PhD thesis

Isomorphs and Pseudoisomorphs
in Molecular Liquid Models

Zahraa Sheydaafar, *May 31, 2021*
supervisor: Thomas B. Schrøder
co-supervisor: Jeppe C. Dyre

Glass and Time, IMFUFA
Department of Science and Environment,
Roskilde University, Denmark

Abstract

This thesis investigates new generic methods of identifying isomorphs and pseudoisomorphs in molecular viscous liquids using computer simulation.

Isomorph theory has been studied for the last ten years in the Glass and Time group at Roskilde University. Strongly correlating liquids, so-called Roskilde simple liquids, are found to have invariant curves in their phase diagram, termed as isomorphs. The structure and dynamics of Roskilde simple liquids are invariant along isomorphs. These curves exist not only in atomic liquid models but also in molecular systems. Isomorphs usually are determined along configurational adiabats and also via the direct isomorph check method. In this work, we introduce new generic "force methods" to generate isomorphs in rigid bonded models and pseudoisomorphs in harmonic spring bonded models.

The atomic force method is introduced by Schrøder for the first time; it has been shown that this method works properly for the Kob-Andersen binary Lennard-Jones system [1]. In this thesis, we introduce the molecular force and the torque methods which identify isomorphs in three small molecular models: asymmetric dumbbell, symmetric inverse power law (IPL) dumbbell and Lewis-Wahnström o-terphenyl (OTP). The advantage of force methods is that only a single configuration is required to predict isomorphs via these methods. The ability of these methods to predict isomorphs also are tested on a larger molecular model, i.e. flexible Lennard-Jones chains model with constraint bonds. In addition to the atomic and molecular forces, the segmental force is also investigated in the Lennard-Jones chains model.

It has been shown that harmonic spring bonded molecular models have a poor correlation between the constant-density equilibrium virial and potential-energy fluctuations, and subsequently they are not supposed to have isomorphs. In 2016, Olsen *et. al* found invariant structure and dynamics in harmonic models, behaving like isomorphs which are termed pseudoisomorphs [2]. Olsen *et. al* used a challenging method to determine pseudoisomorphs, while we suggest much easier methods, ("force methods") to identify pseudoisomorphs in harmonic small and large molecular models. Two different scaling approaches, i.e. atomic scaling and center-of-mass scaling, are used to scale the configurations. We quench the system in order to generate pseudoisomorphs in harmonic models at high densities. Different minimization schemes are presented and developed to find the local minima. At low densities, pseudoisomorphs are identified in harmonic models via the force methods without quenching.

The molecular force method can be considered as a general method to identify isomorphs and pseudoisomorphs in small molecular models at low and high densities. However, the force methods do not predict the isomorphic points in long flexible Lennard-Jones chains model along the large density change; but it is possible to identify pseudoisomorphs via atomic

and segmental forces in this model.

Resumé

Denne afhandling undersøger nye generiske metoder til at identificere iso-morfer og pseudoisomorfer i molekylære viskøse væsker ved hjælp af com-putersimuleringer.

Isomorfteori er i de sidste ti år blevet studeret af Glas og Tid-gruppen ved Roskilde Universitet. Her har man opdaget at stærkt korrelerede væsker, også kaldet Roskilde simple væsker, har kurver i deres fasediagram, kaldet isomorfer, hvor struktur og dynamik er invariant. Disse kurver eksisterer ikke kun i atomare væskemodeller, men også i molekylære systemer. Isomor-fer er ofte bestemt ved at finde de konfigurationelle adiabater, eller via den direkte-isomorf-tjek-metode. I denne afhandling introducerer vi nye gener-iske "kraftmetoder" til at generere isomorfer i modelsystemer med rigide bindinger og pseudoisomorfer i modelsystemer med harmoniske fjederbindinger.

En kraftmetode til at generere isomorfer i atomare modelsystemer er blevet introduceret af Schrøder, og denne metode er blevet testet for Kob-Andersen binære Lennard-Jones-system [1]. I denne afhandling introducerer vi den molekylære kraftmetode og drejningsmomentmetoden, til at iden-tificere isomorfer i tre molekylære modeller: den asymmetriske dumbbell model, den symmetriske inverse power law (IPL) dumbbell model og Lewis-Wahnström o-terphenyl (OTP) modellen. Fordelen ved kraftmetoderne er at kun en enkelt konfiguration er nødvendig for at kunne identificere iso-morfer. Disse metoder er også testet på den fleksible Lennard-Jones kæde-model. Udover de atomare og molekylære kræfter er den segmentale kraft også blevet undersøgt i Lennard-Jones kæde-modellen.

Det er blevet vist at molekylære harmoniske fjederbindings-modeller har en ringe korrelation mellem fluktuationer af virialet og den potentialle en-ergy i ligevægt ved konstant densistet, hvorfor det ikke er forventeligt at disse systemer skulle have isomorfer. I 2016 fandt Olsen et al. dog kurver med invariant struktur og dynamik i harmoniske modeller, der opførte sig lige-som isomorfer, og disse blev kaldt pseudoisomorfer [2]. Olsen et al. benyt-tede en relativ kompliceret metode til at bestemme pseudoisomorferne, hvor vi her foreslår simplere metoder (kraftmetoderne) til at detektere pseudoi-somorfer i harmoniske molekylemodeller. To forskellige skaleringstilgange; atomarisk skalering og massecenter-skalering, er anvendt til at skalere kon-figurationerne. For at generere pseudo-isomorfer i harmoniske modeller ved høje densiteter, formindskes systemet (quenching) hvorefter to forskellige minimeringsfunktioner er anvendt til at finde de lokale minima. Pseudo-isomorfer er tilsvarende identificeret i harmoniske modelsystemer ved lave densiteter via kraftmetoderne, uden behov for quenching.

Den generelle metode til at identificere isomorfer og pseudo-isomorfer i molekylære modelsystemer ved lave og høje densiteter er den molekylære kraftmetode. Kraftmetoderne forudser ikke isomorfer i den fleksible Lennard-Jones kæde-model under store densitetsændringer; men det er muligt at

generere pseudo-isomorfer via de atomare og segmentale kræfter i modellen.

Preface

This doctoral thesis describes some of the work done of the Danish PhD program, between Feb 1st 2018 and June 1st 2021. The work has been supervised by Thomas B. Schrøder and Jeppe C. Dyre and was done in the *Glass and Time* group at Roskilde University.

Acknowledgements

Contents

Chapter 1

Background

This chapter provides a general background concerning glasses and viscous liquids. The *Glass and Time Group* at Roskilde University has been investigating the properties of ultra-viscous liquids over the last few decades. Here, we provide a brief introduction about supercooled liquids by avoiding crystallization and modelling them through simulation methods.

1.1 Glass

Glasses are defined as disordered materials which behave like solids from the mechanical aspect but lack the periodicity of crystals [3]. Glasses usually refer to transparent, shiny objects like bottles on the tables or windows in common everyday life. Several different types of substances like metallic alloy or organic molecules can form glasses. Besides, glasses have a prominent role in current technology. For example, amorphous materials play a critical role in developing non-volatile electronics and also revolutionize superconductor technology [4–10]. It is interesting to know that the most water in the Universe might be glassy [11]. Over the last century, scientists have had many challenges with the fundamental questions provided by the glasses and supercooled liquids. Developing experimental strategies and increasing ingenuity in computer simulations in the last decades have helped significantly to characterizing these materials.

1.1.1 Glass Transition

In general, a supercooled liquid can be made by cooling a viscous liquid fast to avoid crystallization [12–14]. Most of the substances can be supercooled at the right cooling rate. After cooling a liquid, particles usually solidify

and form an ordered lattice structure at temperature T_m. But if liquid is cooled sufficiently fast, particles can not sample crystal, and liquid is falling out of the equilibrium. The resulting material is supercooled at a temperature below T_m. One of the main features of supercooled liquids is that the enthalpy depends on the temperature at constant pressure (see Figure 1.1). Besides, the glass can be formed at temperature T_g where the enthalpy slope for liquids suddenly changes to the same slope of crystals. The cooling rate is one of the main factors in forming glasses through a continuous transition.
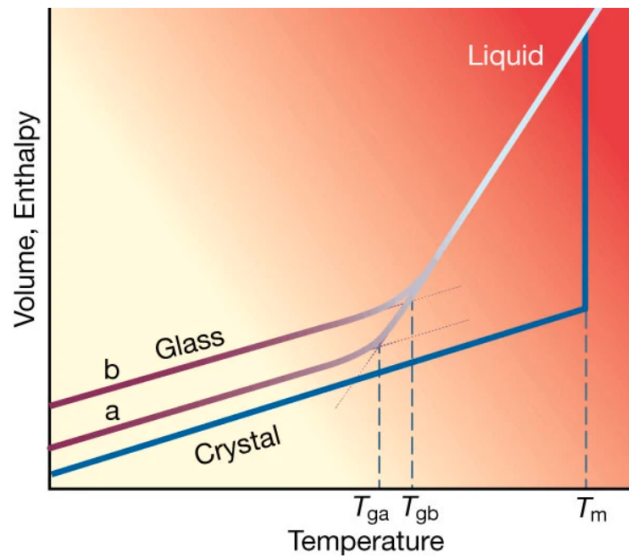
Figure 1.1: The volume V and enthalpy h at constant pressure in liquid, glass and crystalline state dependent on temperature. T_m is the melting temperature. The glass is formed at glass transition temperature T_{ga} with slow cooling rate, and at T_{gb} when the cooling rate is fast. The thermodynamic properties, isobaric heat capacity $c_p = (\partial h/\partial T)_p$ and the thermal expansion coefficient $\alpha_p = (\partial \ln V/\partial T)_p$ change significantly at T_g in a continuous manner. Taken from Ref. [3].

Figure 1.1 shows that the enthalpy decreases continuously with decreasing temperature. It means that the glass transition is not a phase transition because no discontinues changes take place. The glass transition temperature changed through out the process because of a narrow temperature interval in transition. If a cooling rate is low, more time is available for a liquid to adjust its configuration, and liquid stay at equilibrium state at low temperature (i.e. T_{ga} in Figure 1.1). The glass transition temperature T_g depends on the cooling rate, which means that the glass properties depend on how the process is done. For instance T_g increases if the cooling rate increases (i.e. T_{gb} in Figure 1.1). If a liquid is cooled at a slower cooling rate, the resulting material has a higher viscosity and lower enthalpy (Figure

1.1a) compared to the fast-cooled material (Figure 1.1b).

1.1.2 Viscouse Liquids

The definition of a glass transition can be explained in another way when the viscosity and relaxation time reach a certain value. By cooling supercooled liquid, the viscosity gets larger and larger. In addition, the dynamics become slower and subsequently the relaxation time decreases. The particles move slower and slower, so the liquid will be out of equilibrium and forming the glass. The glass transition causes the shear viscosity to increase massively by a factor of 10^4, this increase in viscosity is used to determine the glass transition temperature T_g. The time required for bringing the liquid back to equilibrium, called structural relaxation time, increases significantly. The viscosity is extremely sensitive to the temperature in the region, closed to T_g in some melts. For silica this behavior is defined by the Arrhenius functionality $\eta = A \exp(E/k_{\mathrm{B}}T)$.
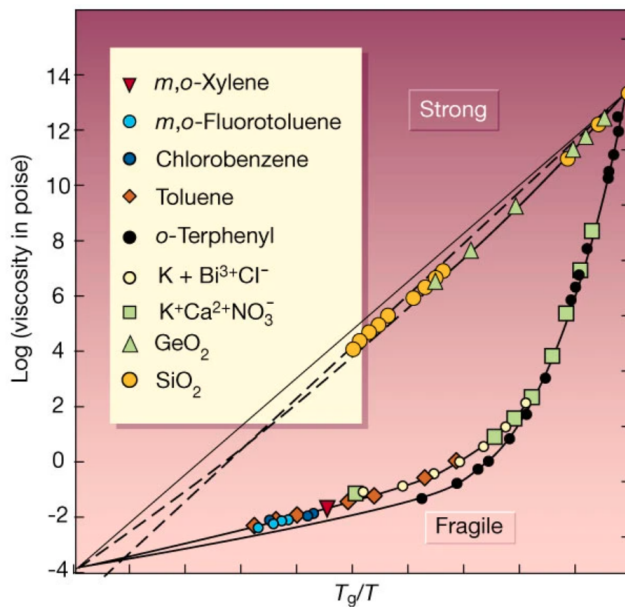
Figure 1.2: The well-known Angell plot showing the viscosity of many glass forming liquids versus inverse temperature. Strong liquids as straight lines obey the Arrhenius function. The non-type Arrhenius behavior liquids like o-terphenyl (OTP) are so-called fragile, and follow the curved line. Taken from Ref. [3].

Figure 1.2 is the famous so-called "Angell plot" [12] which classifies glass-forming liquids in "strong" and "fragile" categories. Here, the "strong" liquids refer to those liquids which have Arrhenius-type behavior like the SiO_2 (yellow circles following a straight line in Figure 1.2). Whereas the liquids in which their viscosity increases dramatically by lowering the temperature

(non/super-Arrhenius behaviour) are considered "fragile" liquids. An example of a fragile liquid is the o-terphenyl (OTP) seen in Figure 1.1 as black circles, and studied in this thesis. It is still a challenge to explain the glass transition by the non-Arrhenius-type liquids, and several theories has been proposed in Ref. [5, 15–17].

1.2 Molecular Dynamics

The technique used in this work to study various model liquids is called Molecular Dynamics (MD) simulation and it solves the classical equations of motion of N molecules for each small time step [18, 19]. This method is mainly used for many-body systems in which the particles' motion obey Newtonian classical mechanics. Furthermore, for a system confined in a simulation box, periodic boundary conditions are considered to avoid effects of the edges [19]. According to periodic boundary conditions, if a particle leaves the box from the left side, another identical particle with the same momentum enters the box from the right side. To understand the periodic boundary conditions, consider the identical simulation boxes replicated around the original box (see Figure 1.3). The particles in replicate boxes (denoted as image particles) behave the same as the original particles and the number of N particles remain fixed. To avoid counting the interaction of the original particle with its image twice, the cutoff radius r_c is defined as the distance beyond which interactions are set approximately zero.

The Lennard-Jones pair potential for atoms or molecules in liquids consists of two part, representing repulsive and attractive forces [21]. It is given by,

$$u_{ij}(r_{ij}) = 4\epsilon_{ij} \left[\left(\frac{\sigma_{ij}}{r_{ij}} \right)^{12} - \left(\frac{\sigma_{ij}}{r_{ij}} \right)^{6} \right], \tag{1.1}$$

in which ϵ_{ij} and σ_{ij} define the energy and length scale of the interaction between the i, j particles. The most important term is the short ranged repulsive force (i.e. r^{-12}-term), created from the outer electron shells. It has a main role in characterising the liquid structure. Whereas the long-ranged attractive force (i.e. r^{-6}-term) has a minor contribution in regulating the liquid state [22]. The cutoff can be defined in several ways for the Lennard-Jones potential $u(r)$:

1. The cutoff is given by the so-called, "truncated and shifted potential (SP)", where the potential is zero above the cutoff and shifted below in a way that ensures the potential is continuous at r_c [18, 23]. More precisely ,

$$f_{SP}(r) = \begin{cases} f_{LJ}(r) & \text{if } r < r_c \\ 0 & \text{if } r > r_c, \end{cases} \tag{1.2}$$
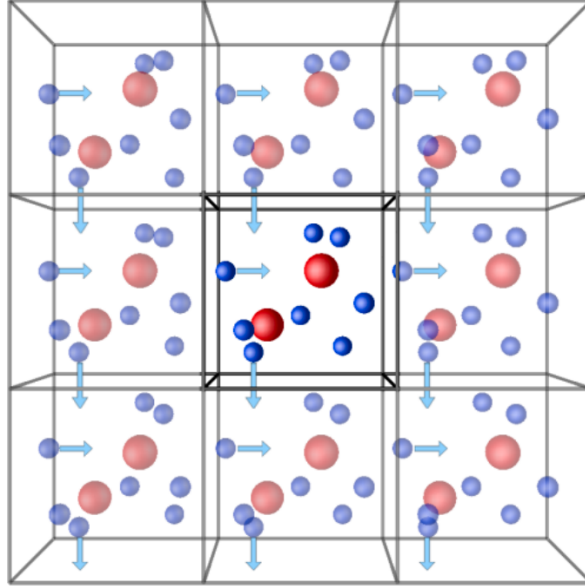
Figure 1.3: An illustration of replicated simulation boxes around the original box in MD simulation. It illustrates the schematic representation of periodic boundary condition. A main particle is replaced with an identical image particle with the same momentum when it leaves the box. Taken from Ref. [20].

where the radial force is obtained by $[f_{LJ} = -u'_{LJ}(r)]$.

2. The "truncated and shifted forces (SF)" cutoff, in which the force decreases to zero continuously at r_c, which is obtained by subtracting a constant term $f_{LJ}(r_c)$ [23, 24],

$$f_{SF}(r) = \begin{cases} f_{LJ}(r) - f_{LJ}(r_c) & \text{if } r < r_c \\ 0 & \text{if } r > r_c. \end{cases} \tag{1.3}$$

The shifted force cutoff has become popular recently because it needs the smaller cutoff distance and the errors reduce significantly.

1.2.1 Leap-Frog Algorithm

The Newton's equations of motion, specifically Newton's second law $\mathbf{F} = m\mathbf{a}$ is solved numerically by MD simulation via discretizing the time coordinate. The force of a system can be extracted as the gradient of the potential energy,

$$\mathbf{F} \equiv -\nabla U(\mathbf{R}), \tag{1.4}$$

which can be the Lennard-Jones potential given for pair interactions in this work. Thus the pair force between the particles i and j is the derivation of Lennard-Jones potential,

5

$$\mathbf{f}_{ij}^{LJ}(\mathbf{r}_{ij}) = -24\epsilon_{ij} \left[2\frac{\sigma_{ij}^{12}}{r_{ij}^{13}} - \frac{\sigma_{ij}^{6}}{r_{ij}^{7}} \right] \hat{\mathbf{r}}_{ij}. \qquad (1.5)$$

The total force is obtained by summing over the pair forces in equation 1.5,

$$\mathbf{f}_i = \sum_{j \neq i} \mathbf{f}_{ij}(\mathbf{r}_{ij}). \qquad (1.6)$$

Newton's equation of motion is given by,

$$\frac{d\mathbf{r}_i}{dt} = \mathbf{v}_i(t), \qquad (1.7)$$

and

$$\frac{d\mathbf{v}_i}{dt} = \frac{\mathbf{f}_i(t)}{m_i}. \qquad (1.8)$$

To solve equation 1.7 and 1.8 numerically by MD simulation time must be discretized in small time steps Δt. The time evolution of equation of motion can be evaluated with different protocols. Here, we use the Leap-Frog algorithm which is modified version of the Verlet algorithm [25, 26]. The Leap-Frog algorithm has advantages in compared to the Verlet algorithm. It avoids the time step squared needed to update the system state and can save the position and velocity at different times. Moreover, it is more stable in computer simulation [25]. With the Leap-Frog algorithm the velocities and positions can be determined by half time step Δt. If time is discretized by time steps around time t, e.g. $..., t - 2\Delta t, t - \Delta t, t + \Delta t, t + 2\Delta t, ...$, the time evolution of velocity and position of particles are obtained by,

$$\mathbf{v}_i(t + \Delta t/2) \quad = \quad \mathbf{v}_i(t - \Delta t/2) + \Delta t \frac{\mathbf{f}_i}{m_i}, \qquad (1.9)$$

$$\mathbf{r}_i(t + \Delta t/2) \quad = \quad \mathbf{r}_i(t) + \Delta t \mathbf{v}_i(t + \Delta t/2). \qquad (1.10)$$

To compare the model systems with real systems, the NVT ensemble (i.e. the temperature is constant) is more often used and it can be simulated by above mentioned algorithm. In this thesis the most part of the simulations are done with canonical ensemble simulations (NVT-simulations). The Nosé-Hoover thermostat is implemented to keep the temperature constant [19, 27–30].

1.3   GPU Computing, RUMD

RUMD is a high-performance Molecular Dynamics simulation package developed at Roskilde University over the last ten years. RUMD is an abbreviation of Roskilde University Molecular Dynamics. The package is running

on graphical processing units (GPU's) instead of central processing units (CPU's) [31]. GPUs are used a lot in the scientific community since they have substantial computational horsepower. They are much faster than CPUs in processing due to several thousands of cores [32] and can process more floating-point operations per second. Moreover, GPUs are cheaper and more efficient from an energy consumption perspective. GPUs can make identical parallel operations on different blocks of the same data and they are good candidates for MD simulation. NVIDIA's CUDA programming environment, released in 2007, promotes the calculation capabilities of GPU [33], which is used in RUMD.
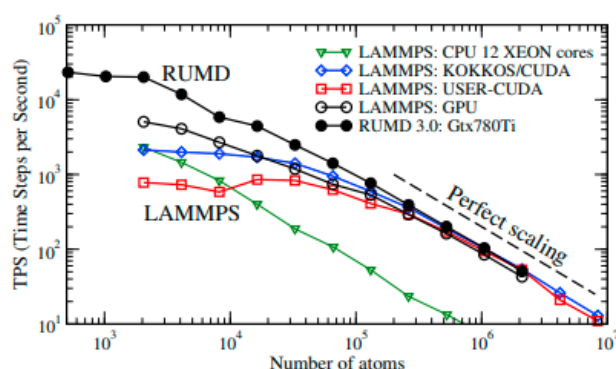
Figure 1.4: Comparing RUMD performance with well-known simulation package, LAMMPS, as a function of system size. RUMD is much faster than LAMMPS for small system sizes and it is seen perfect scaling for large system sizes. Taken from Ref. [31].

RUMD is an open-source program that can be downloaded at `http://rumd.org/`. The package includes a library that is written in C++. It also consists of Python interface and tools to perform post-simulation data analysis. RUMD is optimized for small and medium system sizes while still being comparable with other packages (e.g. LAMMPS, Gromacs, ...) for a large system. This is illustrated in Figure 1.4 which compares the performance of RUMD with different version of LAMMPS benchmark results. RUMD is relatively faster for small system sizes in comparison to LAMMPS with three different GPU versions. All simulations and results in this manuscript are produced and analyzed by RUMD.

1.4 Minimization Functions

The gradient descent is the most well-known optimization algorithm to find the local minimum introduced in 1847 by Cauchy [34]. It starts from a random initial point and takes steps corresponding to the negative gradient of the function to find the minimum via gradient descent. At each step,

we move in the direction where the function declined fastest because the negative gradient points are in the steepest descent. Furthermore, gradient descent is a first-order optimization algorithm. However, this method is quite inefficient because it uses very limited local information and makes small step sizes at each iteration.

1.4.1 Newton's Methods

Another optimization method is Newton's method that finds the extremum (minima and maxima) using information of the curvature [35]. In this method, the second-order function's derivation is considred [36]. Newton's method estimates the function at a random point with a paraboloid and then finds the minimum of the function by approximating the minimum of the paraboloid. The step size is determined by the distance to the minimum of the point's parabola, so it takes less steps to converges to the minimum in comparison with the gradient descent. Even though, Newton's method is faster; it might return a maximum or a saddle point instead of minimum because it is strongly dependent on the local behaviour of the initial point. The Jacobian or the Hessian is required in this method. Computation of the Hessian scales as $O(n^2)$ in Newton method and is therefore more computationally expensive compared with the gradient descent which scales $O(n)$ operations [37]. In 1959, Davidon *et al.* suggested the quasi-Newton algorithms for the first time. These methods are known as secant methods which are the generalization of Newton's methods that address the above mentioned issues [38]. In this method, it is not necessary to compute the Hessian matrix, and instead of approximating the new quantities at each iteration, it takes the information from the previous iteration information to process the next iteration of minimization, it is thus much less computationally expensive.

1.4.2 BFGS Optimization

The minimum of the convex function can be reached by gradient descent (strongly initial point dependent, moves down slowly opposite the gradient), Newton's methods (needs fewer steps, considering the second-order behaviour of the function but costly in time) and quasi-Newton algorithms, the secant methods, (much faster by imposing further constraints in the minimization process).

The BFGS method is one the popular quasi-Newton algorithms which are proposed by Broyden, Fletcher, Goldfarb, and Shanno, in 1970 [34–36, 39, 40, 40]. Newton's methods are required to compute the inverse of Hessian, which costs $O(n^2)$ operations; but using the BFGS method, the inverse Hessian can be estimated directly, which is of course more efficient. BFGS method is used in chapters 5 and 6 to find the local minima of supercooled

liquids.

Chapter 2

Isomorph and Pseudoisomorph

This chapter gives a general overview of isomorph theory in constraint bonded models and pseudoisomorph in harmonic spring bonded models. Isomorphs are invariant curves in the phase diagram of Roskilde simple models. Besides, pseudoisomorphs are found in models with harmonic intramolecular interactions, which behave like isomorphs meaning that structure and dynamics are invariant along these curves. Isomorph and pseudoisomorph have been developed extensively in a series of publications of the Glass and Time group at Roskilde University (Bailey *et al.*, 2008 [41, 42]; Gnan *et al.*, 2009 [43]; Ingebrigtsen *et al.*, 2012 [44]; Pedersen *et al.*, 2009 [45]; Schrøder *et al.*, 2009, 2014 [46, 47]; Dyre, 2014, 2020 [48, 49], Veldhorst *et al.* 2014 and Olsen *et al.*, 2016 [2, 50]).

2.1 Simple Liquids

Traditionally, simple liquids are referred to as many-body systems in which classical particles interact via radially symmetric pair potentials. There are ongoing debates about how to characterize the simple liquids. If the liquids are only defined by the pair potential energy function, how provide a quantitative criterion to define these classes of liquids? In 2012, Ingebrigtsen *et al.* classified simple liquids as systems with strong correlation between viral and potential energy equilibrium fluctuations in the NVT ensemble [44]. The class of simple liquids can be identified with the strongly correlating systems, since the properties of these systems are simpler than the other liquids in general and they are named Roskilde simple liquids [51–

53]. Because the name of strongly correlating systems was confused with the strongly correlating quantum systems, they are named Roskilde simple systems [44]. Simple liquids include not only atomic systems but also some molecular systems [54].

2.2 Roskilde Simple Liquids

Over the last ten years, isomorph theory has been developed and evaluated by the Glass and Time group at Roskilde University [41–43, 45, 46, 50, 55–59]. The theory depends on the correlation between the configurational part of pressure and energy fluctuations in the canonical constant volume ensemble (NVT) of liquids, solids and gas [43, 56, 60]. These two parts depend on the positions of the particles $\mathbf{r_i}$. On the other hand, kinetic energy and temperature only depend on the momenta of the particles $\mathbf{p_i}$,

$$
\begin{aligned}
E &= K(\mathbf{p}_1 + \cdots + \mathbf{p}_N) + U(\mathbf{r}_1 + \cdots + \mathbf{r}_N), & (2.1) \\
pV &= Nk_{\mathrm{B}}T(\mathbf{p}_1 + \cdots + \mathbf{p}_N) + W(\mathbf{r}_1 + \cdots + \mathbf{r}_N). & (2.2)
\end{aligned}
$$

An example of these strong correlations for an asymmetric dumbbell model is given in Figure 2.1. This correlation leads the Glass and Time Group to identify the so-called "hidden scale invariance" in R-simple systems [43]. Indeed, these systems have curves in their thermodynamic phase diagram, along which structure and dynamic properties are invariant. These invariant curves are named "isomorphs".
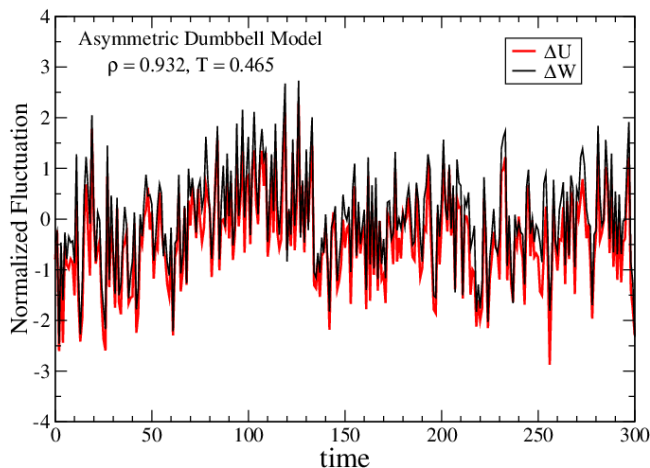
Figure 2.1: Correlation between potential energy and virial of an asymmetric dumbbell model at state point $(\rho, T) = (0.932, 0.465)$. The potential energy and virial per particle are normalized by subtracting the mean and dividing by the standard deviation. The collapse illustrates strong correlation between potential energy and virial.

Since isomorph theory is applicable for strongly correlating system, it is required to define a quantitative measure of this correlation [41]. The degree of correlation is calculated from the standard Pearson correlation coefficient, given by,

$$R(\rho, T) = \frac{\langle \Delta W \Delta U \rangle}{\sqrt{\langle (\Delta W)^2 \rangle \langle (\Delta U)^2 \rangle}}, \tag{2.3}$$

where angular brackets $\langle \rangle$ indicate thermal NVT ensemble averages and Δ denotes the instantaneous deviations from the equilibrium mean value, W the virial and U the potential energy of the system. This correlation is investigated in many different models [41] which are assumed to be a Roskilde simple model when $R > 0.9$. Isomorphs do not exist only in strongly correlating liquids, but also metallic systems can have isomorphs [55, 60].

The slope γ of the W, U-correlations is characterized by $\Delta U = \gamma \Delta W$, and it is given by the linear regression slope of a scatter plot between U and W (see Figure 2.2) [61–63],

$$\gamma = \frac{\langle \Delta W \Delta U \rangle}{\langle (\Delta U)^2 \rangle}, \tag{2.4}$$

which depends on the state point.
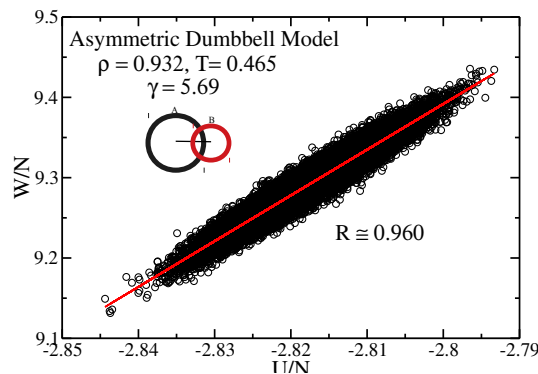
Figure 2.2: Scatter plot of W, U-correlations for asymmetric dumbbell model consisting of 5000 molecules at state point $(\rho, T) = (0.932, 0.465)$. The system is strongly correlated with $R = 0.960$ and $\gamma = 5.69$. Taken from ref. [54]

The correlations of most liquids or solids dominated by van der Waals or weakly ionic and dipolar interactions is much stronger than the correlations of systems with hydrogen or covalent bonds or strong Coulomb forces. Furthermore, isomorph theory is only exact for systems with an Euler-homogeneous potential energy function, which is perfectly strong correlated, for example, systems interacting via an inverse-power-law (IPL) pair-potential [41, 42]. All microconfigurations of an IPL system have $W = \gamma U$

with $\gamma = \dfrac{n}{3}$ and the correlation coefficient is exactly $R = 1$. Since R depends on the temperature T and density ρ strong correlations appears only in part of the phase diagram of liquids models; For example, the correlation coefficient usually decreases to below 0.9 when approaching the critical point.

It is important to note that isomorph invariance refers to structure and dynamics reported in the so-called reduced (state-point dependent) units. In this unit system the particle number density $\rho \equiv N/V$, where N is the particle number and V the system volume defines the length unit l_0, the temperature T defines the energy unit e_0, and the density and the thermal velocity define the time unit t_0. Thus if m is the particle mass, the length, energy, and time units are given by [41, 43, 44],

$$l_0 = \rho^{-1/3}, \quad e_0 = k_{\mathrm{B}}T, \quad t_0 = \rho^{-1/3}.\sqrt{m/k_{\mathrm{B}}T}$$

2.3   Isomorph Theory

In this section, we present an overview of versions of isomorph theory introduced by Gnan. *et al.* [43] and developed by Schrøder. *et al.* [47] and Dyre [48]. Isomorphs theory is defined by two similar approaches, and both start with reduced microconfigurations. By considering a system with N particles, microconfiguration $\mathbf{R}$ is the coordinates vector of all particles $\mathbf{R} \equiv (\mathbf{r}_1, \mathbf{r}_2, ..., \mathbf{r}_N)$. Since isomorph theory refers to quantities given in reduced units, a microconfiguration is scaled by density, $\tilde{\mathbf{R}} \equiv \rho^{1/3}\mathbf{R}$, to make it a reduced microconfiguration. From the original formulation, two configurations with the same reduced coordinates $\rho_1^{1/3}\mathbf{R}_1 = \rho_2^{1/3}\mathbf{R}_2$ at state points (ρ_1, T_1) and (ρ_2, T_2) have identical canonical probability Boltzmann factors,

$$\exp[-U(\mathbf{R}_2)/k_{\mathrm{B}}T_2] \cong C_{12}\exp[-U(\mathbf{R}_1)/k_{\mathrm{B}}T_1], \tag{2.5}$$

C_{12} is a constant which does not depends on the specific configurations, but on the considered state points. Furthermore, the identical Boltzmann factors propose the identical structure and dynamics in reduced units.

The generic version of isomorph theory was formulated by Schrøder and Dyre in 2014 [47]. The existence of isomorphs in R-simple liquids is expressed in "hidden scale invariance" identity, which is called that way because the scaling behavior of potential energy surface (see Figure 2.3) is not obvious.

The potential energy surface of two configurations $\mathbf{R}_1, \mathbf{R_2}$ with identical reduced coordinates, are scaled by,

$$U(\mathbf{R}_2) \cong h_1(\rho_2)U(\mathbf{R}_1) + g_1(\rho_2), \tag{2.6}$$

$$U(\mathbf{R}) \cong h(\rho)\tilde{\Phi}(\rho^{1/3}\mathbf{R}) + g(\rho)$$
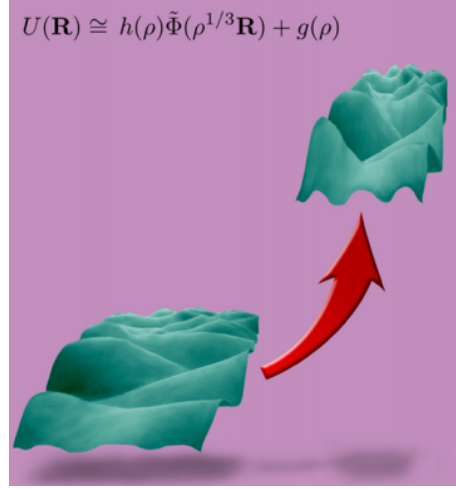
Figure 2.3: Potential energy surface scaling behaviour on which isomorph theory is valid. Taken from Ref. [48]

when density ρ_1 changes to ρ_2. In this version, the R-simple systems with the Euler homogeneous pair potentials ($v(\lambda r) = \lambda^\alpha v(r), \lambda \in \mathbb{R}$), obeys the condition:

$$U(\mathbf{R}_1) < U(\mathbf{R}_2) \Rightarrow U(\lambda \mathbf{R}_1) < U(\lambda \mathbf{R}_2). \tag{2.7}$$

where λ is the scaling factor [47]. The new isomorph condition (equation 2.7) restates the isomorph condition or *hidden scale invariance*. Since the configurations can be scaled back and forth at the set of the densities, $\Rightarrow$ can be replaced to $\Leftrightarrow$ in equation 2.7. If the potential energies of configurations of a R-simple system are same, they are same after scaling,

$$U(\mathbf{R}_1) = U(\mathbf{R}_2) \Leftrightarrow U(\lambda \mathbf{R}_1) = U(\lambda \mathbf{R}_2). \tag{2.8}$$

R-simple systems obey the isomorph condition showed in equation 2.8. In the new formulation, excess isochoric heat capacity, C_V^{ex} is not invariant, whereas it was predicted to be invariant in the original version of isomorph theory [47]. The first-order approximation was taken in the original derivation, while most thermodynamic functions are derived from second-order derivation in the new version [47].

Isomorph can be generated along invariant excess entropy or configurational adiabats curves. The system's entropy is the sum of the ideal gas entropy and configurational contribution, i.e. the excess entropy, $S = S_{id} + S_{ex}$. For an ideal gas, the excess entropy is zero, and for any other systems, $S_{ex} < 0$, because they must be less disordered in comparison to an ideal gas. According to isomorph theory, the excess entropy must be invariant along isomorphs [54, 64–66]. It is defined as the thermodynamic equilibrium ex-

cess entropy of configuration R with average potential energy $U(\mathbf{R})$ at the state point with density ρ,

$$S_{ex}(\mathbf{R}) \equiv S_{ex}(\rho, U(\mathbf{R})). \tag{2.9}$$

On the other hand, the potential energy $U(\mathbf{R})$ can be expressed as the function of density and thermodynamic excess entropy S_{ex},

$$U(\mathbf{R}) = U(\rho, S_{ex}(\mathbf{R})). \tag{2.10}$$

The above formulations can be applied for any systems [67] but if we focus on R-simple systems in which the configurations at two different densities obey the hidden scale invariance (equation 2.8), $\mathbf{R}_2 = \lambda \mathbf{R}_1$ where $\lambda = (\rho_1/\rho_2)^{1/3}$. Considering equation 2.9, it has been shown that the excess entropy of system can be identical at two densities, $S_{ex}(\mathbf{R}_1) = S_{ex}(\mathbf{R}_2)$ [47, 48] and it only depends on the reduced configuration,

$$S_{ex}(\mathbf{R}) = S_{ex}(\tilde{\mathbf{R}}). \tag{2.11}$$

So then equation 2.10 can be represented by,

$$U(\mathbf{R}) = U(\rho, S_{ex}(\tilde{\mathbf{R}})). \tag{2.12}$$

The new formulation in equation 2.12, which connects the microscopic potential energy to equilibrium average potential energy, leads us to achieve the invariant reduced units structure and dynamics.

One of the invariant dynamical properties is the reduced-force derived from Newton's second law in reduced coordinates, $d^2(\tilde{\mathbf{R}})/d\tilde{t}^2 = \tilde{\mathbf{F}}$. All particle forces are expressed as a single vector force, $\mathbf{F}$ which is $\tilde{\mathbf{F}} \equiv \mathbf{F}\rho^{-1/3}/k_{\mathrm{B}}T$ in reduced units and it can be obtained by $\mathbf{F} = -\nabla U$. With regards to $\nabla = \rho^{1/3}\tilde{\nabla}$ and considering equation 2.12, we have,

$$\begin{aligned} \mathbf{F} &= -\rho^{1/3}\tilde{\nabla}U(\rho, S_{ex}(\tilde{\mathbf{R}})) \tag{2.13} \\ &= -\left(\frac{\partial U}{\partial S_{ex}}\right)_\rho \rho^{1/3}\tilde{\nabla}S_{ex}(\tilde{\mathbf{R}}). \end{aligned}$$

Because $\left(\dfrac{\partial U}{\partial S_{ex}}\right)_\rho = T$, the reduced force is equal to,

$$\tilde{\mathbf{F}} = -\tilde{\nabla}S_{ex}(\tilde{\mathbf{R}}), \tag{2.14}$$

which implies that force must be invariant in reduced units. In the next chapter we use the invariant reduced forces to identify isomorphs in R-simple molecular models.

2.4 Pseudoisomorph

There are several systems in which isomorph theory is not valid, like system with Coulomb interactions or molecular liquid models with harmonic interaction. In 2016, Olsen *et. al* found invariant curves in spring models, which resemble isomorphs, named pseudoisomorphs. Since the W, U-correlations break down in harmonic models, the scaling exponent γ can not be used to find the invariant dynamics and structure. However, the pseudoisomorphs are predicted by quenching the system and eliminating the unscaled degrees of freedom of harmonic bonds. See paper [2] for more details. In chapter 5 we use small stiff molecular models with intramolecular harmonic bonds to predict pseudoisomorphs via our newly developed force methods. Large flexible molecular models are investigated in chapter 6.

2.5 Identifying Isomorphs and Pseudoisomorphs

There are several different ways to identify isomorphs and pseudoisomorphs. In this section, we explain two prominent methods. The first one is based on the invariant excess entropy curves named configurational adiabats used to generate isomorphs; the second method uses the potential energy surface, named direct isomorph check method (DIC) used to find both isomorphs and pseudoisomorphs. Additional methods based on invariant reduced forces are introduced in the next chapter.

2.5.1 Configurational Adiabat

To find the curves of constant excess entropy (i.e. configurational adiabat), the scaling exponent γ is used [43]. For an IPL system with the 100% W, U-correlation ($R = 1$), the invariant curves are represented by $\rho^\gamma / T = const.$ and $\gamma = n/3$. In general for strongly correlating systems with correlation coefficient $R > 0.9$, scaling exponent γ as mentioned is the slope of the linear regression fit of equilibrium fluctuations of potential energy and virial in constant volume. The slope of configurational adiabats in $(\log \rho, \log T)$-phase diagram of a strongly correlating system gives the scaling exponent γ. Since the excess entropy remain constant along configurational adiabats and isomorphs are configurational adiabats, dS_{ex} is set to be zero [43]. Besides, the excess entropy can be written as a function of volume and temperature,

$$dS_{ex} = \left(\frac{\partial S_{ex}}{\partial T} \right)_V dT + \left(\frac{\partial S_{ex}}{\partial V} \right)_T dV = 0. \tag{2.15}$$

Using the volume-temperature Maxwell relations for the configurational degrees of freedom, $(\partial S_{ex}/\partial V)_T = \partial \left((W/V)/\partial T \right)_V$, equation 2.15 is written as,

$$\left(\frac{\partial S_{ex}}{\partial T}\right)_V T d\ln T = \left(\frac{\partial W}{\partial T}\right)_V d\ln\rho. \qquad (2.16)$$

By considering $dU = TdS - PdV$ we have,

$$\left(\frac{\partial U}{\partial T}\right)_V d\ln T = \left(\frac{\partial W}{\partial T}\right)_V d\ln\rho, \qquad (2.17)$$

Using the fluctuation relations $(\partial W/\partial T)_V = -\langle \Delta W \Delta U \rangle, (\partial U/\partial T)_V = -\langle (\Delta U)^2 \rangle$ gives the scaling exponent,

$$\gamma = \left(\frac{d\ln T}{d\ln\rho}\right)_{S_{ex}} = \frac{\langle \Delta W \Delta U \rangle}{\langle (\Delta U)^2 \rangle}. \qquad (2.18)$$

Equation 2.18 can be applied for any system to find the configurational adiabat curves [43]. Firstly, to find isomorphs, one must assure that the system has the strong W, U-correlation by measuring R. Isomorphs are mapped out step-by-step by changing the density using equation 2.18. γ can be measured from the equilibrium simulation at any given state point implementing the different numerical integration. The density step size depends on which integral is implemented in simulation. In the Euler integration method, the density should change by a factor of 1%, whereas it can be changed more in each step in the Runge-Kutta integration method [68]. The dynamics and structure are invariant along configurational adiabats in both atomic and molecular models with rigid bonds as long as they are considered as R-simple models.

2.5.2 Direct Isomorph Check

The second way we are checking in this thesis is the direct isomorph check (DIC) method. This method predicts the temperatures by using the isomorph definition directly (equation 2.5). DIC method evaluates the Boltzmann factor proportionality of two different isomorphic state points. Consider two state points with different densities ρ_1 and ρ_2 have the same reduced microconfiguration $\rho_1^{1/3}\mathbf{R}_1 = \rho_2^{1/3}\mathbf{R}_2$, then the potential energy surface at these state points are compared by equation 2.5 which can be written,

$$U(\mathbf{R}_2) \cong h_1(\rho_2)U(\mathbf{R}_1) + g_1(\rho_2). \qquad (2.19)$$

Equation 2.19 indicates the change in the potential energy surface by changing the density and describes how the energy surface at density ρ_1 changes when the micro configuration is scaled to a different density. $h_1(\rho_2)$ and $g_1(\rho_2)$ only depend on density ρ_1. Equation 2.19 is the original formulation of isomorph theory, in which calculating the potential energy at a given density and then scale the system to a second-density, it gives the potential at the new density. Then by calculating the slope of correlation

between these two potentials, by considering the condition $T_2/T_1 = h_1(\rho_2) = h(\rho_2)/h(\rho_1)$, one can identify the isomorphic state points.
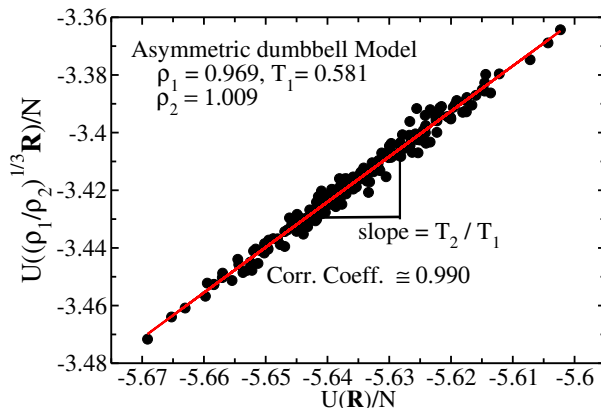

Figure 2.4: The correlation of potential energy surface and direct check of equation 2.19 for the asymmetric dumbbell model (a large and a small LJ particle connected by a rigid bond) at two state points $(\rho_1, T_1) = (0.969, 0.581)$ and $\rho_2 = 1.009$. Different equilibrium configurations are selected from a NVT simulation at the first state point $\rho_1 = 0.969$ in LJ units and then scaled to the second density $\rho_2 = 1.009$. The high correlating shows that the energies at the two densities are related in some way.

Figure 2.4 shows the potential energy correlations of the configurations at density $\rho_1 = 0.969$ and the scaled configurations at density $\rho_2 = 1.009$ of the asymmetric dumbbell model with constraint bond. The correlation coefficient is quite high about 0.990, which implies that the state points are isomorphic. As explained, the temperature of the second density is predicted by the slope of the plot. The density can change more in each jump through this method compared to the configurational adiabats. We test this method in the next chapters to trace isomorphs and pseudoisomorphs in small and large molecular models with constraint and harmonic bonds.

2.6 Invariant Structure

The structure of R-simple liquids is assumed to not change along isomorphs. Considering equation 2.5, the probability of configurations do not change by scaling to other isomorphic state points. The canonical reduced microconfigurations probability distribution function is derived by,

$$P(\tilde{\mathbf{R}}) = \frac{\exp[-U(\tilde{\mathbf{R}})/k_{\mathrm{B}}T]}{\int \exp[-U(\tilde{\mathbf{R}})/k_{\mathrm{B}}T]d\tilde{\mathbf{R}}}. \tag{2.20}$$

It is invariant at isomorphic state points which indicates that the reduced equilibrium structure is invariant in configurations with the same probability distribution. To investigate the system's structure, we measure one of the

typical structural quantities, i.e. the radial distribution function (rdf). This property is defined as the probability of finding a particle at a distance r from another particle. The rdf of the strongly correlating systems are found to be invariant [43], and it is extensively used in this manuscript to test the invariance of the structure.

2.7 Invariant Dynamics

Besides the structure, the dynamics in reduced units are predicted to be invariant along isomorphs and pseudoisomorphs. As shown in section 2.3, the reduced force is invariant since two configurations scaled at different isomorphic points has the same potential energy except for an additive constant (equation 2.19) [47, 69]. Mean square displacement in reduced units, $\langle[\tilde{\mathbf{r}}(\tilde{t}-\tilde{\mathbf{r}}(\tilde{0})]^2\rangle$, and intermediate scattering function given by time correlation function of the spatial Fourier transform of the number density $\rho(q)$,

$$F(\tilde{q},\tilde{t}) = \frac{\langle\rho(\tilde{q},\tilde{t})\rho(-\tilde{q},0)\rangle}{\langle\rho(\tilde{q},0)\rho(-\tilde{q},0)\rangle} \tag{2.21}$$

are main dynamical properties used many times in this thesis. Besides, we calculate the orientational autocorrelation function of end-to-end vector to investigate the rotational dynamics. Figure 2.5 demonstrates the invariant intermediate scattering functions and the orientational autocorrelation function of end-to-end vector in reduced units along isomorph in flexible long Lennard-Jones chains (LJC). The relaxation time and diffusion constant are also used to compare the isomorph methods. See reference [43] to find more invariant dynamic properties. Isomorph theory is in agreement with Rosenfeld's excess entropy scaling because not only dynamics but also excess entropy are invariant along isomorphs [70, 71].

Isomorph theory has been identified on different classes of systems, including simple atomic systems in both liquid and solid phases [43, 45, 54, 56, 57], molecular systems like the rigid-bond asymmetric dumbbell model and the symmetric inverse-power law dumbbell model [54], the 10-bead Lennard-Jones chain [50], the Lewis-Wahnström's three-site model of OTP [54], the seven-site united-atom model of toluene [46], the EMT model of liquid Cu [41]. Furthermore, it has been possible to verify isomorph-theory predictions in experiments on van der Waals bonded organic liquids, and for supercritical argon [58, 59]. However, pseudoisomorphs are identified in the molecular models with poor W, U-correlation [2, 50] e.g. the models with harmonic bond. In this work, we intend to predict isomorphs in molecular models with rigid bonds and pseudoisomorphs in the harmonic spring molecular models via *force-based* methods and compare the results of these methods with the configurational adiabats and the direct isomorph check methods.
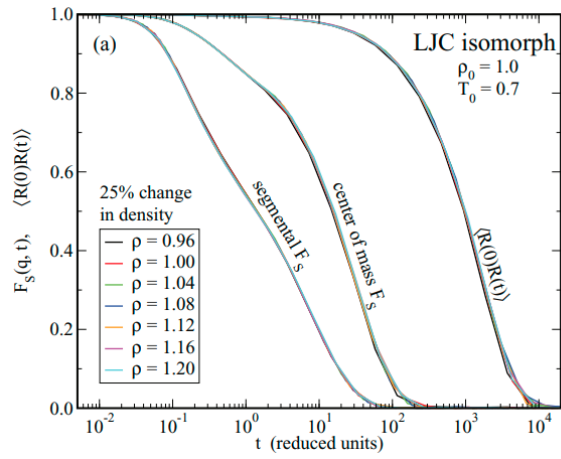
Figure 2.5: The segmental and center of mass incoherent intermediate scattering function F_s, and normalized orientational autocorrelation function of the end-to-end vector $\langle R(0)R(t)\rangle$ in reduced units are invariant along isomorph in the LJC model. Taken from [50].

Chapter 3

Generating Isomorphs in Small Molecular Liquids

This chapter introduces a number of force-based methods to identify isomorphs in three molecular R-simple systems. Schrøder tested the atomic force method on Kob-Andersen binary Lennard-Jones system [1]. We introduce molecular force and torque methods and test them on the asymmetric dumbbell (ASD), symmetric inverse power law (IPL) dumbbell and Lewis-Wahnström o-terphenyl (OTP) with rigid bonds.

3.1   Introduction

The invariant reduced units force concept raises from the potential energy surface scaling at different state points. The potential energies surface at two state points are proportional by a constant factor plus an additive constant (chapter 2). The scaling behaviour of the potential energy surface reveals that the force is one of the quantities, which is invariant in the reduced units according to isomorph theory. In the next section, we show that one can predict isomorphs via simple and efficient methods, i. e. "force methods".

3.2   Finding Isomorphs via Invariant Forces

According to the isomorph theory, two configurations at two state points have the same coordinates in reduced units, $\rho_1^{1/3}\mathbf{R}_1 = \rho_2^{1/3}\mathbf{R}_2$. Not only the structure is invariant along isomorphs but also the dynamics are supposed to be constant along isomorphs at two different state points. So, the potential energy gradient of a strongly correlating liquids is invariant along isomorphic

state points. By considering, $\tilde{\mathbf{F}}_{\mathbf{R}} = -\nabla_{\tilde{\mathbf{R}}}\tilde{U}$, forces also should be invariant along isomorphs which indicates,

$$\tilde{\mathbf{F}}(\mathbf{R}_1) = \tilde{\mathbf{F}}(\mathbf{R}_2). \tag{3.1}$$

The reduced-forces at two state points are derived by,

$$\tilde{\mathbf{F}}(\mathbf{R}_1) = \frac{\mathbf{F}(\mathbf{R}_1)}{k_{\mathrm{B}}T_1}\rho_1^{-1/3}, \tag{3.2}$$

and

$$\tilde{\mathbf{F}}(\mathbf{R}_2) = \frac{\mathbf{F}(\mathbf{R}_2)}{k_{\mathrm{B}}T_2}\rho_2^{-1/3}. \tag{3.3}$$

With regards to equation 3.2 and equation 3.3 one can predict the temperature of the next state point using the forces by,

$$T_2 = \frac{|\mathbf{F}(\mathbf{R}_2)|}{|\mathbf{F}(\mathbf{R}_1)|}\left(\frac{\rho_1}{\rho_2}\right)^{(1/3)} T_1. \tag{3.4}$$

The most prominent advantage of these methods is that one can use only a single equilibrium configuration to generate isomorphs, which is not possible in using the scaling exponent γ and the direct isomorph check method. Four different force-based methods are assumed to predict isomorph in molecular systems: atomic force, molecular force (or center-of-mass force), segmental force and torque methods.

3.3   Atomic Force Method

Currently, Schrøder tested the atomic force method on Kob-Andersen binary Lennard-Jones system and predicted good isomorphic points [1]. In this section, we intend to test this method to identify isomorph in three different constrained molecular model, namely asymmetric dumbbell model (ASD), symmetric IPL dumbbell model (IPL) and Lewis- Wahnström o-terphenyl (OTP) model. This force is measured by considering the particles' intramolecular interactions and summing up the force of atoms in a configuration. So the external force of intermolecular interaction is excluded in calculating atomic force.

3.3.1   Test the Method on ASD Model

Asymmetric dumbbell model (ASD) including 5000 molecules is a first model that we pick to test the atomic force method. ASD is a toy model of toluene which consists of two different sized Lennard-Jones (LJ) spheres, a large (A) and a small (B) particles, rigidly bonded. The equilibrium length of the bonds is 0.584 in the LJ units defined by the large sphere ($\sigma_{AA} \equiv 1$,
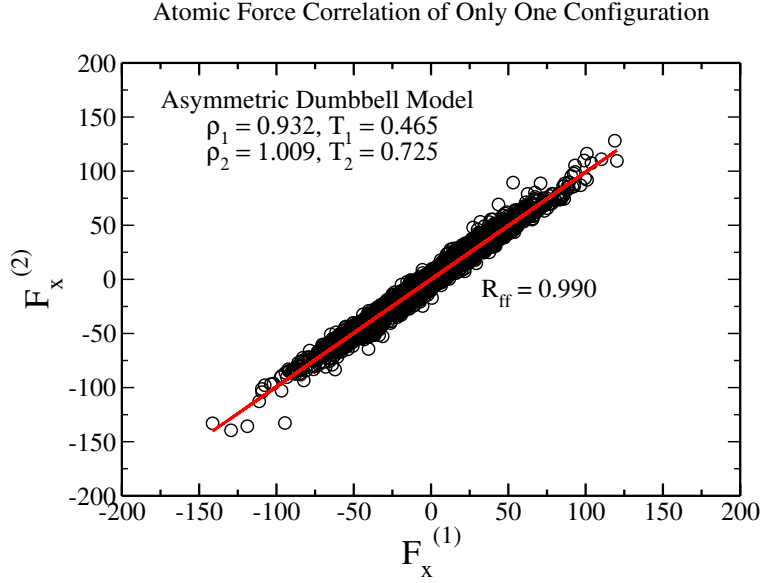
Atomic Force Correlation of Only One Configuration

Figure 3.1: Shows the strong correlation $R_{ff} = 0.990$ between x-component of non-reduced atomic forces at two different state points of the asymmetric dumbbell model. $(\rho_1, T_1) = (0.932, 0.465)$ is considered as a reference point. We predict $T_2 = 0.725$ by scaling a configuration to $\rho_2 = 1.009$ via equation 3.4

$\epsilon_{AA} \equiv 1$, and $m_A \equiv 1$). The parameters of the model were chosen to mimic toluene ($\sigma_{AB} = 0.894$, $\sigma_{BB} = 0.788$, $\epsilon_{AB} = 0.342$, $\epsilon_{BB} = 0.117$, $m_B = 0.195$) [64]. The inter-molecular pair potential interactions obey the Lennard-Jones potential in ASD,

$$v_{ij}(r_{ij}) = 4\epsilon_{ij} \left[\left(\frac{\sigma_{ij}}{r_{ij}} \right)^{12} - \left(\frac{\sigma_{ij}}{r_{ij}} \right)^{6} \right]. \tag{3.5}$$

As expected, the atomic forces have strong correlation at two state points, $\rho_1 = 0.932$ and $\rho_2 = 1.009$, see Figure 3.1. We calculated $T_2 = 0.725$ at density $\rho_2 = 1.009$ by considering atomic forces in the equation 3.4 and using one individual equilibrium configuration at first state point $(\rho_1, T_1) = (0.932, 0.465)$. 152 configurations, taken from the equilibrium simulation at reference point $(\rho_1, T_1) = (0.932, 0.465)$, are used to improve the statistics of temperature prediction. Figure 3.2 represents the distribution of T_2 by scaling the configurations to $\rho_2 = 1.009$.

We measure center-of-mass mean square displacement (msd), center-of-mass incoherent intermediate scattering function (F_{sCM}) and orientational autocorrelation function of end-to-end vector ($\langle \mathbf{R}(0)\mathbf{R}(\tilde{t}) \rangle$) in reduced units to see if translational and rotational dynamics of ASD are invariant along the predicted state points or not?! Figure 3.3 demonstrates center-of-mass mean square displacement in reduced units, whereas Figure 3.4 shows the

Atomic Force Method, $\rho = 1.009$
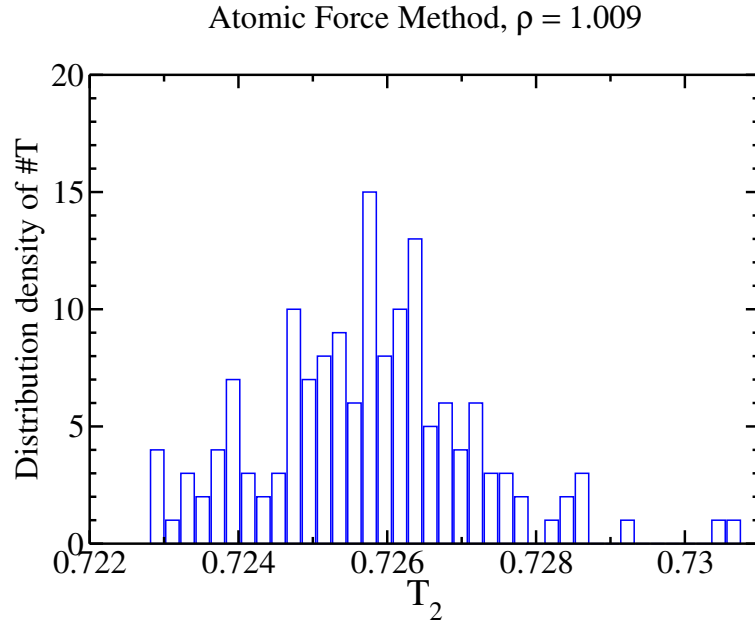
Figure 3.2: Distribution of T_2 by using 152 configurations. T_2 is predicted via atomic force method.
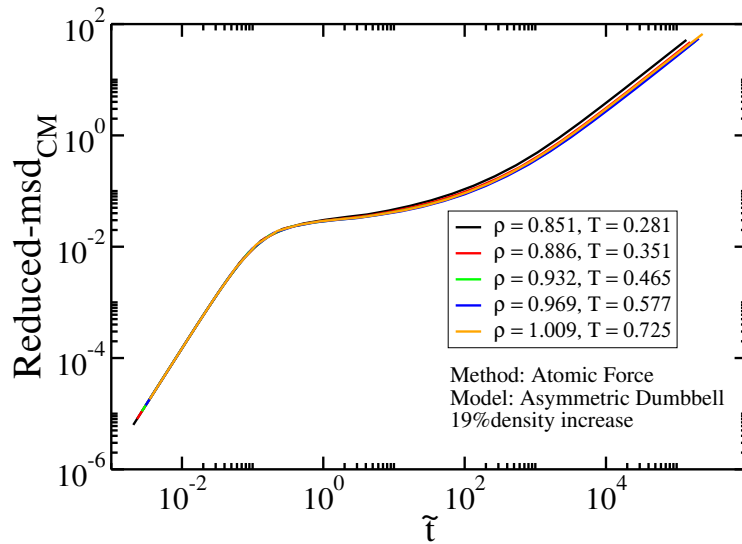
Figure 3.3: Center-of-mass mean square displacement in reduced units of ASD model along the state points which are predicted via atomic force method (equation 3.4). The reference configurations are taken from equilibrium simulation at $(\rho_1, T_1) = (0.932, 0.465)$. Density changes about 19%.

26
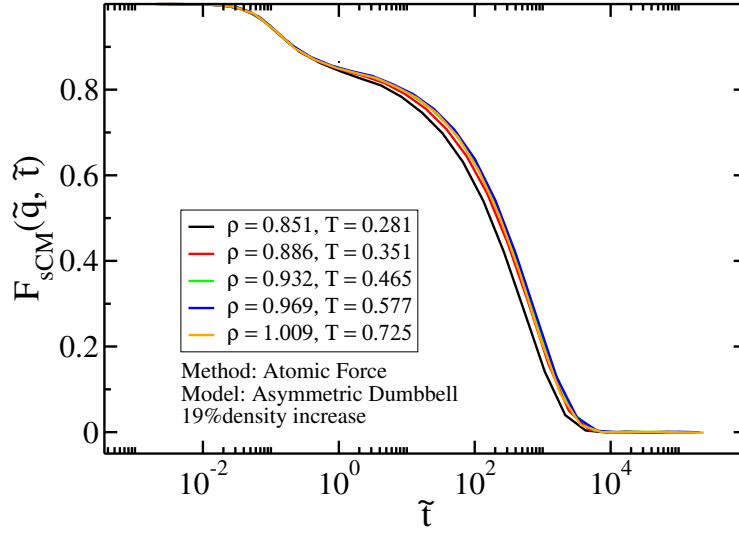
Figure 3.4: Testing the translational dynamics of ASD model via center-of-mass incoherent intermediate scattering function in reduced units along the same state points which are shown in Figure 3.3. The reduced wave-vector is given by $\tilde{q} = q(\rho/0.932)^{1/3}$
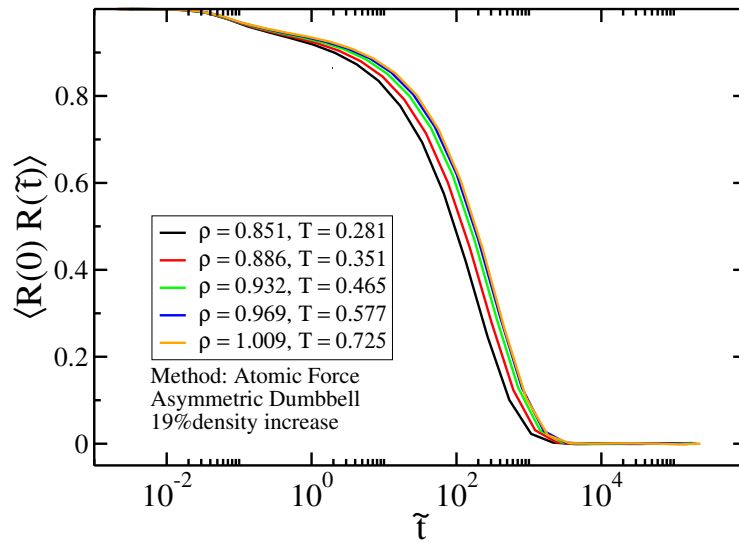
Figure 3.5: Testing the rotational dynamics of ASD model via orientation's auto-correlation function in reduced units along the same state points which are predicted by similar method shown in Figure 3.3 and 3.4
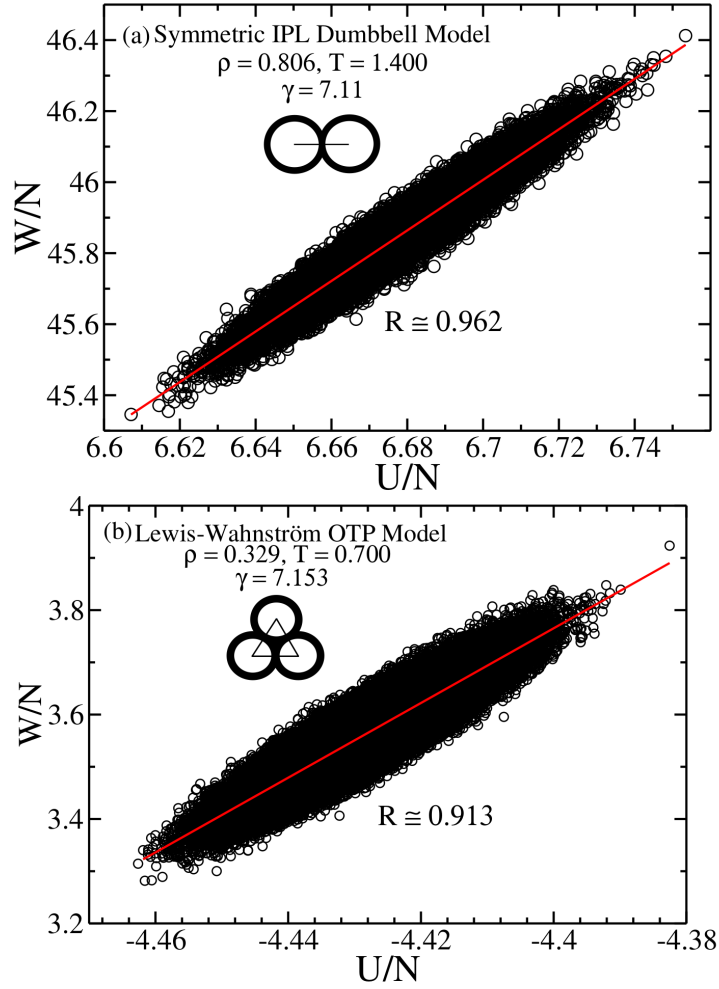
Figure 3.6: The fluctuation of potential energy and virial for symmetric IPL dumbbell and OTP models. (a) The correlation coefficient at the reference state point $(\rho_1, T_1) = (0.775, 1.054)$ is $R = 0.964$ and the linear slop of regression is about $\gamma = 7.04$ for asymmetric dumbbell model, (b) $R = 0.913, \gamma = 7.153$ for OTP model at state point $(\rho_1, T_1) = (0.329, 0.700)$. Reproduce results from ref. [44]

center-of-mass reduced-intermediate scattering function along different predicted state points via the atomic force method. The rotational dynamics are evaluated by considering the reduced orientational autocorrelation function of end-to-end vector in Figure 3.5. The atomic force method identify isomorphic state points in ASD model.

In the following, we represent the results of testing the atomic force method in symmetric IPL dumbbell model (IPL) and Lewis- Wahnström o-terphenyl (OTP) model with rigid bonds. IPL and OTP models are classified as strongly correlating systems (Figure 3.6), and atomic force method is

assumed to predict isomorphic state points in these two models.

Atomic Force Method
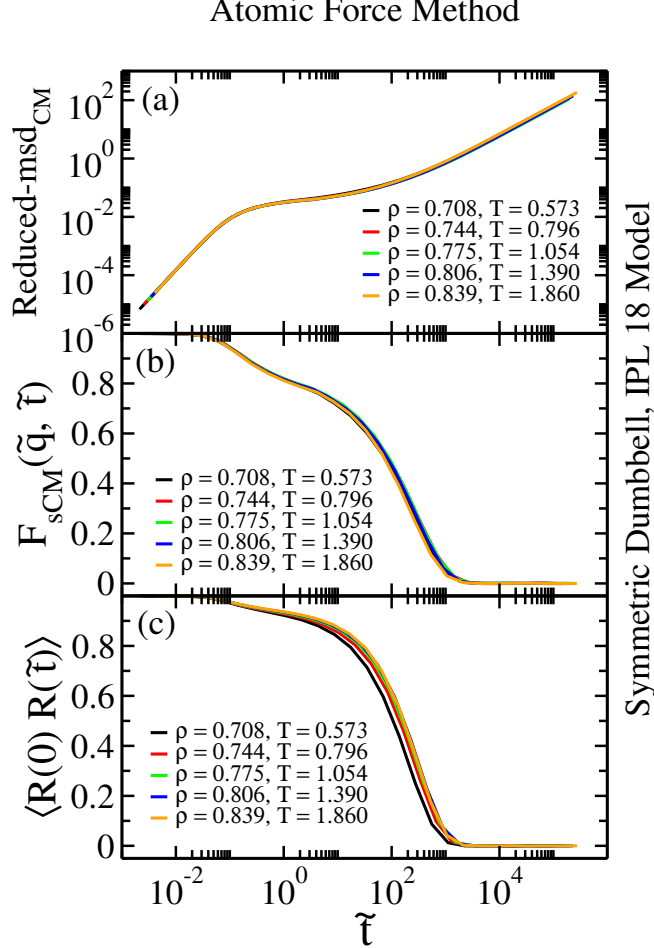
Figure 3.7: Translational and rotational dynamics of IPL model along the predicted temperature via atomic force method using equation 3.4. The reference point is $(\rho_1, T_1) = (0.775, 1.054)$. (a) The mean-square displacement versus time in reduced units. (b) The incoherent intermediate scattering function in reduced wave-vector $\tilde{q} = q(\rho/0.775)^{1/3}$. (c) The orientational auto-correlation function of end-to-end vector in reduced units.

3.3.2 Test the Atomic Force Method on IPL Model

The symmetric IPL dumbbell model consists of two identical particles. As same as ASD, the particles have rigid bonds with length $r_{ij} = 0.584$. 5000 molecules interact via the IPL potential,

$$v_{ij} = \epsilon_{ij} \left(\frac{\sigma_{ij}}{r_{ij}} \right)^n \tag{3.6}$$

in which exponent is $n = 18$. All IPL parameters and particles' masses are unity. The unscaled configurations are taken from the equilibrium simulation at reference point, $(\rho_1, T_1) = (0.775, 1.054)$. The density variation is about 19% taken from ref. [44]. The same dynamics quantities in Figure 3.3, Figure 3.4 and Figure 3.5 ($msd, F_{sCM}, \langle \mathbf{R}(\tilde{t})\mathbf{R}(0) \rangle$) are considered to check dynamics of IPL model along force methods. Figure 3.7 represents that dynamics of IPL are invariant at predicted state points by atomic force method (equation 3.4). However, the translational dynamics (msd, F_{sCM}) have better collapse compared to rotational dynamics ($\langle \mathbf{R}(\tilde{t})\mathbf{R}(0) \rangle$).
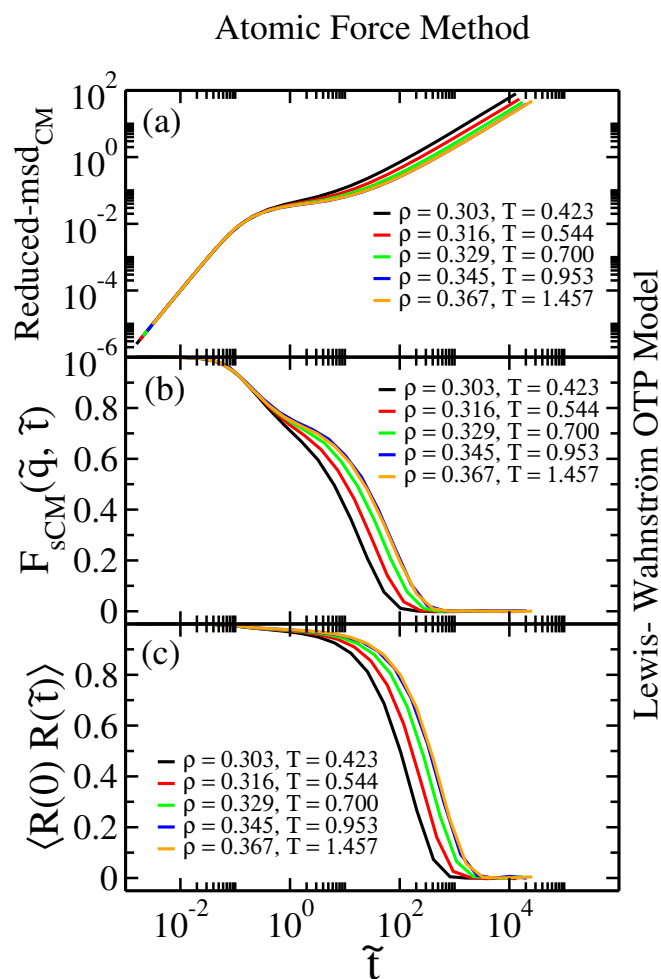
Figure 3.8: Same dynamical properties from Figure 3.7 in OTP model along the predicted temperature via atomic force method. The reference state point is $(\rho_1, T_1) = (0.329, 0.700)$. (a) The mean-square displacement versus time in reduced units. (b) The incoherent intermediate scattering function at the reduced wave-vector $\tilde{q} = q(\rho/0.329)^{1/3}$. (c) The orientational auto-correlation function in reduced units.

Atomic Force Method
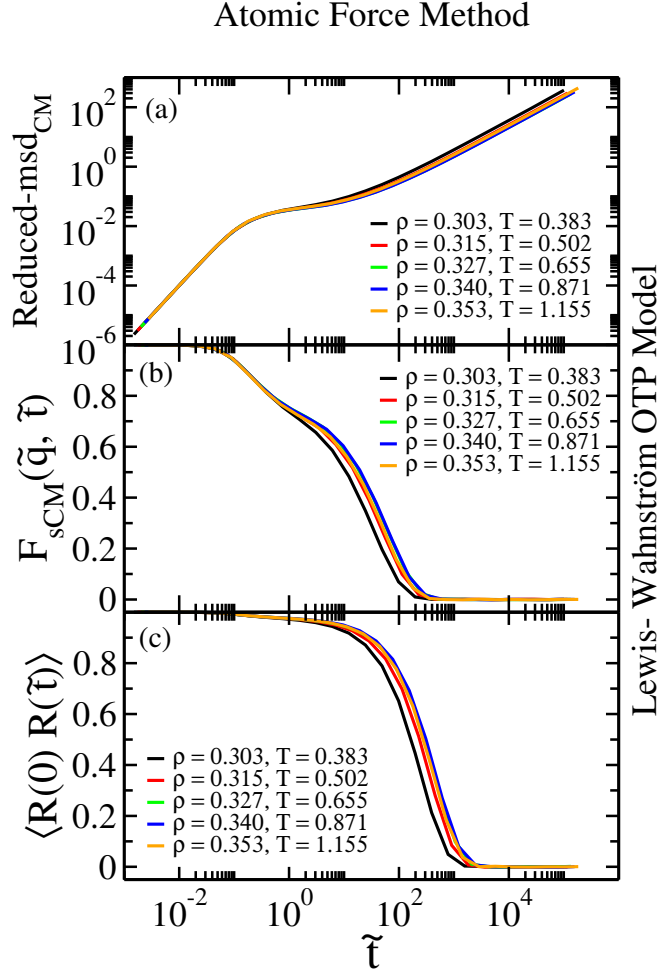
Figure 3.9: Testing the same dynamics properties from Figure 3.8 on OTP model along the invariant atomic force from the reference point $(\rho_1, T_1) = (0.303, 0.383)$. (a) The mean-square displacement versus time in reduced units. (b) Shows the incoherent intermediate scattering function at the reduced wave-vector $\tilde{q} = q(\rho/0.303)^{1/3}$. (c) The orientational auto-correlation function of end-to-end vector in reduced units.

3.3.3   Test the Atomic Force Method on OTP Model

The Lewis- Wahnström OTP model has three identical LJ particles. Atoms are connected by rigid bonds in an isosceles triangle with sides of $r_{ij} = 1.00$ and top angle of 75° which is different from the real 1,2-diphenylbenzene molecule with 60°. All LJ parameters are set to be unity in this model. Figure 3.8 shows that the dynamics of the system is not invariant along predicted state points via atomic force methods. The reference state point is $(\rho_1, T_1) = (0.329, 0.700)$. The dynamics have a good collapse by scaling system to higher density, $\rho = 0.345, 0.367$. The collapse is vanished by scaling at lower density, (see Appendix A). The results improve by scaling the system to only higher density from the reference state point in Figure 3.9. We consider $(\rho_1, T_1) = (0.303, 0.383)$ as the reference point and density increases about 16% overall. This density changes issue only appears for OTP model, which is still the mystery. Hence, state point $(\rho_1, T_1) = (0.303, 0.383)$ is considered as the reference point for OTP model.

3.4   Center-of-mass Force Method

One may consider the center-of-mass force, so-called "molecular force", to identify isomorphs in molecular models. The molecular force is calculated by summing up atoms' forces in each molecule. For example it can be obtained by $\sum F_i = \sum F_{A,i} + F_{B,i}$ in ASD model. The external force is considered in measuring molecular force while the intramolecular forces (due to the bonds) are cancelled out. The molecular forces of two different state points have a strong correlation (see Figure 3.10).

Using the molecular force method in ASD model predicts $T = 0.730$ at density $\rho = 1.009$, which is quite different from predicted temperature via the atomic force method (Figure 3.1). The difference of predicting temperature via atomic and molecular force methods at $\rho = 1.009$ is shown in Figure 3.11.

We continue testing the molecular force method to check whether dynamics are invariant or not in ASD, IPL and OTP models. Figure 3.12 shows that the molecular force method predicts appropriate isomorphic state points along which dynamics are invariant for three models. The molecular force method predicts the better isomorphic points than the atomic force method (see Figure 3.3, 3.4, 3.5, 3.7, 3.9). Besides, the rotational dynamics of molecules should be invariant in reduced units, and it can be expressed by torque. The following section introduces the torque method as the third method to predict isomorphs in strong correlating molecular liquid models.
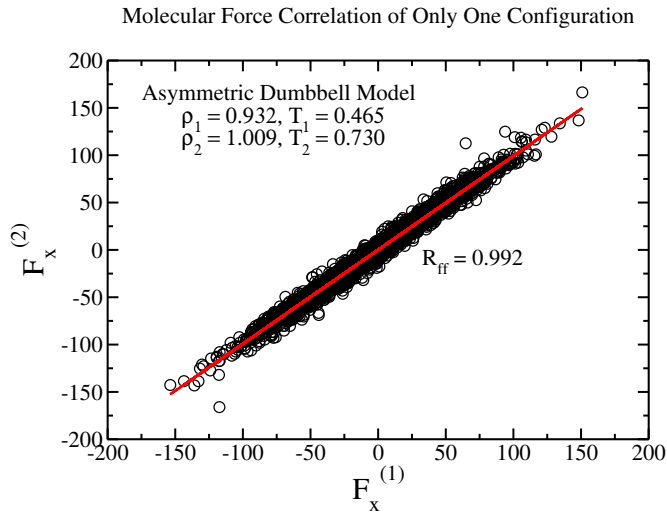
Figure 3.10: Shows the strong correlation $R_{ff} = 0.992$ between x-component of non-reduced center-of-mass forces ("molecular forces") at two different state points of the asymmetric dumbbell model. $(\rho_1, T_1) = (0.932, 0.465)$ is considered as the reference point and by scaling to $\rho_2 = 1.009$ via equation 3.4 we predict $T_2 = 0.730$.
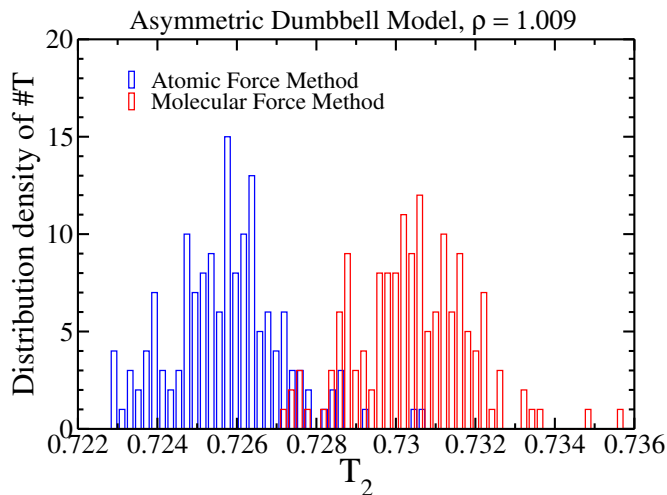
Figure 3.11: Comparing the distribution of predicted temperature via atomic force method (blue) and molecular force method (red) of 152 configurations of ASD models at density $\rho = 1.009$.
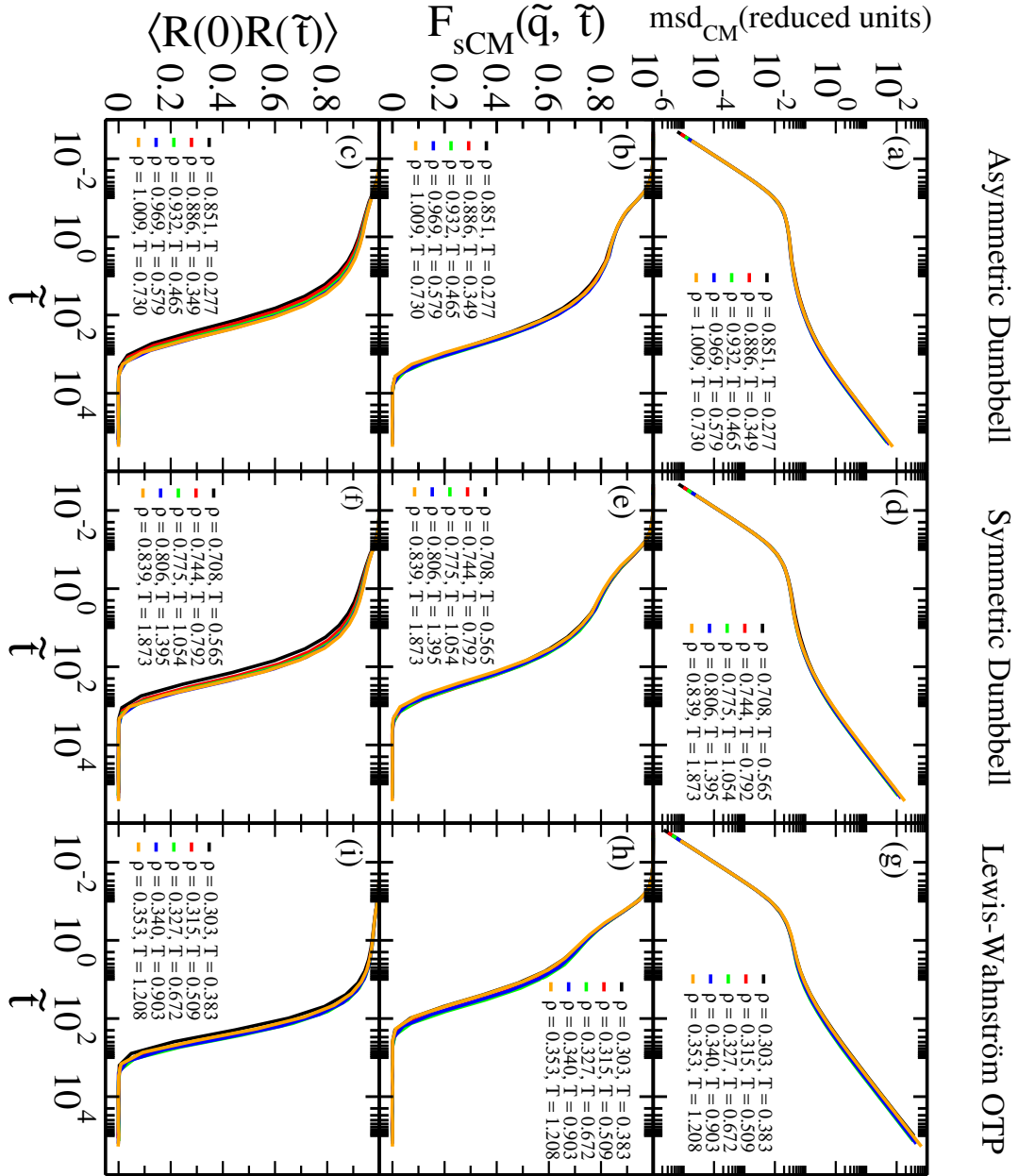
Figure 3.12: Testing the molecular force method on three models, ASD, IPL and OTP. Isomorphs are generated based on a single equilibrium configuration. (a), (b), (c) The mean square displacement, incoherent intermediate scattering function and orientational auto-correlation function in reduced units of the ASD model, which are invariant. Reference point is $(\rho_1, T_1) = (0.932, 0.465)$. (d), (e), (f) The similar dynamical quantities of the IPL model in which we consider $(\rho_1, T_1) = (0.775, 1.054)$ as the reference point. (g), (h), (i) Results for similar dynamics properties of the OTP model. The state point $(\rho_1, T_1) = (0.303, 0.383)$ is starting point.

3.5 Invariance of Reduced Torques

The force acting on one molecule contains two terms,

$$\mathbf{F_{Mol}} = \sum_i (\mathbf{F_{ex,i}} + \mathbf{F_{cons,i}}), \tag{3.7}$$

in which $\mathbf{F_{ex,i}}$ is the force due to the intermolecular interaction of *ith* atom and $\mathbf{F_{cons,i}}$ is the contribution of rigid bond forces (i.e. intramolecular interactions).

To calculate torque, we consider the rotational motion of each atom around the center-of-mass of the molecule. Here, the intramolecular forces ($\mathbf{F_{cons,i}}$) are cancelled out and external forces calculate torque by,

$$\boldsymbol{\tau}_{Mol} = \sum_i \mathbf{r_{cm,i}} \times \mathbf{F_{ex,i}}, \tag{3.8}$$

where $\mathbf{r_{cm,i}}$ is distance between the atom *ith* to center-of-mass in the relevant molecule. In reduced units, torque is given by $\tilde{\tau} = \frac{\tau}{k_B T}$, which should be invariant at two isomorphic state points, $\tilde{\boldsymbol{\tau}_1} = \tilde{\boldsymbol{\tau}_2}$. So one can predicts new temperatures by,

$$T_2 = \frac{\boldsymbol{\tau_2}}{\boldsymbol{\tau_1}} T_1. \tag{3.9}$$

As presented in section 3.3 and section 3.4, isomorph curves have been seen in molecular systems, which are generated by force methods (equation 3.4). We now test the torque method on small molecular models (e.g. ASD, IPL and OTP models). As exTorques of two state points have strong correlation in ASD model (Figure 3.13). The temperature, $T_2 = 0.763$, at the density 1.009 is predicted quite differently via this method compared to predicted T_2 via atomic force method (Figure 3.1) and molecular force method (Figure 3.10).

The precision of methods in predicting temperatures is shown in Figure 3.14. We calculate atoms' temperature through atomic force and molecules' temperature using molecular force and torque methods, $T_2^{(i)}$, at density $\rho_2 = 1.009$. It is shown that the prediction accuracy of the molecular force method is better than the accuracy of another two methods. Figure 3.15 represents the dynamical properties of ASD, IPL and OTP systems along generated state points by torque method using equation 3.9. The dynamics of ASD and IPL models are not invariant using the torque, while there is a good collapse in the dynamics of OTP model. The molecular force method is the only method that predicts the proper isomorphic points in all three molecular models. However, the atomic force method gives good results in IPL model, and the torque method provides the proper results in OTP model.

Torque Correlation of Only One Configuration
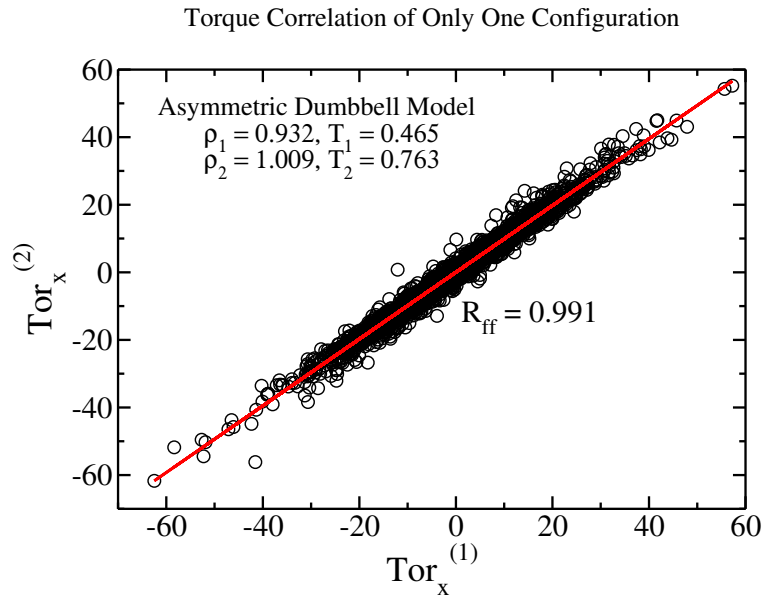
Figure 3.13: Torque correlation of molecules in a given configuration at reference point $(\rho, T) = (0.932, 0.465)$ and scaled configuration at $\rho = 1.009$ for ASD model. The temperature is predicted, $T_2 = 0.763$, by using equation 3.9.
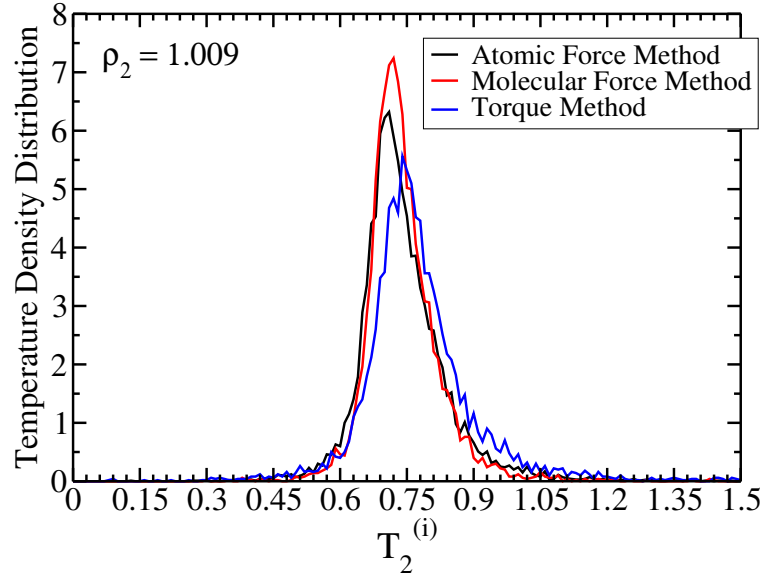
Figure 3.14: Comparing force methods and torque method in predicting the temperature of each particle at density ($\rho = 1.009$) for ASD model. The estimation of the statistical uncertainty of atoms' temperature predicted via atomic force is compared to the precision measuring of molecules' temperature predicted via molecular force and torque. The molecular force method is seen to be more accurate than atomic force and torque methods.
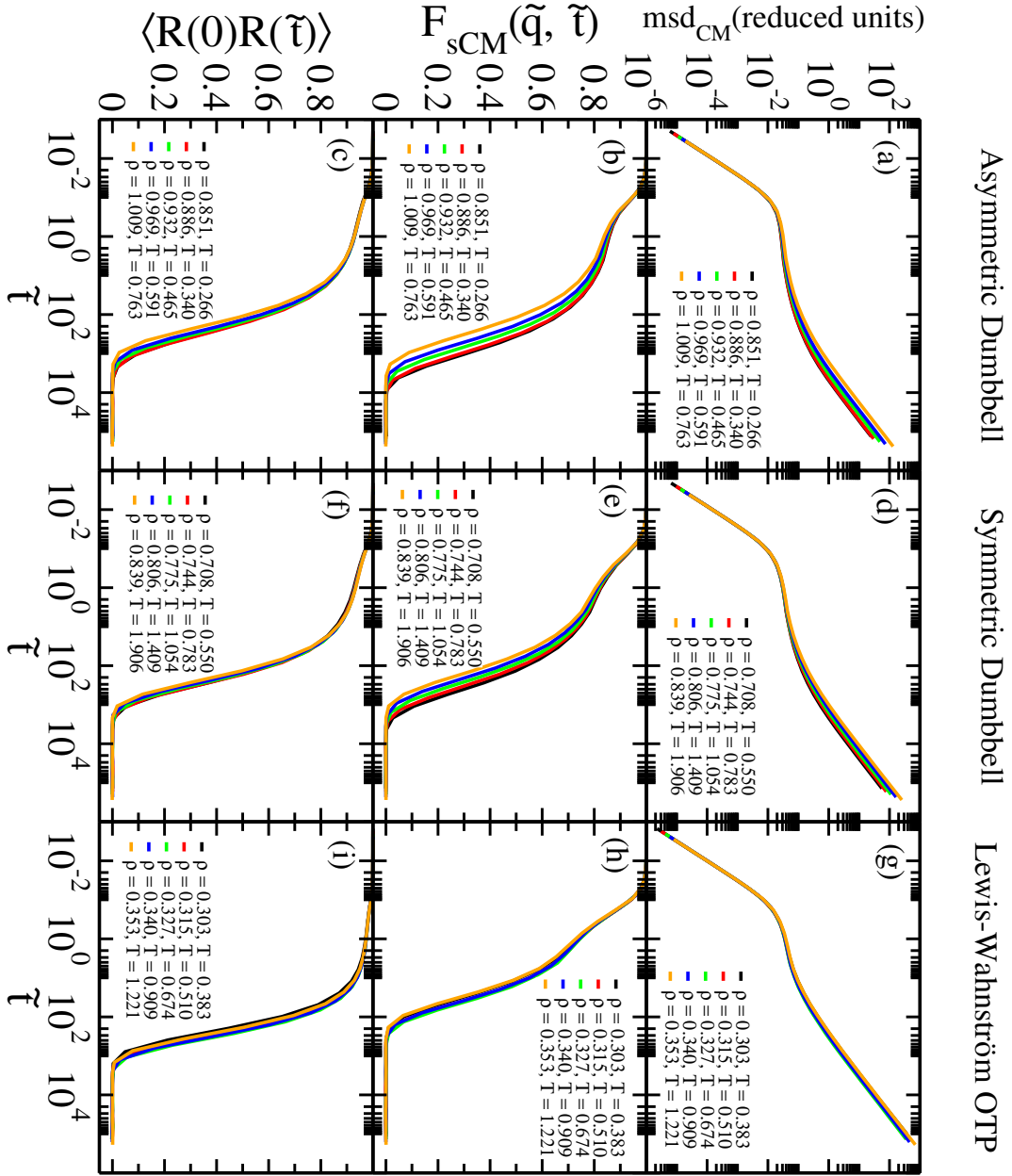
Figure 3.15: Testing the torque method on three models, ASD, IPL and OTP. The same reference points in Figure 3.12 are considered. (a), (b), (c) mean square displacement, incoherent intermediate scattering function and orientational auto-correlation function in reduced units of ASD model, which are not invariant. The molecular force method provide better results (see Figure 3.12). (d), (e), (f) similar dynamical quantities of IPL model. Molecular force method gives nice invariant dynamics in this model in Figure 3.12. (g), (h), (i) results for similar dynamical properties of OTP model. The results of torque method is comparable with molecular force method in Figure 3.12.

3.6　Comparing Isomorph Methods

In the previous section, we used force methods to predict isomorphic state points for three models in which the dynamics behave differently through the various methods. To investigate which methods work better in which model, we measure the relaxation time and diffusion coefficients in this section. By testing the force methods on molecular systems one may wonder how results of these methods are comparable with results of configurational adiabats and direct isomorph check method. In 2012, Ingebrigtsen *et. al* [44] generated isomorphic state points along configurational adiabats in ASD, IPL and OTP models. The temperature is estimated by changing the density 1% in each jump based on equation 2.18. The density can be changed about 15% in force methods, which is a rather large change. The results of configurational adiabats are shown in Figure 3.16 which demonstrates the invariant structure and dynamics in ASD, IPL and OTP models.

Besides, we have created isomorphs by using the direct isomorph check (DIC) method. As explained in section 2.5.2, DIC method identifies new temperatures by using potential energy based on equation 2.5. We find isomorphic state points via this method by starting from a point in the phase diagram and then change the density by a factor of 10%. Density change is rather big compared to configurational adiabats, but it is not comparable with forces methods. Figure 3.17 illustrates the invariant dynamics generated via DIC method in ASD, IPL and OTP models.

We measure translational and rotational relaxation times and center-of-mass diffusion coefficient in reduced units to investigate how these dynamical properties vary through different isomorph methods. The translational relaxation time $\tilde{\tau}_cm$, is calculated from the intermediate scattering function when it has decayed to 0.2. In contrast, the rotational relaxation time $\tilde{\tau}_rot$, is defined as the time when the orientational autocorrelation function of end-to-end vector reaches 0.2. We measure both relaxation times at state points predicted via configurational adiabats, DIC, force methods and isotherm for ASD model in Figure 3.18. The top panel (a) shows the data of translational relaxation time versus changing the density. Likewise, the rotational relaxation time is given in the bottom panel of Figure 3.18(b). As we expected, the relaxation times are invariant along the isomorphs method in comparison with isotherm.

The methods also create isomorphs along which the relaxation times remain constant in IPL and OTP models (Figure 3.19, 3.20). The relaxation times along different isomorph methods are constant along isomorphs in comparison with the relaxation times along isotherm in three models.

Table 3.1 provides another interesting comparison of various methods in the ASD model. It shows the ratio of reduced diffusion coefficient, translational and rotational relaxation times to density. The diffusion coefficient is obtained from the slope of the mean square displacement in diffusive regime,
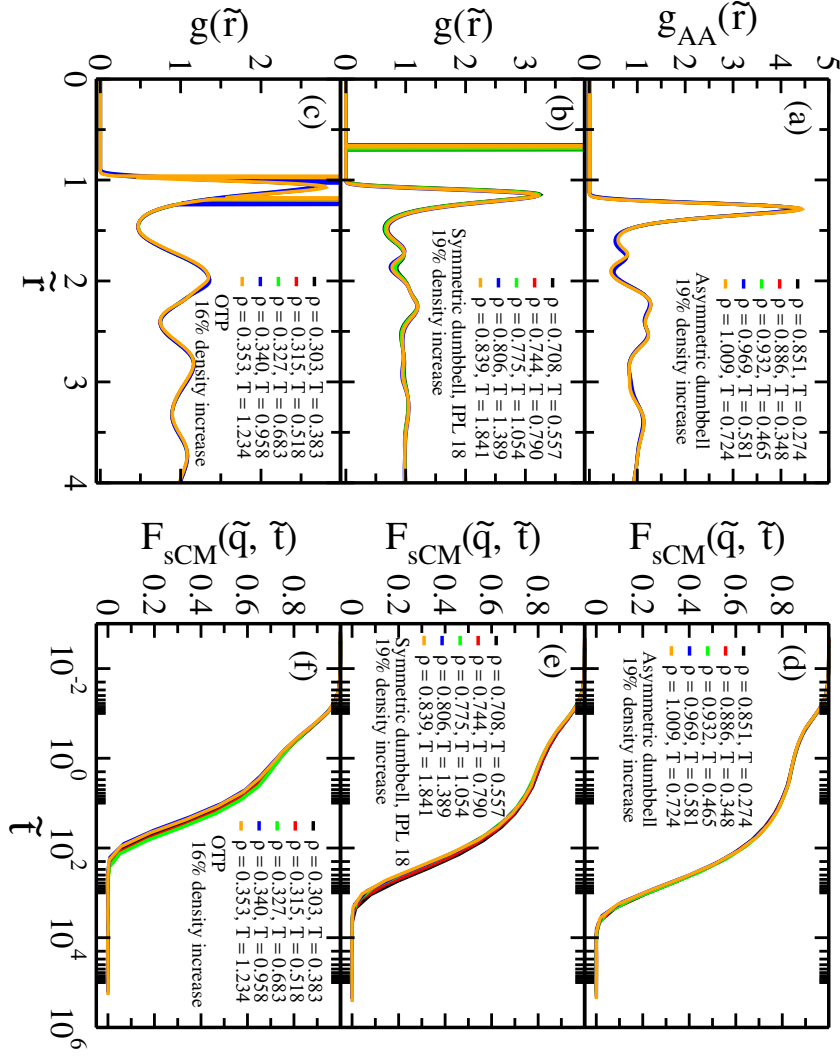
Figure 3.16: Isomorphs along configurational adiabats using equation 2.18 in three ASD, IPL and OTP models. (a), (d) the radial distribution function (*rdf*) and center-of-mass intermediate scattering function (*F$_s$*) in reduced units in ASD model. Results are reproduced from ref. [44] (b), (e) the similar structural and dynamical quantities for IPL model. Here, we consider $(\rho_1, T_1) = (0.775, 1.054)$ as the reference point. (c), (f) the structure and dynamics of OTP model are invariant along constant excess entropy curves. State point $(\rho_1, T_1) = (0.303, 0.383)$.
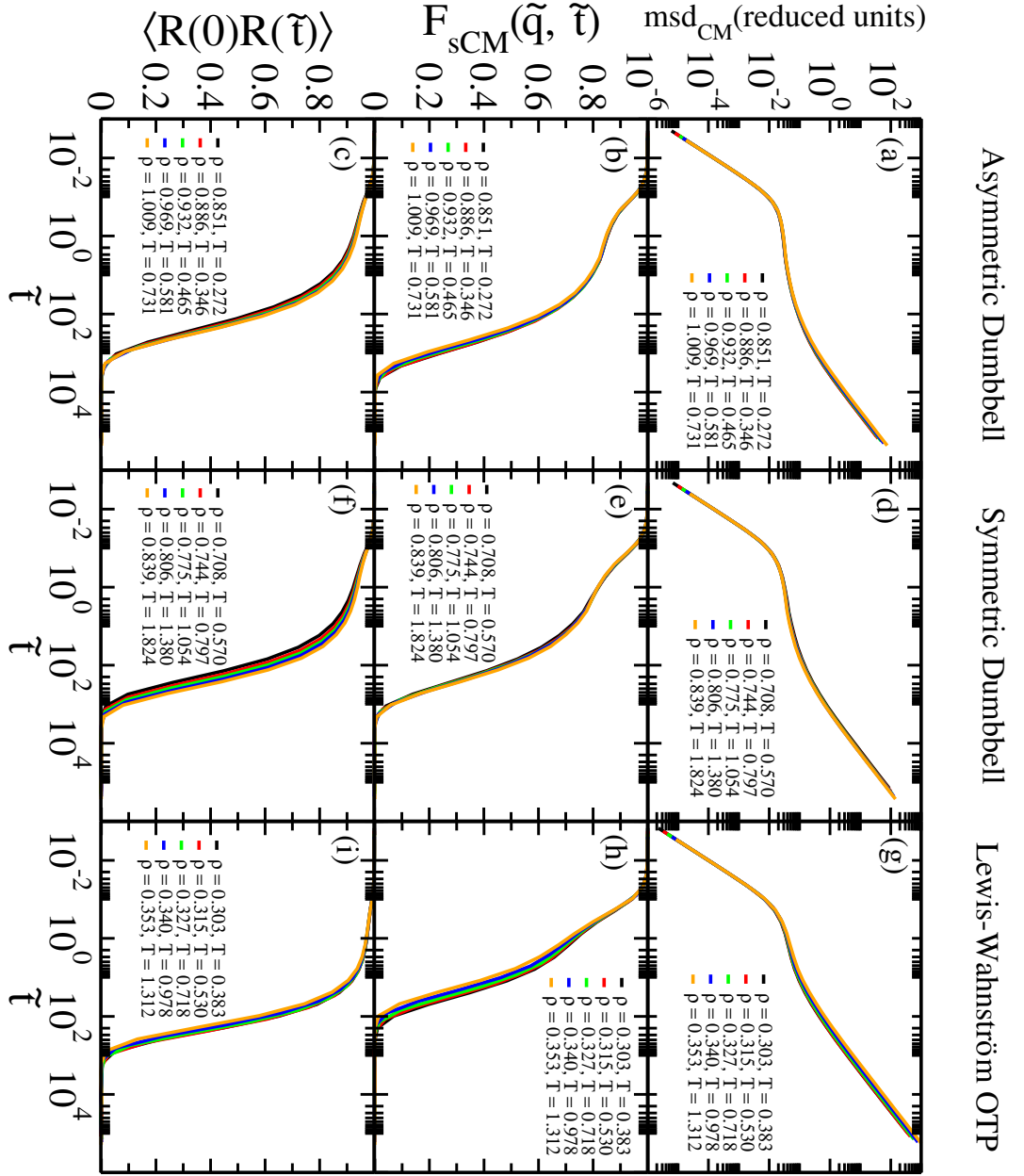
Figure 3.17: Generated isomorphic state points via DIC method in three models. (a), (b), (c) The dynamical properties msd, F_s and $< R(0)R(\tilde{t})$ in reduced units of ASD model. (d), (e), (f) The similar dynamical quantities for IPL model. (g), (h), (i) The similar dynamical quantities for OTP model. Same reference points in Figure 3.16 are considered here.

Asymmetric Dumbbell Model
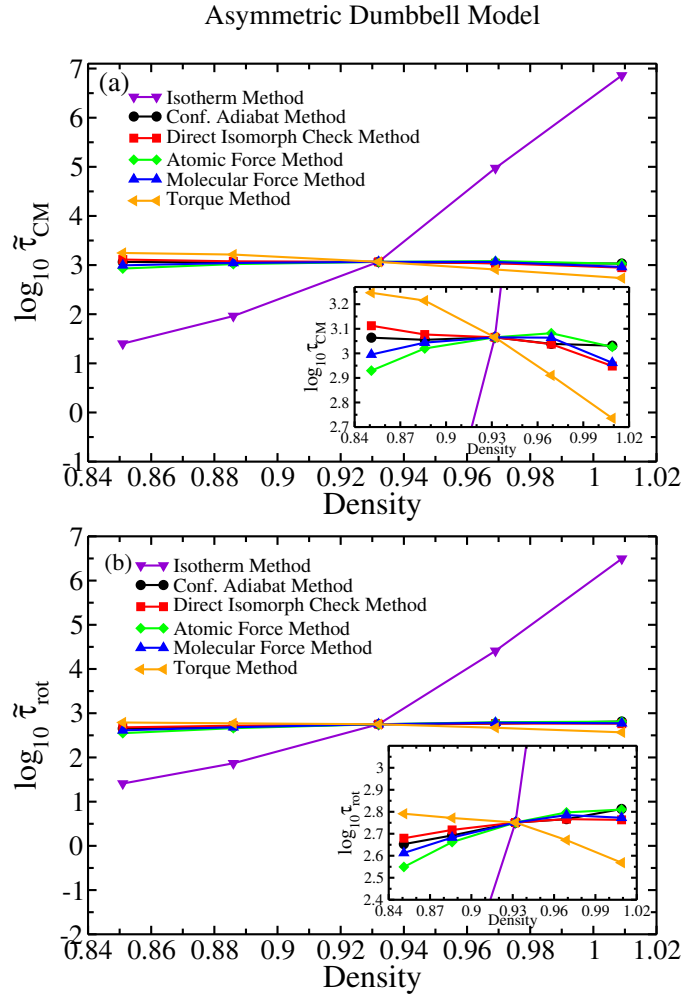
Figure 3.18: Comparing the dynamics of ASD model through different methods with isotherm (purple). Relaxation times are approximately same along four isomorphs predicted by atomic (green) and molecular (blue) force methods, configurational adiabats (black) and direct isomorph check(red) method at densities $\rho = 0.852, 0.969$, but the torque method (orange) generate quite different dynamics. (a) the reduced translational relaxation time against the density changes along curves predicted via different methods for ASD model. (b) shows the orientational relaxation time along curves in reduced units of similar model.
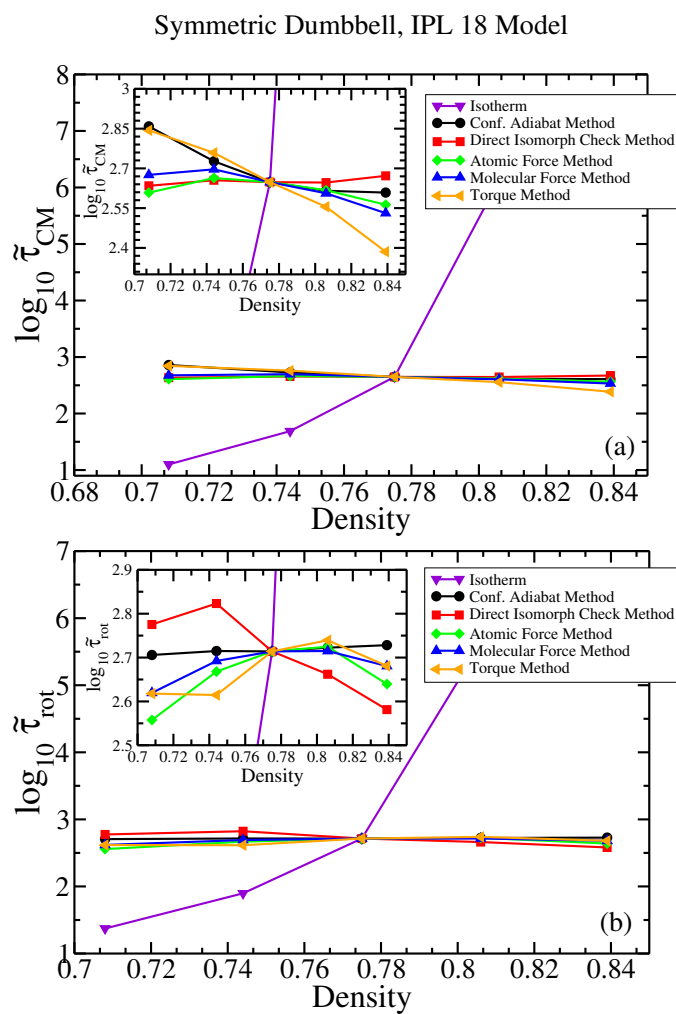
Figure 3.19: The relaxation times variation against density through the isomorph methods and isotherm in IPL model. Here, the dynamics are also invariant along isomorph methods. However, Each isomorph method predicts a different temperature at the same density.
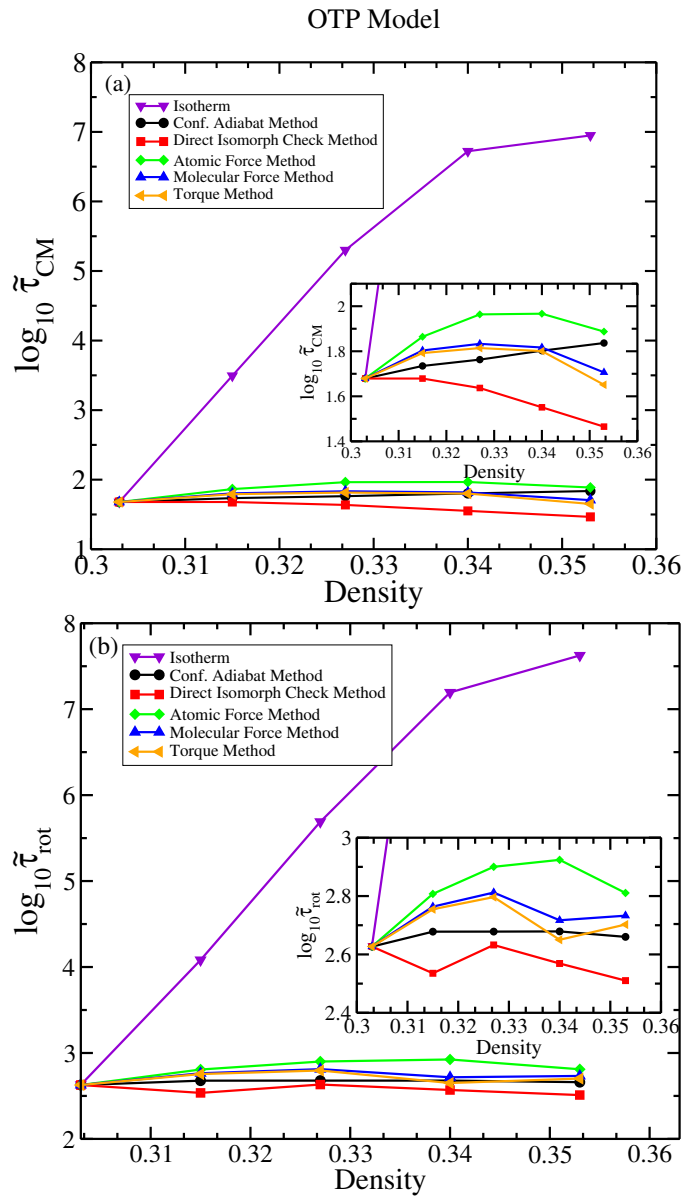
Figure 3.20: Comparing same dynamical properties along isomorph methods from Figure 3.18 in OTP model. The results of molecular force method (blue) is comparable with results of torque method (orange).

$$(\mathbf{r_i}(t) - \mathbf{r_i}(0))^2 \simeq 6Dt \tag{3.10}$$

In molecular systems we calculate the diffusion coefficient by fitting to the center-of-mass mean square displacement for,

$$(\mathbf{r_{cm,j}}(t) - \mathbf{r_{cm,j}}(0))^2 > 10. \tag{3.11}$$

Table 3.1: Comparison between the reduced-unit density variation of the diffusion coefficient (first row), the translational relaxation time (second row) and rotational relaxation time (third row) estimated from different methods and isotherm in ASD model. The second column shows large values obtained by isotherm, non-invariant curves. The third to seventh columns represent the results of configurational adiabats, direct isomorph check, atomic and molecular forces and torque methods. The configurational adiabats and the molecular force method generates better results than other isomorph methods.

	Isotherm	γ	DIC	F_{Atom}	F_{Mol}	Torque
$\dfrac{\partial log\tilde{D}}{\partial log\rho}$	-70(2)	-0.5(4)	1.1(4)	-1.4(2)	-0.9(4)	7.47(6)
$\dfrac{\partial \log \tilde{\tau}_{cm}}{\partial \log \rho}$	77(3)	-0.4(1)	-1.0(1)	1.60(7)	0.5(1)	-7.8(1)
$\dfrac{\partial \log \tilde{\tau}_{rot}}{\partial \log \rho}$	65(3)	1.9(1)	1.26(2)	3.47(3)	2.62(7)	-2.6(2)

Table 3.2: Checking the reduced-units variation of the same dynamical quantities, presented in Table 3.1, for the symmetric dumbbell IPL model. Here, diffusion coefficient and relaxation times keep more invariant along atomic force method. However, the molecular force and torque generate isomorph in IPL model.

	Isotherm	γ	DIC	F_{Atom}	F_{Mol}	Torque
$\dfrac{\partial log\tilde{D}}{\partial log\rho}$	-113.4(6)	1.9(1)	-0.78(7)	-0.2(2)	-0.462(5)	3.9(3)
$\dfrac{\partial \log \tilde{\tau}_{cm}}{\partial \log \rho}$	126.7(7)	-0.4(3)	-0.04(2)	-0.21(7)	-0.42(1)	-0.95(4)
$\dfrac{\partial \log \tilde{\tau}_{rot}}{\partial \log \rho}$	107.9(6)	0.16(1)	-0.7(2)	0.2(2)	0.10(9)	0.5(3)

The variation of the diffusion coefficient and relaxation time along isomorphs must be zero. Since the isomorph theory is approximate, the variations are close to zero. The molecular force method generates better state points in ASD model compared to atomic force and torque methods (Table 3.1). Both atomic and molecular force methods are rather more accurate than the torque method in the IPL model (Table 3.2). In contrast, the torque method identifies better results in the OTP model (see Figure 3.20).

3.7   Structure

In the previous section, we investigated how dynamical properties behave through the state points calculated by new force methods. Besides, it has been shown that the structure of molecular systems should remain invariant along isomorphs produced by configurational adiabats and DIC method in ref. [44]. Therefore, we measure the radial distribution function (rdf) as a function of reduced displacement at state points created by atomic, molecular force and torque methods in ASD, IPL and OTP. Figure 3.21 indicates that the structure of three molecular models is invariant along isomorphs created via force methods.
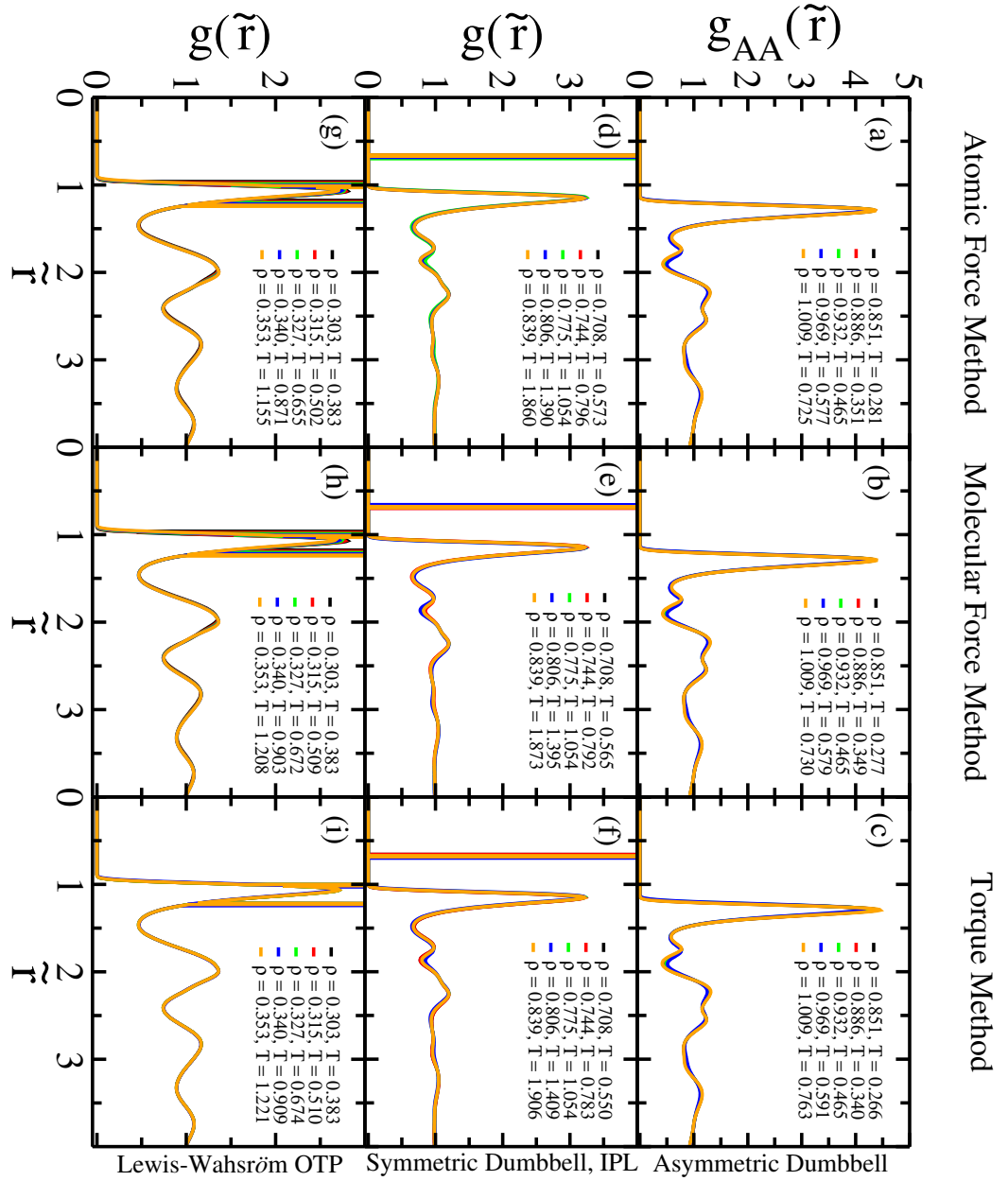
Figure 3.21: The structure of three models along force methods. (a), (b), (c) the radial distribution function in reduced units of ASD along atomic, molecular and torque methods. The reference point is $(\rho, T) = (0.932, 0.465)$. (d), (e), (f) the similar structural property at state points predicted by same methods in IPL model. The reference point is $(\rho, T) = (0.775, 1.054)$. (g), (h), (i) *rdf* of OTP model in reduced units. The reference point is $(\rho, T) = (0.303, 0.383)$.

Chapter 4

Generating Isomorph in a Large Molecular Liquid

In this chapter, we test the force-based methods to identify isomorphs in long flexible Lennard-Jones chains (LJC). In addition to the atomic, molecular and torque methods, we consider another force-based method, named segmental force to create isomorph in the LJC model.

4.1 Introduction

As discussed in chapter 3, isomorphs can be created by newly developed force methods in most or all small molecular systems. Using these methods is beneficial because only a single configuration is sufficient to generate isomorphs. Force methods are also expected to predict isomorphs in real liquids, i.e. the former glass liquids which obey the power-law density scaling and polymers are considered as a large part of real liquids which obey this scaling. In 2014 Veldhorst *et al.* confirmed the isomorphs existence in flexible Lennard-Jones chains (LJC) with rigid bonds [50]. It was found that reduced units dynamics and intermolecular structure of the LJC model have a good collapse at state points generated by configurational adiabats (see Figure 2.5). On the other hand, not all of the structural properties of the LJC model are necessarily invariant, e.g. the intramolecular structures are not constant along isomorph. Since the bond lengths are constant at different densities, they do not remain invariant in reduced units.

LJC model is made of sets Lennard-Jones particles connected by either rigid bonds or springs. Since this model is a simple coarse-grained model of polymers and alkanes, it was first used to study the properties of polymeric

liquids by Grest and Kremer [72–74]. The chain model is more complicated than the simple atomic and small molecular models. Because of the long entangled chain, the particles have to move in specific ways in which the monomers are supposed not to cut each other. The particles represent groups of atoms, like the CH_n unit in alkane or monomers in a polymer.

Here, the LJC model used in simulation consists of 10 beads connected via rigid bonds and represented as a model of viscous polymer melts close to the glass transition [75–78]. Even though one segment is considered as several monomers, a chain of ten beads can barely be called a polymer in the chemical or physical sense. The reason for simulating such short chains is that one is usually interested in the viscous liquid's equilibrium properties. Increasing the chain length enhances the equilibration time dramatically and increases the viscosity, so there is always a trade-off to be done [79, 80].

Since the LJC model has been shown to obey the power law density scaling [81], and Rosenfeld's excess entropy scaling [81–84], it would be an appropriate model to test the new isomorph approaches. Therefore, the equations 3.4 and 3.9 are used to generate isomorph in the (LJC) model in this chapter.

4.2   Simulation Details

Particles in different molecules and non-bonded particles interact via the standard LJ potential, cutting and shifting the forces at 2.5σ. We simulated 1000 chains in a cubic bounding box considering periodic boundary conditions in the NVT ensemble using a Nosé-Hoover thermostat. The time step we used was $t = 0.0025$. All particles were the same type. The potential parameters and the bond lengths were set as unity $\sigma = 1, \epsilon = 1, l = 1\sigma$.

The bonds remain rigid during the simulation [18] using the constraint dynamics, and the forces are from the non-bonded particle pairs interactions. The external force preserves the relative velocities of bonded particles zero along the bond directions, using the Gauss principle of least constraint [85]. We used constraint algorithm developed by Toxværd *et al.* [86] in which the energy and time symmetry preserve.

The correlations between the virial and potential energy of the LJC model is less than correlations of the liquids considered as R-simple liquids [42], and less than the standard single component Lennard-Jones (SCLJ) liquid [41]. The correlation coefficient is estimated about $R = 0.861$ in Figure 4.1. The slope γ of the U-W fluctuations is also considerably different from the SCLJ liquid value, which is $4 < \gamma < 6.5$ [41]. But it is still in the range of the γ value for the OTP model, which has $6.3 < \gamma < 8.0$ [54]. Although the correlation is not sufficiently strong, the dynamics and structure remain constant on isomorphs generated along configurational adiabats and DIC method [50].
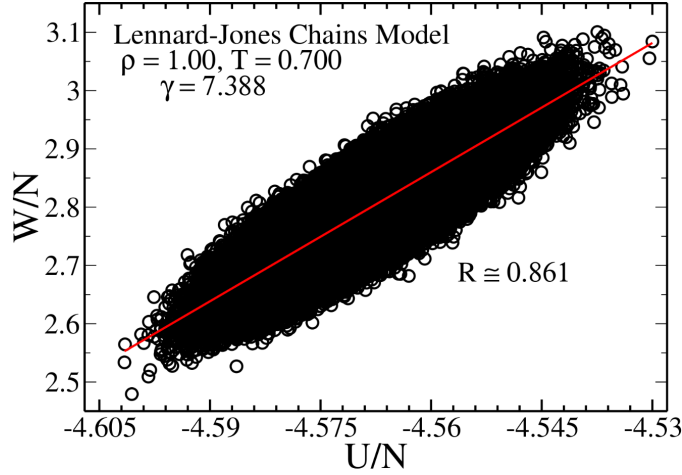
Figure 4.1: Correlations between the virial and potential energy in the LJC model with ten segments at the state point ($\rho = 1.00, T = 0.700$). The correlation coefficient and slope γ are obtained by linear regression to be $R = 0.861$ and $\gamma = 7.388$.

4.3 Segmental Force Method

In addition to the atomic and molecular forces and torque methods, we introduce the segmental force to identify isomorph in the LJC model. There are ten segments in each molecule of the LJC model, so the summation of segment forces gives the molecular force,

$$\mathbf{F}_{Mol} = \sum_{j=1}^{9} \mathbf{F}_{Seg,j}, \tag{4.1}$$

and by using the,

$$\mathbf{F}_{Seg,j} = \frac{1}{d_j}\mathbf{F}_j + \frac{1}{d_{j+1}}\mathbf{F}_{j+1}, \tag{4.2}$$

where d_j and d_{j+1} are the number of bonds in which particle *jth* and $(j+1)th$ are involved sequentially, one can calculate segmental force. In the previous chapter, the molecular force method generates better isomorphic state points in small molecular systems at rather large density changes.

4.4 Testing the Force Methods on LJC Model

In this section, we generate curves on constant reduced forces and torque for the Lennard-Jones chains (LJC) model. The same densities of the ref. [50] are considered to compare the new force methods results with the old-fashioned constant excess entropy results (configurational adiabats). We start from state point $(\rho_1, T_1) = (1.00, 0.700)$ then scale the configuration to

49

densities to $0.96, 1.04, 1.08, 1.12$. Density changes spread over 17%. For $T = 0.700$, the lowest density is determined $\rho = 0.96$ before the pressure reaches negative values and phase transition occurs and highest density is considered $\rho = 1.20$ to prevent the crystallization. New temperatures are obtained by using equations 3.4, 3.9, 4.1. Similar dynamical quantities from Figure 3.15 are considered to check if the dynamics are invariant along reduced invariant force curves or not. We probe the dynamics through the four methods, atomic, molecular, segmental forces and torque methods in Figure 4.2. However, they work very well in the small stiff molecules; they do not predict isomorphic state points in the LJC model. The larger molecular models, like polymers, inherit the intramolecular degrees of freedom which impact the dynamics and structure.

In contrast, the structure of the LJC, measured by the radial distribution function(rdf), have good collapses. We measure rdf along predicted state points via three forces and torque methods. In Figure 4.3 we have plotted four structural quantities in reduced units: the total rdf of segments (a, e, i, m), the segmental intermolecular rdf (b, f, j, n) and segmental intramolecular rdf (c, g, k, o) and center-of-mass rdf (d, h, l, p). As mentioned, the bond lengths do not remain constant in reduced units, so the total segmental distribution function is not invariant, mostly around $\tilde{r} = 1$ due to the nearest neighbour in the molecules. This is also seen in inter-molecular and intramolecular distribution. The intermolecular structure is more invariant than the intramolecular contributions. On the other hand, the radial distribution of center-of-mass is not dependent on state points and represents the nice collapse through all methods.

Besides, we compare the dynamics along the isotherm, configurational adiabats [50], direct isomorph check (DIC) and force methods by plotting the relaxation times obtained from the self intermediate scattering function and orientational autocorrelation function of end-to-end vectors in Figure 4.2. The reduced translational and rotational relaxation times are approximately constant along configurational adiabats and DIC method, whereas they change along the new methods. For comparison, we incorporated the relaxation times of isotherm in Figure 4.4. The state points of the isotherm taken from ref. [50]. However, the density changes about 11%, the dynamics change a lot compared to the isomorphs in which density changes about 25%. The relaxation times are invariant along configurational adiabats and direct isomorph check method and they vary along force methods (Figure 4.4). Nevertheless, the force methods predict better results in a small density changes, 8%, in LJC model (See Appendix B).
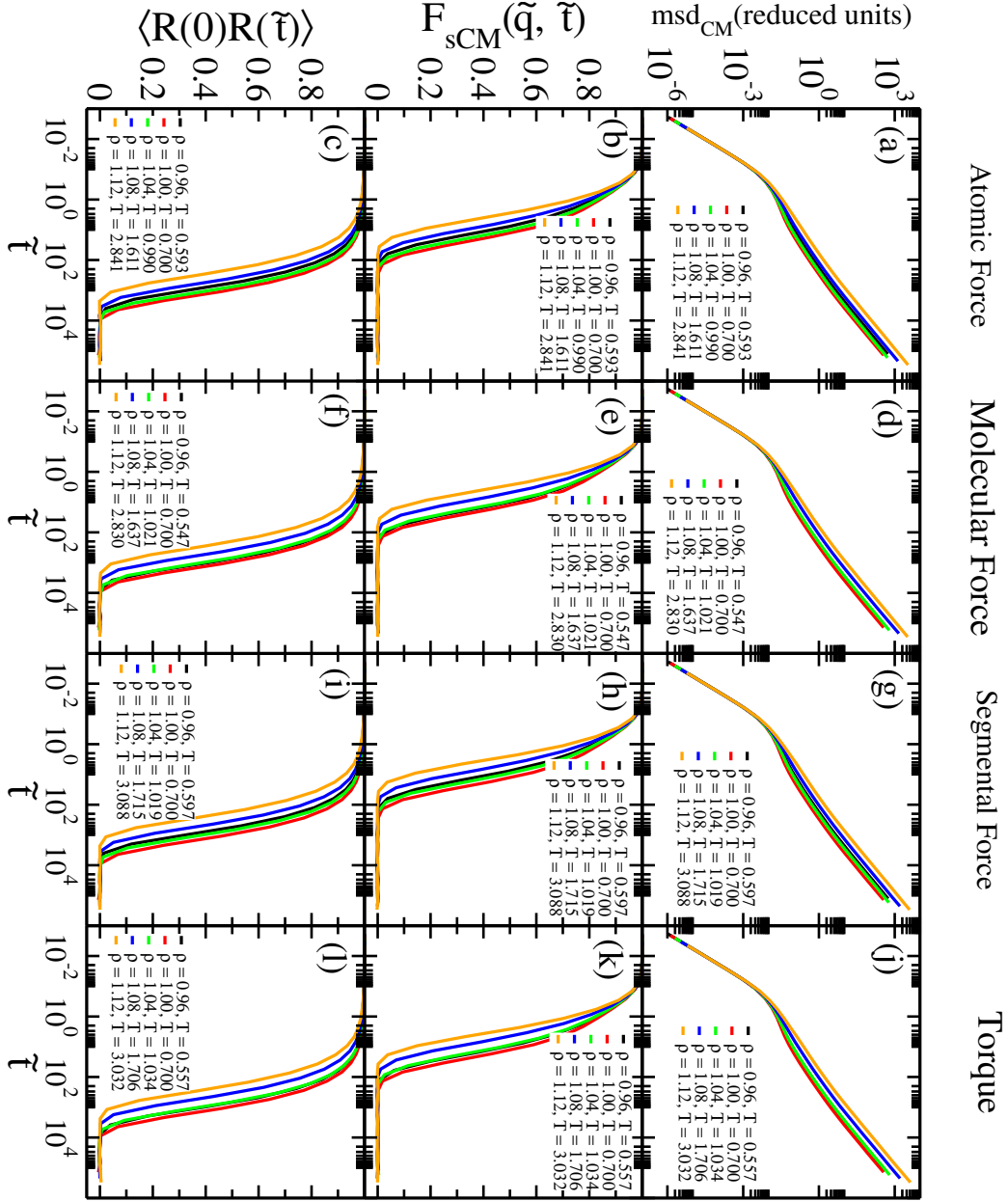
Figure 4.2: Mean square displacement, incoherent intermediate function and orientational autocorrelation function of end-to-end vector in reduced units on invariant reduced forces and torques. Reference point is taken from ref. [50], $(\rho_1, T_1) = (1.00, 0.700)$. The wave vector is kept constant in reduced units $\tilde{q} = 7.09\rho^{1/3}$. The dynamics are not invariant along predicted state points via force methods in this large molecular model.
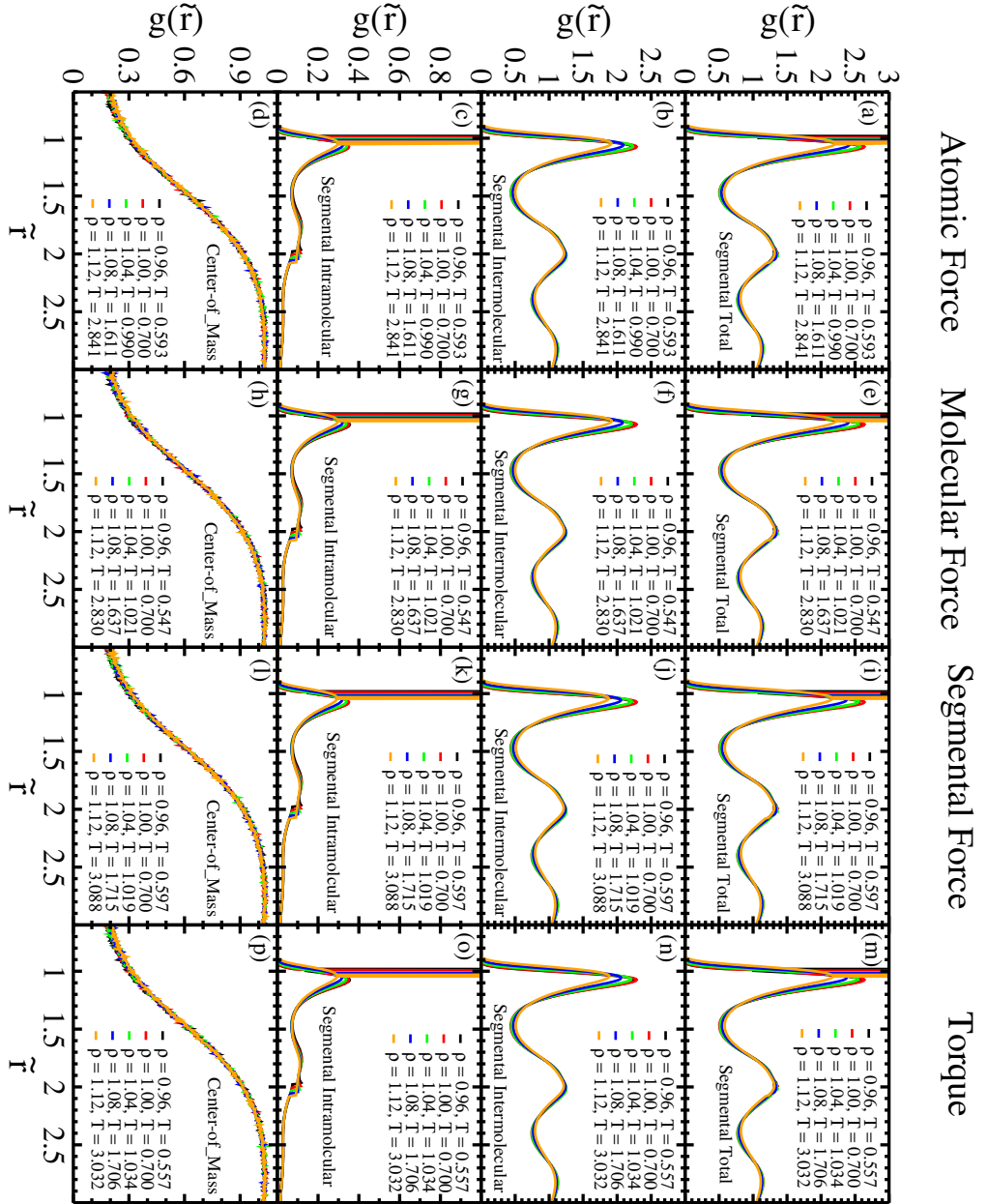
Figure 4.3: Comparing four different radial distribution functions (rdf) through force methods. The reference point is , $(\rho_1, T_1 = 1.00, 0.700)$. (a, e, i, m) The total segmental distribution function in reduced units. (b, f, j, n) The contributions of particle pairs in different chains as intermolecular segmental distribution in reduced units. (c, g, k, o) The reduced intramolecular segmental distribution function due to the contributions from the pairs in the same chain. (d, h, l, p) The radial distribution function of center-of-mass in reduced units.
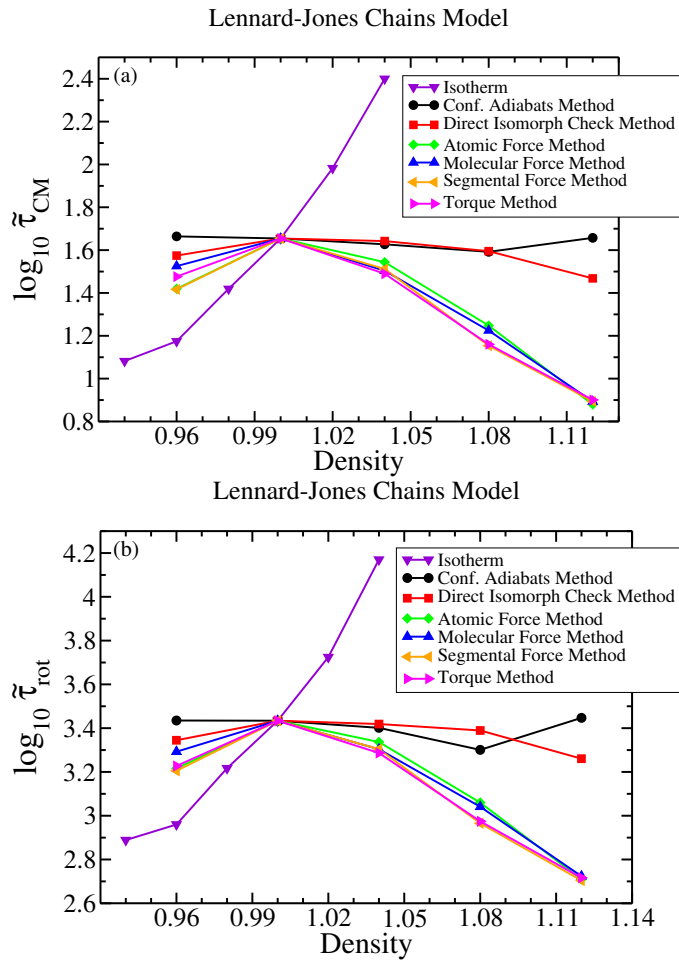
Figure 4.4: Comparing the translational (a) and rotational (b) relaxation time in reduced units along the isotherm and isomorphs methods. The relaxation times hold more invariant along the constant excess entropy and DIC methods, and they are entirely different along the forces methods; however, they fail more along the isotherm.

Chapter 5

Pseudoisomorphs in Small Molecular Models

In this chapter, we test the force methods on small molecular models with harmonic spring bonds. Isomorphs do not exist in harmonic models since they are not strongly correlating. However, there still are hidden scale invariance curves that behave like isomorphs, so-called "pseudoisomorphs". We investigate the force methods to identify pseudoisomorphs in small stiff molecular models, e.g. ASD, IPL and OTP models.

5.1 Introduction

Four newly developed isomorph methods have been tested for the R-simple liquids, e.g. the atomic [1] and molecular models (see chapter 3). Although they all work very well for the atomic [1] and small stiff molecular models, the new force methods do not trace the isomorph in long flexible Lenard-Jones chains at relatively large density change (see chapter 4). In recent papers, [2, 50], it was presented that the models with harmonic bonds do not have isomorph along the configurational adiabats. Besides, the slope γ and the correlation coefficient drop dramatically in the spring models, so they are not assumed to have isomorphs. The small molecules (ASD, IPL, OTP) are considered with spring harmonic potential, given by,

$$v_{ij}(r_{ij}) = -0.5k(r_{ij} - r_0)^2, \tag{5.1}$$

where $k = 3000$ is the spring constant for all models and r_0 is the bond length where the bond energy is zero. The non-bonded molecules interact via Lennard-Jones potential. The same potential parameters explained in

chapter 3 for each model are set here, and the bond lengths are similar. We use the same density from chapter 3 for ASD, IPL and OTP models because the dynamics and the structure of spring bonded models are not significantly different from constrained models. Harmonic bonds are often used in molecular models, which are beneficial since they are faster in the calculation and scaled easier than constraint bonds. The correlation coefficient for harmonic ASD and OTP are about $R = 0.579, 0, 204$ respectively (Figure 5.1) which are not comparable with the corresponding values obtained in constrained model (see Figure 3.6). The IPL system with harmonic interactions still has a robust U-W correlation, $R = 0.878$, but the slope $\gamma = 5.463$ decreases (see Figure 5.2). The correlation coefficient and linear regression slope diminish considerably by substituting the harmonic bonds to rigid bonds in the models due to the springs' fast vibration.
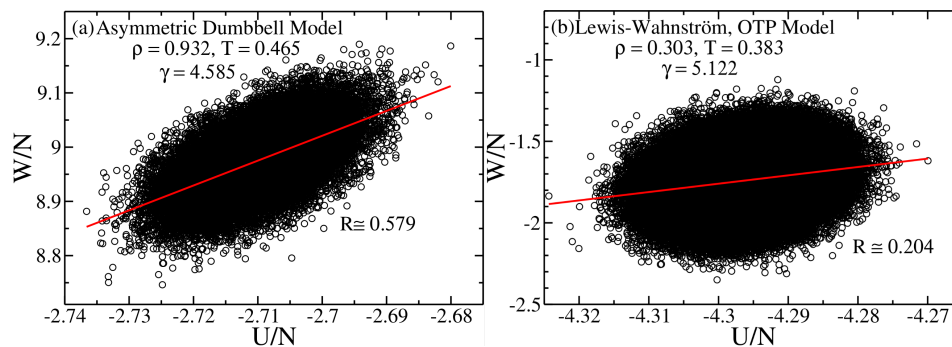
Figure 5.1: The potential energy and virial fluctuations for two models ASD and OTP with harmonic spring intermolecular interactions. (a) The correlation coefficient ($R = 0.579$) and linear regression slope $\gamma = 4.585$ at the state point taken from reference [54] of ASD with spring bonds. Both values drop significantly in compared to ASD with constraint bonds $R = 0.960$, $\gamma = 5.69$. (b) The similar quantities correlations for OTP, including the harmonic bonds. The correlation coefficient for this model also shrink a lot, $R = 0.204$, whereas the constrained OTP model are more strongly correlating $R = 0.894$ and γ declines from 7.953 to 5.122.

Since the springs length are similar to rigid bonds, the dynamics and the intermolecular structure behave like the dynamics and relevant structure of models with rigid bonds. But due to the different spring length distribution, the intramolecular structure is not the same, where the bond's peak is widen in Figure 5.3(b).

Figure 5.4 shows the mean square displacement, incoherent intermediate scattering function and orientational autocorrelation function of the end-to-end vector of ASD to demonstrate the effects of the bond type on the dynamics. The dynamics are vividly faster for a harmonic ASD model. However the bond type have a slight impact on the dynamics, it has a great effect on correlation and consequently on identifying isomorph.

Olsen et al. [2] found that the ASD model dynamics are far from be-
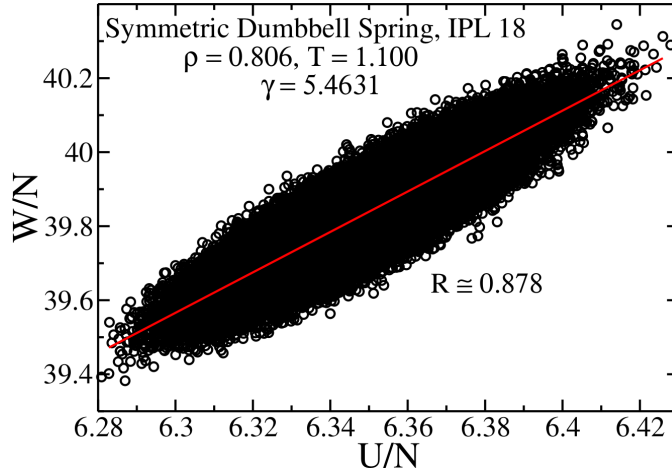
Figure 5.2: The potential energy and virial fluctuations for IPL model consists of harmonic spring interamolecular interactions. It considered as a highly correlated system since $R = 0.878$. The state point taken from ref. [54]. But the slope $\gamma = 5.464$ diminishes comparing with the constraint model in Figure 3.6 (a).
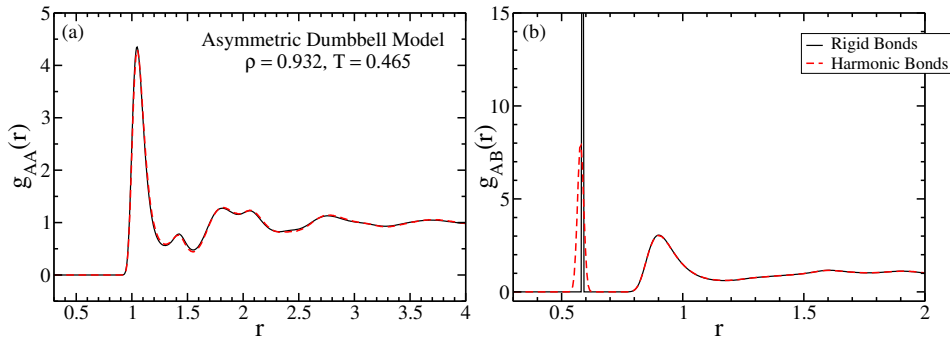
Figure 5.3: Comparing the radial distribution function against r for A-atoms from different asymmetric dumbbell molecules and AB-atoms in each molecules. Black curves indicated the rdf of rigid bonds and the red curve shows a similar quantity for spring bonds. The intermolecular structure (a) is the same, whereas the intramolecular structure (b) differs slightly at the first peak.

ing invariant along the configurational adiabat. In Figure 5.5 we reproduce the dynamical quantities along the configuration adiabats [2] which implies clearly that the models with spring do not have isomorph. Although the dynamics are constant along configurational adiabats in IPL and OTP model with intramolecular constraint bonds, they are not invariant in corresponding harmonic models (See Appendix C).

On the other hand in ref. [2] Olsen et al. traced out the invariant dynamics along pseudoisomorph via the empirical density scaling in the ASD model and identify pseudoisomorph in the same model via quenching the systems to their inherent state. The strong correlation of the systems
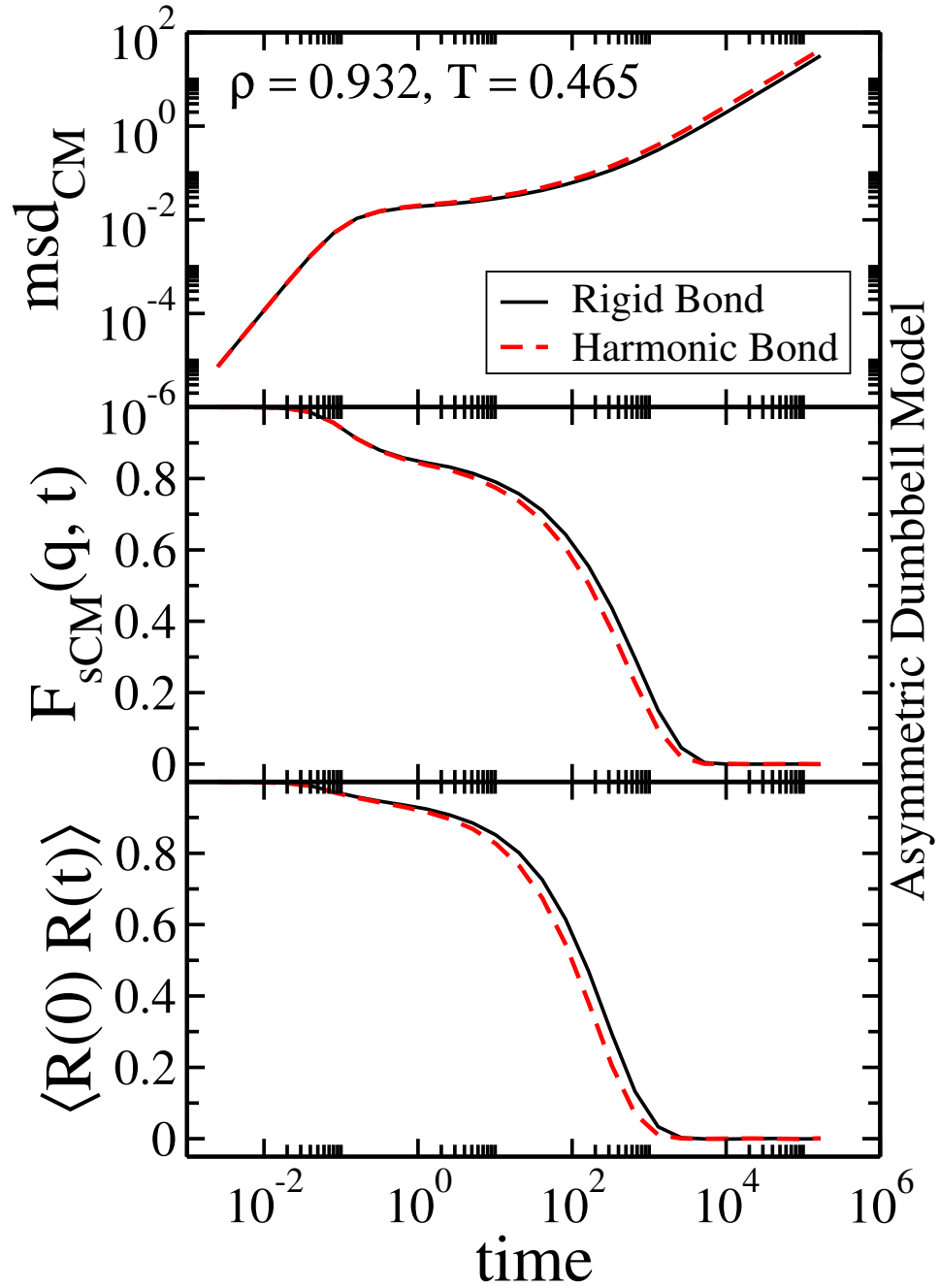
Figure 5.4: Comparing the dynamics of the ASD model with two different bond types. We measure the MSD and intermediate scattering function and orientational autocorrelation function at density $\rho = 0.932$. The springs cause dynamics to be slightly faster.

Figure 5.5: The mean square displacement, incoherent intermediate scattering function, orientational autocorrelation function in reduced units evaluated along the configurational adiabate in ASD model. The state points are taken from ref. [2].

Pseudoisomorph

Figure 5.6: Mean square displacement, incoherent intermediate scattering function and orientational autocorrelation function of end-to-end vector of the ASD model evaluated along the pseudoisomorph at state points are taken from ref. [2].

breaks down due to the vibrational degrees of freedom of springs. So they generate pseudoisomorphs by eliminating these unscaled degrees of freedom and quench the system to an inherent state which is the minimum local potential energy state. The pseudoisomorph has been generated by requiring scale invariance of the inherent-structure low-frequency part of the vibrational spectrum. Results in Figure 5.6 are reproduced from ref. [2] indicates the pseudoisomorph generated with this method. This gives us an idea to test the forces methods to create the pseudoisomorph in models with spring harmonic bonds and, comparing the predicted state points to those reported by Olsen in the Figure 5.6.

As mentioned the dynamical properties of the models with spring are not much affected by harmonic bonds. Moreover, the force is invariant in reduced units in harmonic models, so it is expected the force methods work very well also in harmonic models. In order to test invariant dynamics along forces methods, similar dynamical properties from Figure 5.6 are considered in next sections.

5.2 Pseudoisomorph at High Densities

We now pick the ASD model with 5000 molecules to investigate the dynamics along the invariant reduced-forces. Three methods i.e. atomic and center-of-mass forces and torque methods are chosen to predict the new temperatures and we only need one equilibrium configuration.

In practice, we used 195 configurations to estimate the stability of the procedure which are scaled via center-of-mass (CM) scaling to higher and lower density from reference point $(\rho_1, T_1) = (0.932, 0.465)$. In CM scaling, the position of center-of-mass remain invariant in reduced units at different densities.

Figure 5.7 shows the harmonic bonds cause the force methods do not provide the appropriate state points. There are not any significant collapses in dynamics properties from any of the methods. Besides, the predicted state points are quite different from the pseudoisomorphic points in Figure 5.6. The molecular force method works better due to ignoring stretching intramolecular degrees of freedom in the center of mass force calculation. Apart from the molecular force and torque which are still strongly correlated, $R_f f = 0.975$, (see Figure 5.8(b, c)), the atomic forces correlation declines due to the intramolecular flexible interactions, $R_f f = 0.850$ (see Figure 5.8).

As expected, the harmonic spring force leads to the poor invariant dynamics along the atomic force method, predicted T_2 by the molecular force method should result in better invariance. Figure 5.9 demonstrates that the statistical uncertainty of each atom temperature $T_2^{(i)}$, via atomic force method prediction compared to each molecule's temperature predicted via molecular force and torque methods at highest density $\rho = 1.060$.
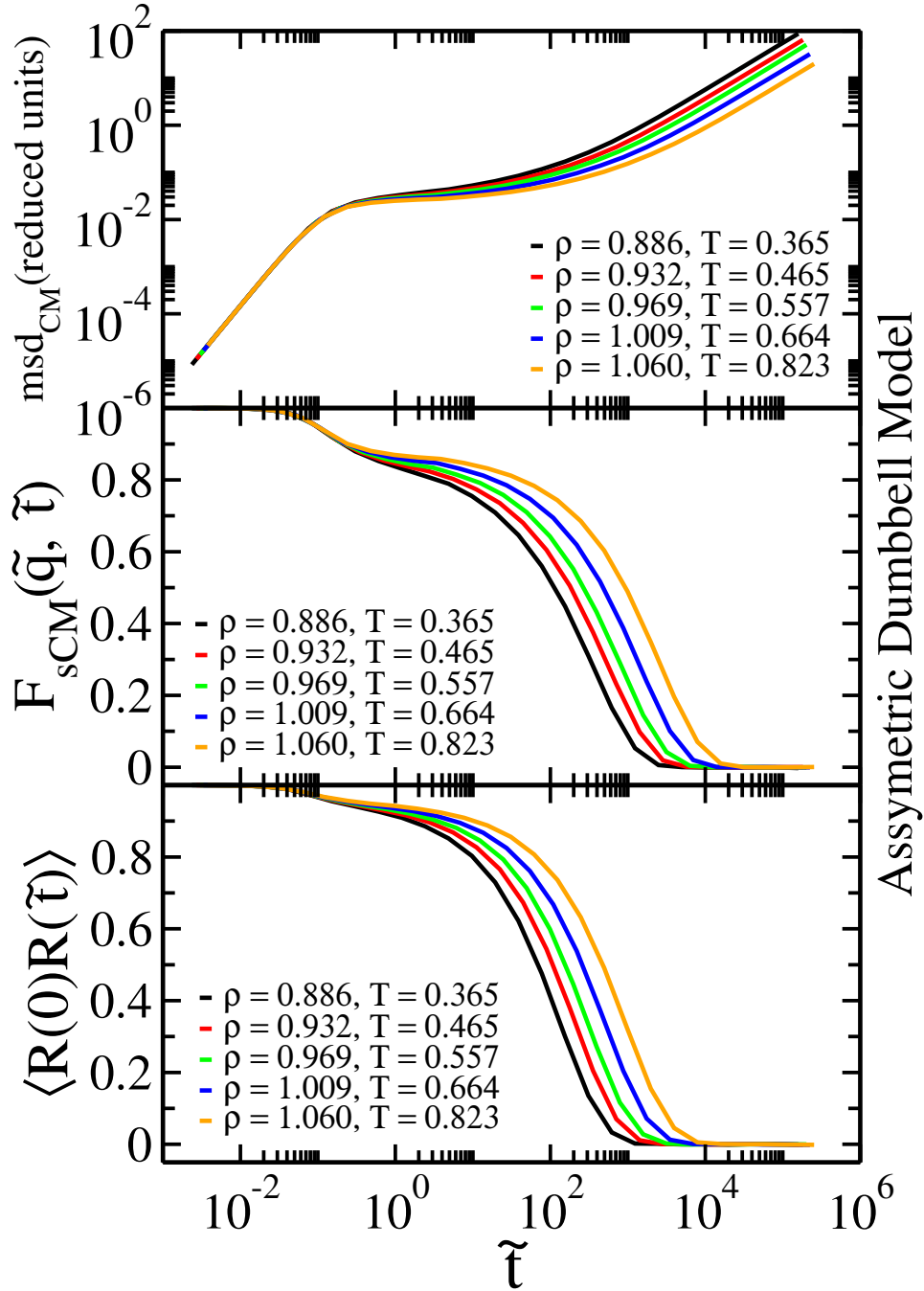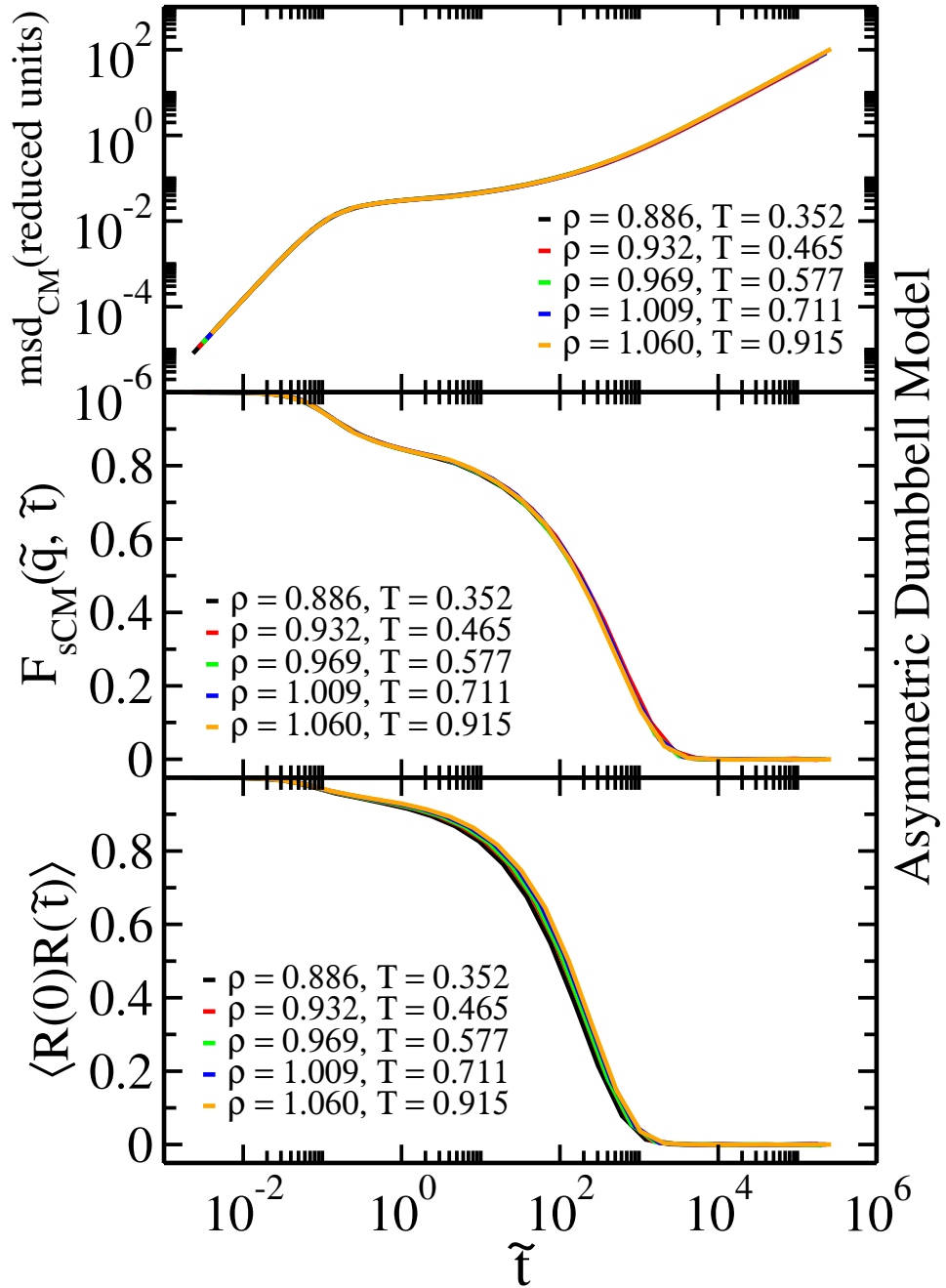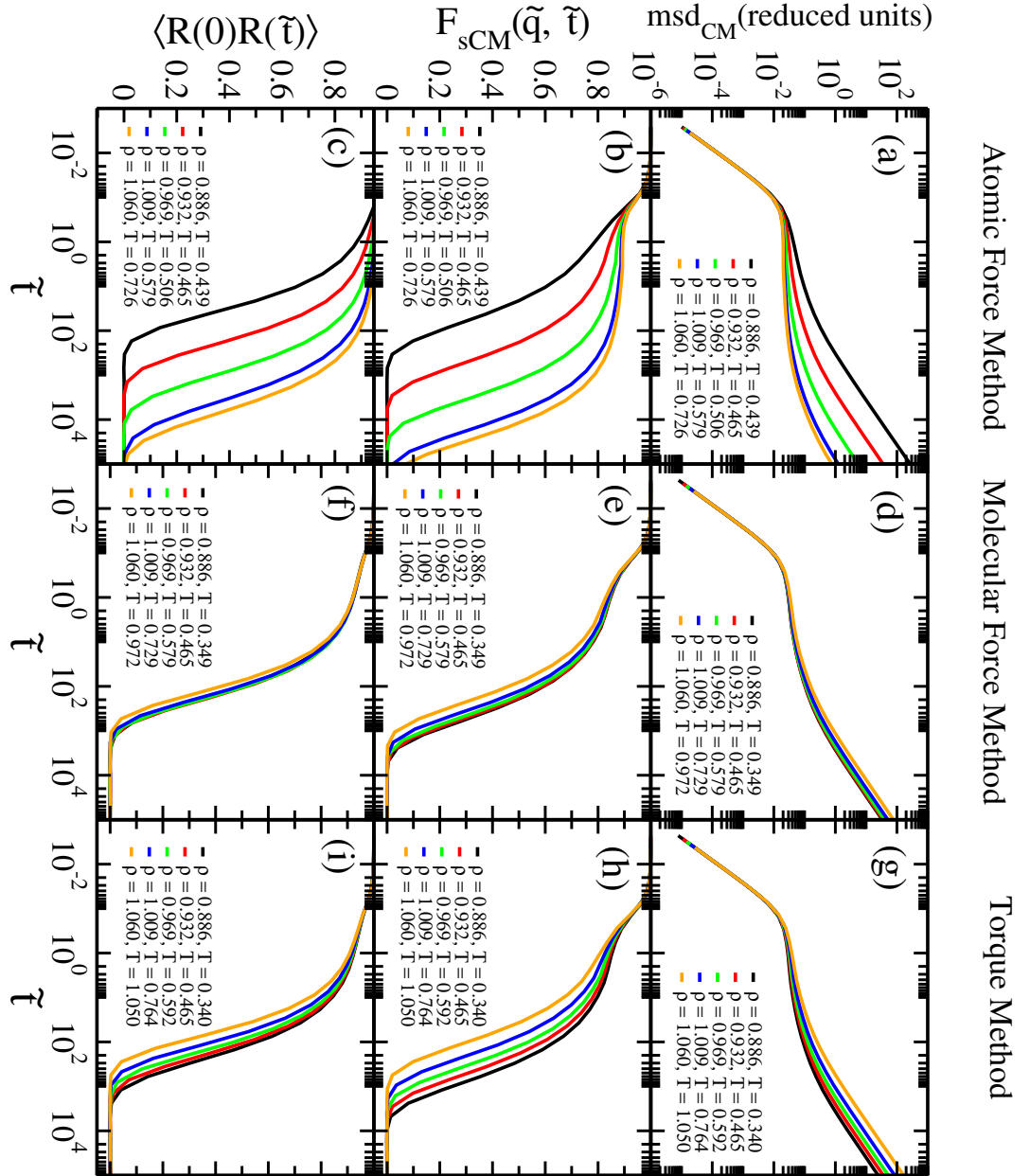
Figure 5.7: Mean square displacement, incoherent intermediate scattering function and orientational autocorrelation function of end-to-end vector of the ASD model with harmonic spring bonds evaluated along invariant forces through the CM scaling in reduced units. Reference point is $(\rho_1, T_1) = (0.932, 0.465)$ taken from ref. [2]. The density changes above 19%
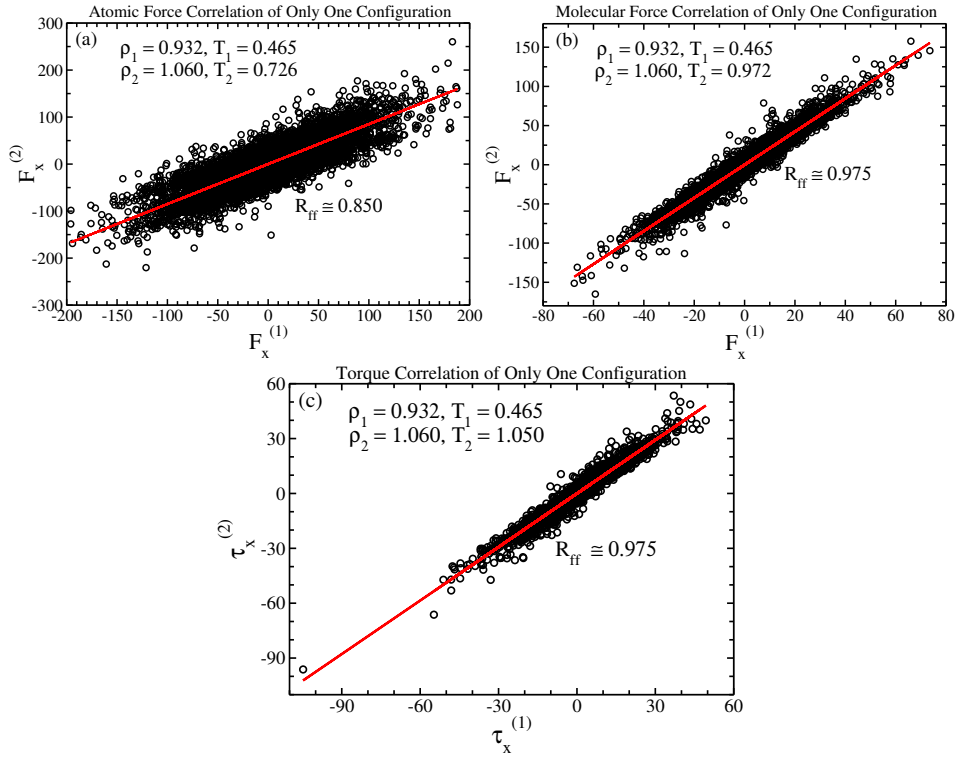
Figure 5.8: Correlation of atomic force (a) molecular force (b) and torque (c) of molecules. One configuration is taken from equilibrium simulation at $(\rho_1, T_1) = (0.932, 0.465)$. Then the temperature at $\rho_2 = 1.060$ is predicted by using equations 3.4, 3.9.
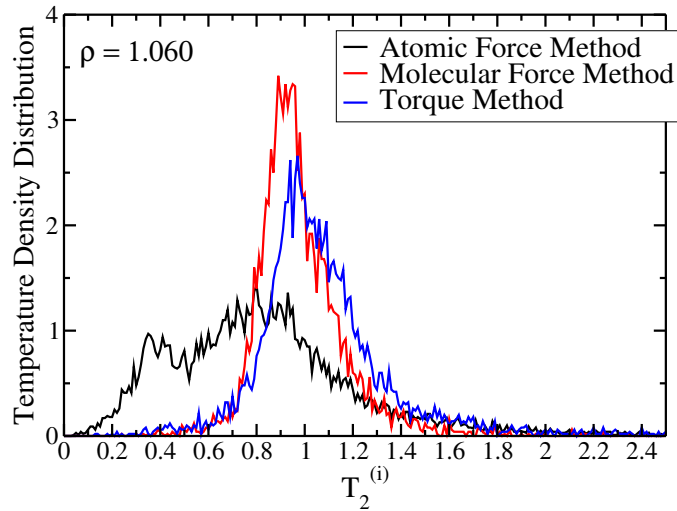
Figure 5.9: Comparing the results of temperature of each particle (through atomic force method) and each molecule (through the molecular force and torque methods), which is seen to be the sharpest for the molecular-force method.

It is evident that the springs cause the atomic force method breaks down and this gives the idea to calculate the atomic force by removing the harmonic contribution. In Figure 5.10 we measure the intermediate scattering function along the invariant atomic force in the absence of spring forces' contribution $F_s = k(r_{ij} - r_0)$ by set the spring stiffness $k = 0$, and temperature produces via the equation 3.4. The results get better but there is not still any collapse.
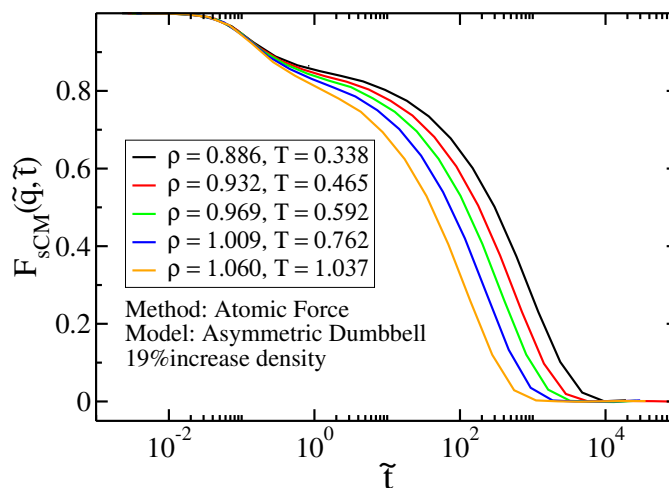
Figure 5.10: Self incoherent intermediate scattering function in reduced units along the state points predicted via atomic force method without spring force contribution by applying the CM scaling. Densities are taken from Figure 5.7. The dynamics prediction improves in comparison with Figure 5.7 (a, b, c) but still far from invariance.

5.2.1 Center-of-Mass Scaling vs Atomic Scaling

As mentioned, the results reported above are achieved using CM scaling. In the following, we test the effect of using instead atomic scaling, where the atomic force correlation get worse when we scale from $\rho_1 = 0.932$ to $\rho_2 = 1.060$ (see Figure 5.11 (a)). Using the atomic scaling allows atoms move freely, which achieve the poor atomic force correlation. However, the molecular force correlation improves because of ignoring the spring force (see Figure 5.11 (b)) and torque has the approximate same correlation in compared to using the CM scaling in Figure 5.8.

In Table 5.1, we use the forces and torque methods to find the new temperature in ASD model. The predicted temperatures are quite different from pseudoisomorphic points predicted by Olsen after quenching the system (Figure 5.6) and also they are different from results in Figure 5.7.
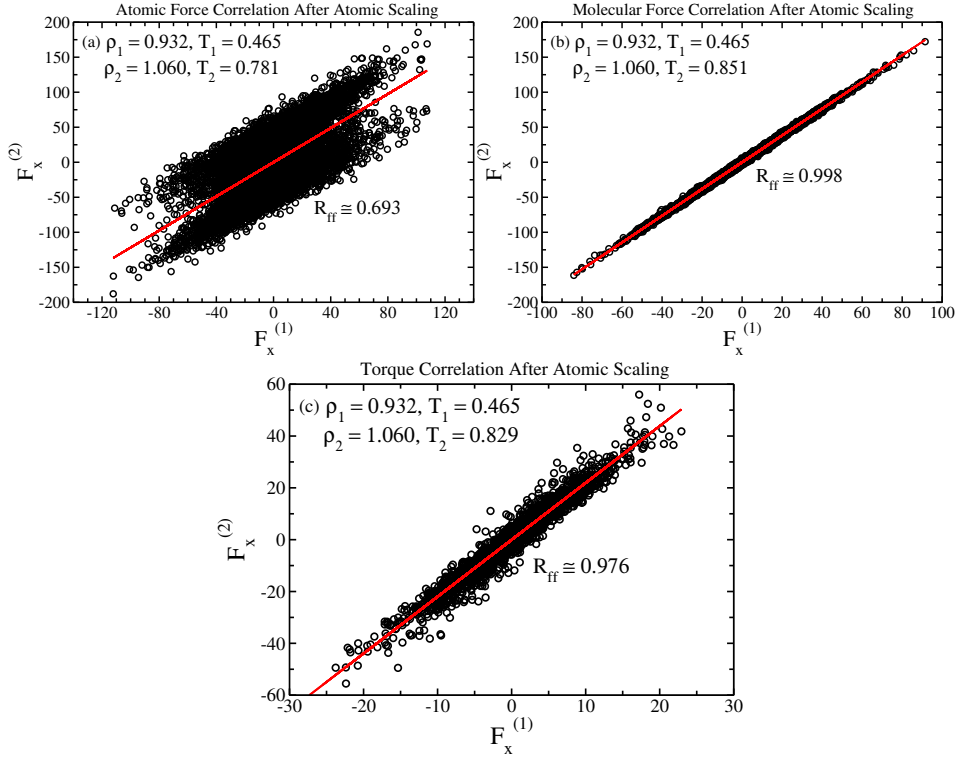
Figure 5.11: Correlation of atomic force (a) molecular force (b) and torque (c) after using the atomic scaling method. One configuration is taken from equilibrium simulation at $(\rho_1, T_1) = (0.932, 0.465)$. Then we scale the configuration at $\rho_2 = 1.060$ via atomic scaling method. Comparing the correlation with Figure 5.8 in which we used the CM scaling indicates the atomic force correlation decreases and splits into two parts. While the molecular force correlation improves and torque correlation dose not change much.

Table 5.1: Calculating the new temperatures via the forces and torque methods on flexible ASD model under the atomic scaling method instead of CM scaling. The configurations are taken from equilibrium simulation at $(\rho_1, T_1) = (0.932, 0.465)$. Second column show the pseudoisomorphic points from ref. [2]; third, fourth and fifth columns show the temperatures predicted by atomic, molecular force method and torque method.

Density	T(Pseudoisomorph)	$T(F_{Atomic})$	$T(F_{Mol})$	T(Torque)
0.886	0.352	0.525	0.363	0.368
0.932	0.465	0.465	0.465	0.465
0.969	0.577	0.515	0.560	0.555
1.009	0.711	0.622	0.677	0.666
1.060	0.915	0.781	0.851	0.829

5.3   What's the problem
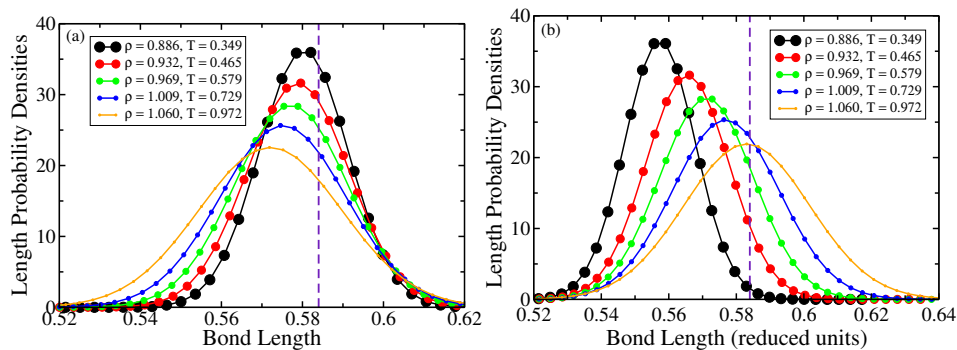
Figure 5.12: Distribution of bonds length along a molecular force method around the reference length of the spring (purple dashed line) (a); The Figure demonstrates that bonds are compressed when the density increases from $\rho_1 = 0.932$. This affects not just the intramolecular, but also the intermolecular forces. The distribution of bonds length in reduced units indicates that the reduced bonds length are compressed and shifted a lot by decreasing the density (b).

The force methods are assumed to generate pseudoisomorphic points in flexible molecules at high densities regardless the spring bonds. It is revealed that the bonds are compressed when the density is increased whereas in reduced units the distribution shifts by decreasing the density. Figure 5.12 shows the average (a) bond lengths and (b) reduced bond lengths distribution for state points generated by the molecular force method. Scaling the system at higher densities rises the intramolecular interaction and affects the force methods predict the inconsistent temperatures, see Figure5.7. Now to organize the scale and unscaled configuration to have the same distribution of spring length, We eliminate the unscaled degrees of freedom through quenching the system and minimizing the potential energy surface.

5.4   The Local Minima of PES

Considering the $3N$ dimensional vector denoted as $\mathbf{R}$, the potential energy surface (PES) is described as the function of these configuration space $U(\mathbf{R})$. Any configuration R can be mapped to its "inherent structure", which corresponds to the local minima. Since the potential energy surface increase by any small displacement, there is a local minima surrounded by uphills. Any steps reach uphills around this minima. The gradient of potential energy corresponded the equilibrium configuration, vanishes, $\nabla U = 0$ at local minima, consequently all forces get zero value. There can find several local minima on PES, but there is only one lowest energy, termed global minimum. Since finding the global minimum of a high-dimension PES in liquids requires a

great deal of effort and sometimes is impossible, we organize several ways to find the local minimum in the next section.

5.5 Finding the Local Minima

For simplicity, in the ASD model composed of two particle connected with flexible bonds, we consider the variation potential by changing the bond length, $U(l)$. If the potential energy surface is only considered as a function of bond length, one can find the minimum of the potential by keeping fixed the center-of-mass of molecule position and bond length orientational direction. Hence so the first condition is given,

$$d\mathbf{R}_{CM,k} = 0, \tag{5.2}$$

where the center-of-mass position of *kth* molecule remains fixed and the new bond length is reached without changing the bond orientational direction,

$$\mathbf{R}'_{ij} = \mathbf{R}_{ij} + l_k \hat{\mathbf{l}}_k, \tag{5.3}$$

in which the distance between two atoms $\mathbf{R}'_{ij}$ in each molecules changes along the *kth* bond direction $\hat{\mathbf{l}}_k$. On the other hand to change the bonds length, we have,

$$L'_k = L_k + dl_k, \tag{5.4}$$

in which L'_k is the new bond length of *kth* molecule obtained by changing the initial bond length L_k with small dl_k. Developing a function to quench the system to its minimum considering mentioned constraint conditions (equations 5.2, 5.4) requires simple mathematics. Consider each molecule composed of *jth* atom which should move along the *kth* bond direction. The new position of atom ($\mathbf{r}'_\mathbf{j}$) is described by,

$$\begin{cases} \mathbf{r}'_\mathbf{j} = \mathbf{r}_\mathbf{j} + \alpha \mathbf{d}\hat{\mathbf{l}}_\mathbf{k} & j \leq k \\ \mathbf{r}'_\mathbf{j} = \mathbf{r}_\mathbf{j} + \beta \mathbf{d}\hat{\mathbf{l}}_\mathbf{k} & j > k \end{cases} \tag{5.5}$$

in which $\mathbf{d}\hat{\mathbf{l}}_\mathbf{k}$ is unit vector of bond length variation. In regards to equations 5.2, 5.5 to keep fixed the center-of-mass position of molecules,

$$d\mathbf{R}_{CM,k} = \frac{\sum_j m_j d\mathbf{r}_\mathbf{j}}{\sum_j m_j} = 0. \tag{5.6}$$

By substituting equation 5.5 in equation 5.6 we have,

$$\sum_{j=0}^{i} m_j d\mathbf{r}_\mathbf{j} + \sum_{j=i+1}^{N-1} m_j d\mathbf{r}_\mathbf{j} = 0, \tag{5.7}$$

so then,

$$\alpha \mathbf{d}\hat{\mathbf{l}}_{\mathbf{k}} \sum_{j=0}^{i} m_j + \beta \mathbf{d}\hat{\mathbf{l}}_{\mathbf{k}} \sum_{j=i+1}^{N-1} m_j = 0. \tag{5.8}$$

In general one can obtain the α and β relation, which is,

$$\beta = -\frac{\sum\limits_{j=0}^{i} m_j}{\sum\limits_{j=i+1}^{N-1} m_j} \alpha. \tag{5.9}$$

Consider small stiff molecules, like asymmetric dumbbell model, we have two particles (large A, Small B) with different masses ($m_A = 1, m_B = 0.195$), according to the equation 5.9 we have,

$$\beta = -\frac{m_A}{m_B}\alpha. \tag{5.10}$$

In equation 5.5, displacement of atoms A and B in the *kth* molecule is derived by,

$$\begin{pmatrix} \mathbf{dr_{A,k}} \\ \mathbf{dr_{B,k}} \end{pmatrix} = \begin{pmatrix} \alpha \\ -\dfrac{m_A}{m_B}\alpha \end{pmatrix} \times \mathbf{dl_k} \tag{5.11}$$

To calculate α we start from moving the atoms along bonds direction by $\mathbf{dl_k}$,

$$|\mathbf{dl_k}| = |\mathbf{dr_{B,k}} - \mathbf{dr_{A,k}}|, \tag{5.12}$$

In regards to equation 5.11, we have,

$$|\mathbf{dl_k}| = |-\frac{m_A}{m_B}\alpha\mathbf{dl_k} - \alpha\mathbf{dl_k}| \tag{5.13}$$

So the α is obtained,

$$\alpha = \frac{m_B}{m_A + m_B}. \tag{5.14}$$

By substituting α and β in equation 5.11 and considering $\mathbf{dl_k} = dl_k\hat{\mathbf{l}}_{\mathbf{k}}$ we have,

$$\begin{pmatrix} \mathbf{dr_{A,k}} \\ \mathbf{dr_{B,k}} \end{pmatrix} = \begin{pmatrix} \dfrac{m_B}{m_A + m_B} \\ -\dfrac{m_A}{m_A + m_B} \end{pmatrix} \times dl_k\hat{\mathbf{l}}_{\mathbf{k}}. \tag{5.15}$$

We now know how to move the particle to keep the center-of-mass of molecules and orientational bond direction fixed by a scalar function (i.e. equation 5.15) and find the minimum potential by 'scipy.optimize.minimize()' function implementing Broyden–Fletcher–Goldfarb–Shanno (BFGS) algorithm [34]. The same calculation can be easily used for symmetric IPL dumbbell molecule composed two atoms with identical mass. Both scaling approach, center-of-mass and atomic scaling are applied to create pseudoisomorphs via force and torque methods after quenching the system.

Increasing the density causes the bond length to shift from length measured at equilibrium. Figure 5.13 demonstrates that the bonds length distribution of unscaled configuration at $\rho = 0.932$ before minimization (black curve) and indicates how the bonds compressed by scaling to highest density $\rho = 1.060$ (red curve) whereas they differ from their equilibrium measures (green curve). This difference vanishes (blue curve) by quenching the system via the described function. Since the bonds length of unscaled configuration at $\rho = 0.932$ avoid shifting (see Figure 5.12), they remain unchanged after minimization (orange curve). In this section we defined the function which used the scalar dl to find the local minimum while quenching the system via the function based on the vector dl is represented in section 5.9
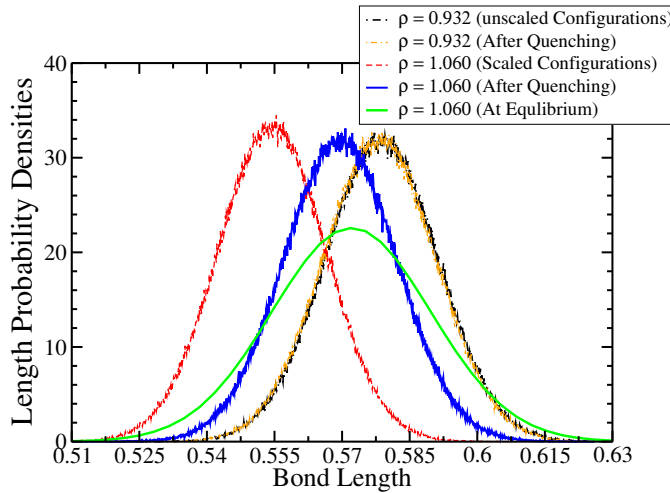
Figure 5.13: The bond length distribution of one unscaled configuration at $\rho = 0.932$ before minimization (black) shifts by scaling to higher density $\rho = 1.060$ whereas it should correspond to the lengths at equilibrium (green). The distribution of lengths for unscaled configuration at $\rho = 0.932$ is not affected by minimization (orange curve). CM scaling is used. Quenching the configuration at relevant density gives the better distribution (blue) consistent with the equilibrium bond lengths.

5.6 Forces Correlation After Quenching

Quenching the configuration to minimum state improves the correlation of forces and torque. In this effort, we take a configuration from equilibrium simulation at reference point $(\rho_1, T_1) = (0.932, 0.465)$, then use the scalar function (equation 5.15) to quench the configuration via BFGS method. After minimization, we scale the configuration at a new density and do the same minimization process. We now calculate the forces and torque of unscaled and scaled configuration at two different density to predict the temperature via equations 3.4, 3.9 after quenching.

We implement two different scaling approaches atomic (AS) and center-of-mass scaling (CMS). In Figure 5.14, all three quantities correlation via atomic and CM scaling boost in comparison with relevant correlations before minimization (5.8). Atomic force correlation after scaling the system by CM scaling is slightly better than correlation in case of atomic scaling (Figure 5.14(a, b)). On the other hand, the molecular force has the same correlation via both scaling approaches (Figure 5.14(c, d)) and torque correlation differs a little (Figure 5.14).

5.7 Identify Pseudoisomorphs After Quenching

We take the ASD model with harmonic bonds to minimize and evaluate the scaling methods, and they give different potential energy and minimum. The atomic force method provides different results along atomic and CM scaling due to intramolecular interactions. In contrast, the molecular force and torque methods create the same temperatures (see Tables 5.2, 5.3).

Table 5.2: Potential and minimum potential energy after quenching and scale the configuration via CM scaling. Then the temperatures are created via three methods (atomic, molecular forces and Torque). $(\rho_1, T_1) = (0.932, 0.465)$ is reference point.

density	U	U_{min}	$T(F_{Atomic})$	$T(F_{Mol})$	Torque
0.886	-30720.936	-30722.153	0.438	0.352	0.345
0.932	-27156.659	-27152.223	0.465	0.465	0.465
0.969	-22804.725	-22850.120	0.498	0.573	0.581
1.009	-16338.726	-16545.582	0.574	0.710	0.730
1.060	-4989.757	-5706.172	0.634	0.917	0.957

The method we used works as follows. A single configuration is selected from an equilibrium simulation at the reference state point (density ρ_1). This configuration is scaled uniformly to the density of interest, ρ_2 . Both scaled and unscaled configurations were quenched as described above in order to eliminate the bond vibrational degrees of freedom. After this, the
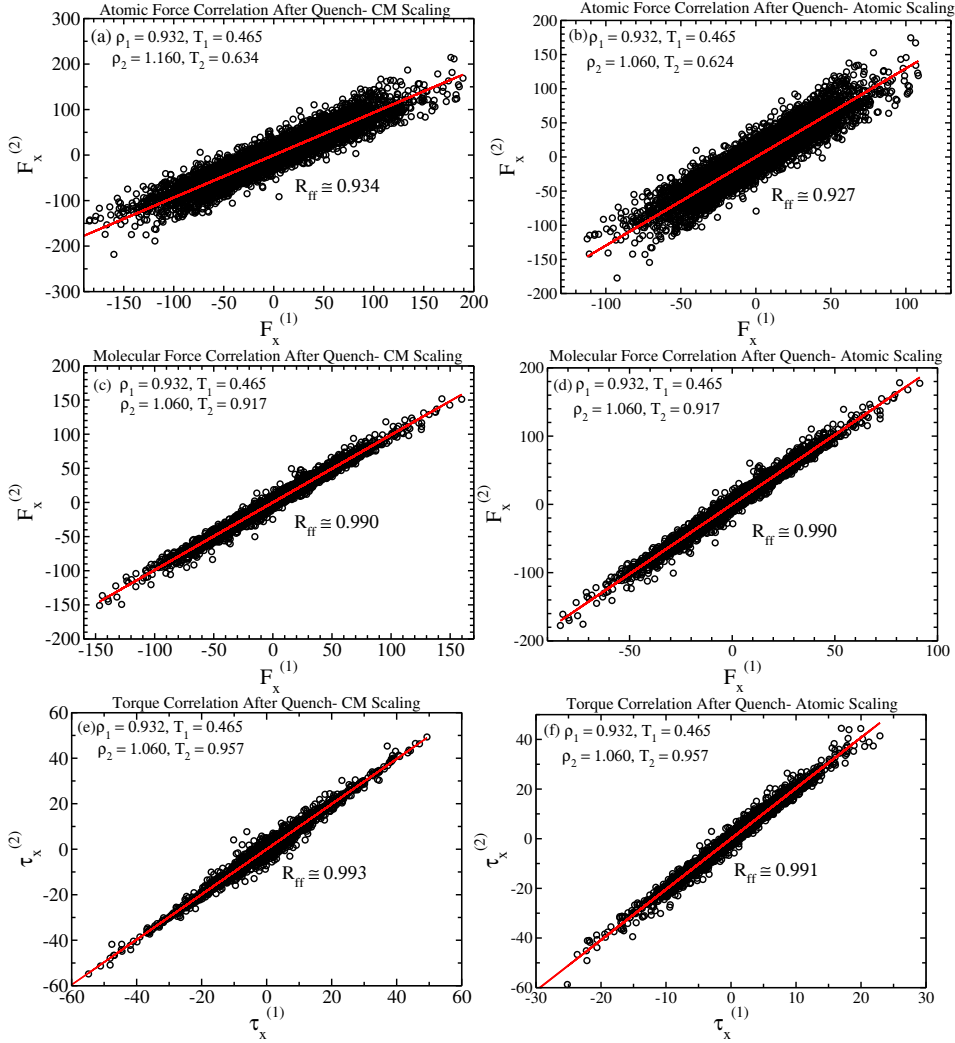
Figure 5.14: Correlation of atomic force (a,b) molecular force (c,d) and torque (e.f) of molecules via both scaling method after quenching. One configuration is taken from equilibrium simulation at $(\rho_1, T_1) = (0.932, 0.465)$ and be quenched. Then we scale the configuration at higher density $\rho_2 = 1.060$ via CM scaling (left panels) and atomic scaling (right panels) and quench again. Then the new temperature is predicted by forces and torque using equations 3.4, 3.9.

Table 5.3: Potential energy and minimum of potential energy after minimization using the atomic scaling. The atomic force method provide different temperatures compared to table 5.2. But molecular force and torque methods identify same state points.

density	U	U_{min}	$T(F_{Atomic})$	$T(F_{Mol})$	Torque
0.886	-30148.038	-30682.507	0.444	0.352	0.345
0.932	-27156.659	-27152.223	0.465	0.465	0.465
0.969	-22666.736	-22874.548	0.494	0.573	0.581
1.009	-15743,463	-16605.424	0.540	0.710	0.730
1.060	-3775.484	-5800.853	0.624	0.917	0.957

relevant forces / torques were evaluated and the temperature T_2 was determined from equations 3.4, 3.9. Note that the system is scaled before quenching. We chose the CM scaling to evaluate the dynamics in Figure 5.15.

The best results are obtained from molecular force method which is also the one that worked best in Figure 5.7. For this method we find excellent collapse of the reduced center-of-mass mean-square displacement as a function of time, as well as of the center- of-mass incoherent intermediate scattering function, while the directional autocorrelation function shows slightly worse collapse but nevertheless significantly better than without quenching. Comparing the results of the torque method with and without quenching shows that quenching also significantly improves the dynamics to be invariant. Since the atomic force method include the harmonic oscillations, it does not produce the appropriate results after quenching. To remove the harmonic bonds effects we calculate the atomic force without considering the spring force after quenching. Both scaling approaches provide the same temperatures. In Figure 5.16 removing the spring force contribution leads to better results but there is not any good collapse.

5.8 DIC Before and After Quenching

Pseudoisomorph is traced out in small molecular model (e.g. ASD, IPL, OTP) via molecular force method after we minimize the potential. In this section, we intend to test the direct isomorph check method (DIC) to investigate if pseudoisomorphs can be identified by this method or not.

As explained in chapter 3, the isomorphic points are predictable by calculating the potential energies slope at the first and second state point. We now pick the equilibrium ASD configurations at $(\rho_1, T_1) = (0.932, 0.465)$ composed of spring bonds. Applying two scaling approaches approximate different potential energy (Tables 5.2, 5.3) consequently slope will be different. The configuration at $(\rho_1, T_1) = (0.932, 0.465)$ is scaled at higher density
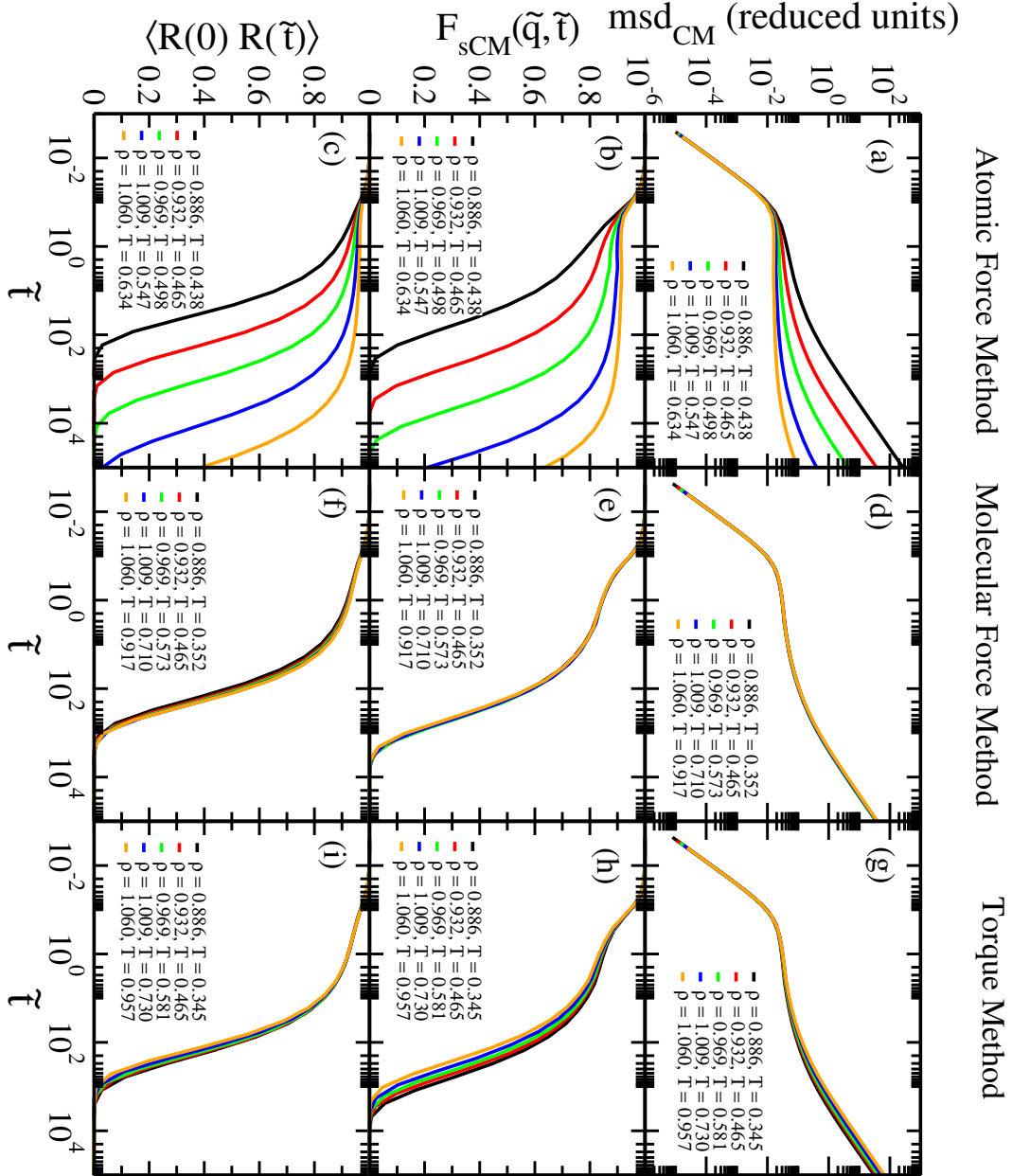
Figure 5.15: The mean square displacement, incoherent intermediate scatter-
ing function, orientational autocorrelation function in reduced units evaluated
along the forces methods in ASD. We apply the CM scaling on 195 configura-
tions and predict T_2 after minimization. The molecular force method provides
the proper pseudoisomorphic points. The results of torque method improve in
comparison with Figure 5.7. But the atomic force method does not work due to
the intramolecular interaction.
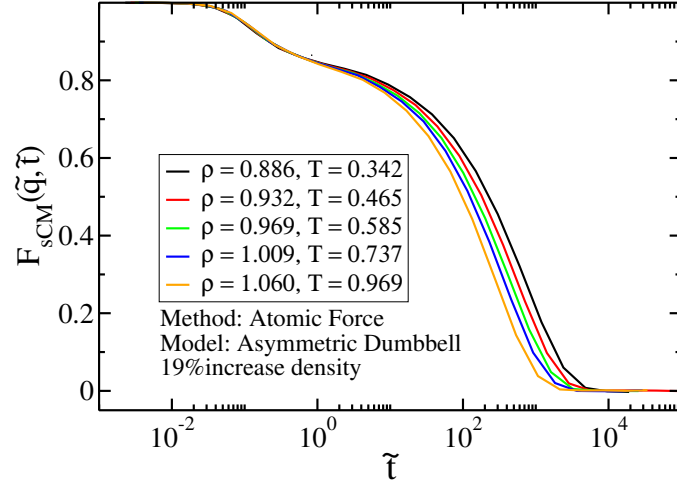
Figure 5.16: The intermediate scattering function in reduced units along invariant atomic force after quenching the configuration without spring contribution. This Figure should be compared with Figure 5.15(a,b,c), which demonstrates the results get better but still there is no collapse.
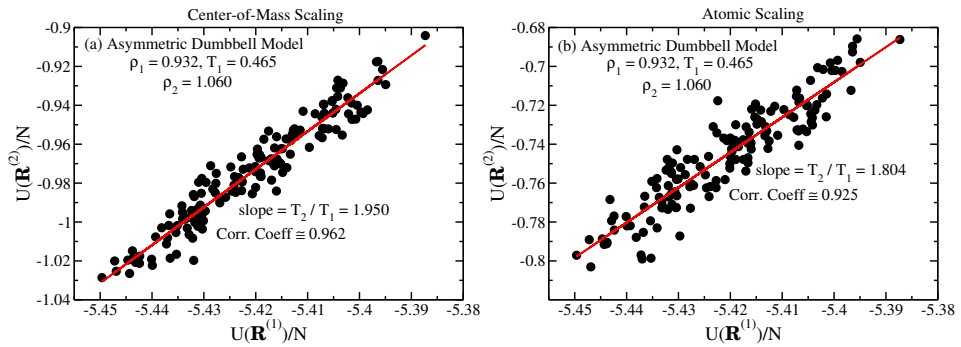
Figure 5.17: The potential energy correlation of unscaled configurations at $(\rho_1, T_1) = (0.932, 0.465)$ and scaled configurations at $\rho_2 = 1.060$. (a) The data of CM scaling method in which the slope and correlation coefficient are $1.950, 0.962$, respectively. (b) The atomic scaling affects the slope value and correlation coefficient where 'slope $= 1.804$' and 'Corr. Coeff $= 0.925$'.

$\rho_2 = 1.060$ by CM scaling in which the slope of the potential energy correlation plot reach 1.950 (see Figure 5.17 (a)). Whereas the slope is obtained 1.804 via atomic scaling (see Figure 5.17 (b)). The ASD model dynamics through CM scaling and atomic scaling is demonstrated in Figure 5.18. The temperatures are created by DIC method before quenching. The CM scaling results are better than the atomic scaling results.
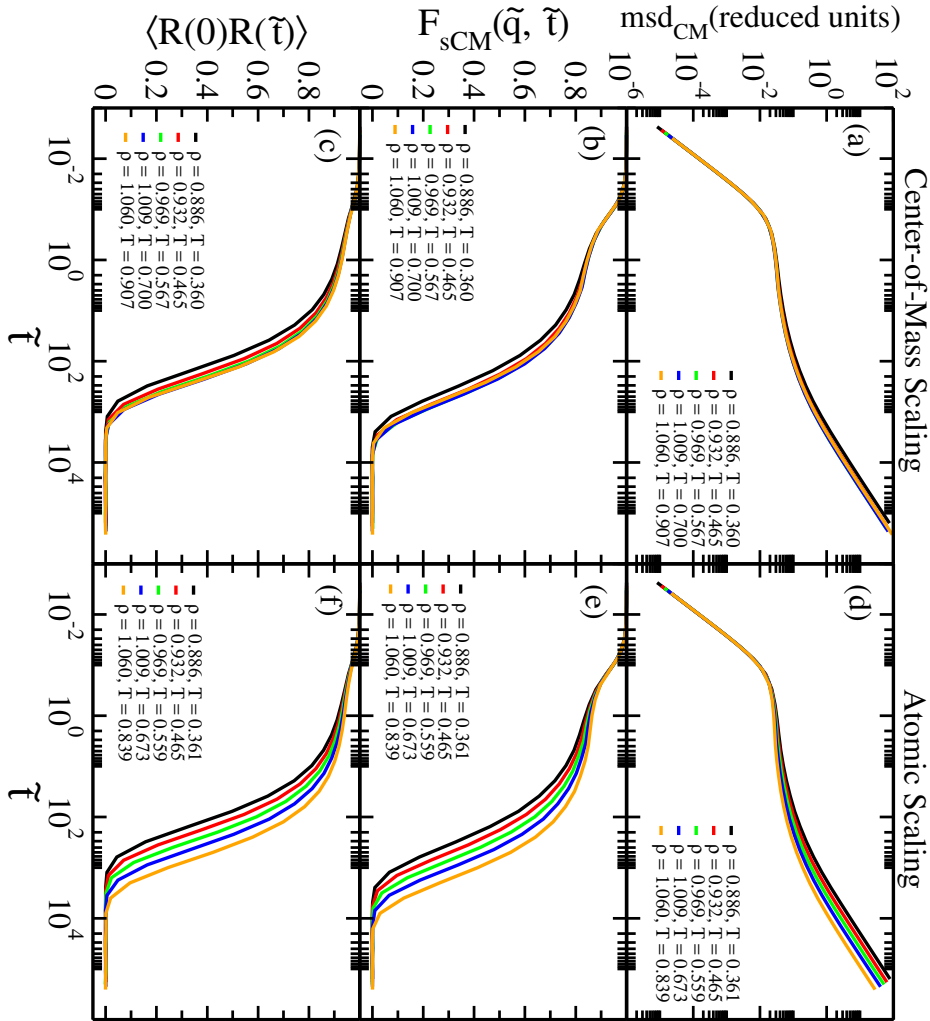
Figure 5.18: Dynamics of the ASD model with harmonic bonds along temperature generated via DIC method without quenching. Both scaling are used. The CM scaling results (a, b, c) are comparable with pseudoisomorphic points in Figure 5.6. But the Atomic scaling results (d, e, f) are quite different.

Table 5.4 indicates that removing the spring contribution does not improve the results, especially at the highest density. Temperatures predicted by CM and atomic scaling after abolishing the harmonic potential are quite

different from the pseudoisomorphic points (Figure 5.6).

Table 5.4: Potential energy and temperatures after removing the harmonic potential and scale the system via CM and atomic scaling. The first column shows the density, the second column shows the potential energy without spring contribution using the CM scaling, and the third column indicates the temperature calculated through the DIC method using the CM scaling. Fourth and fifth columns show the same quantities when we implement the atomic scaling.

density	$U_{CM-Scaling}$	$T_{CM-Scaling}$	$U_{Atomic-Scaling}$	$T_{Atomic-Scaling}$
0.886	-32098.247	0.348	-31480.013	0.362
0.932	-28552.965	0.465	-28552.965	0.465
0.969	-24201.031	0.578	-25080.788	0.561
1.009	-17735.032	0.723	-20068.564	0.679
1.060	-6386.063	0.947	-11556.348	0.854

Eliminating the degrees of freedom by quenching the system causes collapse in CM scaling plot vanishes in Figure 5.19 (a, b, c), but it improves the dynamics along atomic scaling (Figure 5.19 (d, e, f)). If we eliminate the harmonic potential after quenching, it still does not accomplish the invariant dynamics. The potential decrease a lot after minimization and abolishing the harmonic contribution in Table 5.5 (comparing the results with Table 5.4).

Table 5.5: Shows the similar quantities of table 5.4 after quenching and removing the springs. Results are still far from pseudoisomorphic points in Figure 5.6.

density	$U_{CM-Scaling}$	$T_{CM-Scaling}$	$U_{Atomic-Scaling}$	$T_{Atomic-Scaling}$
0.886	-32053.309	0.294	-32001.792	0.296
0.932	-28584.887	0.465	-28552.965	0.465
0.969	-24486.450	0.477	-24457.225	0.455
1.009	-18545.079	0.504	-18601.898	0.548
1.060	-8523.956	0.703	-8461.582	0.655

Figure 5.19: The dynamics get worse after quenching the ASD configurations in comparison with Figure 5.18 by using the CM scaling (a, b, c). However, quenching helps the atomic scaling give the better results (d, e, f).

5.9 Quenching via Vector Function

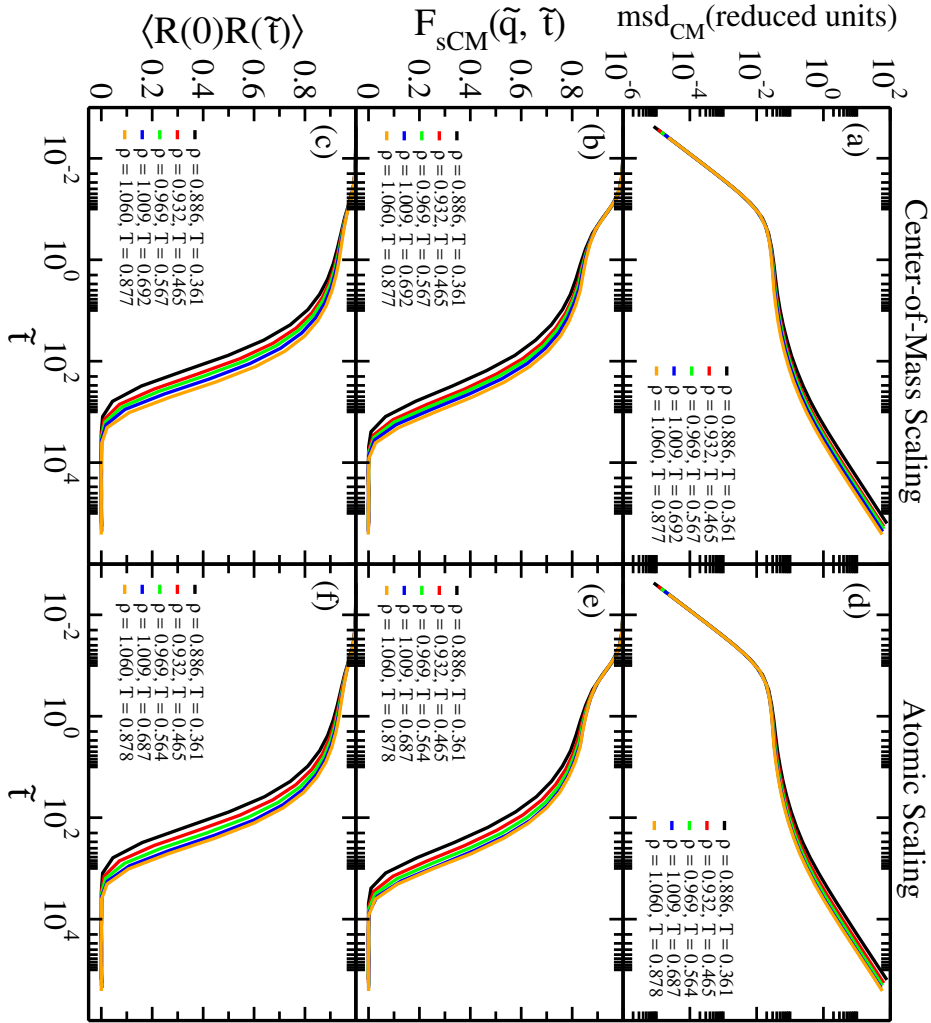In this section, we implement other function, i.e. the vector-based function in which dl is a vector matrix to fine the local minimum. It means that the bonds length vary by different number while in section 5.5 we defined the function in which all length change by a single number. We aim to find the minimum of high-dimensional properties so the Conjugate Gradient (CG) method would be a proper choice. This method has benefits of using the gradient. For calculating the gradient of potential in constraint space for *kth* molecule we have,

$$
\begin{aligned}
\frac{\partial U(\mathbf{L_k})}{\partial \mathbf{L_k}} &= \frac{U(L_{k,k+1} + dl_{k,k+1}) + U(L_{k,k+1})}{dl_k} \\
&= \frac{\dfrac{\partial U}{\partial \mathbf{r_k}} d\mathbf{r_k} + \dfrac{\partial U}{\partial \mathbf{r_{k+1}}} d\mathbf{r_{k+1}}}{dl_k}.
\end{aligned}
\tag{5.16}
$$

By substituting $d\mathbf{r_k}, d\mathbf{r_{k+1}}$ from equation 5.15, we have,

$$
\begin{aligned}
\frac{\partial U(\mathbf{L_k})}{\partial \mathbf{L_k}} &= \frac{m_B}{m_A + m_B} \frac{\partial U}{\partial \mathbf{r_k}} \hat{\mathbf{l}}_\mathbf{k} - \frac{m_A}{m_A + m_B} \frac{\partial U}{\partial \mathbf{r_{k+1}}} \hat{\mathbf{l}}_\mathbf{k} \\
&= \frac{m_B}{m_A + m_B} F_A - \frac{m_A}{m_A + m_B} F_B.
\end{aligned}
\tag{5.17}
$$

The minimum potential is obtained by using the vector dl and considering two conditions, keep the center-of-mass position fixed and move the particle only along the direction of the bond length (equation 5.15) and using the gradient (equation 5.17). In BFGS method, we define a scalar function to change the bond length by a scalar number, but we here pick the vector-matrix to update the length. We use the 'scipy.optimize.minimize()' function implementing conjugate gradient (CG) algorithm based on the vector function. The bond length probability distribution is compared for unscaled configuration at $\rho_1 = 0.932$ and scaled configuration at $\rho = 1.06$, before and after quenching by scalar and vector function in Figure 5.20. Quenching the unscaled configuration via vector function gives the quite different distribution (purple curve) compared to results of the scalar function (orange curve) at $\rho = 0.932$. Moreover, for scaled configuration, the vector function (pink curve) does not provide the correct distribution bond length (green curve). Quenching system via the scalar function (blue curve) reach better results.

Again, we check both scaling method (CM and atomic scaling) and then after quench the system we use the force methods and DIC method to calculate the temperatures. Table 5.6 and Table 5.7 show the potential and minimum of potential via CM and atomic scaling after quenching by the vector function. Using the CM scaling or atomic scaling gives the same
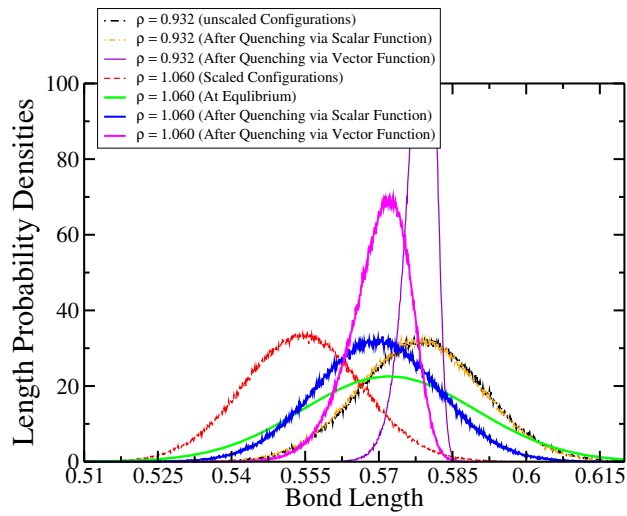
Figure 5.20: Comparing the bond length distribution at reference point $\rho_1 = 0.932$ (black) and scale the system at $\rho_2 = 1.06$ before and after quenching. The bonds of unscaled configuration have quite different length distribution (purple curve) after quenching via vector function in compared to before quenching (black curve). Minimization via scalar function gives the proper results for unscaled configuration (orange curve). The bond length (red) shifts from equilibrium length (green) by scaling the system. Quenching the system by scalar function provide the proper length (blue) corresponding to the equilibrium, which is explained in Figure 5.13. However, the length distribution is narrow after quenching by vector function (pink). Here, we apply the CM scaling.

minima (second column). The temperatures are approximately equivalent. The vector function quench the system to different local minima in comparison with the scalar function (Table 5.2, 5.3). The predicted temperatures are quite different from pseudoisomorphic points in Figure 5.6.

Table 5.6: Minimum of potential and predicted temperatures via vector function using the CG algorithm after CM scaling. The all force methods and DIC are considered to predict the temperatures. The reference point is $(\rho_1, T_1) = (0.932, 0.465)$. The vector function minimize the system more than the scalar function (Table 5.2), but it does not provide the proper pseudoisomorphs.

density	U	U_{min}	$T(F_{Atomic})$	$T(F_{Mol})$	Torque	Direct Iso
0.886	-30720.936	-31864.362	0.354	0.354	0.347	0.351
0.932	-27156.659	-28314.342	0.465	0.465	0.465	0.465
0.969	-22804.725	-24032.457	0.573	0.570	0.577	0.573
1.009	-16338.726	-17777.382	0.700	0.701	0.719	0.708
1.060	-4989.757	-7044.952	0.894	0.895	0.931	0.907

Table 5.7: Using the CG algorithm based on the vector function after scale system with atomic scaling approach gives the same minima when we use the CM scaling (Table 5.6) and the temperatures are the same approximately.

density	U	U_{min}	$T(F_{Atomic})$	$T(F_{Mol})$	T(Tor)	T(DIC)
0.886	-30148.038	-31864.362	0.354	0.354	0.347	0.351
0.932	-27156.659	-28314.342	0.465	0.465	0.465	0.465
0.969	-22666.736	-24032.458	0.573	0.570	0.578	0.573
1.009	-15743,463	-17777.381	0.700	0.701	0.719	0.708
1.060	-3775.484	-7044.951	0.894	0.895	0.931	0.907

So far, the pseudoisomorph is identified in ASD molecular model at high densities by molecular force method after eliminating the unscaled degrees of freedom and considering two constrain condition. We investigate the generating pseudoisomorphs in IPL model (See Appendix D). In IPL model, the molecular force method also predicts proper pseudoisomorphs after quenching.

5.10   Pseudoisomorphs at Low Densities

In this section, we trace pseudoisomorphs in ASD model at low densities. We start from the state point $(\rho_1, T_1) = (0.785, 0.174)$ and scale the system to lower densities $\rho = 0.738, 0.761$ and higher densities $\rho = 0.808, 0.832, 0.856$. The bonds are not compressed by increasing density. Figure 5.21 implies

that there is no significant shifting in bond lengths distribution at higher densities from reference point $(\rho_1, T_1) = (0.785, 0.174)$.
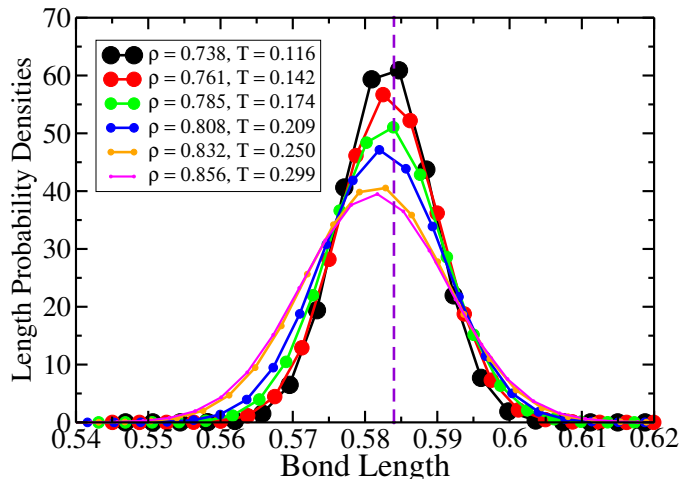
Figure 5.21: Bond lengths distribution of ASD model with harmonic spring bonds at lower densities than densities we used in Figure 5.12. The state points re predicted via molecular force method. The bonds have a roughly similar distribution at different densities and the shifting seen in Figure 5.12 vanishes here. The reference density is $\rho_1 = 0.785$. The density changes over 16%.

To investigate the force methods, the configurations are taken from equilibrium simulation at reference point $(\rho_1, T_1) = (0.785, 0.174)$ and we scale them via CM scaling then calculate the new T by equations 3.4 and 3.9. In this case, we reach pseudoisomorphic points via the molecular force except for the lowest density, $\rho = 0.738$ (see Figure 5.22). Furthermore, the appropriate pseudoisomorphic points are identified without quenching the system. The atomic force method results are still far from adequate T due to the intramolecular harmonic bonds. While the molecular force method find the pseudoisomorph and the torque results are comparable with results of the molecular force method.

To get more information of configurations at state point $(\rho, T) = (0.738, 0.116)$ at which the dynamics behave strange in Figure 5.22 (d, e, f), we plot structure which is represented by radial distribution function in reduced units in Figure 5.23. It seems that the system has phase separation at state point $(\rho, T) = (0.738, 0.116)$. While it has a perfect invariant structure at other state points. Figure 5.24 illustrates the molecular force method is more precise in identifying pseudoisomorphs in the ASD model.

In addition to CM scaling, we measure the temperatures via force methods after using atomic scaling. As shown in table 5.8 the temperatures are quite different from the CM scaling approach results which are different from pseudoisomorphic state points in Figure 5.22. Since the OTP model has the low viscosity, the pseudoisomorphic points are identified via molecular force
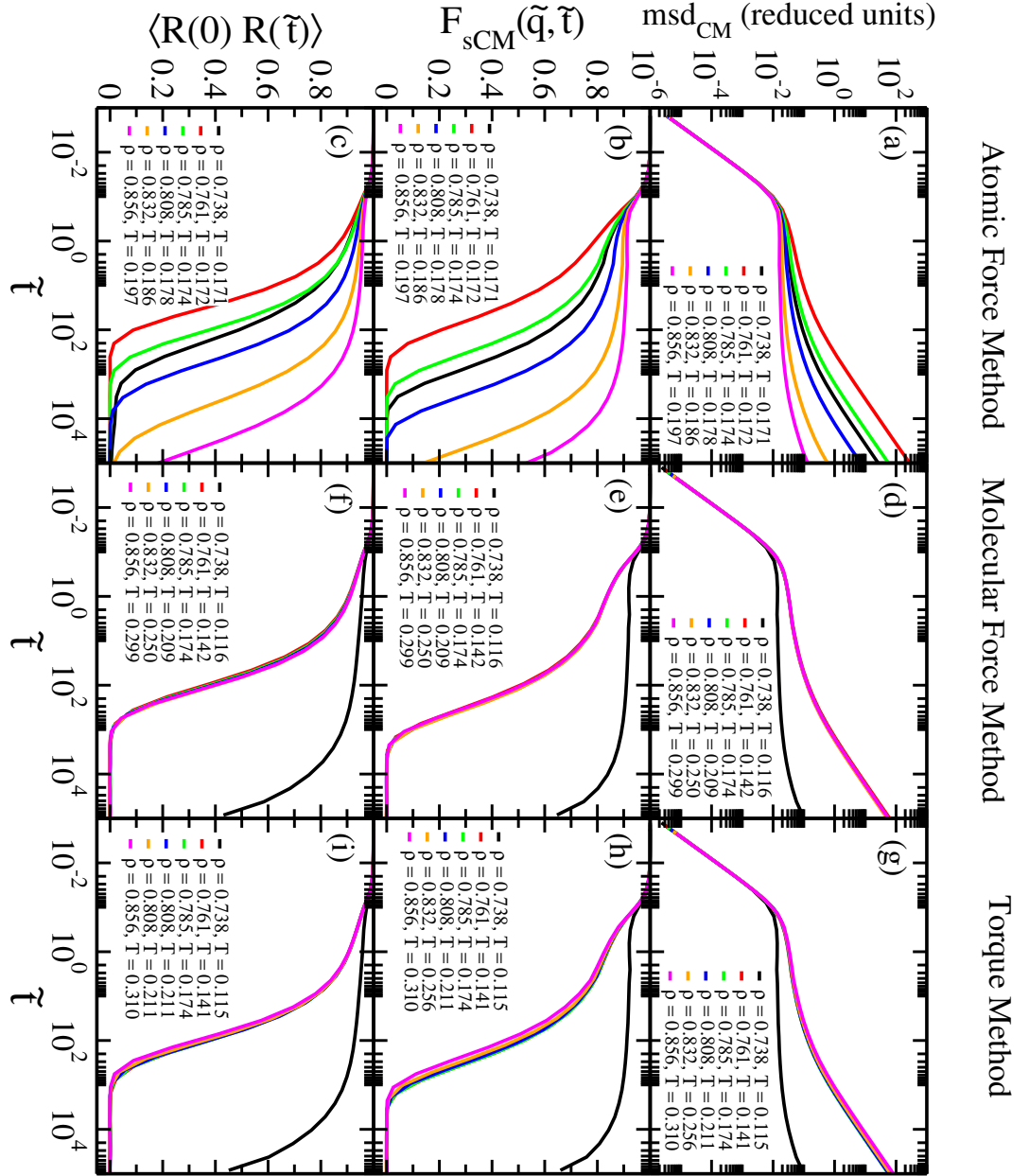
Figure 5.22: The low viscous ASD model dynamics does not demonstrate any invariant along predicted state point via atomic force method (a, b, c). In contrast, there are considerable collapses predicted by molecular force method (d, e, f) and torque method(g, h, i) except at the lowest density $\rho = 0.738$. The equilibrium configurations at $(\rho_1, T_1) = (0.785, 0.174)$ are scaled to lower and higher densities by CM scaling. The density spreads about 16%.

Molecular Force Method
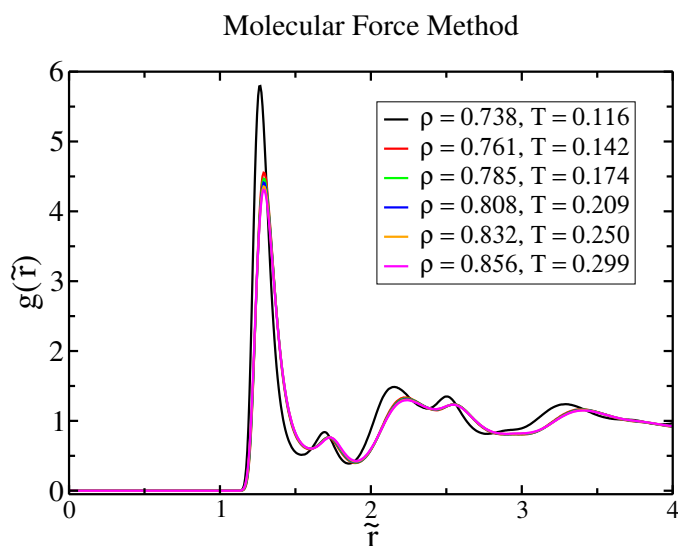
Figure 5.23: Radial distribution function in reduced units of ASD model along the state points predicted via molecular force method. The structure is invariant except for the lowest density, at which system has liquid-gas phase separation. The density spreads about 16%.
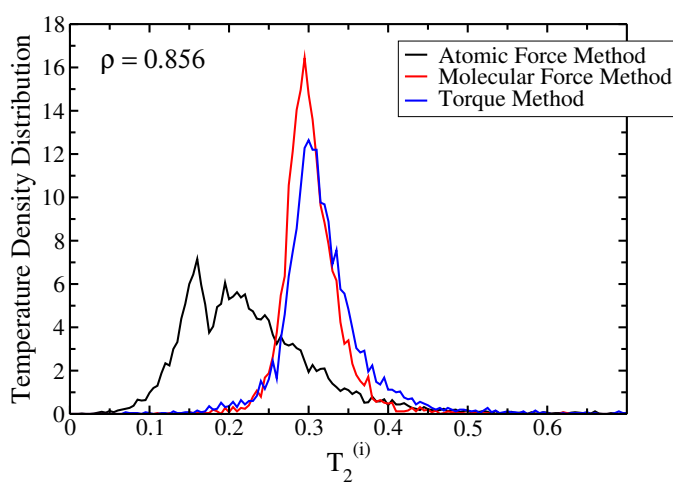
Figure 5.24: Comparing the accuracy of force methods in predicting the temperature of each particle through the atomic force and each molecule via molecular force and Torque methods. At the highest density at which configuration is scaled by CM scaling, the molecular force is the most accurate method, then the torque is in the second rank. While the atomic force method is placed in the third rank in predicting the temperature in harmonic models.

and torque methods without any minimization required(see Appendix C).

Table 5.8: Predicted new T along invariant forces and torques after scaling the system via atomic scaling method. The temperatures are far from anticipated pseudoisomorphic points in comparison with Figure 5.22.

density	$T(F_{Atomic})$	$T(F_{Mol})$	T(Tor)
0.738	0.305	0.123	0.127
0.761	0.214	0.146	0.149
0.785	0.174	0.174	0.174
0.808	0.204	0.203	0.201
0.832	0.275	0.238	0.232
0.856	0.357	0.276	0.266

Indeed, it is interesting that one can identify pseudoisomorph in ASD and OTP model at low densities by molecular force and torque method without minimization.

5.11   Minimization via Scalar Function
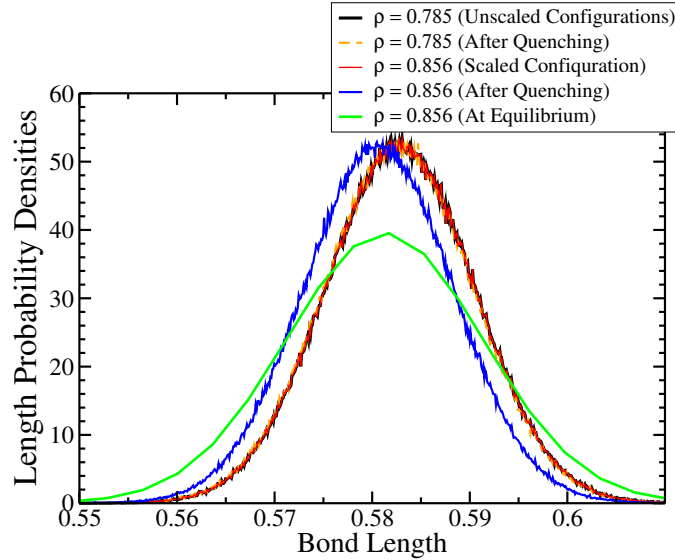
Figure 5.25: The bonds length distribution of unscaled configuration before (black) and after (orange) quenching at reference state point $\rho = 0.785$; and it also illustrates the bonds length have same distribution after scaling to $\rho = 0.856$ via CM scaling (red). Scaled configuration get the better length distribution (blue) after quenching.

The scalar function provided proper results in section 5.5 when we quench the ASD model at rather high densities. Here, we investigate if we can get

invariant dynamics by quenching the ASD model at lower densities or not?! Figure 5.25 demonstrates the configuration at $\rho = 0.785$ has the same bond length before and after quenching (black and orange curves). By scaling it to $\rho = 0.856$ the bonds length avoid to shift (red curve) while they are compressed a little at equilibrium (green curve). Using the scalar function in quenching the system provide the better length distribution (blue curve) which is similar the relevant distribution at equilibrium. On the other hand, quenching this low viscose system gives the approximate same results except at highest density (comparing the predicted T in Table 5.9 with Figure 5.22).

Table 5.9: Predicted new T along invariant forces and torques after quenching via scalar function and applying CM scaling method. The temperatures are about close to results in 5.22.

density	$T(F_{Atomic})$	$T(F_{Mol})$	T(Tor)
0.738	0.171	0.117	0.115
0.761	0.172	0.143	0.142
0.785	0.174	0.174	0.174
0.808	0.177	0.208	0.209
0.832	0.182	0.248	0.253
0.856	0.190	0.294	0.301

Scaling the configurations via atomic scaling and quench the system give different results comparing to the predicted temperature before quenching in Table 5.8. In this case, quenching the system improves the results of atomic force considerably. Results of molecular force and torque method are as same as CM scaling results after quenching in Table 5.9 except for the atomic force method.

Table 5.10: Predicted new T along invariant forces and torques after quenching via scalar function and applying atomic scaling method. The temperatures are about close to results in 5.9.

density	$T(F_{Atomic})$	$T(F_{Mol})$	T(Tor)
0.738	0.174	0.117	0.115
0.761	0.173	0.143	0.142
0.785	0.174	0.174	0.174
0.808	0.176	0.208	0.209
0.832	0.180	0.248	0.253
0.856	0.186	0.294	0.301

We can identify pseudoisomorphs in small molecular models like ASD, IPL and OTP with harmonic bonds via molecular force method. At high densities, the pseudoisomorphs appear after we eliminate the unscaled de-

grees of freedom of springs by defining the scalar function in a constraint space under two conditions and applying the BFGS optimization method. While, at low densities the pseudoisomorphs are generated without quenching which is astonishing.

Chapter 6

Pseudoisomorph in Flexible Lennard-Jones Chains

In this chapter, the large molecular model i.e. flexible Lennard-Jones chains model with harmonic bond is chosen to identify pseudoisomorphs via new force methods. In 2016, Olsen et al. generate pseudoisomorph in LJC model by quenching the system. We consider the atomic, center-of-mass, segmental force and torque methods to identify pseudoisomorphs in this model before and after minimization. The both scaling method, i.e. center-of-mass and atomic scaling are tested.

6.1 Introduction

The flexible Lennard-Jones chains with harmonic intramolecular interactions does not have the U-W strong correlation so it is not expected to have isomorphs. Figure 6.1 demonstrates the weak correlation coefficient $R = 0.284$ and linear regression slope $\gamma = 4.681$ in compared to the relevant quantities in LJC model with rigid bonds (see Figure 4.1). In 2016, Olsen et al. [2] generated pseudoisomorph in the LJC model after they minimize the system to abolish the unscaled degrees of freedom (Figure 6.2).

The force methods have been investigated to identify isomorphs in the constrained Lennard-Jones chain (LJC) model in chapter 4 and in this section, we intend to identify pseudoisomorph via the same methods. First, we test the methods before quenching to investigate the system whether needs to be minimized or not. We again apply both scaling methods (i.e. center-of-mass and atomic scaling). Each configuration contains 1000 molecules. All potential parameters and bond length are similar to the corresponding
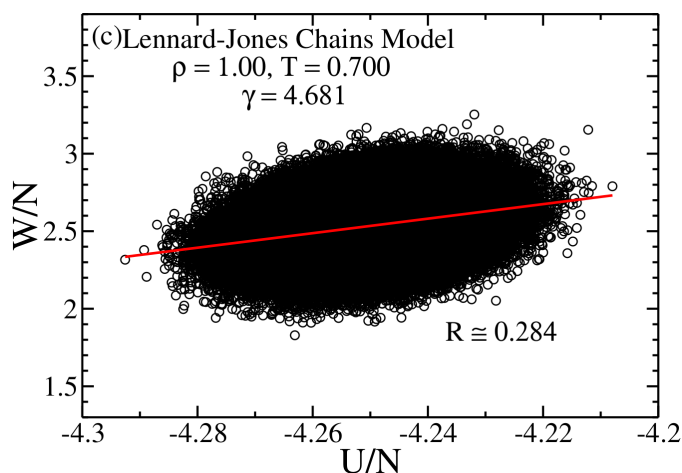
Figure 6.1: Decreasing R, γ also for LJC model when we change the rigid bonds to flexible spring bonds. $R = 0.861$, $\gamma = 7.388$ are obtained for LJC model with constraint and they drop to $R = 0.284$, $\gamma = 4.681$ in harmonic LJC model.

quantities used in section 4.4. Since the LJC model has low viscosity at considered density, the bonds length distribution have no shifting at different state points taken from ref. [2] (see Figure 6.3).

We test the force methods on this model in Figure 6.4 using the CM scaling. Calculating the different type of forces in LJC model in which each molecule contains ten beads is more complicated than small molecular models. How calculating the segmental force is explained in chapter 4. The state points generated in Figure 6.4 via forces methods are not comparable with pseudoisomorphic points in Figure 6.2. On the other hand, Figure 6.5 shows using the potential achieves better results via DIC method after scaling the configurations by CM scaling. The unscaled degrees of freedom of flexible chains cause the dynamics to be not invariant along the force and torque methods. The dynamics are not invariant along the molecular force method, which used the CM force regardless of the spring contributions to calculate T. In calculation of segmental force and torque, the spring force is also removed, but the dynamics still are not invariant. Eliminating the unscaled degrees of freedom by quenching the system might help the methods to identify pseudoisomorphs. As mentioned, finding the minima of liquids system needs lots of effort, and in some cases, it is impossible since the potential energy surface is a high dimensional function.

6.2 Quenching the LJC Model

We explained how to minimize the small molecular model in constrained space via the scalar function in section 5.5. However, the LJC model is

Pseudoisomorph
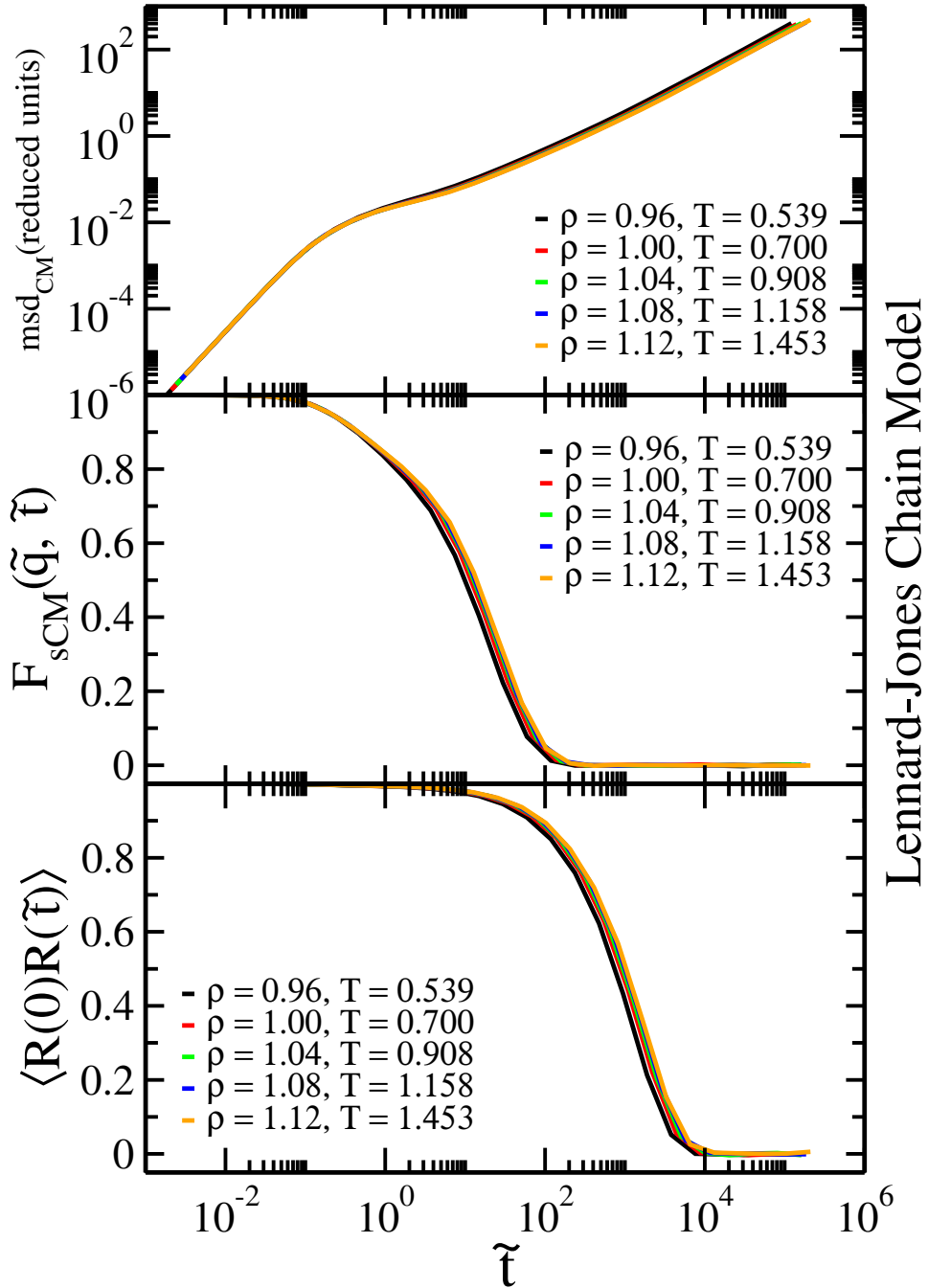
Figure 6.2: The dynamics of harmonic LJC model are invariant along pseudoisomorph. The state points are taken from ref. [2]
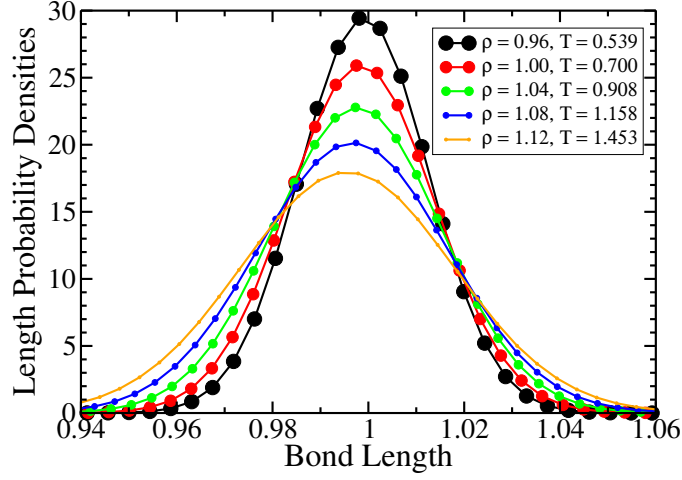
Figure 6.3: The bonds length distribution of harmonic LJC model at pseudoisomorphic points (Andreas paper). The reference point is $(\rho_1, T_1) = (1.00, 0.700)$. The density changes about 17%, and the bonds have an approximate identical length at different densities.

much more complicated, we consider the same conditions to simplify the problem. First, the CM position of each molecule and each segment are assumed to be fixed, $d\mathbf{R}_{CM,i} = 0$ and second the bonds length change along the orientational direction of bonds (equation 5.4). By considering these conditions and change the position of atoms according to equation 5.5, we again reach the equation 5.9. The atoms have the identical mass, $m = 1$, in LJC model, so we have,

$$\beta = -\frac{i+1}{N-i}\alpha. \tag{6.1}$$

According to equation 6.1 and equation 5.5, the position of atoms is derived by,

$$\begin{cases} \mathbf{r'_j} = \mathbf{r_j} + \alpha \mathbf{d\hat{l}_i} & j \leq i \\ \mathbf{r'_j} = \mathbf{r_j} - \dfrac{i+1}{N-i}\alpha \mathbf{d\hat{l}_i} & j > i \end{cases} \tag{6.2}$$

With respect to change the segment length by $d\mathbf{l}$, we have,

$$|\mathbf{dl_i}| = |\mathbf{dr_{j+1}} - \mathbf{dr_j}| \tag{6.3}$$

By substituting equation 6.2 in equation 6.3, we have,

$$|\mathbf{dl_i}| = |-\frac{i+1}{N-i}\alpha \mathbf{d\hat{l}_i} - \alpha \mathbf{d\hat{l}_i}|. \tag{6.4}$$
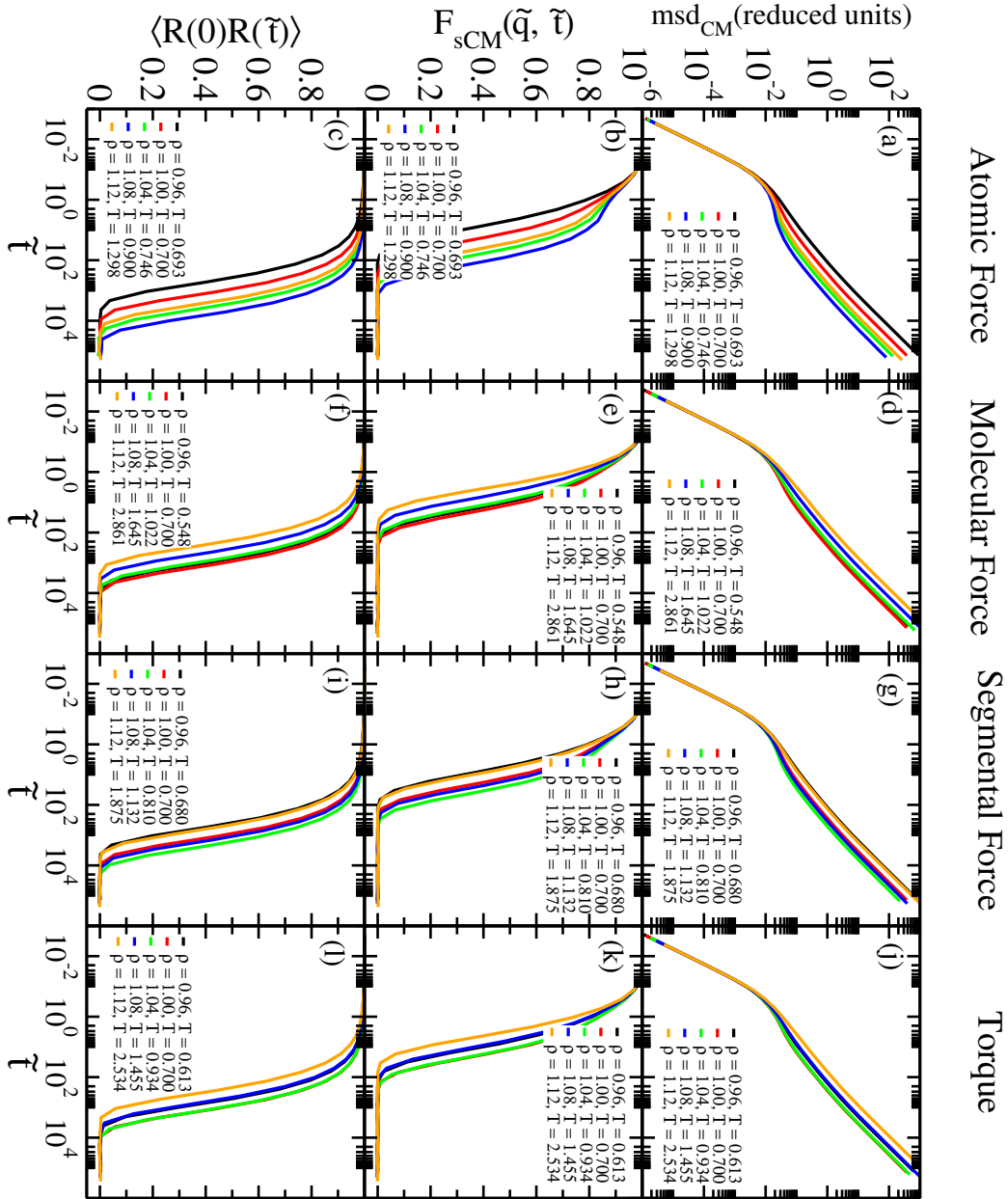
Figure 6.4: The dynamics of LJC model with harmonic bonds. The reference point is $(\rho_1, T_1) = (1.00, 0.700)$. The force methods are tested here before minimization and using the CM scaling. The density increases about 17%. However, the methods do not achieve the pseudoisomorph as expected.

Direct Isomorph Check Method
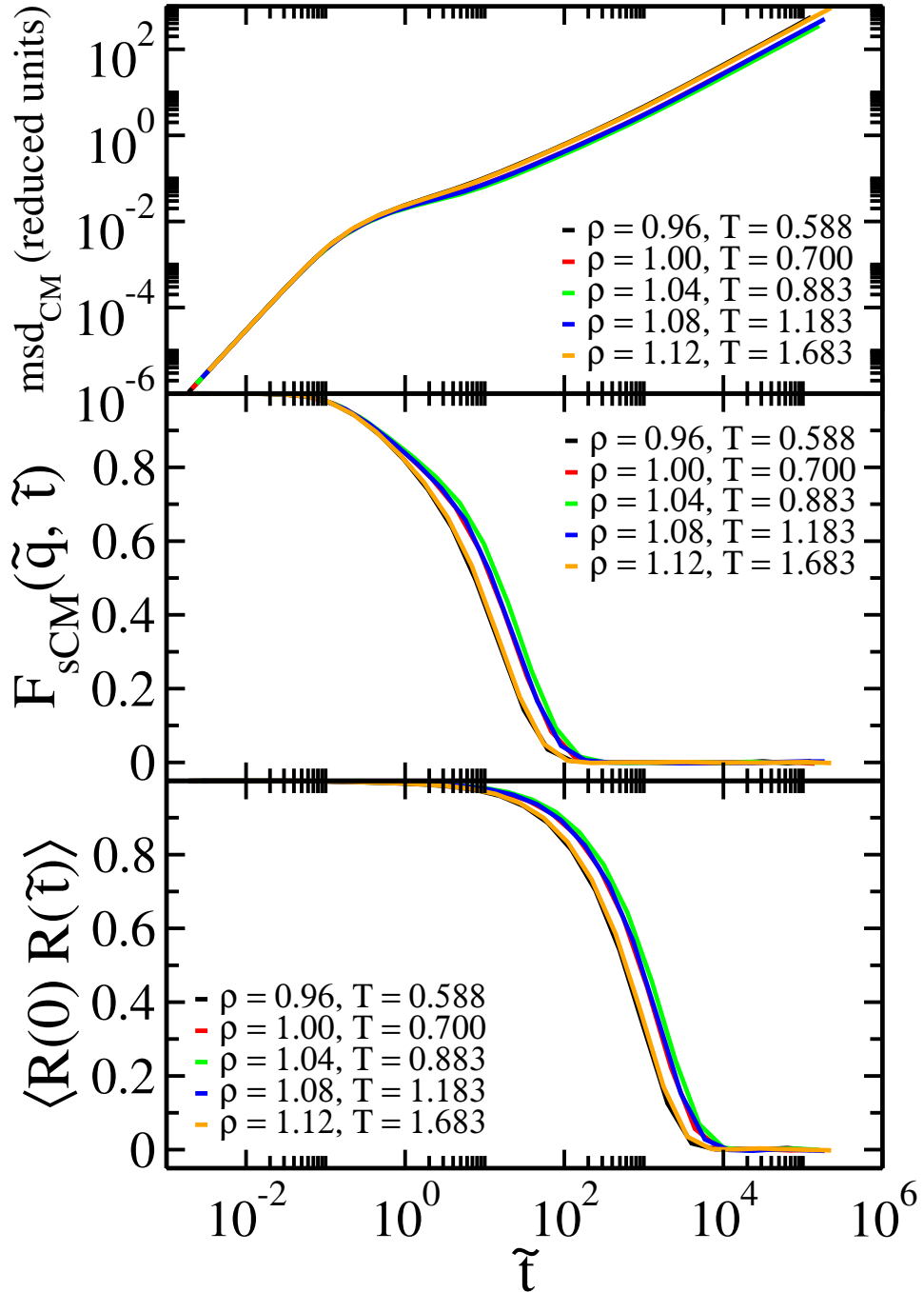
Figure 6.5: The DIC method provides more proper results in LJC model than the force methods in Figure 6.4. The same reference point in Figure 6.4 is considered. Here, the CM scaling is used.

By doing math, we can obtain α and then β,

$$\alpha \;=\; -\frac{N-i}{N+1} \tag{6.5}$$

$$\beta \;=\; \frac{i+1}{N+1} \tag{6.6}$$

So the new position of particles can be obtained by,

$$\begin{cases} \mathbf{r'_j} = \mathbf{r_j} - (\dfrac{N-i}{N+1})\mathbf{d\hat{l}_i} & j \le i \\[2mm] \mathbf{r'_j} = \mathbf{r_j} + (\dfrac{i+1}{N+1})\mathbf{d\hat{l}_i} & j > i \end{cases} \tag{6.7}$$

We now define a function to change the atom's position by a scalar value along the bond direction and keep the CM position fix and then we can quench the system by using the BFGS minimization method [34] in scipy.minimize() function of python.

Table 6.1: Potential and minimum of potential of harmonic LJC model. The minimum of potential are calculated by using the scalar function and scaling the configurations via CM scaling method. The starting point is $\rho_1 = 1.00$.

Density	U	U_{min}
0.96	-42857.147	-42925.848
*1.00	-42656.196	-42658.487
1.04	-40070.162	-40370.622
1.08	-33785.021	-35473.475
1.12	-21726.564	-27425.074

Table 6.2: Calculating the new T using the BFGS algorithm based on the scalar function after scale system with CM scaling approach. Four force methods are applied to generate pseudoisomorphs. However, the results are different from pseudoisomorphic points in Figure 6.2.

| density	$T(F_{Atomic})$	$T(F_{Mol})$	$T(F_{Seg})$	T(Tor)
0.96	0.693	0.676	0.676	0.611
*1.00	0.700	0.700	0.700	0.700
1.04	0.733	0.774	0.774	0.858
1.08	0.817	0.924	0.914	1.118
1.12	0.966	1.152	1.156	1.473

The equilibrium configurations at the reference state point, $\rho_1 = 1.00$, are minimized by the scalar function and then we scale the configurations to lower and higher densities by CM scaling method, then again quench the corresponding configurations. Quenching the high dimensional potential energy surface of LJC model is quite hard specially at lower density

$\rho = 0.96$ and reference point $\rho = 1.00$ (see Table 6.1). The new temperatures are produced via atomic and molecular force method (equation 3.4), segmental force method (equation 4.1) and torque method (equation 3.9) after quenching the system and using the CM scaling. Table 6.2 indicates the predicted state points are not the desired pseudoisomorphs points which found in Figure 6.2. The intramolecular vibrations are removed by quenching and the methods give lower temperature in comparison with predicted T before quenching (see Figure 6.4).
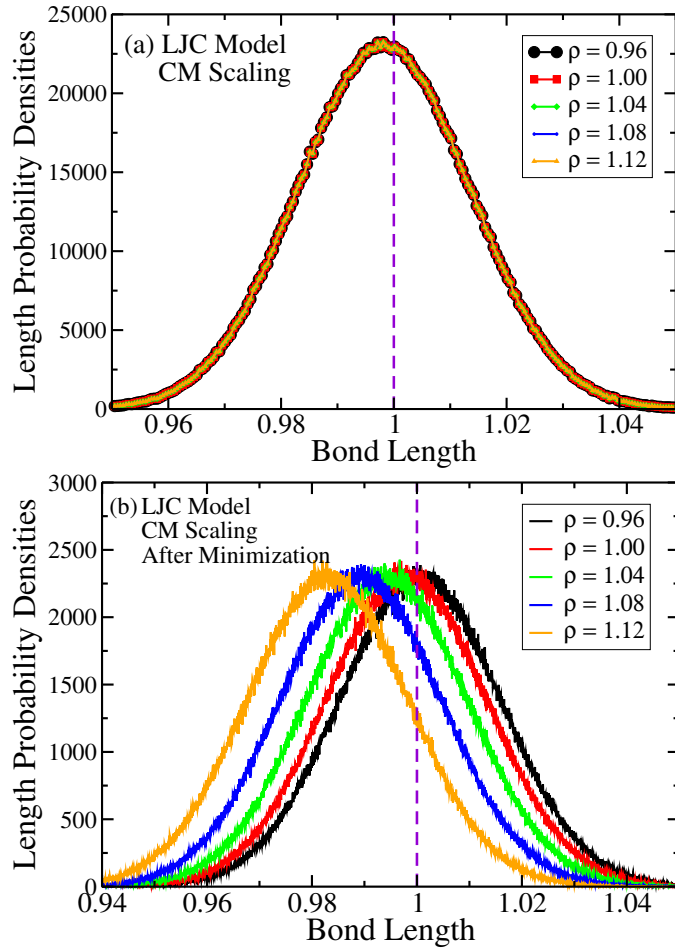
Figure 6.6: The bonds length distribution of harmonic LJC model using the CM scaling before minimization (a), and after we minimize the system via the scalar function in constrained space (b). The reference point is $(\rho_1, T_1) = (1.00, 0.700)$. The bonds shift by quenching the system while approximating the identical distribution in panel (a) before quenching. In both Figures, the CM scaling is implemented.

As shown in Figure 6.6 (a), the springs reject to compress by scaling the configurations to higher densities via CM scaling method. However,
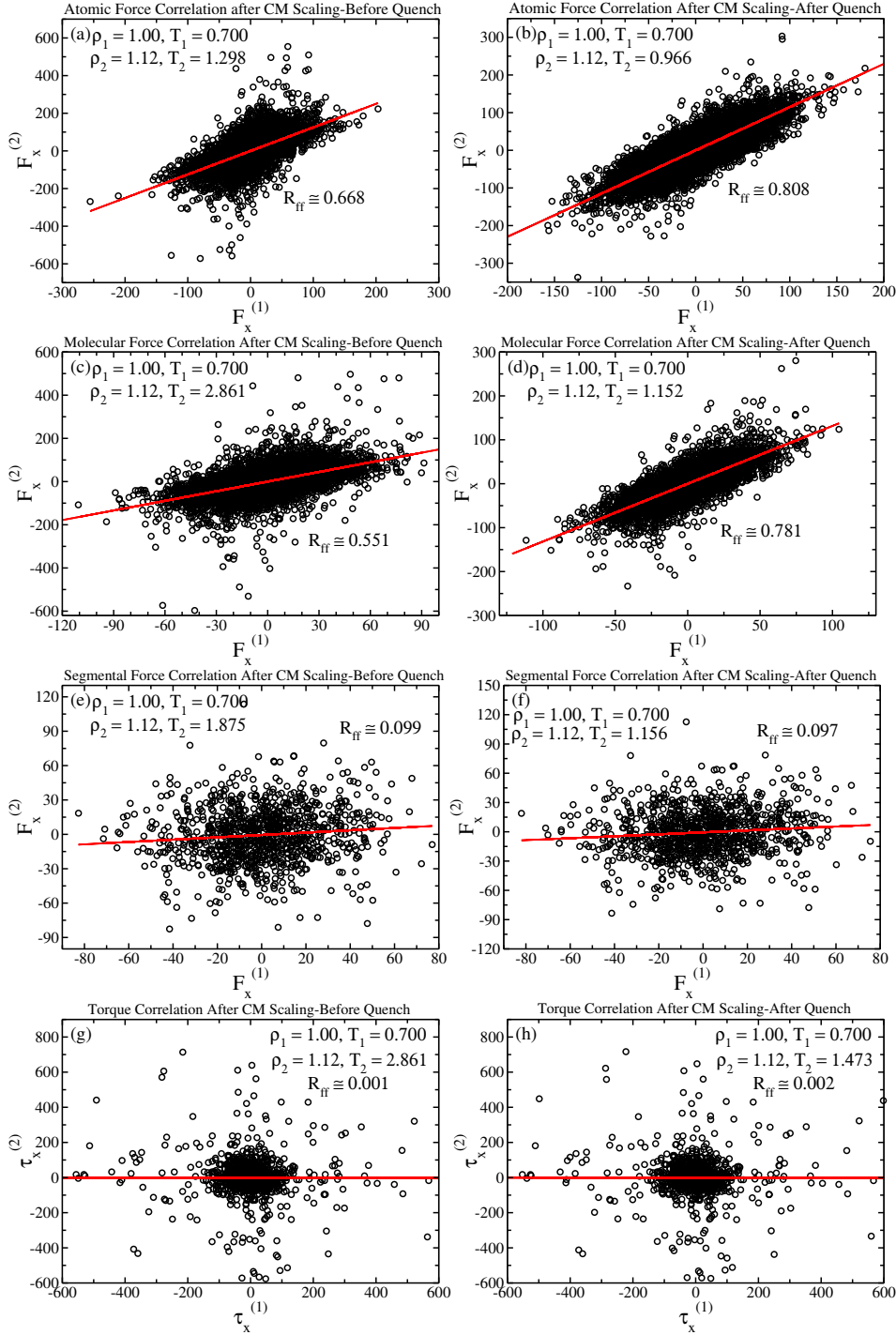
Figure 6.7: Correlation of atomic force (a,b), molecular force (c,d), segmental force (e,f) and torque (g,h) of LJC model with harmonic bonds before and after minimization. One configuration is taken from equilibrium simulation at $(\rho_1, T_1) = (1.00, 0.700)$, after quenching we scale the configuration at higher density $\rho_2 = 1.12$ via CM scaling and do quenching again. Then the new temperature is predicted by forces and torque using equations 3.4, 3.9.

quenching the system after scaling with the same method makes the spring compress (see Figure 6.6). The atomic force and molecular force correlation improve by quenching (see Figure 6.7). In contrast, the segmental force and torque are weakly correlated either before or after minimization (see Figure 6.7).

6.3 Atomic Scaling on Harmonic LJC
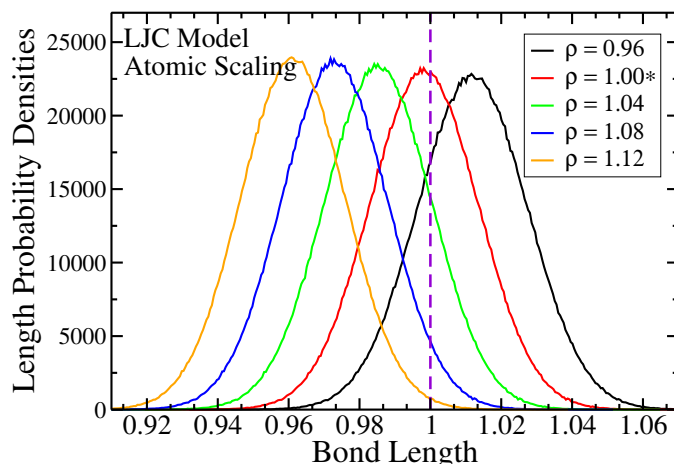
Figure 6.8: The bonds length distribution of harmonic LJC model is shifted by using the atomic scaling. The reference point is $\rho_1 = 1.00$.

The CM scaling method is used in scaling the spring LJC model before and after minimization and the predicted points are far from pseudoisomorph. We now intend to use the atomic scaling method to allow the atoms move freely regardless keeping the CM position fix. In addition, the springs can stretch at lower densities and compress at higher densities from reference length as shown in Figure 6.8, which is not occurred in CM scaling (see Figure 6.6(a)).

The dynamics are invariant along atomic (a, b, c) and segmental force (g, h, i) methods in Figure 6.9 except at lowest density $(\rho, T) = (0.96, 0.883)$ at which pressure is negative. On the other hand, the predicted points via the molecular force method are not pseudoisomorphic (see Figure 6.9(d, e, f)). Consequently, the torque method estimates the appropriate point at densities $\rho = 1.00, 1.04, 1.08, 1.12$, not the lowest and highest densities (see Figure 6.9(j, k, l)).

The atomic scaling method causes the intramolecular interactions increase, so the potential energy is higher than the corresponding quantity obtained from CM scaling (comparing the Table 6.3 with Table 6.1). Furthermore, using the scalar function to quench the system leads to the better minimum potential energy (see Table 6.3). Quenching the system via BFGS
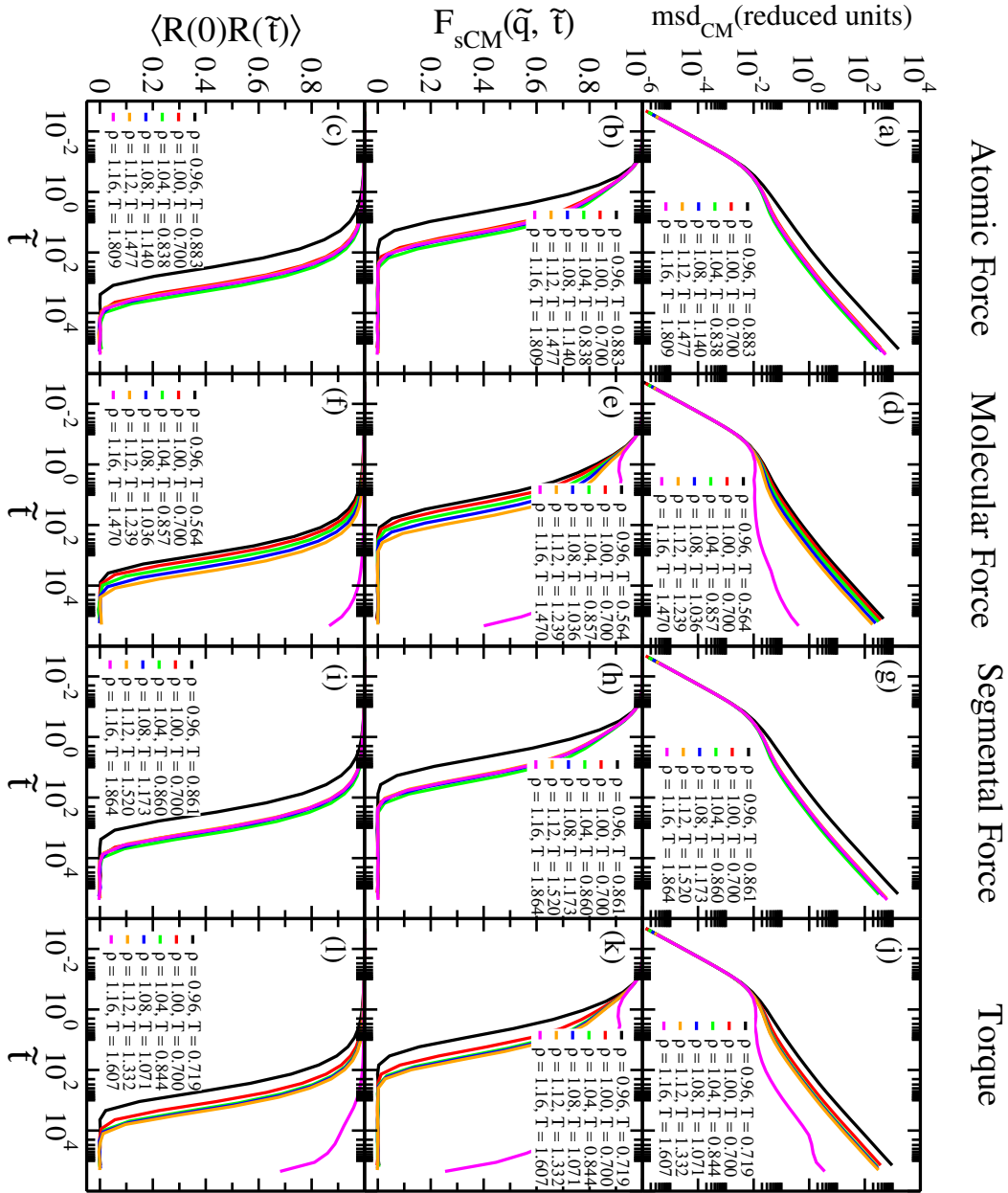
Figure 6.9: The dynamics of the LJC model with harmonic bonds implementing the force methods after using the atomic scaling method. The reference point is $(\rho_1, T_1) = (1.00, 0.700)$. The density increases about 17%. The atomic force method (a, b, c) generate the proper pseudoisomorph at higher densities from the reference point. However, the molecular force method (d, e, f) do not achieve the pseudoisomorphs as expected, the segmental force method (g, h, i) gives the appropriate prediction also at higher densities; And the torque method (j, k, l) provide the good results at some of the densities $\rho = 1.00, 1.04, 1.08, 1.12$.
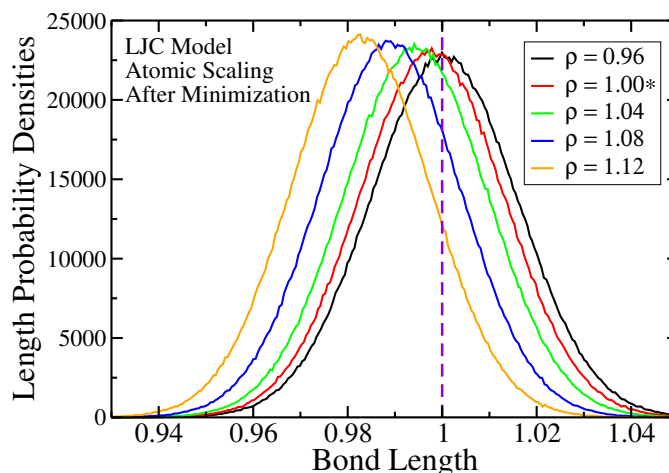
Figure 6.10: Quenching the LJC model by scalar function in constrained space affect the bonds length do not shift a lot at high densities via atomic scaling method. The reference point is $\rho_1 = 1.00$.

method after scale the configurations by atomic scaling, gets better length distribution, not shifted a lot, see Figure 6.10 which indicates that the bonds are not much far from the reference length in compared to Figure 6.8. However, quenching the system does not improve the results and causes the dynamics to change a lot along the atomic force and segmental force methods (see Figure 6.11). The torque method is the only method that gives better dynamics. On the other hand, the predicted temperatures are lower than corresponding results before minimization.

Table 6.3: Using the atomic scaling method before and after quenching the harmonic LJC model. The potential energy increase due to the intramolecular interactions boost in atomic scaling approach. Using the similar minimizing method implemented in Table 6.1, we determine the better minima through the atomic scaling (third column).

Density	U	U_{min}
0.96	-40735.162	-42838.588
*1.00	-42656.196	-42658.487
1.04	-39031.911	-40442.753
1.08	-30469.480	-35603.088
1.12	-17461.024	-27608.887

The structure is measured by segmental total radial distribution function which is invariant along atomic and segmental force methods before we quench the system by using the atomic scaling (Figure 6.12 (a,c)). After Quenching only the torque method gives the invariant structure (Figure 6.12 (h)).
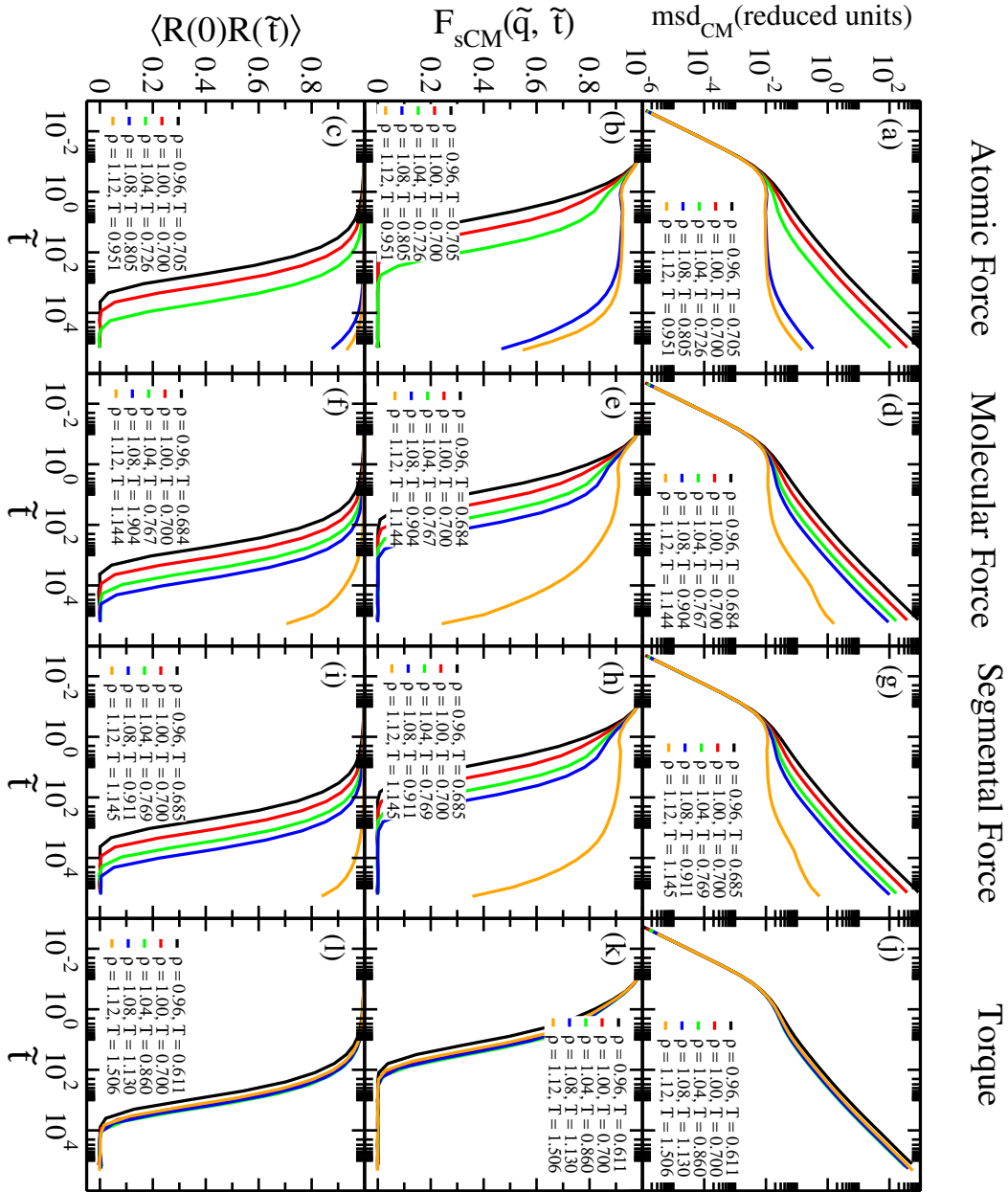
Figure 6.11: Quenching the harmonic LJC model by scalar function and implementing the atomic scaling does not improve the dynamics along invariant forces and torque. The reference point is $(\rho_1, T_1) = (1.00, 0.700)$. The density increases about 17%. The atomic force method (a, b, c), the molecular force (d, e, f), the segmental force (g, h, i) provide poor results compared to Figure 6.9. However, the torque method (j, k, l) achieve good results.
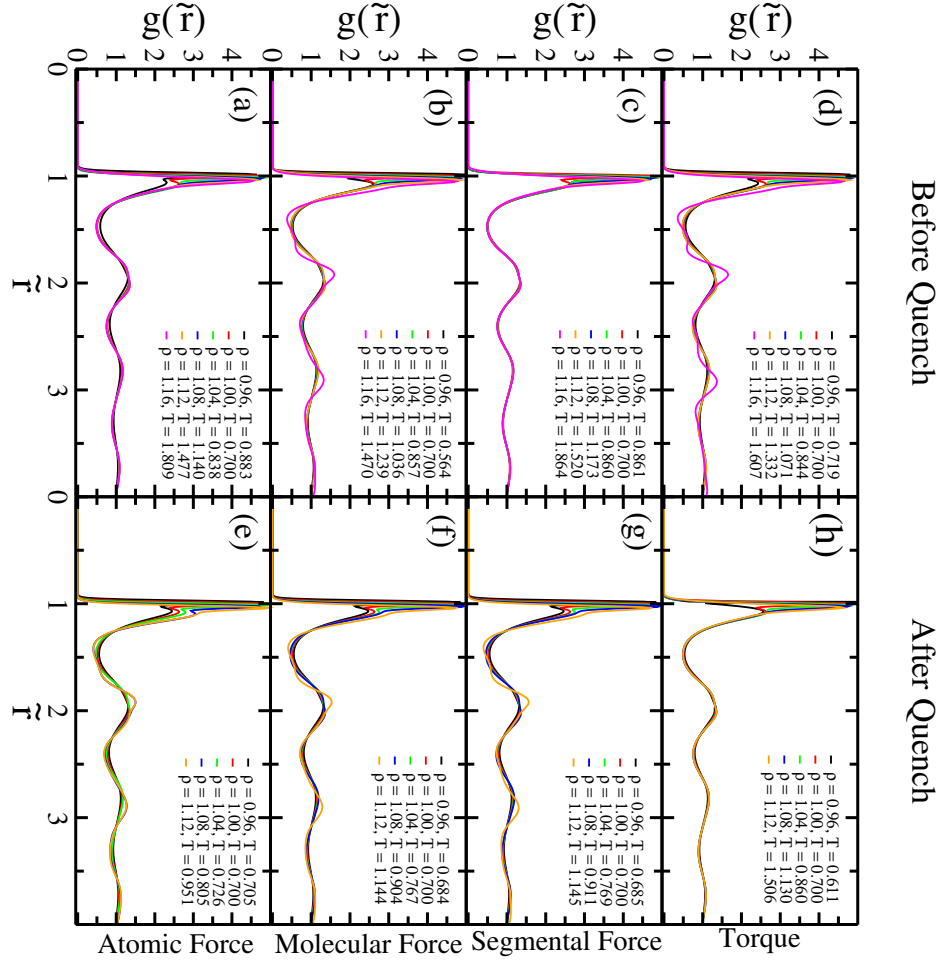
Figure 6.12: The radial distribution function of harmonic LJC model in reduced units along the force methods before and after quenching. The atomic scaling is applied to scale the reference configurations (i.e. equilibrium configurations at state points $(\rho_1, T_1) = (1.00, 0.700)$) to lower and higher densities . The atomic (a) and segmental (c) force predict the better invariant structure before we minimize the system. But the structure are not same at highest density along the molecular force (b) and torque (d) methods. After minimization, the results of torque method get better (h) and the other methods' predictions are not good enough.

Pseudoisomorphs are identified via atomic and segmental force using the atomic scaling method without any quenching in long flexible Lennard-Jones chains model. It is still unknown why the molecular force method is not able to predict pseudoisomorphs in this model and also why the atomic scaling works better than CM scaling approach.

Chapter 7

Conclusions

We have shown, for the first time, an easy and efficient force-based way to trace isomorphs and pseudoisomorphs in molecular systems. Force methods including the atomic, molecular, segmental and torque methods provide astonishing results in small and large molecular liquid models. Isomorphs are usually generated in strongly correlated liquids via configurational adiabats and the direct isomorph check method. Identifying isomorphs via these methods require several number of configurations from a long simulation which is not efficient in time and energy. This issue has disappeared by developing the force methods which only need a single configuration to trace an isomorph. On the other hand, pseudoisomorph can not be generated along configurational adiabats and the direct isomorph check method since W-U correlations break down in harmonic bonded models. The method developed by Olsen *et. al* [2] is a rather tedious method to trace pseudoisomorph; While the force methods are able to generate pseudoisomorphs in harmonic bonded models by using a single equilibrium configuration easily and efficiently.

The atomic force, molecular force and torque methods produce comparable results in comparison with configurational adiabats and the direct isomorph check method in small molecular models with rigid bonds (i.e. ASD, IPL and OTP models). Since the isomorph theory is not exact, there are few differences in details of which method works better in which model but the force methods still provide comparable isomorphic state points. Even so, the intramolecular interactions affect the atomic force calculation but it still finds isomorphs in most of the small molecular models. Overall the molecular force method is considered as a general method to find better invariant curves in all small molecular R-simple models. The torque method also generate appropriate results. The new force methods are also tested on long flexible a Lennard-Jones chains (LJC) model and they do not determine isomorphs in this large molecular model. Even though these methods do not seem to work for flexible Lennard-Jones chains as well as ASD, IPL

and OTP models, it is revealed that the force methods can still predict appropriate isomorphic state points for small density changes.

Identifying pseudoisomorphs in spring bonded models was very difficult and it needed a lots of effort before we developed the force methods. Now, generating pseudoiomorphs in small and large molecular models can be easily done using the force methods. Pseudoisomorphs are found in ASD and OTP models at low densities via molecular force and torque methods, while the atomic force method do not predict the proper temperatures because of the vibrational intramolecular interactions.

If one increases the densities the proper invariant curves predicted via molecular force method disappears due to the bond lengths compression and vibrational intramolecular interactions. At high densities, the pseudoisomorphs appear after we eliminate the unscaled degrees of freedom of springs by defining a scalar function in a constraint space considering two conditions and applying the BFGS optimization method. We try to keep the center-of-mass position of each molecule fixed and update the position of particles along the bond direction in the scalar function and then we use the BFGS method to find the local minima of the potential energy surface. We also find the local minima via a vector function using conjugate gradient method. Force methods are not able to identify pseudoisomorphs after quenching via the vector function in ASD model. In contrast, we create pseudoisomorphs in IPL model via force methods after quenching via the vector function. In addition, two scaling method are considered in spring models, namely atomic scaling (AS) and center-of-mass scaling (CMS) approaches. Both scaling method do not provide the pseudoisomorphic state points for ASD model at high densities before quenching. While, the molecular force method predicts the most proper pseudoisomorphic state points after quenching. The results of molecular force and torque method are the same using the atomic and center-of-mass scaling approaches after we minimize the potential energy. The atomic force method which is affected by the vibrating bonds, does not detect the pseudoisomorph in harmonic ASD model neither before nor after quenching.

Dynamics and structure of flexible Lennard-Jones chains with spring bonds are investigated at low density at which force methods do not predict pseudoisomorphs through the center-of-mass scaling approach. While the atomic and segmental force methods find the invariant curves by applying the atomic scaling method. Pseudoisomorphs in LJC model at low density are found without any quenching.

In summary, we have shown that it is possible to predict invariant structure and dynamics via a density scaling property i.e. invariant force in reduced units in molecular models composed of rigid or spring bonds. Even though, configurational adiabats and direct isomorph check method has been used to detect the isomorphs over ten years, the force methods must be considered as new generic methods. The molecular force method is the most

prominent method not only to generate isomorphs but also to generate pseudoisomorphs in vibrational space in small molecular models. In some cases, the torque method also succeeds to gain proper results.

One of the possible improvements and extension of this work would be to investigate the dynamics of larger molecular models to find a generic force-based method to identify isomorphs in this larger models for the large density changes. Furthermore, generalizing isomorph theory to rigid bonded molecular models and define the pseudoisomorph theory in harmonic spring bonded models can be a subject of ongoing research and requires further work.

Appendix A

Problems Dealing with OTP

OTP model with rigid bonds is one of the molecular models which we consider to test the forces methods. Since there is a strong correlation between the virial and potential energy of this model (Figure 3.6(b)), it has been classified as the R-simple liquid and it has isomorphs. Testing the force methods on OTP reveals that these methods can trace the isomorphs when the system is scaled to higher densities (Figure 3.9). This means that the structure and dynamics predicted by force methods are invariant at higher densities from reference point. Figure 3.12 and Figure 3.15 represents the perfect collapse in dynamics in OTP when we start from point $(\rho_1, T_1) = (0.303, 0.383)$ and then increase the density to $0.315, 0.327, 0.340, 0.353$. But if we start from a point with high density $(\rho_1, T_1) = (0.340, 0.903)$ and decrease the density dynamics is not invariant along the predicted state points via force methods.

Figure A.1 represents this issue via atomic force (a, b, c), molecular force (d, e, f) and torque (g, h, i) methods along curves with 12% density decrease. It is clear that the dynamics are not invariant by jumping down to lower densities. In addition, the relaxation times change along force method more than along the configurational adiabats and DIC method (Figure A.2).

To explain in detail, we investigate the bond length probability distribution of the longer bond in each molecule by jumping up and down in density. Apparently, the bond lengths of molecules are preserved at different densities (Figure A.3). So the scaling affects the OTP configurations neither at high nor at low densities. By looking at the dynamics quantity, e.g. molecular force, it has been found that the molecular forces still have strong correlation by decreasing the density (Figure A.4).

To investigate the effect of scaling on predicting the temperature via the molecular force method, we used one configuration taken from equilibrium simulation at $(\rho, T) = (0.303, 0.383)$ and scaled it to the density $\rho = 0.340$ to measure the statistics of the desired temperature each molecule intend to have. The probability density distribution of each molecule's temperature
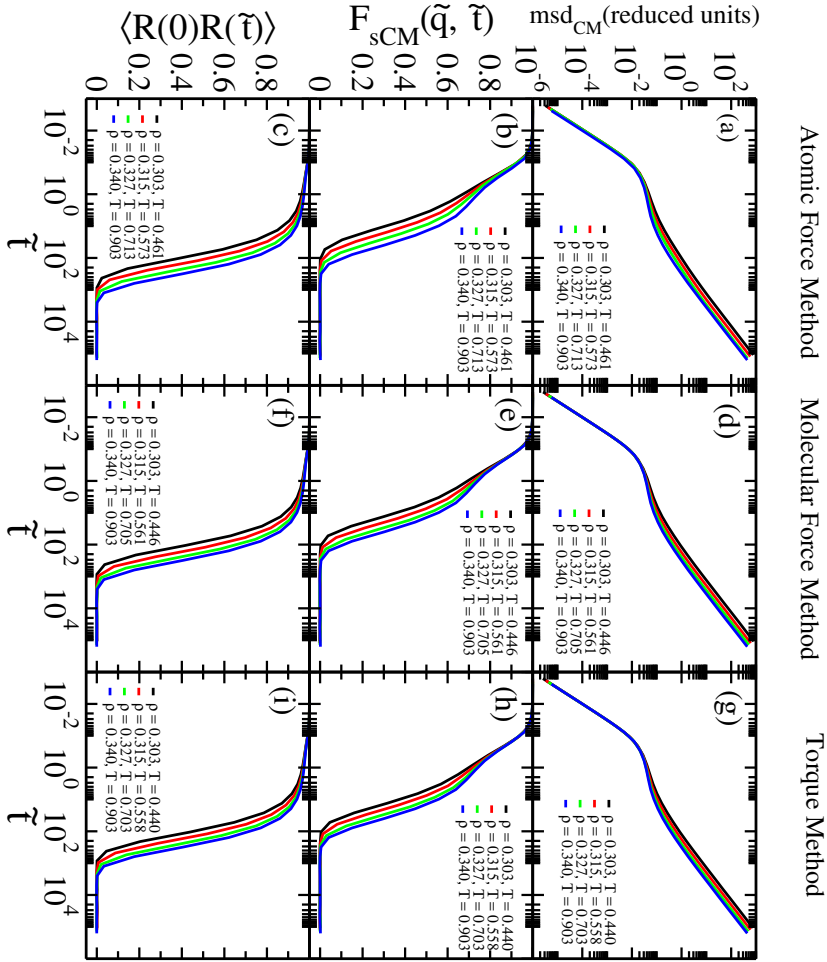
Figure A.1: Investigating the dynamics of OTP through the predicted state points via three new force methods. The similar reduce-units dynamical quantities from Figure 3.9 are considered. Here, the reference state point is $(\rho_1, T_1) = (0.340, 0.903)$. (a, b, c) Show the dynamics deviation along the predicted state points by atomic force method. (d, e, f) Show the results of checking the molecular force. However this method has been confirmed as the best method in ASD, IPL and OTP (Figure 3.12). (g, h, i) Shows the torque method does not also work for OTP by scaling to lower densities.
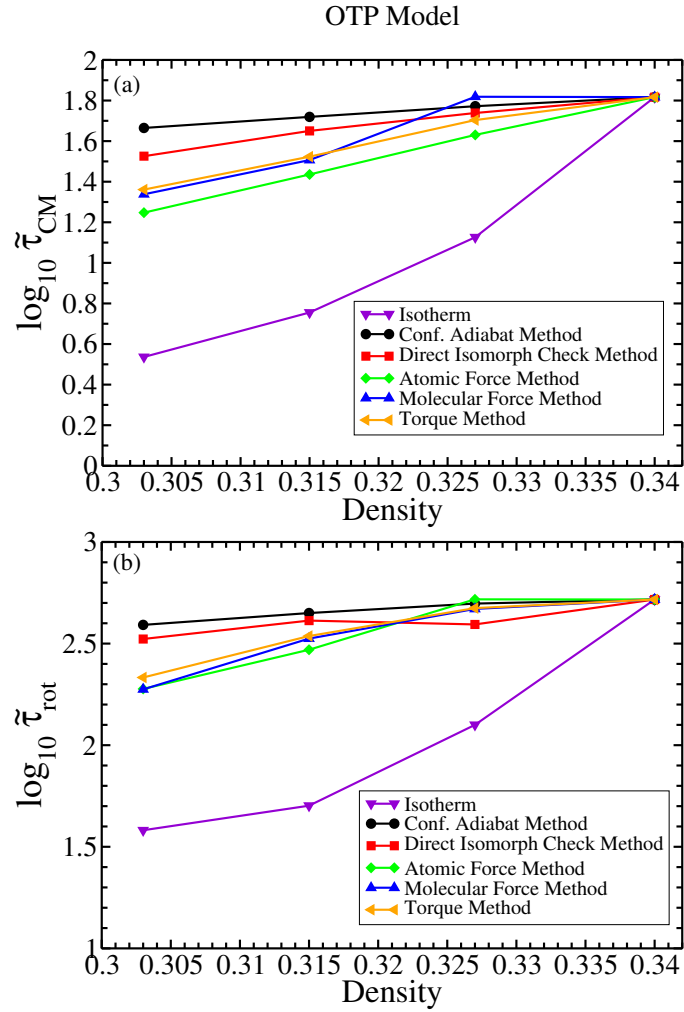
Figure A.2: Show the translational (a) and rotational (b) relaxation times for OTP model by starting from $\rho = 0.340$ and jumping down to lower density. Both relaxation times of isomorph methods do not show the large deviation like isotherm and they are approximately invariant.
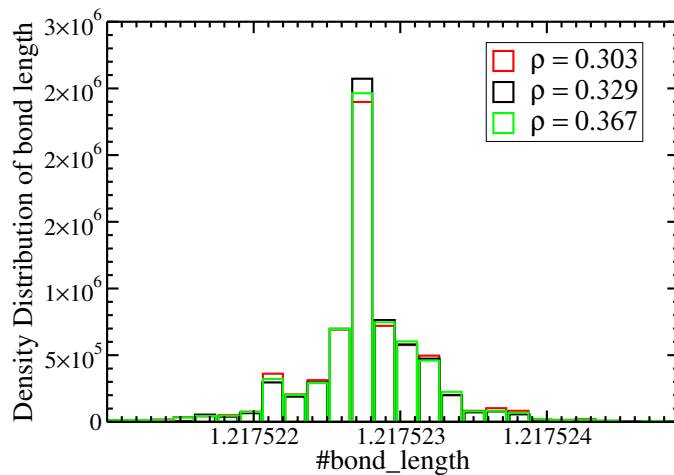
Figure A.3: The probability distribution of longest bond length in OTP molecules. We scale the system at lowest density,$\rho = 0.303$, and highest density, $\rho = 0.367$, by staring from $\rho = 0.329$.

Molecular Force Correlation of Only One Configuration
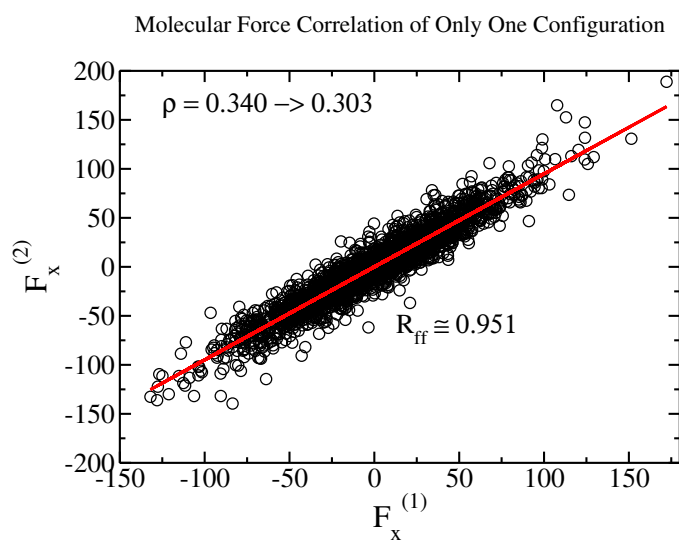
Figure A.4: The correlation of molecules' forces at the $\rho = 0.340$ and jump to $\rho = 0.303$. They still have a strong correlation regardless of which density we start from.

are presented in Figure A.5 which have the peak around $T = 0.903$ (red curve). To check the method gives the right temperature or not, we took an equilibrium configuration at $(\rho, T) = (0.340, 0.903)$ and then scaled it to $\rho = 0.303$ and again change the density to $\rho = 0.340$, it gave the same probability in Figure A.5 (black curve).
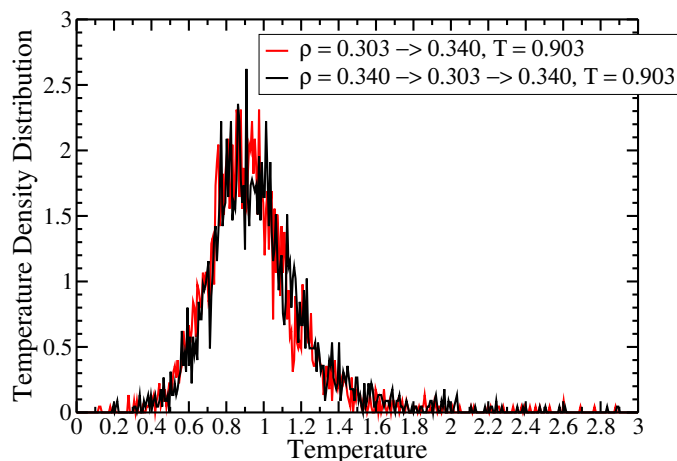
Figure A.5: The probability distribution of the temperature which each molecule desires. Shows the molecular force method always predict the right temperature of the configurations by increasing the density. By scaling to higher density $\rho = 0.340$ from reference point $\rho = 0.303$ we calculated $T = 0.903$ (red). On the other hand, it has been manifested that if we start from density $\rho = 0.340$ and jump down to density $\rho = 0.303$ and then increase the density, it gives the same $T = 0.903$ (black).

So we have clarified that the isomorphs methods work very well for OTP model only if we increase the density. Now we confirm this by showing the statistics of the molecules' temperature when the densities decrease. For the density $\rho = 0.303$ the molecules' temperatures are expected to be $T = 0.383$ regardless which density we choose as the reference point. For instance, if we take a configuration of equilibrium simulation at $\rho = 0.303$ and change the density to 0.340, then back to staring density again the temperature distribution is peaked around 0.383 according to Figure A.6 (black). In contrast, we realized that if we take a equilibrium configuration at $\rho = 0.340$ and decrease the density to $\rho = 0.303$ it predicts $T = 0.440$ which is far from the expected temperature.

The OTP model is the only model struggling with density changes which is still unknown. It has been shown the dynamics of the IPL model remains invariant when the density decreases (see Figure A.7).
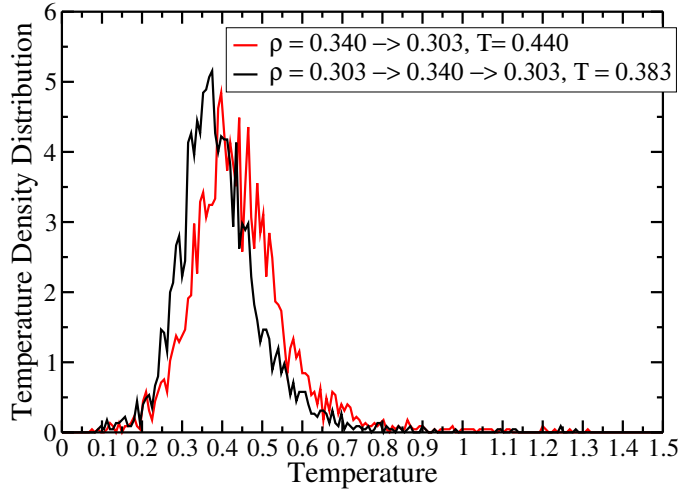
Figure A.6: Shows the similar probability distribution in Figure A.5. But we check the process by jump down in low density. For the state point $\rho = 0.303$ the temperature is anticipated to be about $T = 0.383$ (black), and it is not dependent on starting point, but when we take a uscaled equilibrium configuration $\rho = 0.340$ and scaled it to lower density $\rho = 0.303$ the temperatures are obtained around $T = 0.440$.
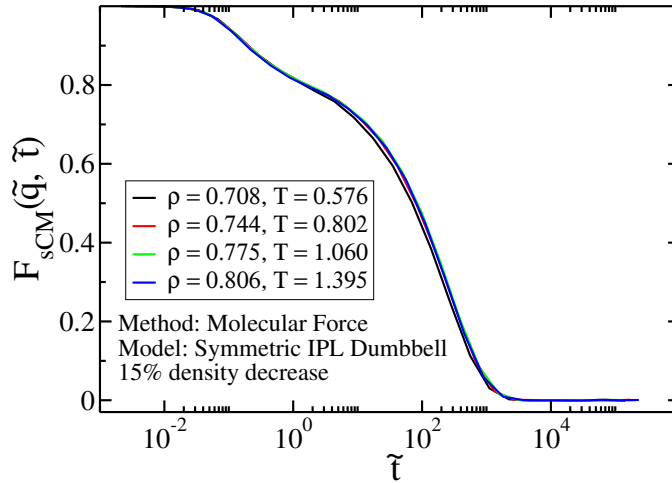
Figure A.7: Testing the molecular force method on IPL model through the density decrease over 15%. It shows the incoherent intermediate scattering function in reduced units is still invariant by scaling the system to lower densities. Here, $(\rho, T) = (0.806, 1, 395)$ is the reference point.

111

Appendix B

Forces Methods in LJC Model

As shown in Figure 4.2 in section 4.4 the new methods do not find the isomorph in rigid bonded LJC model, because of the non-scaled intramolecular bonds. But if we test the force methods in small density changes, the dynamics become invariant. Figure B.1 confirms that the force methods predict isomorphic state points for small density ranges about 8% in LJC model with rigid bonds.

The relaxation times in reduced units improve along the forces methods at small density changes. The translational and rotational relaxation times are plotted in Figure B.2 and they both are invariant in comparison with isotherm.
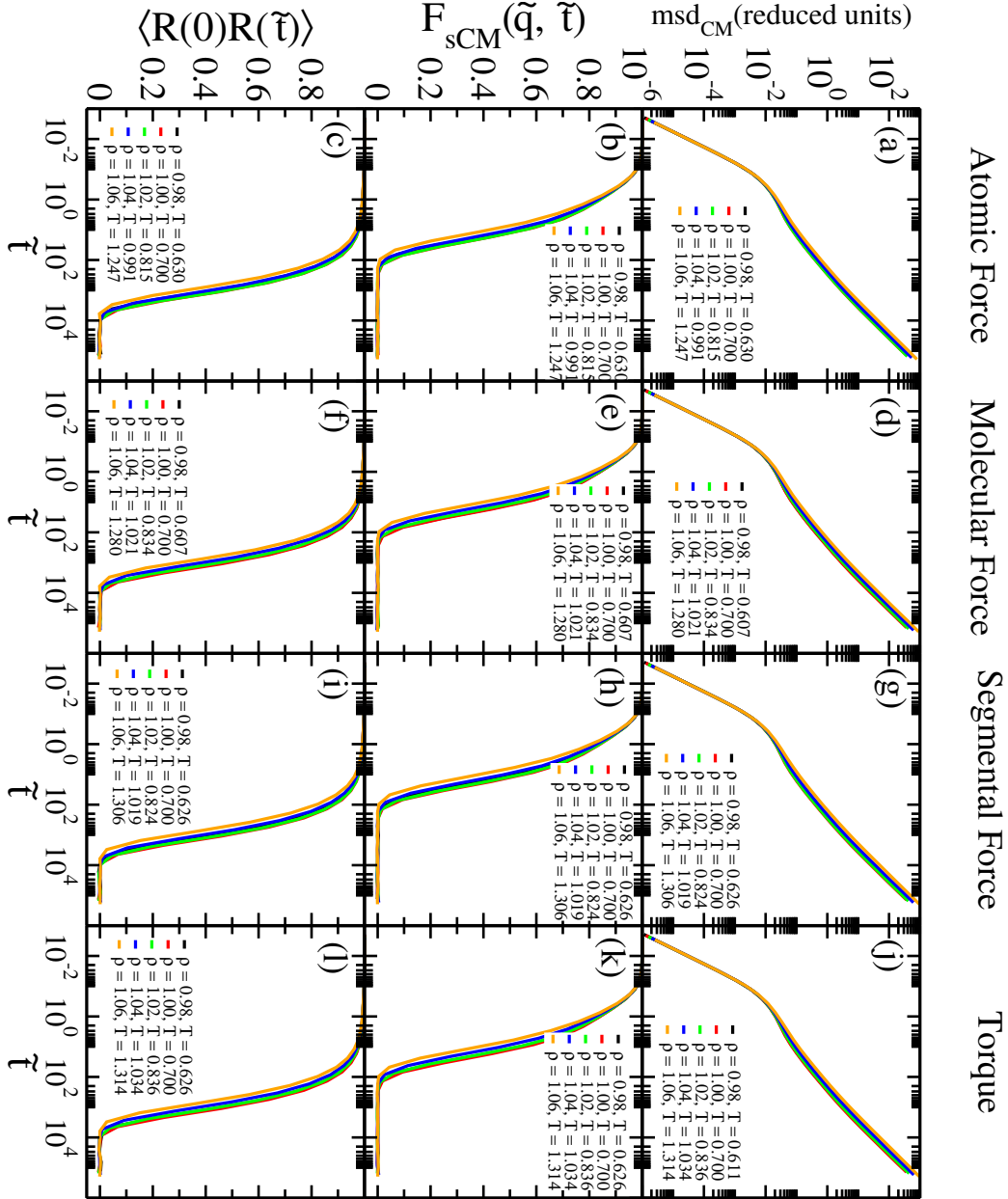
Figure B.1: Show the dynamics of LJC along the invariant reduced atomic force (a, b, c), molecular force (d, e, f), segmental force (g, h, i) and torque (j, k, l) curves. The mean square displacement, incoherent intermediate scattering function and normalized orientational autocorrelation function of the end-to-end vector are invariant in reduced units. The density changes over 8% from the starting point $(\rho_1, T_1) = (1.00, 0.700)$.
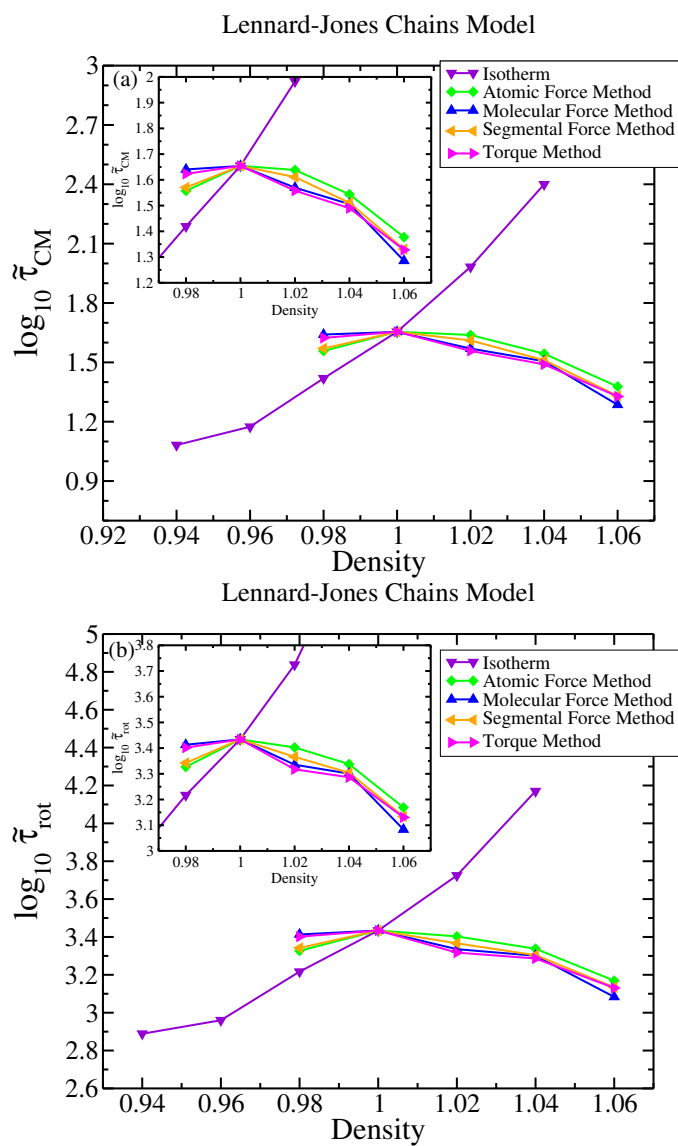
Figure B.2: Comparing the translational (a) and rotational (b) relaxation time in reduced units along the isotherm and forces methods. In low density ranges the relaxation times hold more invariant compared to Figure 4.4, and they are entirely different along the isotherm.

Appendix C

Configurational Adiabats in Spring Bonded IPL and OTP Models

The dynamics of spring harmonic bonded models are not invariant along the configurational adiabats because the excess entropy is not constant in these models and scaling exponent γ can not identify pseudoisomorphs. The dynamics of IPL model and OTP model" are shown to be not invariant along configurational adiabats in Figure C.1. The state points are found by equation 2.18 changing the density by 1% in each jump from the reference point $(\rho_1, T_1) = (0.806, 1.100)$ in IPL model and $(\rho_1, T_1) = (0.329, 0.700)$ in OTP model.
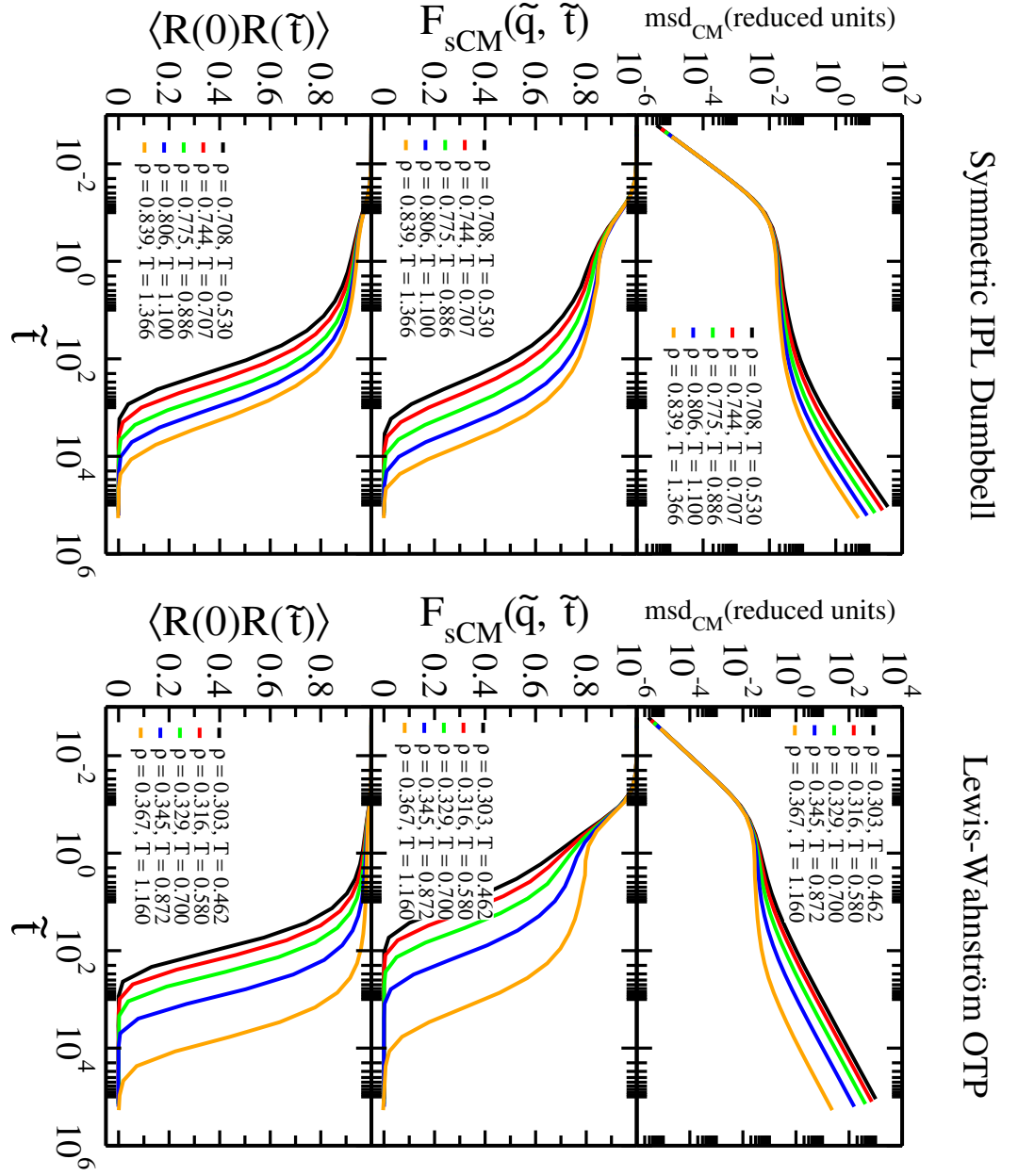
Figure C.1: Show the dynamics of IPL and OTP models with harmonic bonds along configurational adiabats are not invariant. $(\rho_1, T_1) = (0.806, 1.100)$ is the reference point in the IPL model and we consider $(\rho_1, T_1) = (0.329, 0.700)$ as the reference point for OTP. The density increases about 20%.

Appendix D

Pseudoisomorph in IPL Model

We chose the symmetric IPL dumbbell model with harmonic bonds as the second model to identify pseudoisomorph via force methods. IPL model is small molecules systems which are highly viscous. 5000 molecules in this model consist of two identical atoms connected via harmonic oscillations with length $r_{i,j} = 0.584$. The intermolecular interactions obey the IPL potential with exponent $n = 18$ (chapter 2) with unit parameter. The intramolecular interactions are harmonic with spring stiffness $k = 3000$. Since the structure remains invariant in harmonic models, we only check the dynamics in this section.

As shown in Figure C.1, the scaling exponent γ does not provide pseudoisomorphic points because the W- U correlation is broken down in models with harmonic intramolecular interactions. The DIC and force methods also provide incompatible results because of the bending and stretching bonds in Figure D.1. We used the CM scaling in Figure D.1 in which the dynamics vary quite much. On the other hand, atomic scaling gives different results since the potential energy and consequently the forces and torque are ob-

Table D.1: Predicted T via atomic force method (second column), molecular force method (third comĺumn), torque method (fourth column) and DIC method (fifth column) by applying the atomic scaling. The atomic force results are quite unfavourable. Both molecular force and toque create the same results.

density	$T(F_{Atomic})$	$T(F_{Mol})$	T(Tor)	T(DIC)
0.708	1.095	0.505	0.505	0.497
0.744	0.998	0.680	0.680	0.690
0.775	1.011	0.869	0.869	0.880
0.806	1.100	1.100	1.100	1.100
0.839	1.260	1.399	1.399	1.371
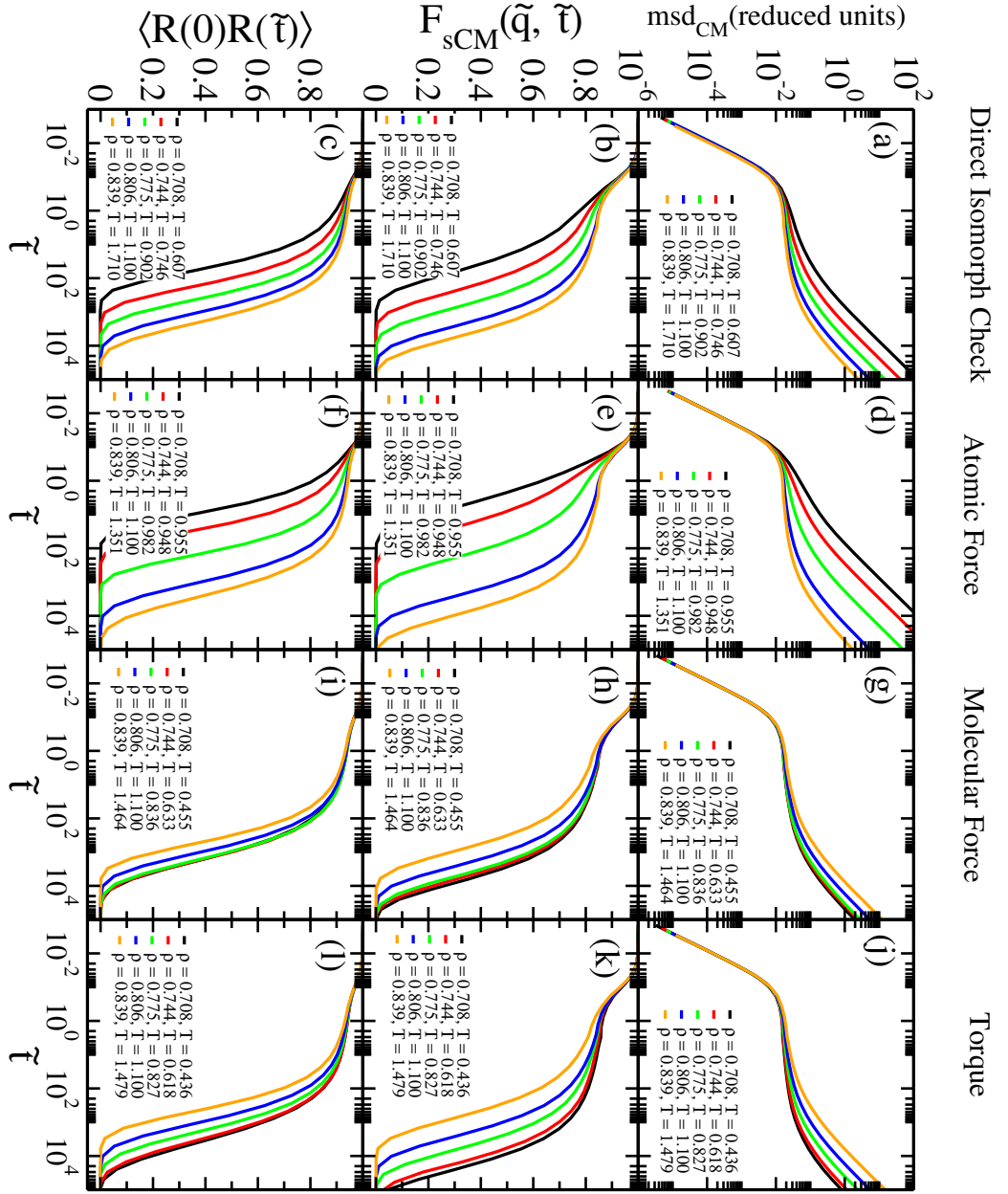
Figure D.1: Show the dynamics of IPL with harmonic bonds along DIC method (a, b, c), atomic force method (d, e, f), molecular force method (g, h, i) and torque method (j, k, l). The reference point is $(\rho_1, T_1) = (0.806, 1.100)$. The density increases about 20%. The dynamics vary along DIC method and also along the force and torque methods. CM scaling is used here.
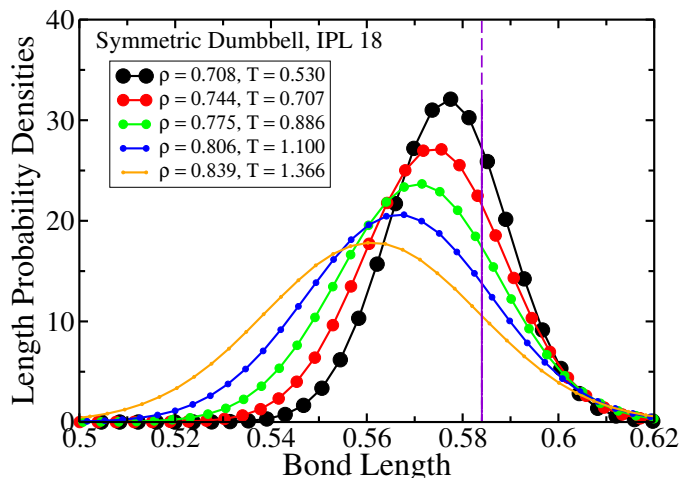
Figure D.2: Show the bond lengths distribution of IPL configurations taken from equilibrium simulation at state points predicted via molecular force method before minimization. The reference point is $(\rho_1, T_1) = (0.806, 1.100)$. It shows the bond lengths decrease by scaling the configurations to higher densities.

tained approximately different. Predicted state points via DIC and force methods through the atomic scaling is presented in Table D.1. The molecular force and torque method predict same temperature using atomic scaling. Any of the methods can not find pseudoisomrphs in IPL model because the bond lengths distribution are compressed by increasing the density in Figure D.2. Hence, the systems need to be quenched to generate pseudoisomorph via force methods.

D.0.1 Quenching via a Scalar Function

It is required to eliminate the unscaled degrees of freedom by quenching the system. We now consider two conditions (i.e. keep the center-of-mass and the bonds' orientational direction fixed) and use both center-of-mass scaling and atomic scaling to test the force methods after quenching. We use both minimization methods, i.e. BFGS and CG method, to create the pseudoisomorphs in this section. Quenching the IPL model is much easier than quenching the ASD model. Since particles in IPL models have identical mass we can use the equation 5.15 with $m_A = m_B = 1$,

$$\begin{pmatrix} \mathbf{dr_{A,k}} \\ \mathbf{dr_{B,k}} \end{pmatrix} = \begin{pmatrix} \dfrac{1}{2} \\ -\dfrac{1}{2} \end{pmatrix} \times dl_k \hat{\mathbf{l}}_{\mathbf{k}}. \tag{D.1}$$

Equation D.1 defines a scalar function which we can use to find the local minima in IPL models via BFGS optimization method. The molecular

Table D.2: Test the atomic force and DIC methods after quenching and remove the spring's contribution in calculating the potential and force. The temperatures are far from pseudoisomorphic state points in Figure D.3 (g, h, i).

density	U	U_{min}	T(DIC)	$T(F_{Atomic})$
0.708	29380.606	25369.488	0.196	0.560
0.744	39082.553	35023.324	0.268	0.646
0.775	50012.381	46063.906	0.434	0.848
0.806	63925.787	58902.953	1.100	1.100
0.839	82791.457	75107.396	0.596	1.418

Table D.3: Using the scalar function to quench the system after scaling via atomic scaling. DIC (fourth column) method and atomic force method (fifth column) create quite distinctive T in compared with Figure D.3. But the molecular force method (sixth column) and torque method (seventh column) approximately estimate comparable T in comparison with using the CM scaling (Figure D.3).

density	U	U_{min}	T(DIC)	$T(F_{Atomic})$	$T(F_{Mol})$	T(Tor)
0.708	30358.672	28708.306	0.571	0.885	0.475	0.465
0.744	39296.630	38777.029	0.707	0.922	0.657	0.649
0.775	50083.806	49964.634	0.880	0.990	0.856	0.852
0.806	63925.787	63919.768	1.100	1.100	1.100	1.100
0.839	82305.139	82300.285	1.339	1.268	1.412	1.416

force and torque methods predict pseudoisomorphic state points by using the CM scaling method after quenching in Figure D.3). Whereas, the direct isomorph check and atomic force method which are affected by harmonic intramolecular interactions can not identify pseudoisomrphs.

The temperatures in table D.2, which are predicted by DIC and atomic force method after quenching via the scalar function and remove the spring force contribution, are still not desirable results in compared to Figure D.3 (g, h, i).

The potential energy and minimum of potential are different when we use atomic scaling approach. Table D.3 shows the results of DIC and force methods after quenching via a similar function (i.e. equation D.1) and atomic scaling method. Since the intramolecular interactions are different along different scaling methods, DIC and atomic force method provide different results comparing with Figure D.3 but molecular force and torque method, in which the effects of the intramolecular interaction are ignored, predict quite the same temperatures. If we abolish the harmonic potential, the DIC method identifies inconsistent results, but the atomic force method provides comparable temperatures according to table D.4 and table D.2.

Figure D.3: The IPL system's dynamics with harmonic bonds after scaling the system with CM scaling method and then quench it via the scalar function (equation D.1). Quenching the system helps methods to identify pseudoiso-morph in IPL model. Direct isomorph check method (a, b, c), atomic force method (d, e, f) do not predict invariant dynamics even after minimization. Whereas, molecular force (g, h, i) and torque method (j, k, l) predict good invariant dynamics.

Table D.4: Minimum of potential and predicted temperatures after applying atomic scaling and quenching via scalar function without spring contributions. DIC method results are entirely inappropriate and the atomic force method generates quite comparable results in comparison with the Table D.2.

density	U	U_{min}	T(DIC)	$T(F_{Atomic})$
0.708	30358.672	25325.066	0.159	0.560
0.744	39296.630	35122.698	0.245	0.646
0.775	50083.806	45847.652	0.202	0.850
0.806	63925.787	58902.953	1.100	1.100
0.839	82305.139	75104.077	0.441	1.416

D.0.2   Quenching via a Vector Function

After quenching via scalar function, the molecular force and torque methods identify the proper pseudoisomorph in IPL molecular model with harmonic bonds. In this section, we try the minimize the system by a vector function through the conjugate gradient method (CG). According to the equation for the IPL model with $m_A = m_B = 1$, the function is defined by,

$$
\begin{aligned}
\frac{\partial U(\mathbf{L_k})}{\partial \mathbf{L_k}} &= \frac{1}{2}\frac{\partial U}{\partial \mathbf{r_k}}\hat{\mathbf{l}}_\mathbf{k} - \frac{1}{2}\frac{\partial U}{\partial \mathbf{r_{k+1}}}\hat{\mathbf{l}}_\mathbf{k} \\
&= \frac{1}{2}F_A - \frac{1}{2}F_B.
\end{aligned} \tag{D.2}
$$

Using equation D.1 and equation D.2 via CG optimization method can find the local minima of IPL model. Both scaling methods are tested to investigate this minimization method. Figure D.4 indicates that the system's dynamics improve by using the vector function to minimize the system along DIC method and invariant forces and torque. The atomic force and molecular force produce approximate same results. The torque method provides the proper pseudoisomorphs in Figure D.4. The results of both scaling methods, i.e. CM and atomic scaling are roughly the same (see Table D.5).

The molecular force and torque methods generate pseudoisomorphs in IPL model after we quench the system via both scalar function and vector function, while the atomic force and DIC methods only predict proper invariant dynamics after quenching via the vector function. It is anticipated the force methods can identify pseudoisomorphs in IPL model at lower densities without any minimization.
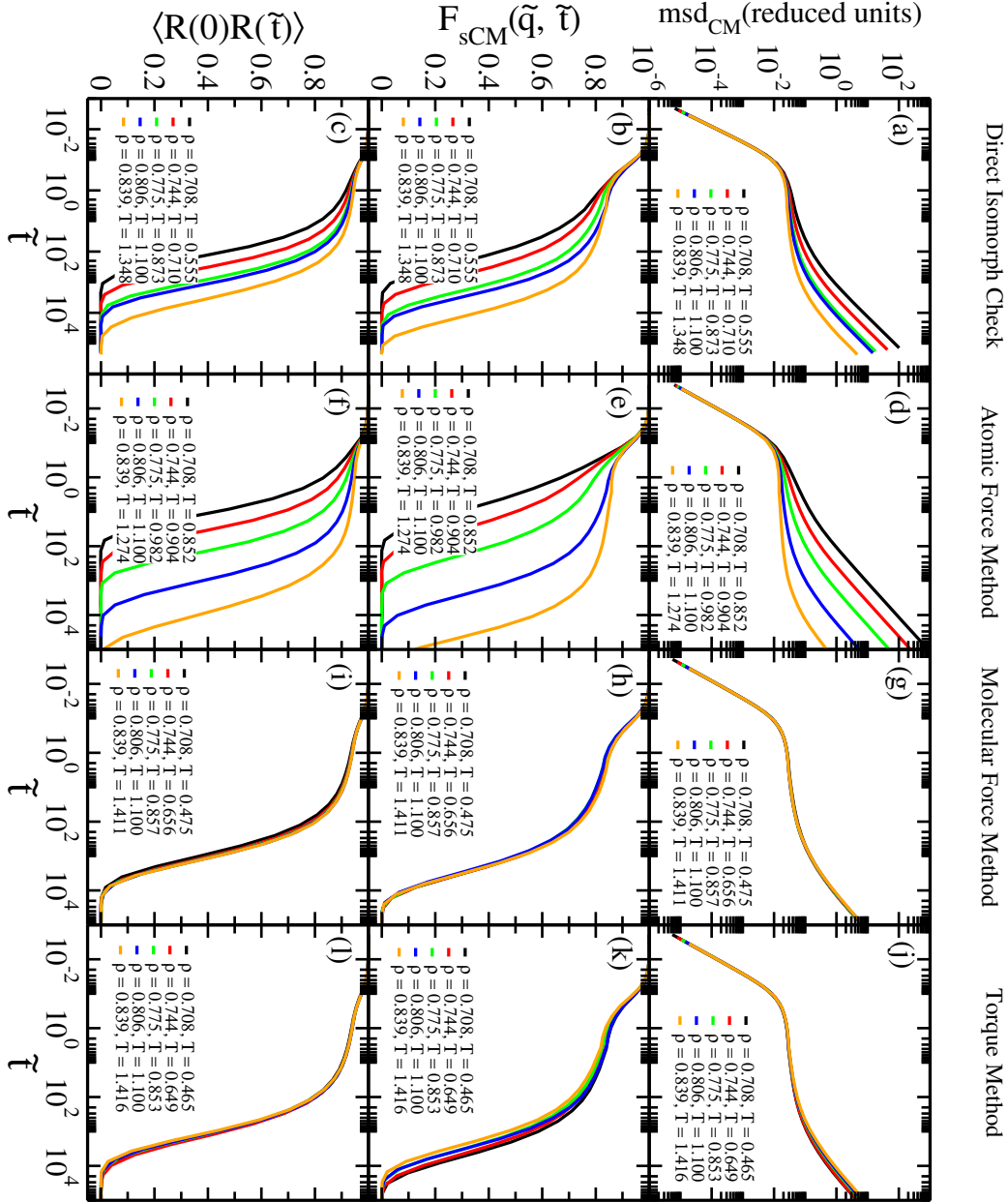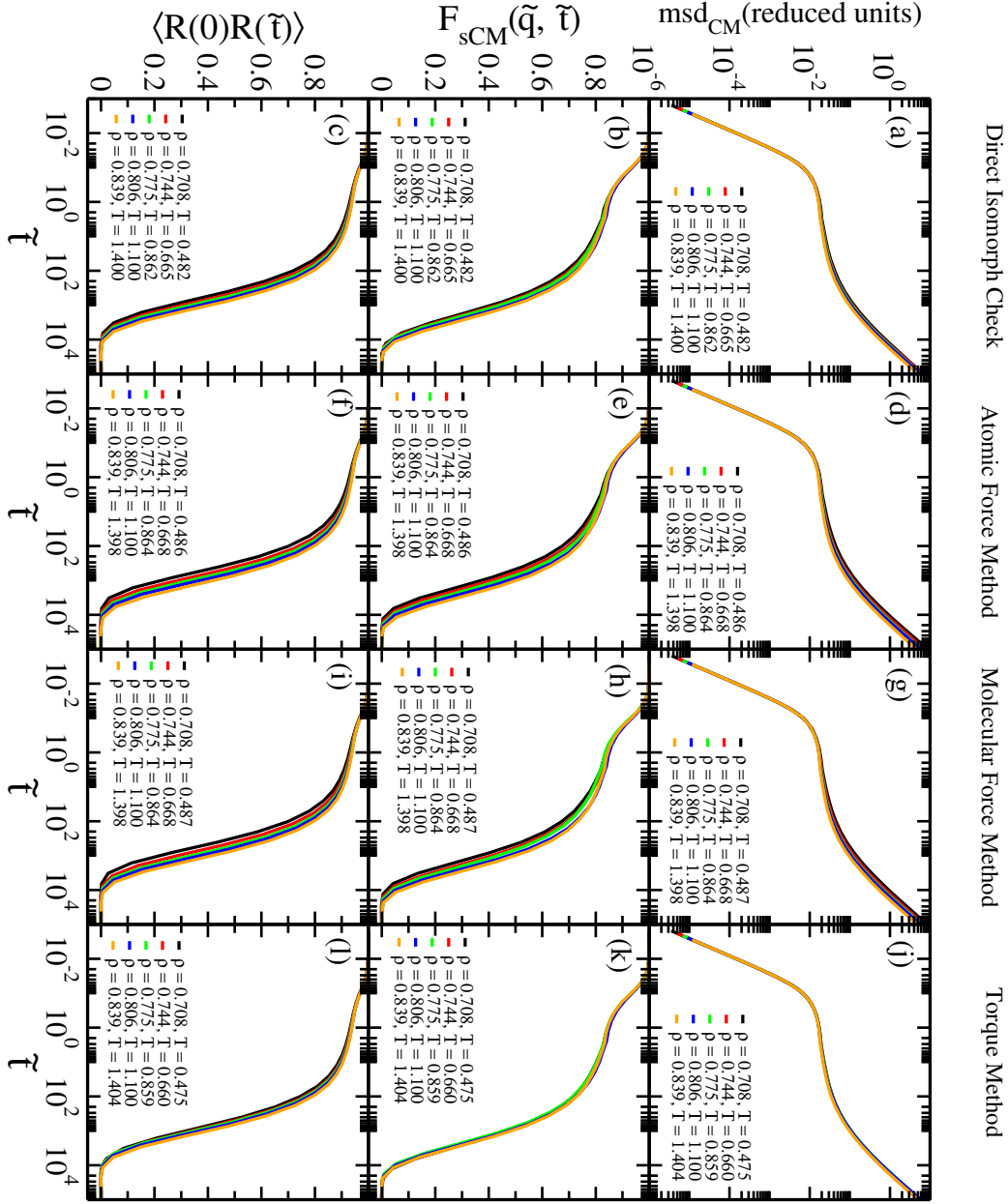
Figure D.4: The IPL system's dynamics with harmonic bonds after scaling the system with CM scaling method and then quench it via the vector function using equations D.2, D.2. The direct isomorph check method (a, b, c), atomic force method (d, e, f), molecular force (g, h, i) and torque method (j, k, l) provide good invariant dynamics.

Table D.5: Potential, minimum of potential and predicted temperatures via atomic scaling and after quenching via vector function by DIC and force methods. Using the vector function reaches much more minima value than the scalar function in Table D.3. The atomic scaling method gives the same results as using CM scaling method.

density	U	U_{min}	T(DIC)	$T(F_{Atomic})$	$T(F_{Mol})$	T(Tor)
0.708	30358.672	25869.033	0.482	0.487	0.486	0.475
0.744	39296.630	36042.350	0.665	0.668	0.668	0.660
0.775	50083.806	47285.757	0.862	0.864	0.864	0.859
0.806	63925.787	61247.613	1.100	1.100	1.100	1.100
0.839	82305.140	79557.679	1.400	1.398	1.398	1.404

Appendix E

Pseudoisomorph in OTP Model

We found isomorph in constraint bonded OTP model via molecular force method (see Figure 3.12) and torque method in Figure 3.15. Furthermore, we recognized that isomorphs are predicted in the OTP model by scaling the configuration at higher densities from the reference state point. This section investigates how to generate pseudoisomorphs in the OTP model with harmonic spring bonds and whether it requires minimization or not.
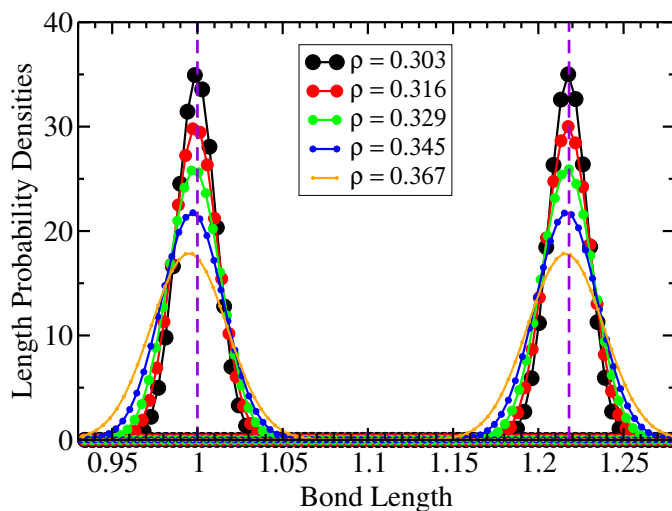
Figure E.1: Show the bond lengths distribution of OTP configurations taken from equilibrium simulation. The reference point is $\rho_1 = 0.329$. It shows that the bond lengths do not compressed by scaling the configurations to higher densities.

By considering the density $\rho = 0.329$ as the reference point, the bond lengths have proper distributions at the different densities, and they prevent to compress since the system is not highly viscous. Since the OTP model

125
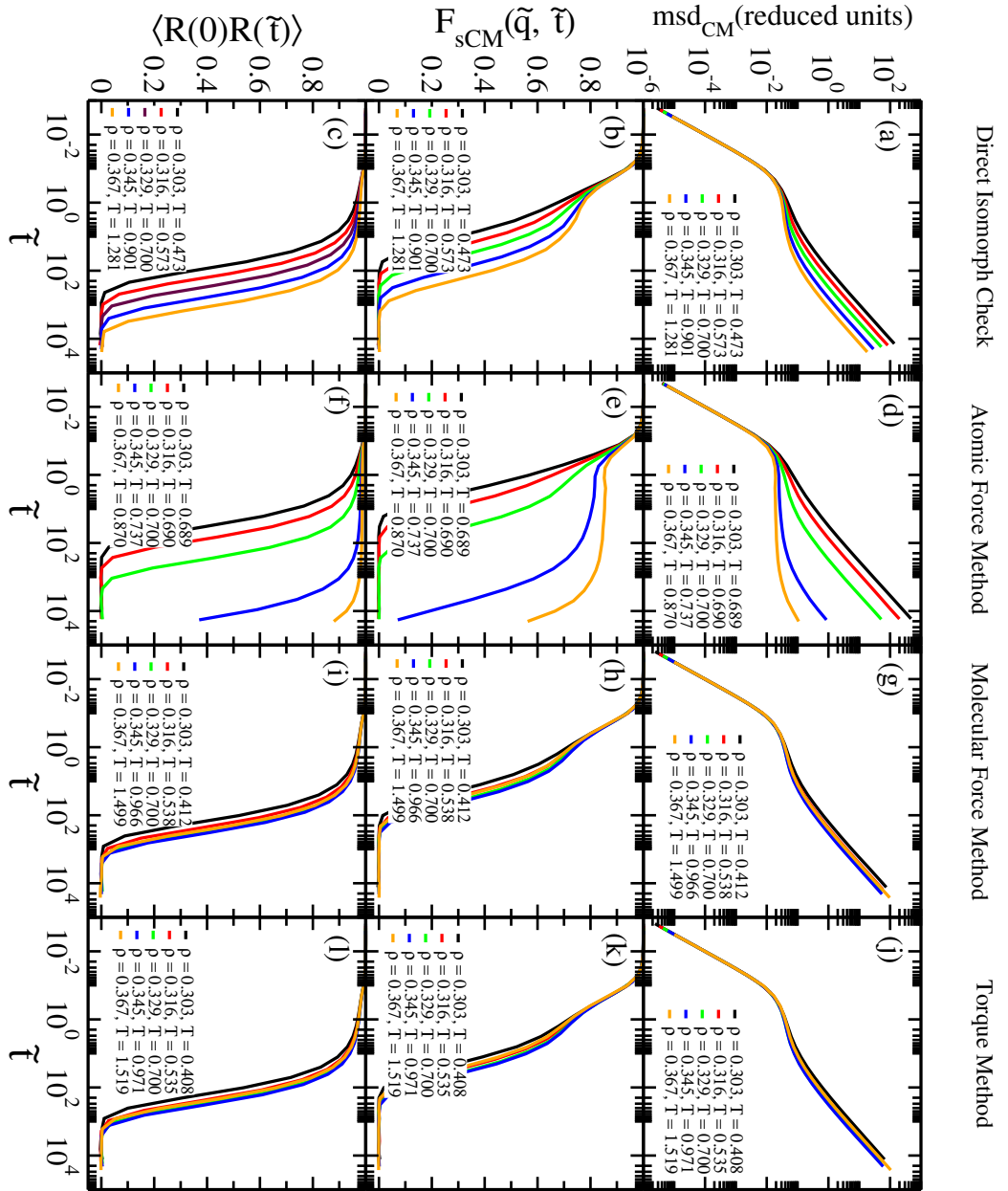
Figure E.2: The dynamics of harmonic bonded OTP model after scaling the system with CM scaling. The reference point is $(\rho, T) = (0.329, 0.700)$. It is anticipated that the direct isomorph check method (a, b, c), atomic force method (d, e, f) are not able to identify pseudoisomorphs. In contrast, molecular force (g, h, i) and torque method (j, k, l) provide better results.

Figure E.3: The dynamics of OTP model improves along DIC and atomic force methods by removing the spring contribution in calculating the potential and atomic force. The reference point is $(\rho, T) = (0.329, 0.700)$. Here, CM scaling method is applied.

Table E.1: Test the atomic scaling on harmonic OTP model. The new temperatures are produced by similar force methods in Figure E.2 at same densities. The temperatures come from DIC method are better than temperatures measured via CM scaling approach (second column). Due to the harmonic intramolecular fast vibration, the predicted state points along atomic force method achieve inconsistency (third column). The molecular force and torque methods be likely to calculate same temperatures.

density	T(DIC)	$T(F_{Atomic})$	$T(F_{Mol})$	T(Tor)
0.303	0.362	1.724	0.452	0.452
0.316	0.527	1.032	0.567	0.567
*0.329	0.700	0.700	0.700	0.700
0.345	0.925	1.080	0.891	0.891
0.367	1.264	1.963	1.209	1.209

has three bonds, two with identical length $l = 1$ and one with different length $l = 1.218$, the bond lengths distribution has two picks in Figure E.1. If we consider $(\rho_1, T_1) = (0.329, 0.700)$ as a starting point and scale the system via CM scaling method, the molecular force and torque methods generate better results in Figure E.2 (g, h, i, j, k, l) than DIC and atomic force methods (Figure E.2 (a, b, c, d, e, f)). As shown, subtracting the harmonic force contribution from intramolecular interactions make the DIC and atomic force determine better results (see Figure E.3). The results of testing the DIC and force methods on harmonic bonded OTP model through the atomic scaling method are demonstrated in Table E.1.

If we consider $(\rho_1, T_1) = (0.303, 0.383)$ as the reference state point and scale the system to only higher density via CM scaling, the molecular force method and torque method generate the pseudoisomorphic state points. Figure E.4 shows that the dynamics are invariant along state points predicted via molecular and torque method. So by considering $(\rho_1, T_1) = (0.303, 0.383)$ as the reference state point we achieve quite better results via molecular force and torque methods in comparison with results of Figure E.2 in which $(\rho_1, T_1) = (0.329, 0.700)$ is the reference point. Table E.2 demonstrates the predicted temperatures via DIC and atomic force methods by subtracting the harmonic intramolecular interactions. Temperatures predicted via DIC method are comparable with pseudoisomorphic points predicted via molecular force in Figure E.4 but atomic force results are still far from pseudoisomorphic state points. The results of atomic scaling method are presented in Table E.3 which are quite different from pseudoisomorphic state points in Figure E.4 along molecular force method.
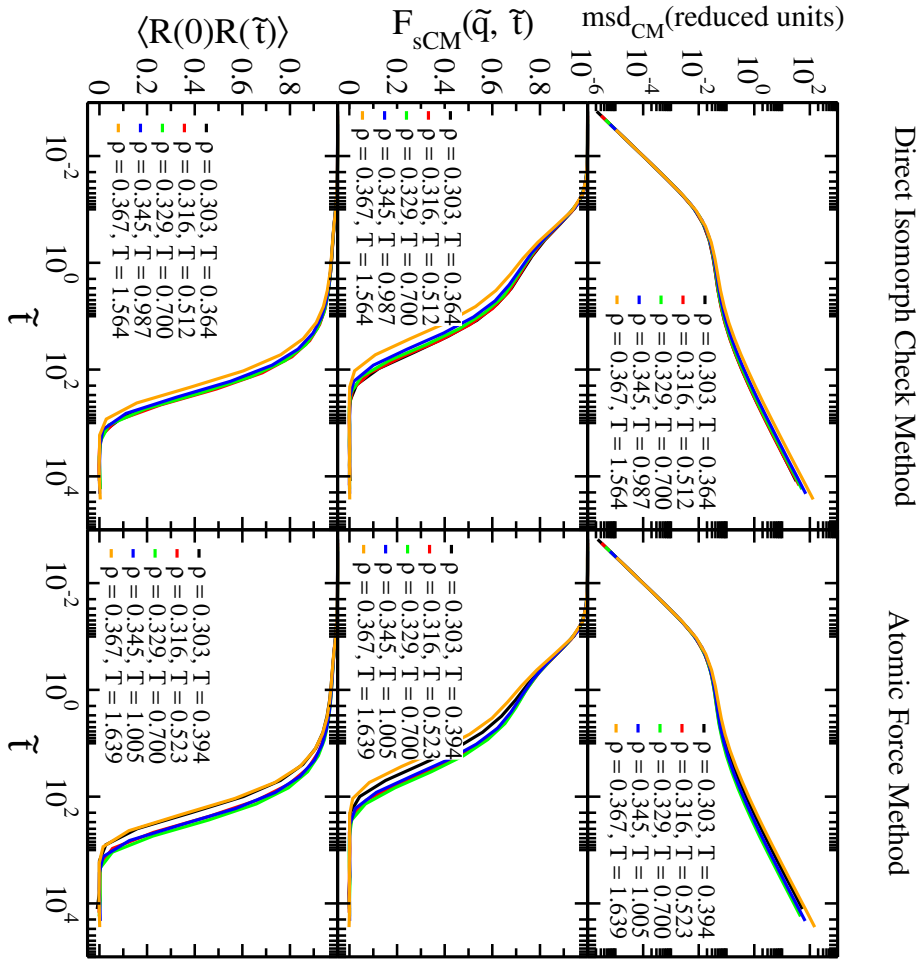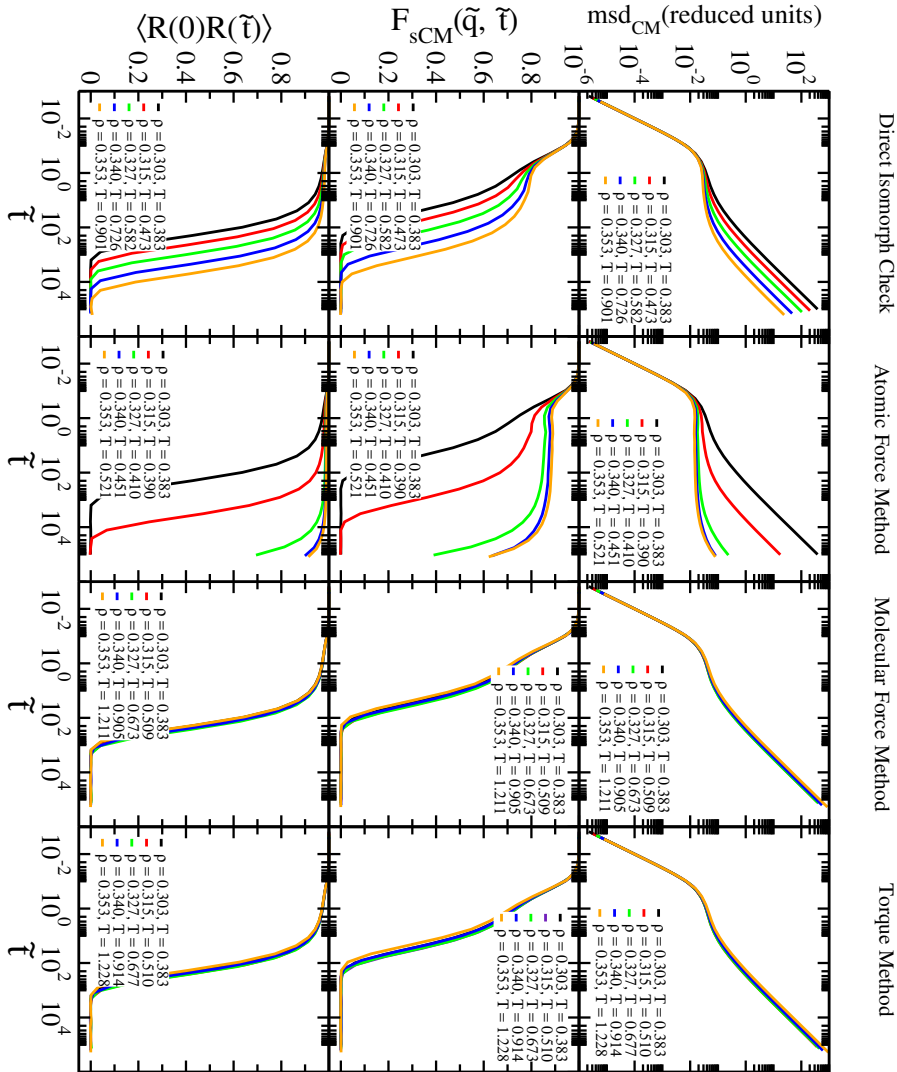
Figure E.4: The dynamics of OTP model with springs along DIC and force methods using the CM scaling. The reference point is $(\rho_1, T_1) = (0.303, 0.383)$. The results of DIC and atomic force method are still inconsistent because of the harmonic intramolecular interactions. The molecular force and torque methods achieve a significant collapse. The density changes over 16%.

129

Table E.2: Results of atomic force and DIC methods after removing the spring's contribution in calculating the potential and atomic force using CM scaling. Both methods determine better results compared to results in Figure E.4.

density	T(DIC)	$T(F_{Atomic})$
*0.303	0.383	0.383
0.315	0.512	0.524
0.327	0.669	0.717
0.340	0.875	0.999
0.353	1.124	1.379

Table E.3: Test the atomic scaling on harmonic OTP model through atomic scaling by considering $(\rho_1, T_1) = (0.303, 0.383)$ as the reference point. The new temperatures are produced by similar methods in Figure E.4 at same densities. DIC and force methods achieve inconsistency results which are quite far from pseudoisomorphic state points.

density	T(DIC)	$T(F_{Atomic})$	$T(F_{Mol})$	T(Tor)
*0.303	0.383	0.383	0.383	0.383
0.315	0.400	0.648	0.475	0.475
0.327	0.432	1.082	0.581	0.581
0.340	0.481	1.547	0.714	0.714
0.353	0.547	1.981	0.866	0.866

Appendix F

Subtracting Harmonic Interactions in LJC Model

The molecular force, segmental force and torque methods are not affected by harmonic intramolecular interactions. So we only consider the atomic force and DIC method to calculate temperatures before and after quenching by removing the harmonic intramolecular interactions in this section. We implement the CM scaling for both cases, and we calculate T after removing the spring contribution. We start from state point $(\rho_1, T_1) = (1.00, 0.700)$ and we subtract the spring force, then scale the system via CM scaling at different densities again remove the spring force from corresponding scaled configurations. Then we use the atomic force method (equation 3.4) and DIC method. Table F.1 show the predicted temperature via atomic force method (third column), and DIC method (fourth column) which are different from pseudoisomorphic points from ref. [2] (second column).

Table F.1: Predicted temperature via atomic force and DIC methods through CM scaling and removing the harmonic potential. The second column results from ref. [2] along which the dynamics are invariant. Comparing the atomic force results (third column) and DIC (fourth column) method implies that they are not pseudoisomorphic state points, especially at the highest density.

Density	T(Pseudoisomorph)	$T(F_{Atomic})$	T(DIC)
0.96	0.539	0.566	0.517
*1.00	0.700	0.700	0.700
1.04	0.908	1.030	0.979
1.08	1.158	1.694	1.409
1.12	1.453	2.966	2.083

On the other hand, quenching the system causes the intramolecular interaction declines, and the methods calculate lower temperatures after minimization, but still, they are not pseudoisomorphic. We use force methods

after quenching and scaling via CM scaling and again remove the spring forces in Table F.2. The predicted T are lower than the corresponding T in table F.1, but they are quite different from pseudoisomorph results taken from ref. [2].

Table F.2: Using the atomic force method and DIC method after quenching the system and using CM scaling method and removing the harmonic contribution.

Density	T(Pseudoisomorph)	$T(F_{Atomic})$	T(DIC)
0.96	0.539	0.559	0.411
*1.00	0.700	0.700	0.700
1.04	0.908	0.956	0.724
1.08	1.158	1.340	0.725
1.12	1.453	1.843	0.817

Atomic force and DIC methods do not find pseudoisomorph in harmonic LJC model before and after quenching and removing harmonic intramolecular interactions.

Appendix G

Reprints of Articles

Predicting scaling properties of fluids from individual configurations: Small molecules

Zahraa Sheydaafar,* Jeppe C. Dyre, and Thomas B. Schrøder†

Glass and Time, IMFUFA, Department of Science and Environment,

Roskilde University, P.O. Box 260, DK-4000 Roskilde, Denmark

(Dated: May 28, 2021)

Abstract

Isomorphs are curves in the phase diagram along which both structure and dynamics to a good approximation are invariant. There are two main methods to trace out isomorphs in both atomic and molecular systems, the configurational adiabat method and the direct isomorph check method. We introduce and test a new family of force based methods on three molecular models; the asymmetric dumbbell model, the symmetric inverse power law dumbbell model, and the Lewis-Wahnström model of o-terphenyl. A unique feature of the force based methods is that they only require a single configuration to trace out an isomorph. The atomic force method was previously shown to work very well for the Kob-Andersen binary Lennard-Jones mixture, but we show that it does not work for molecular models. In contrast, we find that a new method based on molecular forces works well for all three molecular models.

PACS numbers: Valid PACS appear here

---

* samaneh@ruc.dk

† tbs@ruc.dk

I. INTRODUCTION

Isomorphs are curves of invariant structure and dynamics in the thermodynamic phase diagram. They occur in systems with strong correlations between the constant-volume canonical-ensemble equilibrium fluctuations of potential energy and virial [1, 2], which characterize the so-called R-simple (strongly correlating) systems [3–6]. The Pearson correlation coefficient R between the thermal equilibrium fluctuations of potential energy U and virial W is given by (where sharp brackets denote NVT canonical averages, and 'Δ' denotes the deviation from equilibrium mean value, e.g., $\Delta U \equiv U - \langle U \rangle$):

$$R = \frac{\langle \Delta W \Delta U \rangle}{\sqrt{\langle (\Delta W)^2 \rangle \langle (\Delta U)^2 \rangle}} \,. \tag{1}$$

For an inverse power-law (IPL) system with pair potential proportional to r^{-n} in which r is the pair distance, the correlation is perfect, $R = 1$, because $W = (n/3)U$ for all microconfigurations. Somewhat smaller correlations still lead to fairly invariant structure and dynamics, and the class of R-simple liquids is defined by $R > 0.9$. Isomorph theory has been applied to different classes of systems, including simple atomic systems in both liquid and solid phases [7, 12–17], molecular systems [18], and the 10-bead Lennard-Jones chain [19]. Furthermore, isomorph-theory predictions have been verified in experiments on van der Waals bonded organic liquids [20, 21].

In 2012, Ingebrigtsen and et al. [18] studied isomorphs for liquid molecular systems composed of small rigid molecules. They found isomorphs in the asymmetric dumbbell model (ASD) (Fig. 1(a)), the symmetric inverse power law (IPL) dumbbell model (Fig. 1(b)), and the Lewis- Wahnström o-terphenyl (OTP) model(Fig. 1(c)). It is important to note that isomorph invariances refer to structure and dynamics reported in the so-called *reduced* (state-point dependent) units. In this unit system, the length unit l_0 is defined by the particle number density $\rho \equiv N/V$ where N is the particle number and V the system volume, the temperature T defines the energy unit e_0, and the density and the thermal velocity define the time unit t_0. Thus if m is the particle mass, the length, energy, and time units are given [1, 3, 7] by

$$l_0 = \rho^{-1/3} \,,\; e_0 = k_B T \,,\; t_0 = \rho^{-1/3} \sqrt{m/k_B T} \,. \tag{2}$$

Reference 18 used the so-caled configurational adiabat method to trace out isomorphs. For
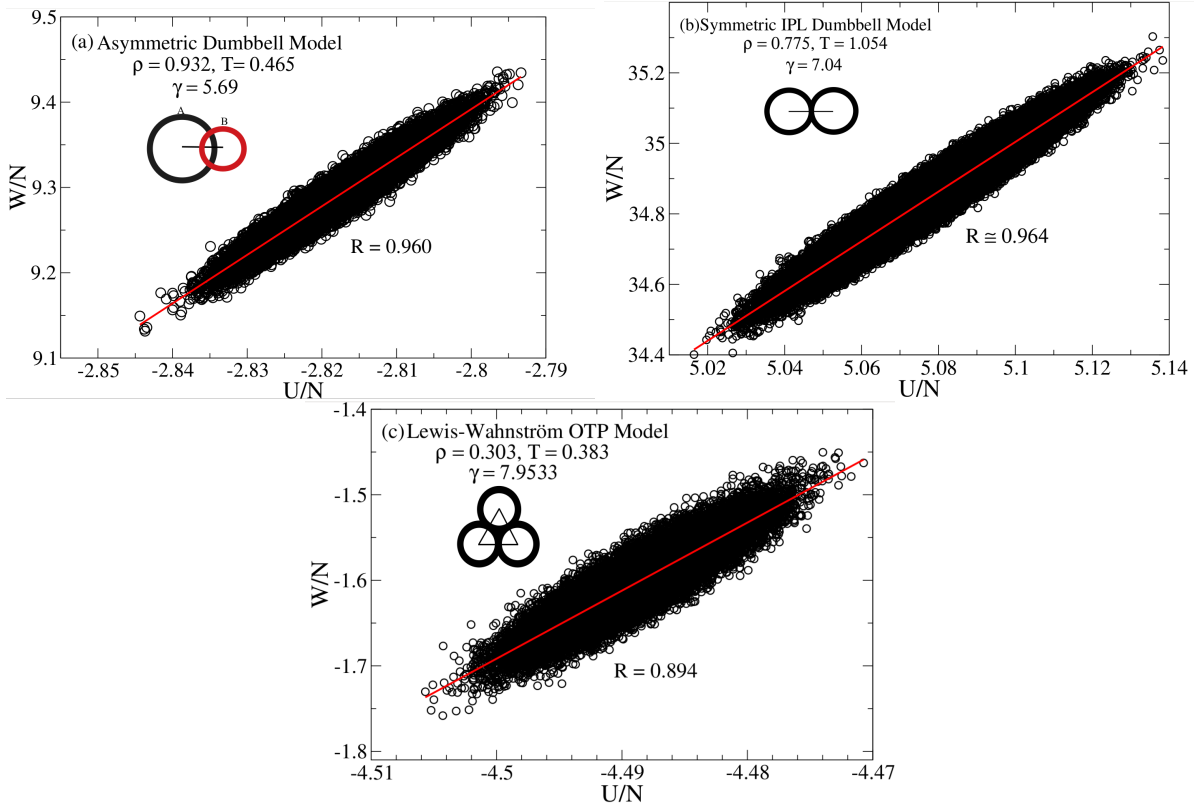
FIG. 1. The fluctuation of potential energy and virial for the asymmetric dumbbell and symmetric IPL dumbbell models and and the OTP model with rigid bonds. (a) The Pearson correlation coeficient at the reference state point $(\rho_1, T_1) = (0.932, 0.465)$ is $R = 0.959$ and the linear slope of regression is $\gamma = 5.69$ for the asymmetric dumbbell model. (b) $R = 0.962, \gamma = 7.11$ for the symmetric dumbbell model at state point $(\rho_1, T_1) = (0.806, 1.400)$. (c) $R = 0.894, \gamma = 7.95$ for the OTP model at state point $(\rho_1, T_1) = (0.303, 0.383)$.

a scatter plot of virial versus potential energy of configurations taken from an equilibrium simulation (see Fig. 1), the linear-regression slope γ is given [7–10] by

$$\gamma \equiv \frac{\langle \Delta U \Delta W \rangle}{\langle (\Delta U)^2 \rangle} = \left(\frac{\partial \ln T}{\partial \ln \rho} \right)_{S_{\text{ex}}} . \tag{3}$$

Recall that S_{ex} is the total entropy minus ideal gas entropy at the same density and temperature ($S_{\text{ex}} < 0$ due to the fact that any system is more ordered than an ideal gas). For R-simple liquids, the isomorph theory predicts invariance of the dynamics along the configurational adiabats defined by $S_{\text{ex}} =$Const [18, 28–30]. For any system, Eq. (3) allows one to generate the configurational adiabats. This is done by calculating the two canonical averages

3

in Eq. (3) at an initial state point, changing density slightly, and from Eq. (3) calculating the corresponding change in temperature. At the new state point the canonical averages are recalculated, and so on.

Another method to generate isomorphs is termed the direct isomorph check, which works as follows. Two configurations of the strongly correlated system have proportional Boltzmann factors, i.e.

$$e^{-U(\mathbf{R}^{(1)})/k_{\mathrm{B}}T_1} = C_{12}e^{-U(\mathbf{R}^{(2)})/k_{\mathrm{B}}T_2}. \tag{4}$$

Here $\mathbf{R}^{(1)}$ and $\mathbf{R}^{(2)}$ are two configurations that scale uniformly into one another, $\mathbf{R}^{(2)} = (\rho_1/\rho_2)^{1/3}\mathbf{R}^{(1)}$, and C_{12} is a constant that depends only on the two state points in question. By taking the logarithm of Eq. (4) we get

$$U(\mathbf{R}^{(2)}) = \frac{T_2}{T_1}.U(\mathbf{R}^{(1)}) + k_{\mathrm{B}}T_2 \ln C_{12}. \tag{5}$$

Thus, taking configurations, $\mathbf{R}^{(1)}$, from an equilibrium NVT simulations at (ρ_1, T_1) and plotting $U(\mathbf{R}^{(2)})$ versus $U(\mathbf{R}^{(1)})$ is predicted to reveal strong correlation, and T_2 can be calculated from the slope.

Below, we investigate new efficient methods for generating isomorphs. They are all based on the scaling properties of a single configuration selected from an equilibrium simulation of a reference state point. This works well for the Kob-Andersen binary Lennard-Jones mixture, which is a R-simple system [23]. The present paper extends the single-configuration idea to deal with three molecular system: the asymmetric dumbbell (ASD) model, the symmetric inverse power law (IPL) dumbbell model, and the Lewis-Wahnström OTP model.

II. SIMULATION DETAILS

We studied three molecular systems with rigid bonds, the asymmetric dumbbell model (N = 5000), symmetric IPL dumbbell r^{-18} model (N = 5000), and the Lewis-Wahnström OTP model (N = 3000). All three models were previously shown to have good isomorphs [18].

Asymmetric dumbbell molecules consist of two different sized Lennard-Jones (LJ) spheres, a large (A) and a small (B) particle, rigidly bonded. The length of the bonds is 0.584 in the LJ units defined by the large sphere ($\sigma_{AA} \equiv 1$, $\epsilon_{AA} \equiv 1$, and $m_A \equiv 1$). The parameters

4

of the model were chosen to mimic toluene ($\sigma_{AB} = 0.894$, $\sigma_{BB} = 0.788$, $\epsilon_{AB} = 0.342$, $\epsilon_{BB} = 0.117$, $m_B = 0.195$) [28]. The inter-molecular pair potential interactions are given by the Lennard-Jones pair potential:

$$v_{ij}(r_{ij}) = 4\epsilon_{ij} \left[\left(\frac{\sigma_{ij}}{r_{ij}} \right)^{12} - \left(\frac{\sigma_{ij}}{r_{ij}} \right)^{6} \right]. \tag{6}$$

The symmetric IPL model consists of two identical particles, connected by a rigid bond of length 0.584. The inter-molecular pair potential interactions are given by the inverse power-law (IPL) potential:

$$v_{ij} = \epsilon_{ij} \left(\frac{\sigma_{ij}}{r_{ij}} \right)^{n} \tag{7}$$

in which $n = 18$. All IPL parameters and particle masses are unity.

The Lewis-Wahnström OTP model consists of three identical LJ particles. Atoms are connected by rigid bonds in an isosceles triangle with side length 1.000 and a top angle of 75°. All LJ parameters are set to unity in this model either.

All Molecular Dynamics simulations were performed in the NVT ensemble with a Nose-Hoover thermostat using RUMD, an open-source package that can be downloaded at `http://rumd.org` [24].

III. THREE SINGLE-CONFIGURATION METHODS FOR IDENTIFYING ISO-MORPHS

Generating isomorphs by means of Eq. (3) for an R-simple system is straightforward but requires, as the numerical calculation of most statistical-mechanical quantities, a time sequence of equilibrium configurations. Good statistics can be obtained, however, from the scaling properties of the forces of a single configuration [23]. The idea is to make use of the fact that *all* reduced forces are isomorph invariant.

To show that the reduced forces are all invariant along an isomorph, we refer to the basic equation of isomorph theory [11],

$$U(\mathbf{R}) = U(\rho, S_{\text{ex}}(\tilde{\mathbf{R}})). \tag{8}$$

Here $\mathbf{R} \equiv (\mathbf{r}_1, ..., \mathbf{r}_N)$ is the configuration vector of all particle coordinates, $U(\rho, S_{\text{ex}})$ is the thermodynamic average potential energy at the state point with density ρ and excess entropy

S_{ex}, $\tilde{\mathbf{R}} \equiv \rho^{1/3}\mathbf{R}$ is the reduced configuration vector, and $S_{ex}(\tilde{\mathbf{R}})$ is the microscopic excess-entropy function as defined in Ref. 11. The fact that the latter function depends only on the configuration's *reduced* coordinates is a consequence of the hidden scale invariance condition $U(\mathbf{R}_a) < U(\mathbf{R}_b) \Rightarrow U(\lambda\mathbf{R}_a) < U(\lambda\mathbf{R}_b)$ in which λ is a uniform scaling parameter [11]. This condition is equivalent to the system having strong virial potential-energy correlations [7].

It follows from Eq. (8) that the vector of all forces on the individual particles, $\mathbf{F} \equiv (\mathbf{F}_1, ..., \mathbf{F}_N)$, is given by

$$\mathbf{F}(\mathbf{R}) = -\nabla U(\mathbf{R}) = -\left(\frac{\partial U}{\partial S_{ex}}\right)_\rho \rho^{1/3}\tilde{\nabla} S_{ex}(\tilde{\mathbf{R}}). \tag{9}$$

Since $(\partial U/\partial S_{ex})_\rho = T$, the reduced force vector $\tilde{\mathbf{F}} \equiv l_0\mathbf{F}/e_0 = \rho^{-1/3}\mathbf{F}/k_B T$ is given by (where $\tilde{S}_{ex} \equiv S_{ex}/k_B$)

$$\tilde{\mathbf{F}} = -\tilde{\nabla}\tilde{S}_{ex}(\tilde{\mathbf{R}}). \tag{10}$$

The fact that $\tilde{\mathbf{F}}$ depends only on the *reduced* coordinates implies invariant dynamics along an isomorph because in this case, the reduced-unit version of Newton's second law, $d^2\tilde{\mathbf{R}}/d\tilde{t}^2 = \tilde{\mathbf{F}}(\tilde{\mathbf{R}})$ [1], has no reference to the state point density. This implies invariant reduced dynamics along the isomorphs.

Given a reference state point (ρ_1, T_1) and a new density, ρ_2, we now derive the equation for calculating the temperature T_2 so that the state point (ρ_2, T_2) is isomorphic with (ρ_1, T_1). If $\mathbf{R}_1$ is a configuration taken from an equilibrium simulation of the reference state point and $\mathbf{R}_2$ is the same configuration scaled uniformly to density ρ_2, the fact that the reduced forces of the two configurations are identical is expressed as follows:

$$\tilde{\mathbf{F}}(\mathbf{R}_1) = \tilde{\mathbf{F}}(\mathbf{R}_2). \tag{11}$$

From this identity T_2 can be determined by:

$$T_2 = \frac{|\mathbf{F}(\mathbf{R}_2)|}{|\mathbf{F}(\mathbf{R}_1)|}\left(\frac{\rho_1}{\rho_2}\right)^{1/3} T_1. \tag{12}$$

The atomic force method was tested for the Kob-Andersen binary Lennard-Jones model in Ref [23]. For a system composed of rigid bonded molecules, in addition to atoms' forces, the center-of-mass forces are expected to be isomorph invariant in reduced units. This paper tests both force methods on the ASD, IPL and OTP systems. The method is illustrated
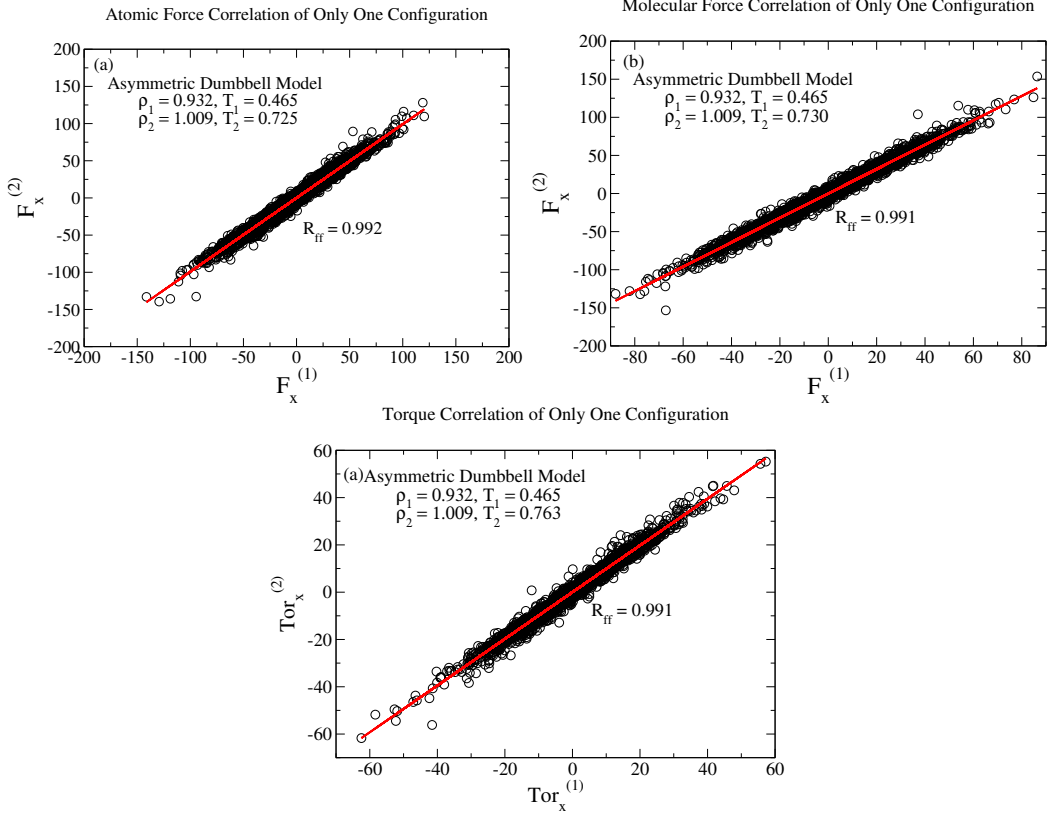
Atomic Force Correlation of Only One Configuration

Molecular Force Correlation of Only One Configuration

Torque Correlation of Only One Configuration

FIG. 2. (a) ["atomic-force method"] shows a plot of all particle forces in one axis direction for a single configuration $\mathbf{R}_1$ of the reference state point $(\rho_1, T_1) = (0.932, 0.465)$ versus for its uniformly scaled version to density ρ_2, $\mathbf{R}_2 = (\rho_1/\rho_2)^{1/3}\mathbf{R}_1$. From the slope of the best-fit line via Eq. (12) one identifies $T_2 = 0.725$. (b) ["molecular-force method"] shows a similar plot based on the center-of-mass forces between the molecules (which ignores the intramolecular forces). Better correlation is obtained here, and the slightly different $T_2 = 0.730$ is arrived at using this method. (c) ["Torque Method] shows the same plot in regard to the rotational motion of molecules. Despite the approximately same correlation, the temperature defined from this method Eq. (13) is quite different, $T_2 = 0.763$.

in Fig. 2 in which (a) for the ADP system shows the x-coordinates of the forces on all particles plotted against the same quantities of the uniformly scaled configuration for a 7% density increase. (b) shows the same for the center-of-mass "molecular" forces between the molecules, which have no contributions from the intramolecular forces. We find a strong correlation in both cases, but a somewhat different prediction for T_2, which is 0.725 by using atomic force method and 0.730 by using center-of-mass force method.

7

Before comparing the two methods by testing for invariant dynamics, we introduce a third method based on the isomorph invariance of the reduced-unit torque on each molecule, i.e., $\tilde{\boldsymbol{\tau}}_1 = \tilde{\boldsymbol{\tau}}_2$ where τ is the torque. Since the torque in reduced units is defined by $\tilde{\boldsymbol{\tau}} \equiv \boldsymbol{\tau}/e_0 = \boldsymbol{\tau}/k_B T$, the invariance requirement means that T_2 is given by

$$T_2 = \frac{|\boldsymbol{\tau_2}|}{|\boldsymbol{\tau_1}|} T_1 \,. \tag{13}$$

This assumes invariance of the reduced rotational dynamics of the particles around the molecules' center-of-mass. This method is used in Fig. 2(c), which shows a quite high correlation of the torques before and after scaling the configuration, but a somewhat higher temperature, $T_2 = 0.763$.
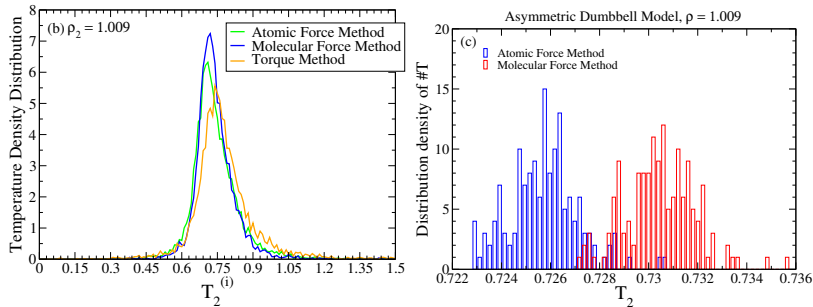

FIG. 3. (a) Distribution of temperatures predicted by applying Eq. (12) and Eq. (13) to individual molecules in a single configuration. For perfect scaling, all the molecules should 'agree', i.e., the distributions should be delta functions. (b) the distribution of T_2 values predicted from 152 independent configurations by using the atomic force (blue) and molecular force (red) methods.

Fig. 3(a) shows the distribution of T_2 predictions, when Eq. (12) and Eq. (13) are applied to individual molecules. The width of the distributions are similar, but smallest for the molecular-force method. Fig. 3(b) shows the distribution of T_2 values predicted by applying Eq. (12) to 152 independent configurations. Using one configuration is a main advantage of the new force based methods considered here. However, for comparison between the methods, we will in the following use the average of the T_2 values predicted from 100-200 independent configurations.

IV. RESULTS

In the following we will test the three different methods on the three models introduced above. Both translational and rotational dynamics is considered; we test the invariance of the reduced molecular center-of-mass mean square displacement (msd), the intermediate incoherent scattering function (Fs), and the orientational time-autocorrelation function.

Tests of the three methods on ASD are shown in Fig. 4. The state point $(\rho_1, T_1) = (0.932, 0.465)$ is the reference point. From this we determined two state points with lower density and two with higher density, spanning in all a density variation of 19%. The configuration was scaled uniformly to the relevant density ρ_2 in order to determine the temperature T_2 at which the reduced forces/torques are the same as at the reference state point. The best results are obtained with the molecular-force method (Fig. 4 (d), (e), and (f)).

TABLE I. Reduced-unit density variation of the diffusion coefficient (first row), the relaxation time of molecular center-of-mass dynamics (second row) and rotational dynamics (third row) for the ASD model. The second column shows large numbers arising from the isotherm, non-invariant curves. The third to seventh columns represent the configurational adiabat, direct isomorph check, atomic and molecular forces and torque methods. The molecular force method is better than other methods for predicting state points of approximately invariant dynamics.

	Isotherm	γ	DIC	F_{Atom}	F_{Mol}	Torque
$\dfrac{\partial log \tilde{D}}{\partial log \rho}$	-70(2)	-0.5(4)	1.1(4)	-1.4(2)	-0.9(4)	7.47(6)
$\dfrac{\partial \log \tilde{\tau}_{cm}}{\partial \log \rho}$	77(3)	-0.4(1)	-1.0(1)	1.60(7)	0.5(1)	-7.8(1)
$\dfrac{\partial \log \tilde{\tau}_{rot}}{\partial \log \rho}$	65(3)	1.9(1)	1.26(2)	3.47(3)	2.62(7)	-2.6(2)

Figure 5 shows the variation of the relaxation times of translational motion (a) and rotational motion (b) for an isotherm (purple), configurational adiabat (black), as well as curves generated by the direct isomorph check (red), atomic force (green), molecular force (blue), and torque methods (orange). Not surprisingly, all the approximate isomorphs are better in representing the invariant relaxation compared to the isotherm. Table I shows the density variation of the diffusion coefficient and translational and rotational relaxation times (first column) in reduced units along the isotherm (second column) and the five approximate isomorphs (third-seventh columns). The diffusion coefficient is calculated from the diffusive
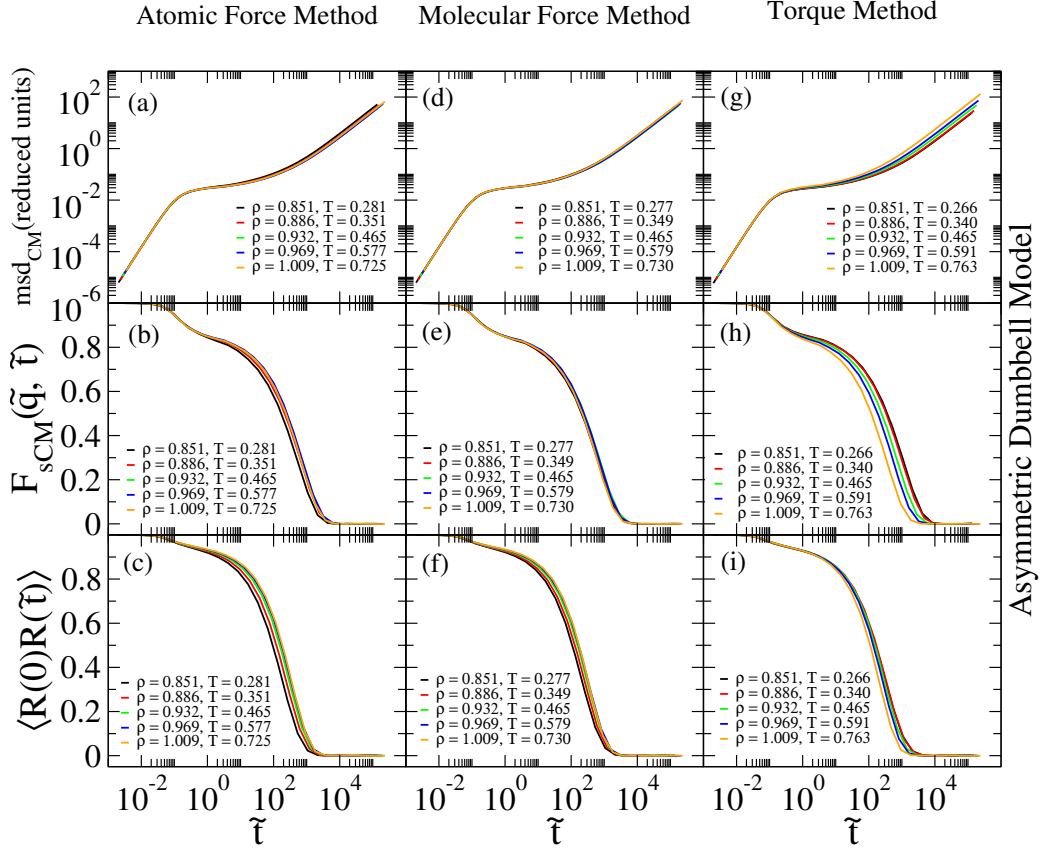
FIG. 4. Testing the ASD model for invariance of the reduced translational and rotational dynamics by three different methods. Each method investigates the reduced center-of-mass mean-square displacement (upper figures), the center-of-mass incoherent intermediate scattering function for the reduced wave-vector $\tilde{q} = q(\rho/0.932)^{1/3}$ (middle figures), and the orientational time-autocorrelation function probed via the autocorrelation of the normalized bond vector (bottom figures). (a), (b), (c) show results for state points generated by the atomic-force method based on requiring invariant reduced forces between all atoms, including the intramolecular contributions (Eq. (12)). (d), (e), (f) show results for state points generated by the molecular-force method requiring invariant reduced center-of-mass forces between the molecules (Eq. (12)). (g), (h), (i) show results for state points generated by the torque method requiring invariant reduced torques on the molecules (Eq. (13)).

part of the mean-square displacement (compare Fig. 4). The variation of relaxation times as functions of density are obtained by calculating the slope of relaxation curves of Fig. 5(a) and (b) at two-state points, lower $\rho = 0.886$ and upper $\rho = 0.969$ points of reference state point.
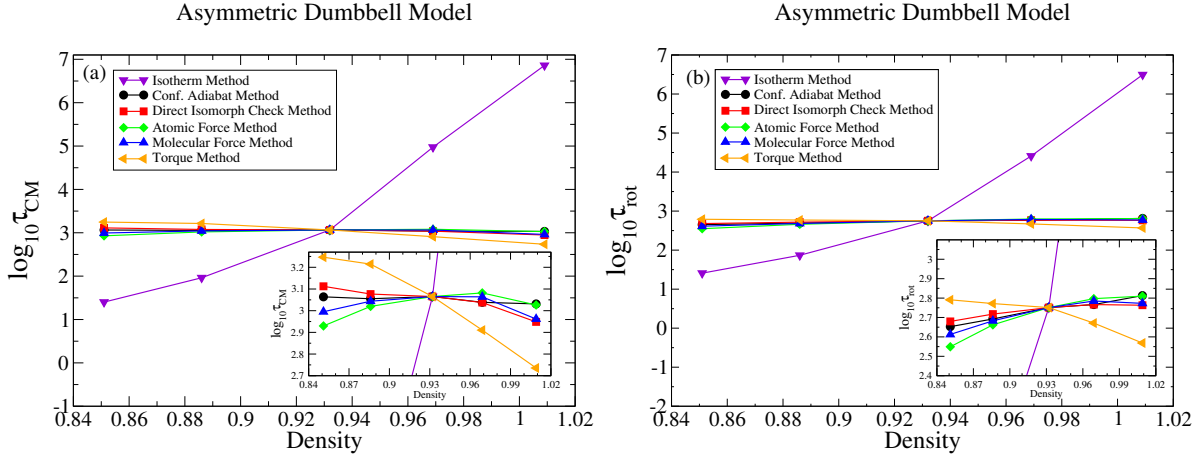
10

FIG. 5. Comparing the relaxation time as a function of the density for the ASD model along an isotherm (purple) as well as for five different methods: configurational adiabat (black), direct isomorph check (red), atomic (green) and molecular (blue) force and torque (orange) methods. (a) shows the translational relaxation time calculated by the intermediate scattering function. (b) shows a similar plot for the rotational relaxation time (derived from the orientational time-autocorrelation function of the molecular end-to-end vector).

TABLE II. Checking the reduced-units variation of the same dynamic quantities as in Table I for the symmetric dumbbell IPL model.

	Isotherm	γ	DIC	F_{Atom}	F_{Mol}	Torque
$\dfrac{\partial log\tilde{D}}{\partial log\rho}$	-113.4(6)	1.9(1)	-0.78(7)	-0.2(2)	-0.462(5)	3.9(3)
$\dfrac{\partial \log \tilde{\tau}_{cm}}{\partial \log \rho}$	126.7(7)	-0.4(3)	-0.04(2)	-0.21(7)	-0.42(1)	-0.95(4)
$\dfrac{\partial \log \tilde{\tau}_{rot}}{\partial \log \rho}$	107.9(6)	0.16(1)	-0.7(2)	0.2(2)	0.10(9)	0.5(3)

An important question is whether the molecular geometry determines which method work for which model or not. The second model we consider is the IPL symmetric dumbbell model to check the invariance properties by use of the single-configuration force methods. The corresponding quantities are shown in Fig. 6, Fig. 7 and Tabel II. We determine two state point with lower density and two with higher density, spanning in all a density variation of 19%. Overall, for the ASD model we find the molecular force approach to produce the best invariance curves. Fig. 7 (a) and (b) represent the variation of both translational and rotational dynamics by plotting both relaxation times.
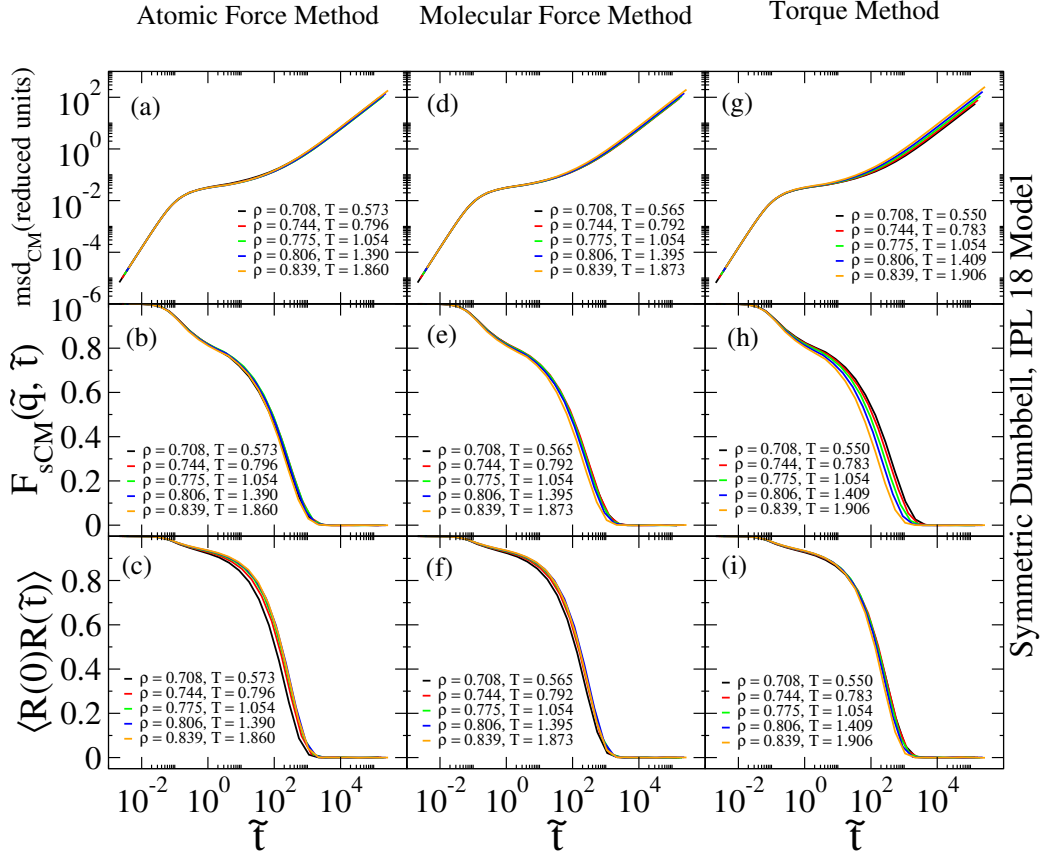
11

FIG. 6. Testing the atomic force, molecular force, and torque methods on the IPL model for invariance of the reduced translational and rotational dynamics. The same dynamic quantities as in Fig. 4 are investigated. The reference point is $(\rho_1, T_1) = (0.775, 1.054)$ and the values of q considered are constant in reduced units, $\tilde{q} = q(\rho/0.775)^{1/3}$. (a), (b), (c) show results for state points generated by the atomic-force method (which includes the intramolecular contributions, Eq. (12)). (d), (e), (f) show results for state points generated by the molecular-force method (Eq. (12)). (g), (h), (i) show results for state points generated by the torque method (Eq. (13)).

So far, the molecular force method has given the best results. We proceed to investigate the three force methods for the OTP model (Fig. 8). In this model, $(\rho_1, T_1) = (0.303, 0.383)$ is the reference point. The same quantities as before are plotted against the reduced time. Again the molecular force method is best for producing approximate isomorphs (Fig. 9).

There is an interesting distinction in regard to which densities are used to analyze the dynamics. Scaling the OTP system to lower density disturbs the prediction process. In Fig. 10(a) we consider the fourth point of the state points of Fig. 8 (d), $(\rho_1, T_1) =$
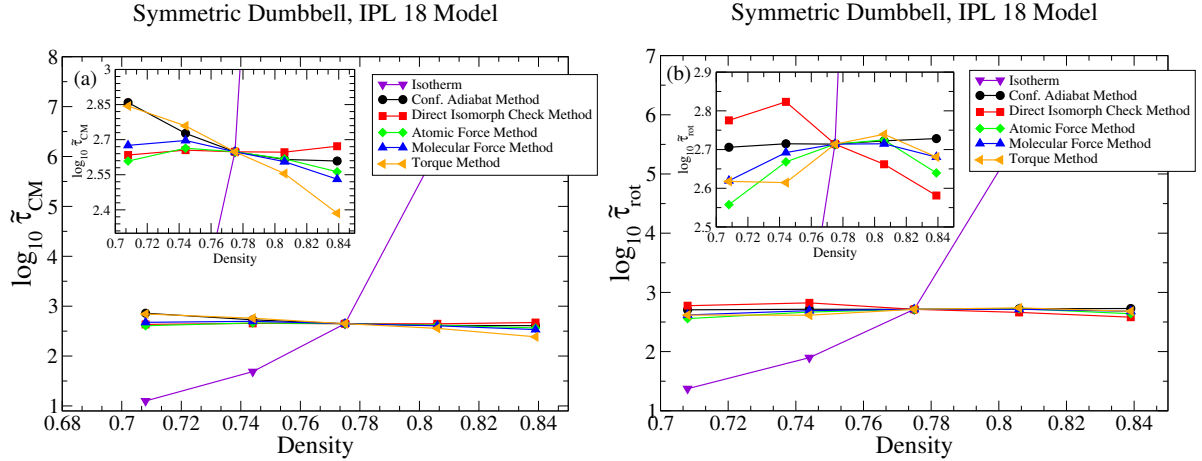
FIG. 7. Comparing the relaxation time as a function of the density for the IPL model along similar curves as in Fig. 5. As shown before, all the approximate isomorph methods are better in representing the invariant relaxation time than the isotherm. (a) shows the translational relaxation time calculated by the intermediate scattering function. (b) shows a similar plot for rotational relaxation time.

$(0.340, 0.903)$, as reference point, and then move to lower densities, spannig about 16%. The invariant intermediate scattering function in Fig. 8 has disappeared by decreasing densities in Fig. 10. On the other hand, the approaches are able to give the proper curves only if scaling the configuration to higher density in OTP system. This issue is only found in OTP model, not the other two models. For example, the IPL model dynamics has been still invariant in reduced units along the molecular force methods. Figure 10(b) shows the reduced incoherent intermediate scattering function of isomorphs points when we start from $(\rho_1, T_1) = (0.806, 1.395)$ (Fig. 6(e)) and decrease the density. The dynamics of IPL model is still invariant however it gives the different state points in comparison with Fig. 6(e) because the isomorphs are approximate.

To investigate the OTP model issue, we calculate the translational and rotational relaxation times through the isotherm and isomorphs methods by decreasing the density (Figure 11). By scaling the configurations to lower density, the configurational adiabats and DIC methods still create the isomorphs along which the dynamics is quite invariant. However, this is clearly not the case for the force methods. Thus, for the OTP model the molecular force method works well, but only if increasing density from the reference point. At the present we do not have an explanation for this
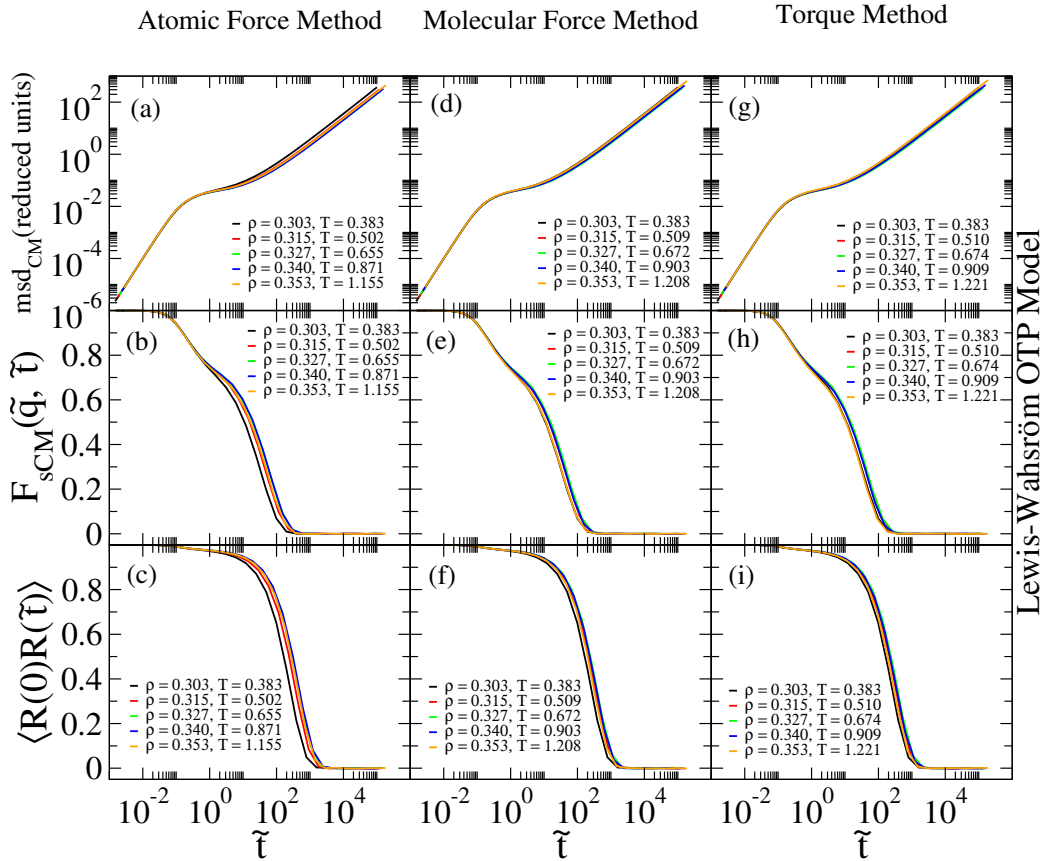
FIG. 8. Testing for invariance of the same reduced dynamics as in Fig. 4 and Fig. 6 for the OTP model. Approximate isomorphs were generated based on a single equilibrium configuration from the reference state point $(\rho_1, T_1) = (0.303, 0.383)$. Results were averaged over 152 configurations to improve statistics. (a), (b), (c) show results for state points generated by the atomic-force method. (d), (e), (f) show results for state points generated by the molecular-force method. (g), (h), (i) show results for state points generated by the torque method.

V. DISCUSSION

Isomorphs exist in systems with strong virial potential-energy correlation, including molecular systems with rigid bonds. For the asymmetric dumbbell, the symmetric dumbbell, and the Lewis-Wahnström OTP models, we have seen that there exists curves along which the dynamics is invariant to a good approximation. Though not our focus here, we note that the structure is invariant to a good approximation for all three methods (Fig. 12).

We tested several methods to generate an approximate isomorph starting from a given
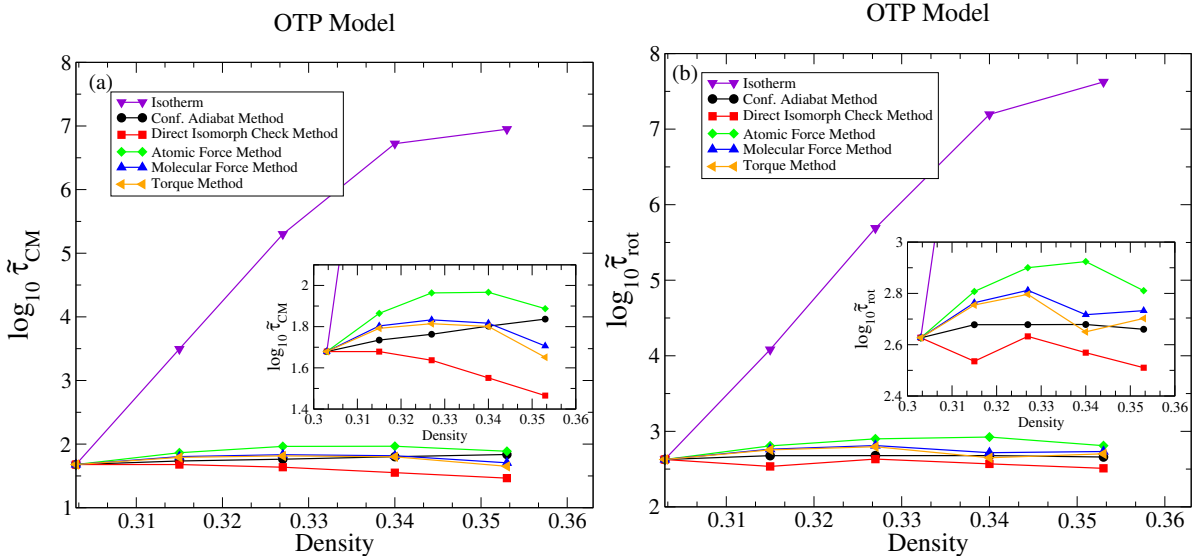
FIG. 9. Comparing the relaxation time as a function of the density in the OTP model along an isotherm and the various approximate isomorph methods. Both translational and rotational relaxation time are invariant compared to the isotherm (purple). (a) shows the translational relaxation time calculated by the intermediate scattering function. (b) shows a similar plot for the rotational relaxation time.

reference state point. The force methods involve in principle a single configuration and its uniformly scaled version, although we averaged over 152 configuration pairs in order to get better statistics and also to be able to estimate the uncertainty of the T_2 predictions. Such averaging is not going to be necessary if a much larger system is simulated than the presently studied (5000 molecules for ASD and IPL, and 3000 molecules for OTP). Apparently, both the intermolecular and intramolecular interactions play an important role in generating potentially isomorphic state points. In particular, the atomic forces are still affected by the intramolecular interactions, and we believe this is why the atomic-force method is not able to identify state points of approximately invariant reduced dynamics in some cases. On the other hand, the molecular-force method based on invariant reduced center-of-mass forces generally works well, while the torque method gave decent results in ASD model. For the IPL and OTP models, the torque method provides good results, as well.

Identifying isomorphs via three new methods is much simpler and computationally cheaper than the method in Ref [18]. The force methods for generating isomorphs have here only been tested on molecular systems composed of molecules with constraint bonds. The question whether the molecular-force based method works well for other molecular system,
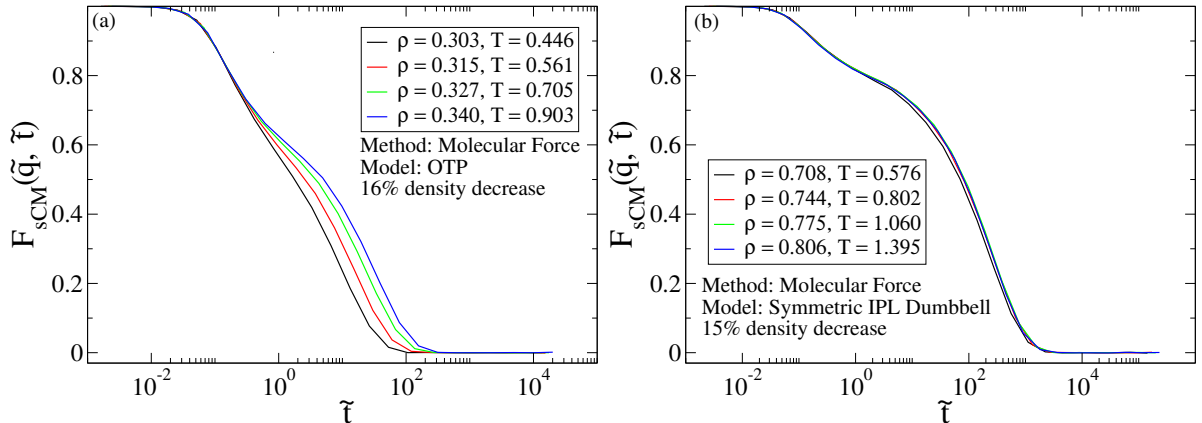
15

FIG. 10. Comparing the dynamics of two model (OTP, IPL) when the density decreased. (a) shows the incoherent intermediate scattering function illustrates that the dynamics of the OTP system is not invariant when state points are generated by decreasing the density. Here the reference state point is $(\rho_1, T_1) = (0.340, 0.903)$. Surprisingly, the molecular force method, which his best for the ASD and IPL methods and also for OTP when increasing the density, does not provide any isomorphic points. (b) shows testing the similar method on IPL model in similar process of decreasing the density. $(\rho_1, T_1) = (0.806, 1.395)$ is the starting point. The reduced dynamics quantity still has a perfect collapse and it is not effected by density changes.

e.g., with harmonic bonds, is important to investigate in future work.

[1] Gnan,Nicoletta and Schrøder,Thomas B. and Pedersen,Ulf R. and Bailey,Nicholas P. and Dyre,Jeppe C. "Pressure-energy correlations in liquids. IV. "Isomorphs" in liquid phase diagrams", The Journal of Chemical Physics, **131**, 234504 (2009).

[2] Dyre, Jeppe C., "Hidden Scale Invariance in Condensed Matter", The Journal of Physical Chemistry B, **118**, 10007-10024 (2014).

[3] Ingebrigtsen, Trond S. and Schrøder, Thomas B. and Dyre, Jeppe C. "What Is a Simple Liquid?", Phys. Rev. X. **2**, 011011 (2012).

[4] Bailey,Nicholas P. and Bøhling,Lasse and Veldhorst,Arno A. and Schrøder,Thomas B. and Dyre,Jeppe C. "Statistical mechanics of Roskilde liquids: Configurational adiabats, specific heat contours, and density dependence of the scaling exponent", The Journal of Chemical Physics. **139**, 184506 (2013).
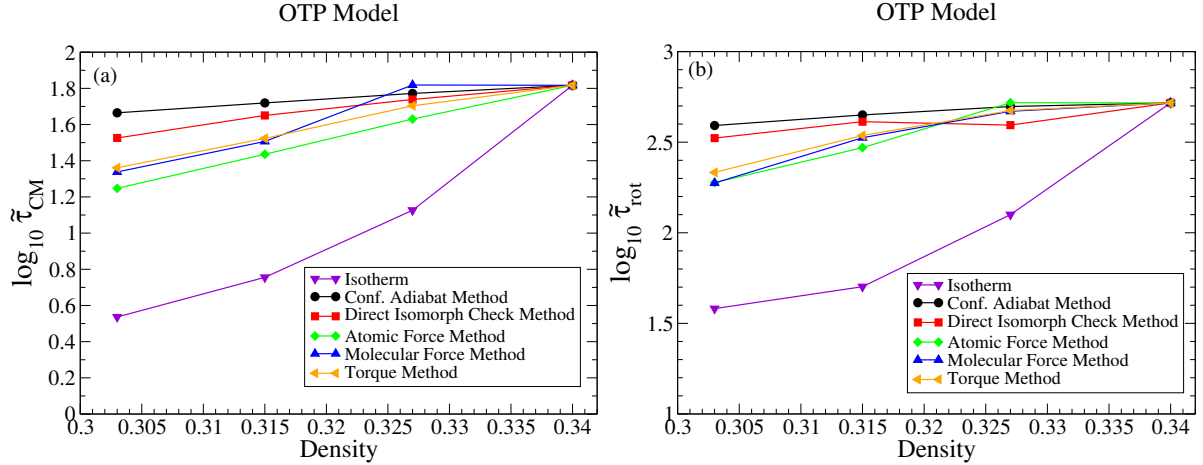
FIG. 11. Comparing the similar dynamical quantity represented in Fig. 9 given by five methods with isotherm. Again the variation of relaxation time is rather more invariant along isomorhphs methods than isotherm (a) Shows the translational relaxation time as the function of density when we decrease the density and (b) shows the relevant quantities of rotational dynamics. In both panel the dynamis is more invariant along the configurational adiabats and direct isomorphs check methods in comparing with Fig. 9. Comparing the force methods shows they identify the proper isomorphic state points only by increasing the density.

[5] Flenner, Elijah and Staley, Hannah and Szamel, Grzegorz, "Universal Features of Dynamic Heterogeneity in Supercooled Liquids", Phys. Rev. Lett. **112**, 097801 (2014).

[6] Prasad,Saurav and Chakravarty,Charusita, "Onset of simple liquid behaviour in modified water models", The Journal of Chemical Physics. **140**, 164501 (2014).

[7] Bailey,Nicholas P. and Pedersen,Ulf R. and Gnan,Nicoletta and Schrøder,Thomas B. and Dyre,Jeppe C. "Pressure-energy correlations in liquids. I. Results from computer simulations", The Journal of Chemical Physics, **129**, 184507 (2008).

[8] Fragiadakis,D. and Roland,C. M. "On the density scaling of liquid dynamics", The Journal of Chemical Physics, **134**, 044504, (2011).

[9] Koperwas,K. and Grzybowski,A. and Paluch,M. "The effect of molecular architecture on the physical properties of supercooled liquids studied by MD simulations: Density scaling and its relation to the equation of state", The Journal of Chemical Physics, **150**, 014501, (2019).

[10] Fragiadakis,D. and Roland,C. M. "Intermolecular distance and density scaling of dynamics in molecular liquids", The Journal of Chemical Physics, **150**, 204501, (2019).

[11] Schrøder,Thomas B. and Dyre,Jeppe C. "Simplicity of condensed matter at its core: Generic

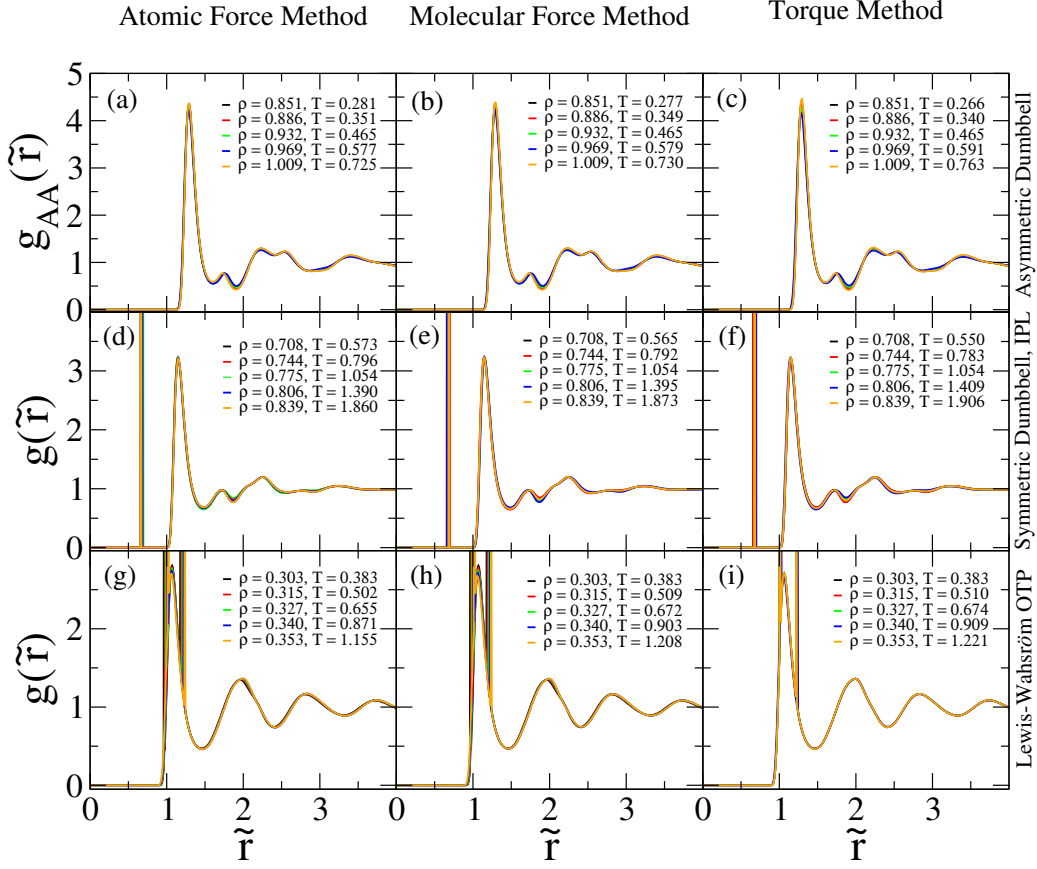Atomic Force Method   Molecular Force Method   Torque Method

FIG. 12.   Testing for invariance of the reduced-unit structure for the three different methods for the ASD, IPL, and OTP models. Results were averaged over 152 configurations to improve statistics. As previously, the configuration was scaled uniformly to the relevant density ρ_2 in order to determine the corresponding temperature T_2. (a), (b), (c) show results for state points generated by the atomic and molecular force and torque method for ASD model. (d), (e), (f) show results for state points generated by the atomic and molecular force and torque for IPL model. (g), (h), (i) show results for state points generated by the atomic and molecular force and torque for OTP model.

definition of a Roskilde-simple system", The Journal of Chemical Physics, **141**, 204502 (2014).

[12] Bailey,Nicholas P. and Pedersen,Ulf R. and Gnan,Nicoletta and Schrøder,Thomas B. and Dyre,Jeppe C. "Pressure-energy correlations in liquids. II. Analysis and consequences", The Journal of Chemical Physics, **129**, 184508 (2008).

[13] Schrøder,Thomas B. and Bailey,Nicholas P. and Pedersen,Ulf R. and Gnan,Nicoletta and Dyre,Jeppe C. "Pressure-energy correlations in liquids. III. Statistical mechanics and ther-

modynamics of liquids with hidden scale invariance", The Journal of Chemical Physics, **131**, 234503 (2009).

[14] Pedersen, Ulf R. and Bailey, Nicholas P. and Schrøder, Thomas B. and Dyre, Jeppe C. "Strong Pressure-Energy Correlations in van der Waals Liquids", Phys. Rev. Lett, **100**, 015701 (2008).

[15] Albrechtsen, Dan E. and Olsen, Andreas E. and Pedersen, Ulf R. and Schrøder, Thomas B. and Dyre, Jeppe C. "Isomorph invariance of the structure and dynamics of classical crystals", Phys. Rev. B, **90**, 094106 (2014).

[16] Bacher,Andreas Kvist and Schrøder,Thomas B. and Dyre,Jeppe C. "The EXP pair-potential system. II. Fluid phase isomorphs", The Journal of Chemical Physics, **149**, 114502 (2018).

[17] Costigliola, Lorenzo and Schrøder, Thomas B. and Dyre, Jeppe C. "Freezing and melting line invariants of the Lennard-Jones system", Phys. Chem. Chem. Phys. **18**, 14678-14690 (2016).

[18] Ingebrigtsen, Trond S. and Schrøder, Thomas B. and Dyre, Jeppe C. "Isomorphs in Model Molecular Liquids", The Journal of Physical Chemistry B, **116**, 1018-1034 (2012).

[19] Veldhorst,Arno A. and Dyre,Jeppe C. and Schrøder,Thomas B. "Scaling of the dynamics of flexible Lennard-Jones chains" The Journal of Chemical Physics, **141**, 054904 (2014).

[20] Wence Xiao and Jon Tofteskov and Troels V. Christensen and Jeppe C. Dyre and Kristine Niss. "Isomorph theory prediction for the dielectric loss variation along an isochrone", Journal of Non-Crystalline Solids, **407**, 190-195 (2015).

[21] Hansen,H.W. and Sanz,A. and Adrjanowicz,K. and Frick,B. and Niss,K. "Evidence of a one-dimensional thermodynamic phase diagram for simple glass-formers", Nature Communications, **9**, 518, (2018).

[22] Olsen,Andreas Elmerdahl and Dyre,Jeppe C. and Schrøder,Thomas B. "Communication: Pseudoisomorphs in liquids with intramolecular degrees of freedom", The Journal of Chemical Physics, **145**, 241103, (2016).

[23] Schrøder,Thomas B. "Predicting Scaling Properties From a Single Fluid Configuration", arXiv:2105.12258 [cond-mat.soft] (2021).

[24] Nicholas P. Bailey and Trond S. Ingebrigsen and Jesper Schmidt Hansen and Arno A. Veldhorst and Lasse Bøhling and Claire A. Lemarchand and Andreas E. Olsen and Andreas K. Bacher and Lorenzo Costigliola and Ulf R. Pedersen and Heine Larsen and Jeppe C. Dyre and Thomas B. Schrøder. "RUMD: A general purpose molecular dynamics package optimized to utilize GPU hardware down to a few thousands particles", SciPost Physics, **3**, 038, (2017).

[25] Jorge Nocedal; Wright Stephen J. "Numerical optimization", Springer, New York, NY, (2006).

[26] William H. Press. "Numerical Recipes", Cambridge University Press, (2007).

[27] Magnus R. Hestenes and Eduard Stiefel. "Methods of Conjugate Gradients for Solving Linear Systems", Journal of Research of the National Bureau of Standards, **49**, 2379, (1952).

[28] Schrøder, Thomas B. and Pedersen, Ulf R. and Bailey, Nicholas P. and Toxvaerd, Søren and Dyre, Jeppe C. "Hidden scale invariance in molecular van der Waals liquids: A simulation study", Phys. Rev. E, **80**, 041502, (2009).

[29] Dyre, Jeppe C. "Simple liquids' quasiuniversality and the hard-sphere paradigm", Journal of Physics: Condensed Matter, **28**, 323001, (2016).

[30] Dyre, Jeppe C. "Perspective: Excess-entropy scaling", The Journal of Chemical Physics, **149**, 210901, (2018).

Predicting scaling properties of fluids from individual configurations: Pseudoisomorphs

Zahraa Sheydaafar,* Jeppe C. Dyre, and Thomas B. Schrøder†

Glass and Time, IMFUFA, Department of Science and Environment,

Roskilde University, P.O. Box 260, DK-4000 Roskilde, Denmark

(Dated: May 31, 2021)

Abstract

Pseudoisomorphs are curves in the thermodynamic phase diagram with invariant structure and dynamics, but not invariant excess entropy. Pseudoisomorphs have been found in molecular models with flexible bonds. Here we present force based methods to trace out pseudoisomorphs, and test them on the asymmetric dumbbell model and the 10-bead Lennard-Jones chain model, both with bonds modeled as harmonic springs. For each model a specific method that work very well in tracing out pseudoisomorphs is presented.

---

* samaneh@ruc.dk

† tbs@ruc.dk

I. INTRODUCTION

Isomorphs are curves in the thermodynamic phase diagram along which structure, dynamics, and excess entropy (the entropy minus that of the ideal gas with same density and temperature) in the appropriate units to a good approximation are invariant. Systems with isomorphs are termed Roskilde-simple, and they are characterized by strong correlation between the canonical-ensemble equilibrium fluctuations of potential energy, U, and virial, W, as quantified by the Pearson correlation coefficient (where sharp brackets denote canonical averages, and Δ denotes the deviation from the mean):

$$R = \frac{\langle \Delta W \Delta U \rangle}{\sqrt{\langle (\Delta W)^2 \rangle \langle (\Delta U)^2 \rangle}} \,. \tag{1}$$

$R > 0.9$ was given as the criteria for being Roskilde-simple, but even systems with slightly lower R values can be found to have isomorphs. The ismorphic invariance of structure and dynamics requires the use of so-called reduced units, where the unit of energy is given by $e_0 \equiv k_B T$, the unit of length is given by $l_0 \equiv \rho^{-1/3}$, and the unit of time is given by $t_0 \equiv \rho^{-1/3} \sqrt{m/k_B T}$, where m is a characteristic mass of the system.

As mentioned, isomorphs have invariant excess entropy, i.e., they are configurational adibats. In all systems, Roskilde-simple or not, configurational adibats can be traced out using the general statistical mechanics relation:

$$\gamma \equiv \left(\frac{\partial \ln T}{\partial \ln \rho} \right)_{S_{\mathrm{ex}}} = \frac{\langle \Delta U \Delta W \rangle}{\langle (\Delta U)^2 \rangle} \,. \tag{2}$$

Evaluating the right-hand side by equilibrium NVT simulations, a configurational adiabat can be identified in the (ρ, T) phase diagram by solving the differential equation, Eq. (2), numerically.

Isomoprhs have been found in both atomic and molecular systems. For molecular systems, isomorphs are found when bonds are modeled by fixed constraints, but not when flexible bonds are used. Fig. 1 shows scatter plots of the virial versus potential energy for asymmetric dumbbell and 10-bead Lennard-Jones chain models, both with harmonic springs. Neither model are Roskilde-simple; the correlation coefficients are 0.579 and 0.284, respectively, and as expected they are found not to have isomorphs. Nevertheless, empirical scaling reveal that both models have curves in the phase diagram with invariant structure and dynamics but *not* invariant excess entropy. These curves are termed "pseudoisomorphs".
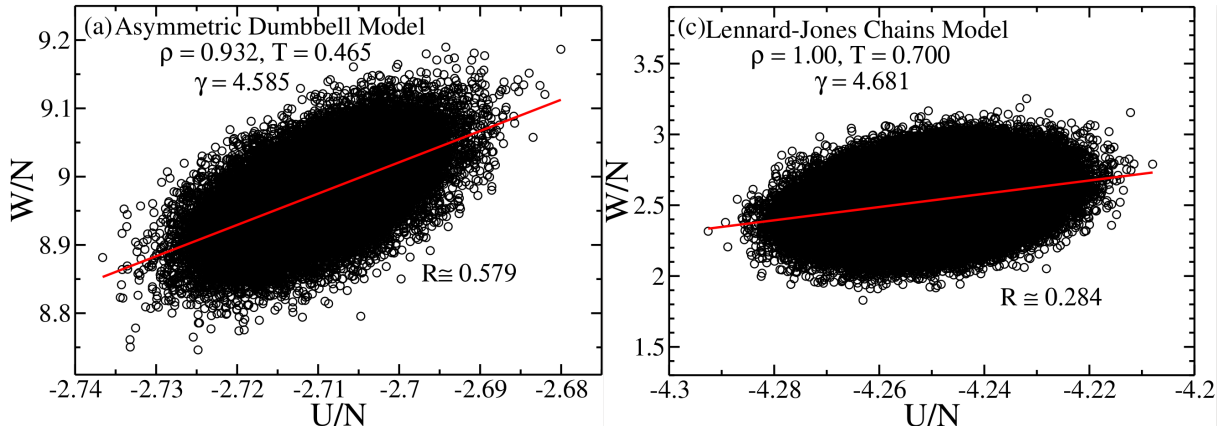
2

FIG. 1. The potential energy and virial fluctuations for two models ASD and LJC with harmonic spring intermolecular interactions. (a) The correlation coefficient ($R = 0.579$) and linear regression slope $\gamma = 4.585$ at state point taken from reference [12] of asymmetric dumbbell model with spring bonds. (b) The similar quantities correlation for flexible Lennard-Jones chain model, including the harmonic bonds. The correlation coefficient for this model also shrink a lot, $R = 0.204$.

Since pseudoisomorphs are not configurational adiabats, Eq. (2) can not be used to identify them. In 2016 Olsen *et al.* presented a method for tracing out pseudoisomorphs; i) a configuration is quenched to the nearest local minimum in the high dimensional potential energy landscape (an "inherent state") ii) the Hessian matrix is set up and diagonalised to find the vibrational spectrum; iii) the high frequency part of the spectrum related to the springs is identified, and the scaling properties of the remaining part of the spectrum is utilized to identify the pseudoisomorph. This method works, but is quite complicated to apply. Fig. 2 demonstrates invariance of dynamics in both the asymmetric dumbbell (ASD) and the flexible Lennard-Jones chain (LJC) along the state points that Ref. [7] determined are pseudoisomorphs.

The present paper investigates much simpler methods for generating pseudoisomorphs. The new methods are based on the scaling properties of the forces in a single configuration. This works very well for atomic systems like the Kob-Andersen binary Lennard-Jones mixture[13], and molecular models like the asymmetric dumbbell model and the Lewis-Wahntrom OTP model with bonds modeled by constraints[14]. The present paper extends the single-configuration idea to deal with a molecular system that does not have strong virial potential-energy correlations, and thus does not have isomorphs, but might have pseudoisomorphs.

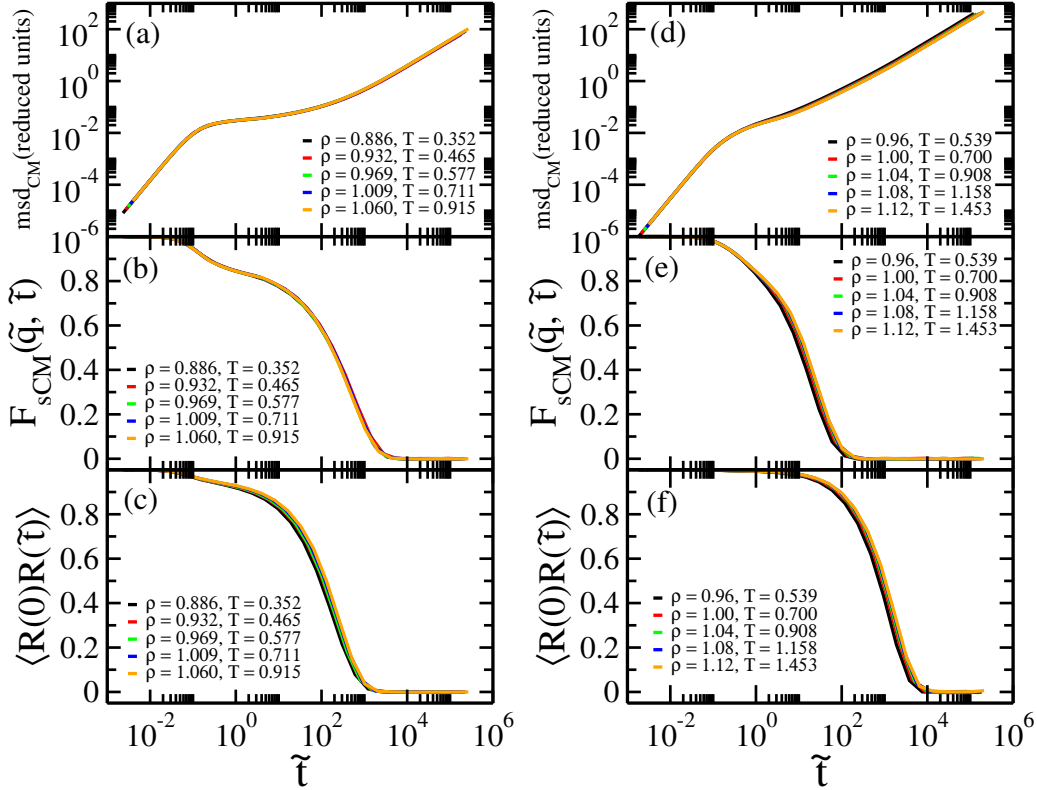Asymmetric Dumbbell   Lennard-Jones Chains

FIG. 2. Test of invariance of dynamics along state points determined by Olsen *et al*[7] to be pseudoisomorphs. (a)-(c) the asymmetric dumbbell with harmonic springs. (d)-(f) the 10-bead Lennard-Jones chain model with harmonic springs. (a, d) show the reduced mean-square displacement of the center of mass plotted as a function of reduced time. (b, e) show the center-of-mass incoherent intermediate scattering function as a function of the reduced time at the reduced wave-vector given by $\tilde{q} = q(\rho_2/\rho_1)^{1/3}$. (c, f) show the normalized end-to-end vector autocorrelation function, which probes the decay of molecular orientation.

II. MODELS AND SIMULATION DETAILS

We simulated the asymmetric dumbbell model (ASD) with 5000 molecules consisting of two different sized Lennard-Jones (LJ) spheres, a large (A) and a small (B) particle. The parameters of the model were chosen to mimic toluene[15]. Adopting the units defined by the large sphere ($\sigma_{AA} \equiv 1$, $\epsilon_{AA} \equiv 1$, and $m_A \equiv 1$), the other LJ-parameters are given by $\sigma_{AB} = 0.894$, $\sigma_{BB} = 0.788$, $\epsilon_{AB} = 0.342$, $\epsilon_{BB} = 0.117$, $m_B = 0.195$. The bonds are modeled

as harmonic spring, with an equilibrium length 0.584, and a spring-constants $k = 3000$.

For 10-bead Lennard-Jones chain (LJC) system, we simulated 1000 molecules. All particles are the same type, with the potential parameters and bond lengths set to unity $\sigma = 1, \epsilon = 1, l = 1\sigma$. Particles in different molecules and non-bonded particles interact via the standard LJ potential, cutting and shifting the forces at 2.5σ.

All Molecular Dynamics simulations were performed in the NVT ensemble with a Nose-Hoover thermostat using RUMD, an open-source package that can be downloaded at `http://rumd.org` [16].

III. IDENTIFYING PSEUDOISOMORPHS VIA FORCE-BASED METHODS

Force methods have been introduced in refs. [14, 17]. Briefly, the idea is the following: Given a configuration, $\mathbf{R}_1$, at state point (ρ_1, T_1) an affine scaling to density ρ_2 is performed: $\mathbf{R}_2 = (\rho_1/\rho_2)^{1/3} \mathbf{R}_1$. For molecules, two variants of this scaling can be applied; i) "molecular scaling", where the center-of-mass of molecules are scaled while orientation and internal degrees of freedom are kept fixed. ii) "atomic scaling", where the affine scaling is applied to positions of all atoms, thus modifying internal degrees of freedom. After the scaling of the configuration, the forces associated with the two configurations, $\mathbf{F}(\mathbf{R}_1)$, $\mathbf{F}(\mathbf{R}_2)$, are compared. If the new temperature, T_2 can be chosen such that forces are the same in reduces units, $\tilde{\mathbf{F}}(\mathbf{R}_1) = \tilde{\mathbf{F}}(\mathbf{R}_2)$, and if this is representative of all the relevant configurations, we can expect structure and dynamics to be invariant in reduced units, since it is the same differential equation being solved when simulating the two state points. In practice, the temperature at density ρ_2 is chosen by,

$$T_2 = \frac{|\mathbf{F}(\mathbf{R}_2)|}{|\mathbf{F}(\mathbf{R}_1)|} \left(\frac{\rho_1}{\rho_2} \right)^{1/3} T_1, \tag{3}$$

which ensures $|\tilde{\mathbf{F}}(\mathbf{R}_1)| = |\tilde{\mathbf{F}}(\mathbf{R}_2)|$. Different variants of the method is arrived at by different interpretations of what exactly $\mathbf{F}(\mathbf{R})$ represents, e.g., the forces on all the atoms in the system, or the center-of-mass force on all molecules. We consider also a special variant, based on invariance of torques in reduced units, $\tilde{\boldsymbol{\tau}}_1 = \tilde{\boldsymbol{\tau}}_2$, leading to:

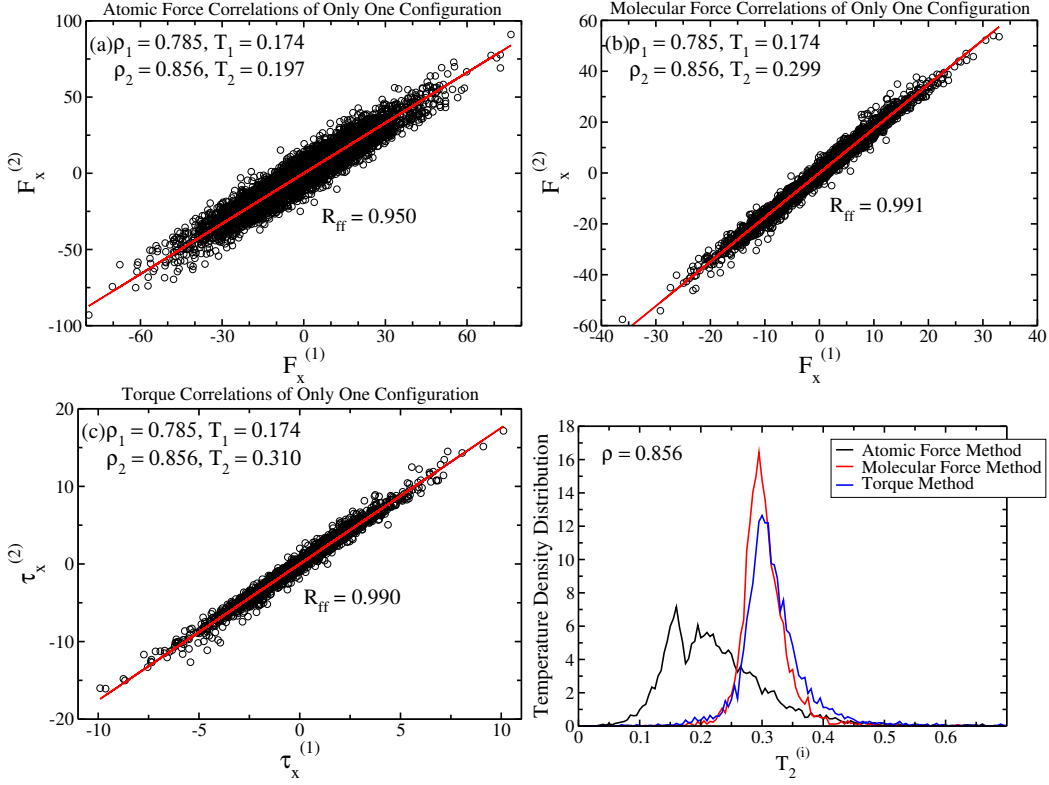$$T_2 = \frac{|\boldsymbol{\tau}_2|}{|\boldsymbol{\tau}_1|} T_1 . \tag{4}$$

5

FIG. 3. Force and torque correlations in harmonic ASD model using molecular scaling. (a) ["atomic-force method"] shows the x-coordinates of the reduced forces on all particles plotted against the same quantities of the uniformly scaled configuration. The new temperatures are identified by Eq. (3). (b) ["molecular-force method"] shows the same for the center-of-mass "molecular" forces between the molecules, which has no contributions from the intramolecular spring forces. (c) ["Torque method"] shows the same correlation between the torque of molecules of unscaled and scaled configuration. (d) show the distribution of predicted temperatures, by applying the methods to individual atoms and molecules.

The three methods are applied in Fig. 3, using molecular scaling for the initial scaling of the configuration, $\mathbf{R}_{2,cm} = (\rho_1/\rho_2)^{1/3}\mathbf{R}_{1,cm}$. $(\rho_1, T_1) = (0.785, 0.174)$ is used as the reference state point and $\rho_2 = 0.856$, i.e., a 9% increase in density. Fig. 3(a) shows a scatter plot of atomic force components, before and after scaling for a single configuration. $T_2 = 0.197$ is found by applying atomic forces in Eq. (3); Fig. 3(b) shows a similar plot based on the center-of-mass, or "molecular", forces between the molecules. Better correlation is obtained, and a quite different $T_2 = 0.299$ is arrived at. Fig. 3(c) shows the torque correlations of molecules of unscaled and scaled configuration. The correlation is comparable with correlation of

6

molecular force. Using Eq. (4) gives $T_2 = 0.310$. Figure 3(d) shows distributions of the temperatures predicted from applying Eq. (3) and Eq. (4) to individual atoms and molecules. If the scaling was perfect, the distribution of predicted temperatures whould be a delta-function, i.e., all atoms/molecules would "agree" on what the new temperature should be. The molecular forces are found to give the smallest width of the distribution of predicted temperatures.

For each of the three methods for identifying state points of possible dynamic invariances, Fig. 4 compares the results for the dynamic signatures of the system studied in Fig. 2. The methods only require a single configuration, but when comparing the methods T_2-values were averaged over 195 independent configurations. We find that the molecular-force method gives very invariant dynamics, with the exception of the lowest density where negative pressure and a phase separation is observed. The torque method gives similar, but slightly worse, results. The atomic force method does not work.

Next we turn our attention to the 10-bead Lennard-Jones chains (LJC). For this model one can use not only the atomic and center-of-mass forces but also the segmental forces, defined as:

$$\mathbf{F}_{Seg,j} \equiv \frac{1}{d_j}\mathbf{F}_j + \frac{1}{d_{j+1}}\mathbf{F}_{j+1}, \tag{5}$$

where d_j and d_{j+1} are the number of bonds in which particle jth and $(j+1)th$ are involved in. Note that the segmental forces here are defined so that:

$$\mathbf{F}_{Mol} = \sum_{j=1}^{9}\mathbf{F}_{Seg,j}, \tag{6}$$

The dynamics are invariant along atomic (a, b, c) and segmental force (g, h, i) methods in Fig. 5 except at lowest density from reference point $(\rho_1, T_1) = (1.00, 0.700)$. Same densities are given from Fig. 1. On the other hand, the predicted points via the center-of-mass force method are not pseudoisomorphic due to the intramolecular interactions (Fig. 5 (d, e, f)). The torque method estimates the appropriate point at densities $\rho = 1.00, 1.04, 1.08, 1.12$, not the lowest and highest densities (Fig. 5 (j, k, l)). The atomic and segmental force methods predict the appropriate state points in LJC model whereas the molecular force method gives better results in small molecular models (i. e. ASD model).
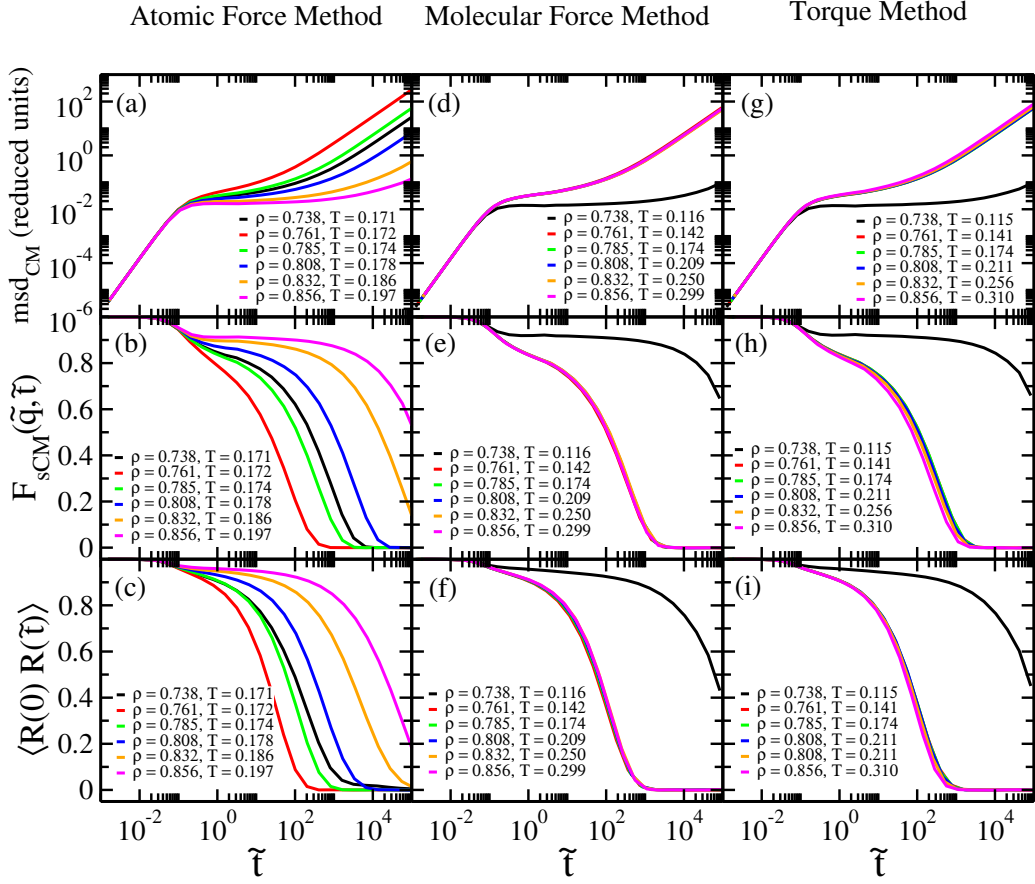
FIG. 4. Testing for invariance of the reduced dynamics for each of three different methods for generating pseudoisomorphs based on a single equilibrium configuration of the reference state point $(\rho_1, T_1) = (0.785, 0.174)$. Each method investigates the reduced center-of-mass mean-square displacement (upper figures), the center-of-mass incoherent intermediate scattering function (middle figures), and the directional autocorrelation function probed via the autocorrelation function of the normalized bond vector (bottom figures). (a), (b), (c) show results for state points generated by the atomic-force method based on requiring invariant reduced forces between all atoms, i.e., including the harmonic bond contributions (Eq. (3)). (d), (e), (f) show results for state points generated by the molecular-force method requiring invariant reduced center-of-mass forces between the molecules (Eq. (3)). (g), (h), (i) show results for state points generated by the torque method requiring invariant reduced torques on the molecules (Eq. (4)).
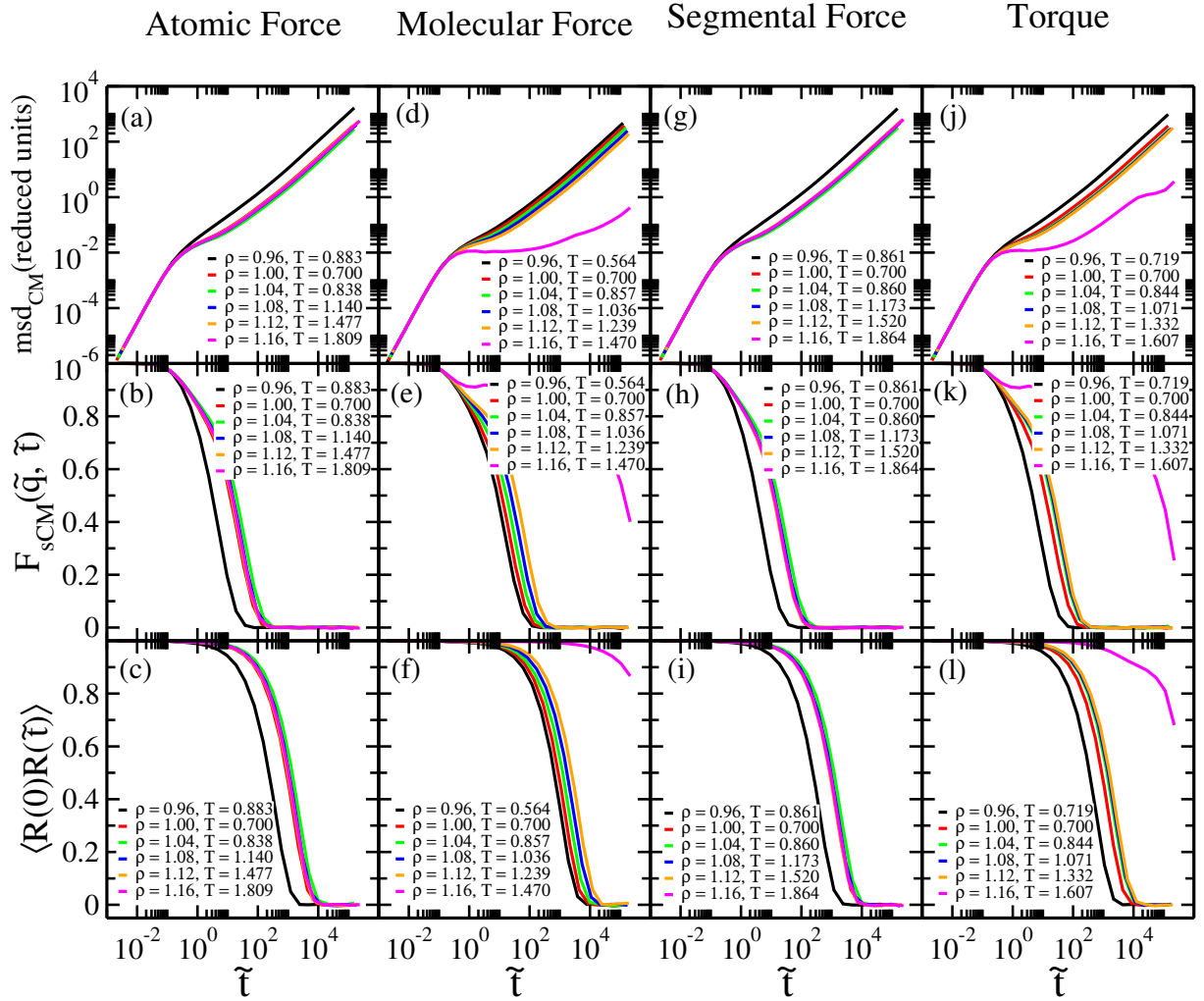
8

FIG. 5. The dynamics of the LJC model with harmonic bonds using the force methods applying the atomic scaling method. The reference point is $(\rho_1, T_1) = (1.00, 0.700)$. The density increases about 17%. The atomic force method (a, b, c) generate the proper pseudoisomorph at higher densities from the reference point. However, the molecular force method (d, e, f) do not achieve the pseudoisomorphs as expected, the segmental force method (g, h, i) gives the appropriate prediction also at higher densities; And the torque method (j, k, l) provides the good results at some of the densities $\rho = 1.00, 1.04, 1.08, 1.12$.

IV. PSEUDOISOMORPHS IN ASD MODEL AT HIGH DENSITIES

In Fig. 4 we applied the force based methods to the ASD and found good invariance of the dynamics using the molecular force method, and to a slightly lesser degree the torque
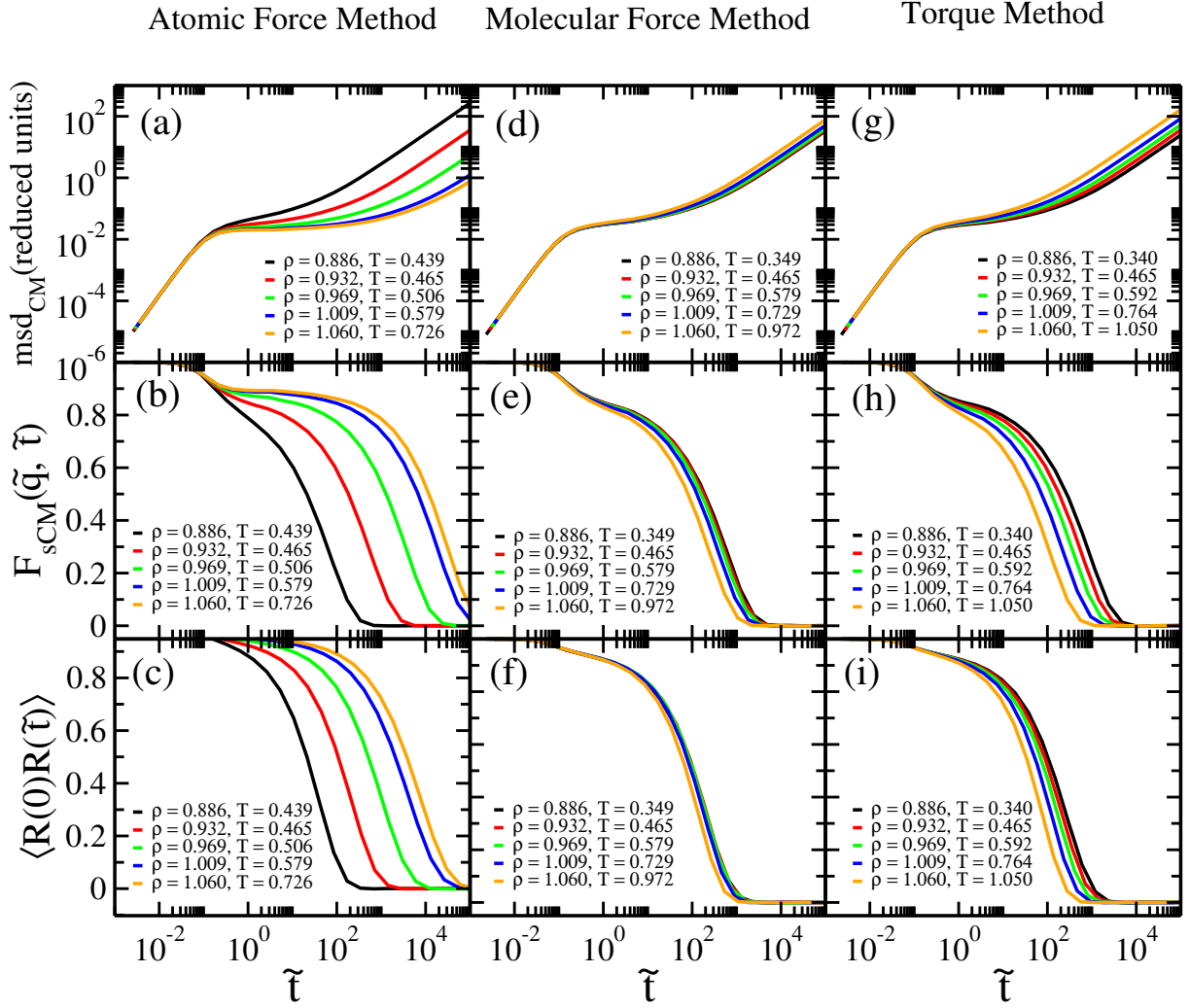
9

FIG. 6. Mean square displacement, incoherent intermediate scattering function and orientational autocorrelation function of end-to-end vector of the ASD model with harmonic spring bonds evaluated along invariant forces through the CM scaling. Reference point is $(\rho_1, T_1) = (0.932, 0.465)$ taken from ref. [7] . The density changes above 19%

method. Note however, that the densities used ($\rho = 0.738 \to 0.856$) are smaller than the densities ($\rho = 0.886 \to 0.972$) applied by Olsen *et al*[7] (Fig. 2). Fig. 6 shows the results of applying the same methods as in Fig. 4, but at the higher densities used by Olsen *et al*[7]. The molecular force method is still the best method, but the invariance of the dynamics is clearly inferior to what was found at low densities.
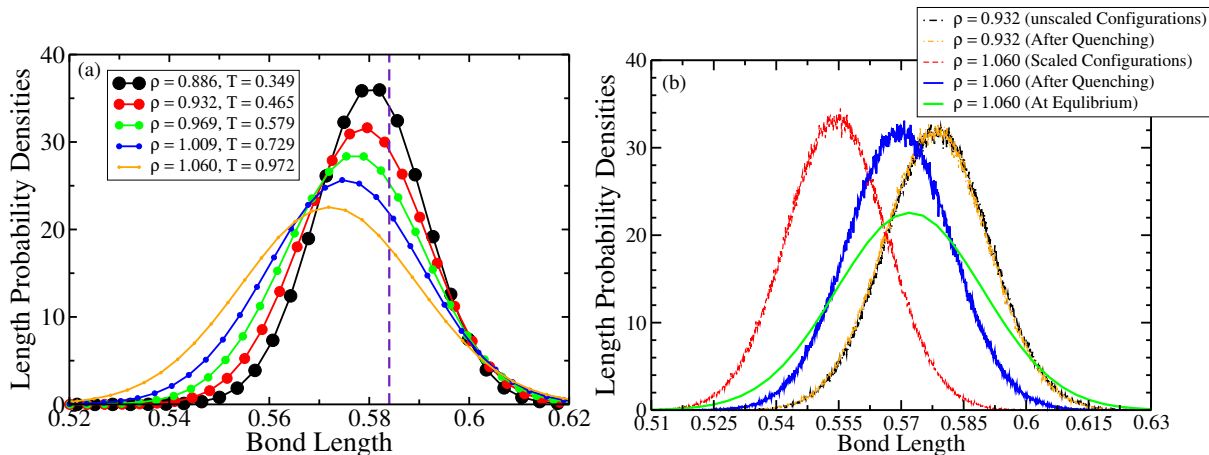
10

A.   What's the problem

FIG. 7. Distribution of bond lengths along the molecular force method around the length of the spring (purple dashed line) and comparing the bond length distribution of unscaled and scaled configurations. The figures demonstrate that bonds are compressed when the density is increased. This affects not just the intramolecular, but also the intermolecular forces. (a) Comparing the bond length of different state points in which $\rho = 0.932$ is the reference point at equilibrium. Bond length is shifting by scaling the system at different densities. (b) Shows quenching the system according to the constraint conditions (fix the centre-of-mass and orientational direction of molecules fix), causes the bonds compressed to their right length at equilibrium (green). Comparing the bond length of unscaled (black) and scaled (red) configurations shows how the bond length decreased by scaling the system at high density before quenching, which is different from the bond length at equilibrium (green). This difference is disappeared by quenching the system (blue).

Fig. 7(a) shows the distributions of bond lengths for equilibrium simulations at the state points generated by the molecular force method. The bonds are compressed when the density is increased, an effect that is not seen at the lower densities used in Fig. 4. This means that when a configuration from the reference state point is scaled to a higher density, this scaled configuration is not representative of equilibrium configurations at the new state point, since the bonds are too long.

In an attempt to eliminate the effects of the harmonic bonds, for any given configuration we kept fixed the center of mass and orientation of each molecule. For this "constrained" system a scalar l was added to all bond lengths, and the potential energy was the minimized

11

as a function of l. In this way any given configuration is mapped into a "quenched" configuration with minimized harmonic bond energy, in effect removing the non-scaling degrees of freedom suspected of causing the poor invariance seen in Fig. 6 and giving the proper bond lengths (Fig. 7 b). Note that the system is scaled before quenching, not the other way around.
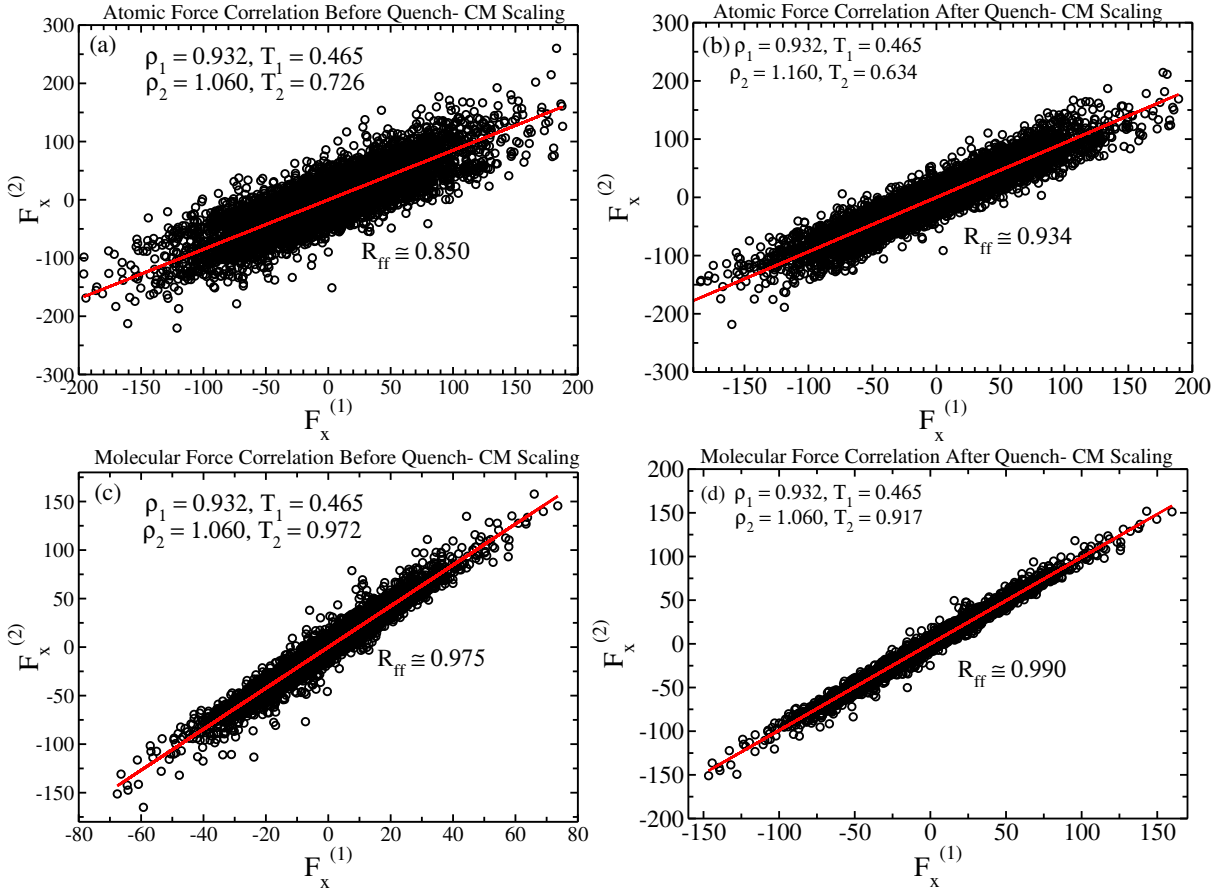

FIG. 8. Correlation of atomic force (a, b) molecular force (c, d) of molecules. One configuration is taken from equilibrium simulation at $(\rho_1, T_1) = (0.932, 0.465)$. Then the temperature at $\rho_2 = 1.060$ is predicted by using Eq. (3). Analog of Fig. 3 for pairs of quenched configurations. For both the atomic-force (b) and the molecular force (d) methods we find better correlation between scaled and non-scaled forces after quenching.

Based on pairs of quenched configurations one may apply again the atomic-force, molecular-force, and torque methods to generate state points with, possibly, the same dynamics. The method we implemented works as follows. A single configuration is selected from an equilibrium simulation at the reference state point (density ρ_1). This configuration

12

is scaled uniformly to the density of interest, ρ_2. Both scaled and unscaled configurations were quenched as described above in order to eliminate the bond vibrational degrees of freedom. After this the relevant forces / torques were evaluated and the temperature T_2 was determined from Eq. (3) and Eq. (4). Figure 8(a) shows the force-force scatter plot of a single scaled configuration versus those of the unscaled configuration before quenching, while (b) shows the better force correlations after quenching. (c, d) show the correlations of center-of-mass forces before and after quenching. The quench method leads to better correlation, with the correlation coefficient increasing from 0.850 to 0.934 for the atomic forces and from 0.975 to 0.990 for the molecular (center-of-mass) forces.
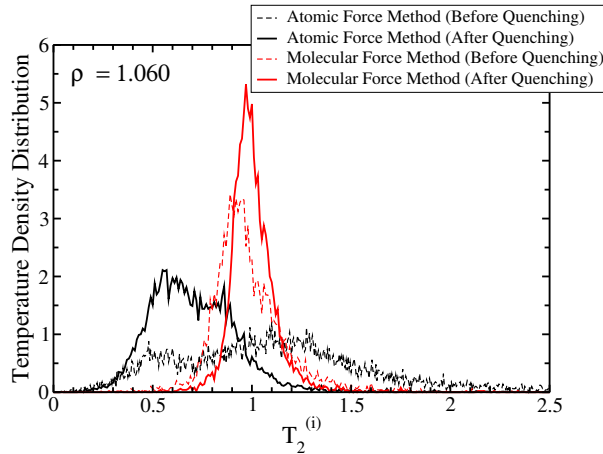

FIG. 9. Distribution of each particles temperature predicted via atomic and molecular forces. For both methods T_2 distributions narrow after quenching (full lines) compared to those of before quenching (dashed lines). These improved consistency results give hope that the quenching procedure results in more invariant dynamics specially by molecular force method; this is tested below in Fig. 10.

High correlation signals an internal consistency of the procedure and also narrow temperatures prediction distribution in Fig. 9 which give hope for a good collapse of the reduced dynamics. This is tested in Fig. 10 that is analogous to Fig. 6 except that all temperatures T_2 are based on quenched configurations. We again averaged over 195 pairs of scaled and non-scaled configurations in order to improve the statistics. The best results are obtained with the molecular-force method, which is also the one that worked best in Fig. 4. For this method we here find excellent collapse of the reduced center-of-mass mean-square displacement as a function of time, as well as of the center-of-mass incoherent intermediate
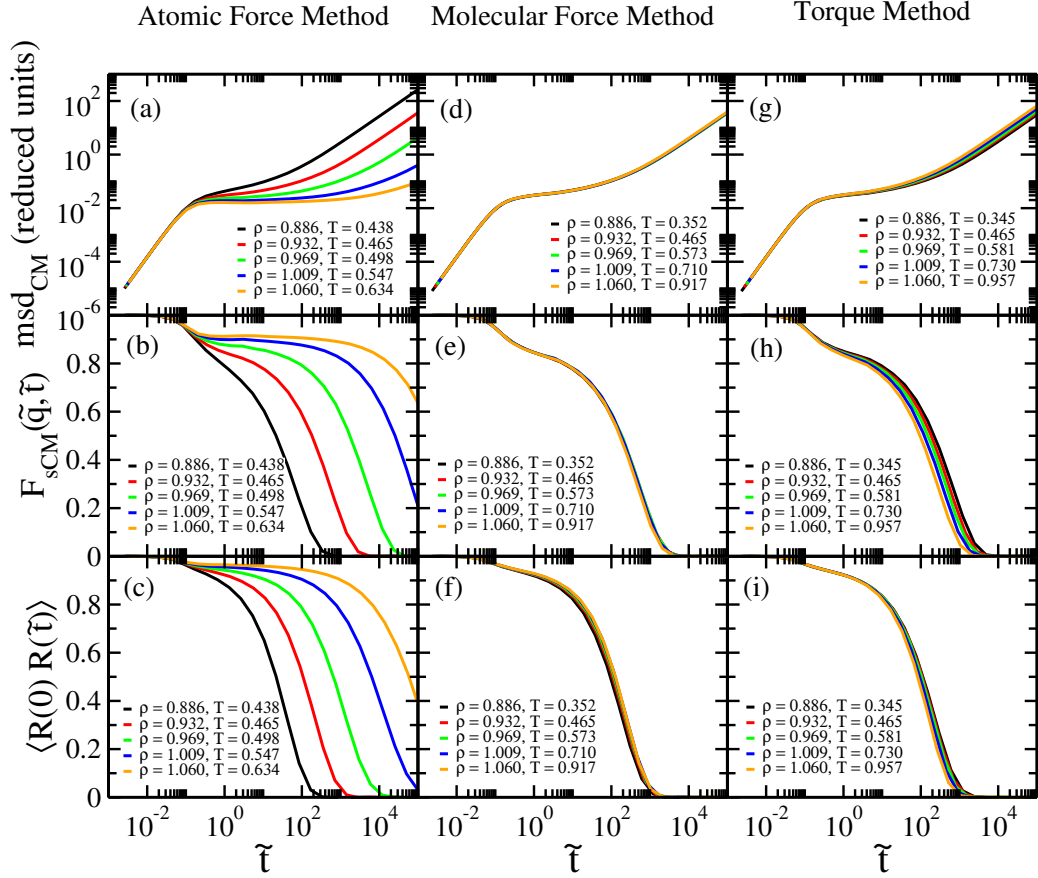
13

FIG. 10. Testing for invariance of the reduced dynamics for the three different "quench" methods for generating pseudoisomorphs based on a single equilibrium configuration from the reference state point $(\rho_1, T_1) = (0.932, 0.465)$. The configuration was scaled uniformly to the relevant density ρ_2 in order to determine the corresponding temperature T_2. In contrast to Fig. 6, the scaled and non-scaled configurations were quenched to a potential-energy minimum to eliminate the harmonic bond degrees of freedom, after which procedure T_2 was determined as above in Fig. 6. (a), (b), (c) show results for state points generated by the atomic-force method requiring invariant reduced forces between all atoms, i.e., including the harmonic bond contributions (Eq. (3)). (d), (e), (f) show results for state points generated by the molecular-force method requiring invariant reduced center-of-mass forces between the molecules (Eq. (3)). (g), (h), (i) show results for state points generated by the torque method requiring invariant reduced torques on the molecules (Eq. (4)).

scattering function, while the directional autocorrelation function shows slightly worse collapse but nevertheless significantly better than without quenching. Comparing the results of the torque method with and without quenching shows that quenching also significantly
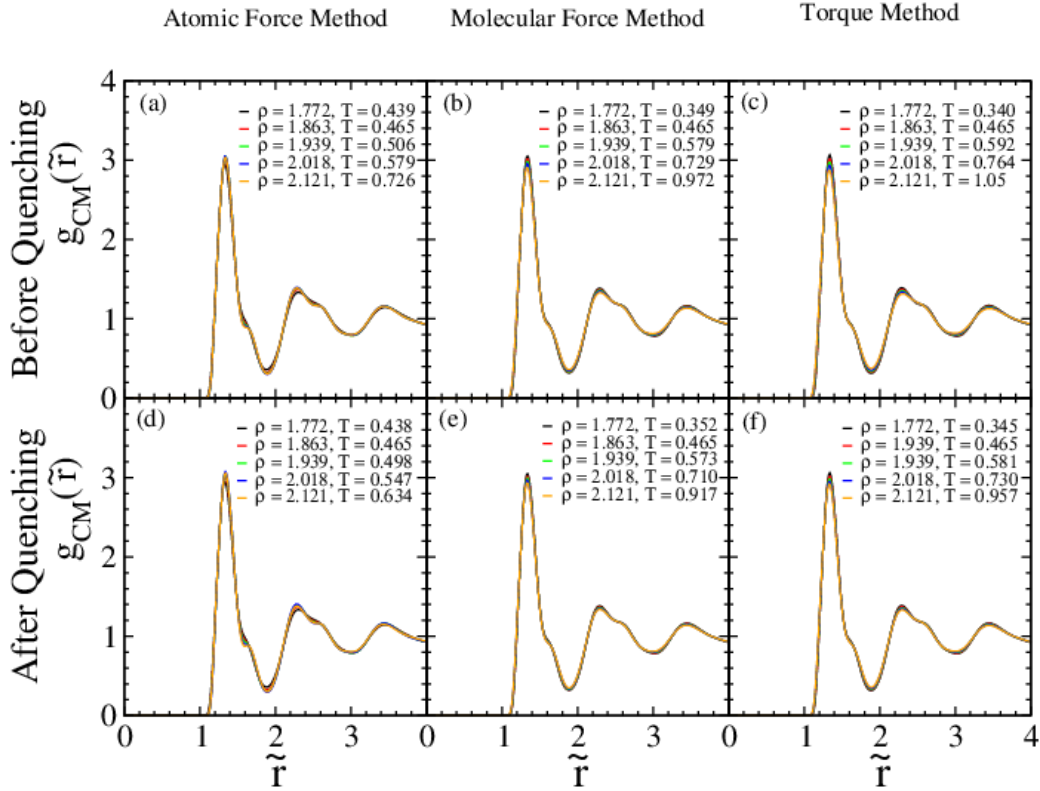
FIG. 11.   Testing for invariance of the reduced-unit structure for the three different methods for without and with quenching for generating pseudoisomorphs based on a single equilibrium configuration from the reference state point $(\rho_1, T_1) = (0.932, 0.465)$. The configuration was scaled uniformly to the relevant density ρ_2 in order to determine the corresponding temperature T_2. (a), (b), (c) show results for state points generated by the atomic and molecular force and torque method before minimization. (d), (e), (f)show results for state points generated by the atomic and molecular force and torque methods after minimization.

improves the invariances. Using the atomic scaling give the same results for molecular force and torque method after we quench the system in Table I while the atomic force gives different results compared to Fig. 10.

V.   DISCUSSION

Genuine isomorphs do not exist in systems without strong virial potential-energy correlations, like systems of molecules with harmonic bonds. For the asymmetric dumbbell model and long flexible Lennard-Jones chains with harmonic springs, we have seen that there ex-

TABLE I. Predicted temperature using the atomic scaling after quenching. The atomic force method provide different temperatures compared to Fig. 10. But molecular force and torque methods identify same state points.

density	$T(F_{Atomic})$	$T(F_{Mol})$	Torque
0.886	0.444	0.352	0.345
0.932	0.465	0.465	0.465
0.969	0.494	0.573	0.581
1.009	0.540	0.710	0.730
1.060	0.624	0.917	0.957

ists, nevertheless, curves along which the dynamics is invariant to a good approximation. Such curves are termed pseudoisomorphs [7]. Though they do not have invariant excess entropy, they still behave like isomorphs, in the sense that they have invariant strucure and dynamics in reduced units. Though not a focus here, we note that the structure is invariant to a good approximation for all three methods both with and without quenching (Fig. 11).

We tested several methods to generate pseudoisomorphs. All methods require only a single configuration. For the ASD model with harmonic bonds, the best method to trace out pseudoisomorphs is the molecular force method with molecular scaling and quencing of the harmonic bonds, see Fig. 10. At low densities, the quenching can be skipped (but it does not hurt), see Fig. 4. Interestingly, the molecular method does not work for the 10-bead LJ-chains. For this model the best method was found to be the atomic force method with atomic scaling.

ACKNOWLEDGMENTS

[1] N. Gnan, T. B. Schrøder, U. R. Pedersen, N. P. Bailey, and J. C. Dyre, *The Journal of Chemical Physics* **131**, 234504 (2009).

[2] J. C. Dyre, *The Journal of Physical Chemistry B* **118**, 10007 (2014), PMID: 25011702.

[3] T. S. INGEBRIGTSEN, T. B. SCHRØDER, and J. C. DYRE, *Phys. Rev. X* **2**, 011011 (2012).

[4] N. P. BAILEY, L. BØHLING, A. A. VELDHORST, T. B. SCHRØDER, and J. C. DYRE, *The Journal of Chemical Physics* **139**, 184506 (2013).

[5] E. FLENNER, H. STALEY, and G. SZAMEL, *Phys. Rev. Lett.* **112**, 097801 (2014).

[6] S. PRASAD and C. CHAKRAVARTY, *The Journal of Chemical Physics* **140**, 164501 (2014).

[7] A. E. OLSEN, J. C. DYRE, and T. B. SCHRØDER, *The Journal of Chemical Physics* **145**, 241103 (2016).

[8] N. P. BAILEY, U. R. PEDERSEN, N. GNAN, T. B. SCHRØDER, and J. C. DYRE, *The Journal of Chemical Physics* **129**, 184507 (2008).

[9] D. FRAGIADAKIS and C. M. ROLAND, *The Journal of Chemical Physics* **134**, 044504 (2011).

[10] K. KOPERWAS, A. GRZYBOWSKI, and M. PALUCH, *The Journal of Chemical Physics* **150**, 014501 (2019).

[11] D. FRAGIADAKIS and C. ROLAND, *The Journal of Chemical Physics* **150**, 204501 (2019).

[12] T. S. INGEBRIGTSEN, T. B. SCHRØDER, and J. C. DYRE, *The Journal of Physical Chemistry B* **116**, 1018 (2012), PMID: 22251282.

[13] T. B. SCHRØDER, *unpublished* .

[14] Z. SHEYDAAFAR, *unpublished* .

[15] T. B. SCHRØDER, N. P. BAILEY, U. R. PEDERSEN, N. GNAN, and J. C. DYRE, *The Journal of Chemical Physics* **131**, 234503 (2009).

[16] N. P. BAILEY, T. S. INGEBRIGTSEN, J. S. HANSEN, A. A. VELDHORST, L. BØHLING, C. A. LEMARCHAND, A. E. OLSEN, A. K. BACHER, L. COSTIGLIOLA, U. R. PEDERSEN, H. LARSEN, J. C. DYRE, and T. B. SCHRØDER, *SciPost Phys.* **3**, 038 (2017).

[17] T. B. SCHRØDER, *unpublished* .

Appendix H

Reprints of Posters

The Structure and Dynamics of Matter

Zahraa Sheydaafar, Thomas Schrøder and Jeppe Dyre

DNRF Centre "Glass and Time", IMFUFA, Department of Sciences, Roskilde University, Denmark

I. Isomorph Theory

According to the isomorph theory, dynamics and structure of strongly correlating liquids system, called simple Roskilde liquids, are invariant in different state points.

The correlation coefficient :

$$R = \frac{\langle \Delta W \Delta U \rangle}{\sqrt{\langle (\Delta W)^2 \rangle}\sqrt{\langle (\Delta U)^2 \rangle}}$$

.

$$R > 0.9$$

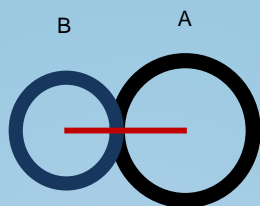Strongly Correlating Systems

Isomorph

II. Asymmetric Dumbbell Model

The asymmetric dumbbell model, mimic of the toluene, consists of two different type of LJ atoms, a large (A) and small (B) atoms, in which the intermolecular pair interaction is demonstrated by the Lennard-Jones potential :

$$u(r_{ij}) = 4\,\varepsilon_{ij}\left[\left(\frac{\sigma_{ij}}{r_{ij}}\right)^{12} - \left(\frac{\sigma_{ij}}{r_{ij}}\right)^{6}\right]$$

$$U = U_{LJ}$$

$$W = W_{LJ} + W_{con}$$

B   A

IV. Finding Isomorph

The scaling exponent :

$$\gamma = \frac{\langle \Delta U \, \Delta W \rangle}{\langle (\Delta U)^2 \rangle} = \left(\frac{\partial \ln T}{\partial \ln \rho}\right)_{S_{ex}}$$

V. Predicting Isomorphs in one configuration
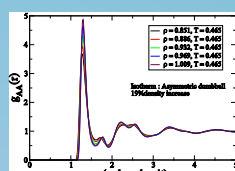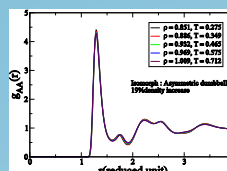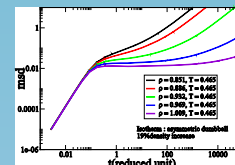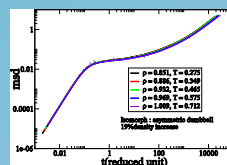
Invariance of reduced unit quantities :

$$\widetilde{R} = \rho^{1/3}R$$

$$\widetilde{F}(R) = \frac{F(R)}{\rho^{1/3}\,k_B T}$$

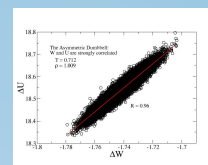$$\widetilde{F}(R_2) \cong \widetilde{F}(R_1)$$

The temperature of the second state point is quantified by :

$$T_2 = \left(\frac{\rho_1}{\rho_2}\right)^{1/3}\frac{|F_1|}{|F_2|}\,T_1$$
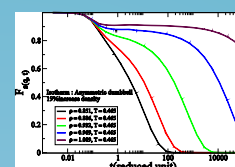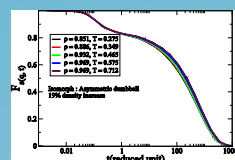
VI. Conclusion

Generating isomorphs via invariant reduced forces indicates the invariance of dynamics and structure of liquids at different predicted state points.
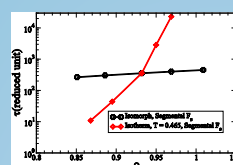
References

N. Gnan, T. B. Schrøder, U. R. Pedersen, N. P. Bailey, J. C. Dyre;" *Pressure-energy correlations in liquids. IV. "Isomorphs" in liquid phase diagrams*"; J. Chem. Phys. **131**, 234504 (2009).

A.E. Olsen, J. C. Dyre and T. B. Schroder; *"Communication : Pseudoisomorph in liquids with intermolecular degrees of freedom"*: J. Chem. Phys. **145**, 241103 (2016).

T. S. Ingebrigtsen, T. B. Schroder, J. C. Dyre; *"Isomorphs in Model Molecular Liquids";* J. Phys. Chem. B; **116**, 1018-1034 (2012).

Dynamical Scaled Approaches in Identifying Isomorphs

Zahraa Sheydaafar, Jeppe Dyre and Thomas Schrøder

DNRF Centre "Glass and Time", IMFUFA, Department of Sciences, Roskilde University, Denmark

I. IsomorphTheory

The strongly correlated liquids, termed Roskilde simple liquids, experience isomorphs. Dynamics and structural properties of Roskilde liquids are invariant along isomorphs curves. Identifying isomorphic state points is an important fundamental issue in the isomorphs theory.

II. Identifying Isomorph Methods

Scaling Exponent Method:

$$\gamma = \frac{\langle \Delta U\, \Delta W \rangle}{\langle (\Delta U)^2 \rangle} = \left(\frac{\partial \ln T}{\partial \ln \rho} \right)_{S_{ex}}$$

Direct Isomorph Check Method:

$$U_2 \simeq \frac{T_2}{T_1} U_1$$
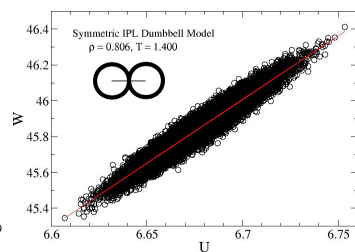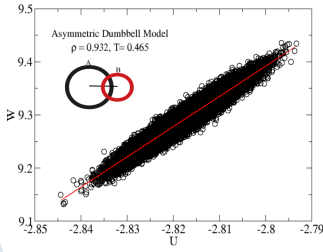
Invariant Dynamical Methods:

Force:

$$\widetilde{F}(R_1) \simeq \widetilde{F}(R_2) \quad , \quad \widetilde{F}(R) = \frac{F(R)}{\rho^{1/3} k_B T}$$

Torque:

$$\tilde{\tau}_1 \simeq \tilde{\tau}_2 \quad , \quad \tilde{\tau} = \frac{\tau}{k_B T}$$
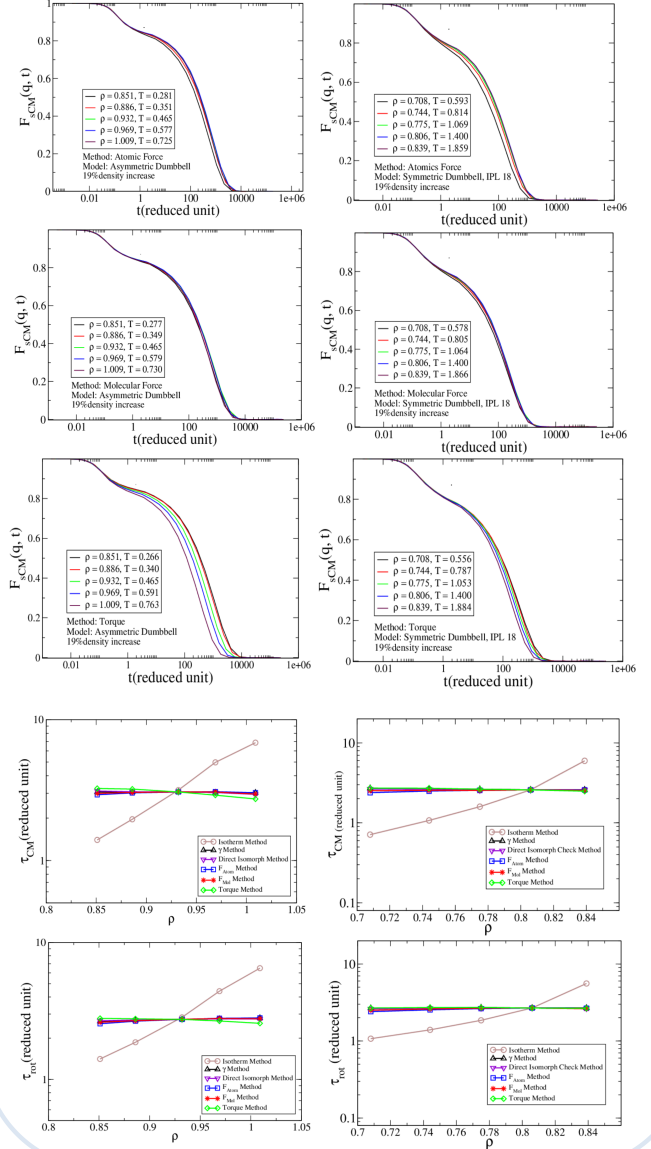
III. Models

$$U(r) = 4\varepsilon \left[\left(\frac{\sigma}{r} \right)^{12} - \left(\frac{\sigma}{r} \right)^6 \right]$$

$$U(r) = \varepsilon \left(\frac{\sigma}{r} \right)^{18}$$

IV. Results

Asymmetric Dumbbell Model

	Isotherm	γ	Dir-iso	F_{Atom}	F_{Mol}	Torque
$\frac{\partial \log \widetilde{D}}{\partial \log \rho}$	-70(2)	-0.5(4)	1.1(4)	-1.4(2)	-0.9(4)	7.47(6)
$\frac{\partial \log \widetilde{\tau_{CM}}}{\partial \log \rho}$	77(3)	-0.4(1)	-1.0(1)	1.60(7)	0.5(1)	-7.8(1)
$\frac{\partial \log \widetilde{\tau_{rot}}}{\partial \log \rho}$	65(3)	1.9(1)	1.26(2)	3.47(3)	2.62(7)	-2.6(2)

Symmetric Dumbbell Model

	Isotherm	γ	Dir-iso	F_{Atom}	F_{Mol}	Torque
$\frac{\partial \log \widetilde{D}}{\partial \log \rho}$	-113.4(6)	2.37(2)	0.88(1)	0.751(2)	1.770(5)	4.80(2)
$\frac{\partial \log \widetilde{\tau_{CM}}}{\partial \log \rho}$	126.7(7)	-1.35(2)	0.06(1)	1.71(1)	0.11(2)	-4.26(1)
$\frac{\partial \log \widetilde{\tau_{rot}}}{\partial \log \rho}$	107.9(6)	-0.87(1)	0.88(2)	0.91(2)	-1.37(3)	-1.807(7)

References

N. Gnan, T. B. Schrøder, U. R. Pedersen, N. P. Bailey, J. C. Dyre;" *Pressure-energy correlations in liquids. IV. "Isomorphs" in liquid phase diagrams"*; J. Chem. Phys. **131**, 234504 (2009)

A. E. Olsen, J. C. Dyre and T. B. Schroder; *"Communication : Pseudoisomorph in liquids with intermolecular degrees of freedom":* J. Chem. Phys. **145**, 241103 (2016).

T. S. Ingebrigtsen, T. B. Schroder, J. C. Dyre; *"Isomorphs in Model Molecular Liquids";* J. Phys. Chem. B; **116**, 1018-1034 (2012)

Predicting scaling properties of fluids from individual configurations

Zahraa Sheydaafar (samaneh@ruc.dk), Jeppe C. Dyre and Thomas Schrøder

DNRF Centre "Glass and Time", Department of Science and Environment, Roskilde University, Denmark

Pseudoisomorph Theory

Pseudoisomorph theory is identified in systems without strong virial potential-energy correlations by identifying lines of invariant dynamics in the phase diagram of spring harmonic bonded models [1]. These curves behave like isomorphs although the excess entropy is not invariant along an pseudoisomorph.

$$R = \frac{\langle \Delta W \Delta U \rangle}{\sqrt{\langle (\Delta W)^2 \rangle \langle (\Delta U)^2 \rangle}}$$
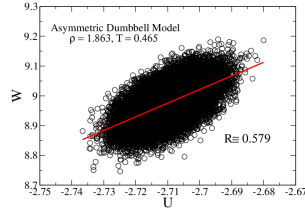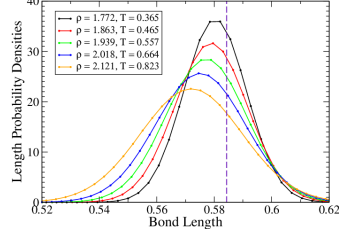

Identifying Pseudoisomorph

- **Invariance Force Method**

$$\tilde{\mathbf{F}}(\mathbf{R}_1) = \tilde{\mathbf{F}}(\mathbf{R}_2) \qquad T_2 = \frac{|\mathbf{F}(\mathbf{R}_2)|}{|\mathbf{F}(\mathbf{R}_1)|} \left(\frac{\rho_1}{\rho_2}\right)^{1/3} T_1$$

- **Invariance Torque Method**

$$T_2 = \frac{|\boldsymbol{\tau}_2|}{|\boldsymbol{\tau}_1|} T_1$$

Why dynamic methods do not work?

- **Minimization of the potential energy surface**

We consider two condition:

$$L_i' = L_i + dl_i$$
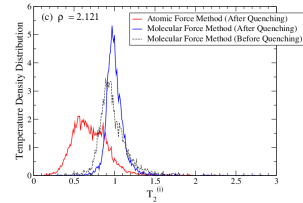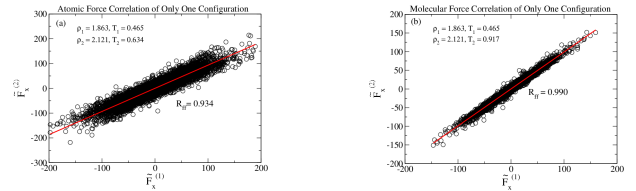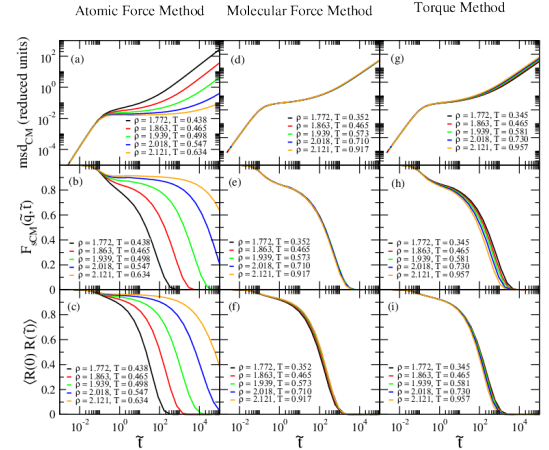
$$d\mathbf{R}_{cm} = 0$$

Update particles' positions:

$$\begin{cases} \mathbf{r}_j' = \mathbf{r}_j + \alpha \mathbf{dl_i} \ j \leq i \\ \mathbf{r}_j' = \mathbf{r}_j + \beta \mathbf{dl_i} \ j > i \end{cases}$$

$$\begin{pmatrix} \mathbf{dr_1} \\ \mathbf{dr_2} \end{pmatrix} = \begin{pmatrix} \dfrac{m_B}{m_A + m_B} \\ -\dfrac{m_A}{m_A + m_B} \end{pmatrix} \times dl_1 \hat{\mathbf{l}}_1$$

Calculate the minimum of potential in l space:

$$\frac{\partial U(\mathbf{L})}{\partial \mathbf{L}} = \frac{m_B}{m_A + m_B} \frac{\partial U}{\partial \mathbf{r_1}} \hat{\mathbf{l}}_1 - \frac{m_A}{m_A + m_B} \frac{\partial U}{\partial \mathbf{r_2}} \hat{\mathbf{l}}_1$$

After Minimization

Another Minimization Method

- Minimum of potential and predicted temperatures via Vector Function

density	U	U_{min}	$T(F_{Mol})$	$T(F_{Atomic})$	Torque
0.886	-30720.936	-31864.362	0.354	0.354	0.347
0.969	-22804.725	-24032.457	0.567	0.573	0.577
1.009	-16338.726	-17777.382	0.701	0.700	0.719
1.060	-4989.757	-7044.952	0.895	0.894	0.931
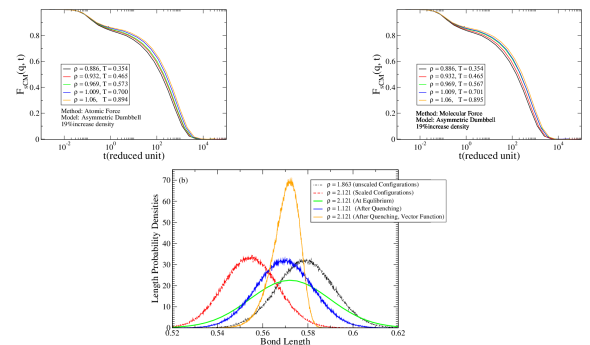
References

[1] A. E. Olsen, J. C. Dyre and T. B. Schrøder, *J. Chem. Phys.* **145**, 241103 (2016).

[2] A. A. Veldhorst, J. C. Dyre and T. B. Schrøder, *J. Chem. Phys.* **143**, 194503 (2015).

[3] T. S. Ingebrigtsen, T. B. Schrøder and J. C. Dyre, *J. Chem. Phys.* **116**, 1018 (2012).

[4] N. Gnan, T. B. Schrøder, U. R. Pedersen, N. P. Bailey and J. C. Dyre, *J. Chem. Phys.* **131**, 234504 (2009).

All simulations are performed in RUMD (Roskilde University Molecular Dynamics) : http://rumd.org/.

Bibliography

[1] Thomas B. Schrøder. Predicting scaling properties from a single fluid configuration, 2021.

[2] Andreas Elmerdahl Olsen, Jeppe C. Dyre, and Thomas B. Schrøder. Communication: Pseudoisomorphs in liquids with intramolecular degrees of freedom. *The Journal of Chemical Physics*, 145(24):241103, 2016.

[3] Pablo G Debenedetti and Frank H Stillinger. Supercooled liquids and the glass transition. *Nature*, 410(6825):259–267, 2001.

[4] M. D. Ediger and Peter Harrowell. Perspective: Supercooled liquids and glasses. *The Journal of Chemical Physics*, 137(8):080901, 2012.

[5] Jeppe C. Dyre. Colloquium: The glass transition and elastic models of glass-forming liquids. *Rev. Mod. Phys.*, 78:953–972, Sep 2006.

[6] VRV Ramanan. Metallic glasses in distribution transformer applications: an update. *Journal of materials engineering*, 13(2):119–127, 1991.

[7] M.F. Ashby and A.L. Greer. Metallic glasses as structural materials. *Scripta Materialia*, 54(3):321–326, 2006. Viewpoint set no: 37. On mechanical behavior of metallic glasses.

[8] Matthias Wuttig and Noboru Yamada. Phase-change materials for rewriteable data storage. *Nature materials*, 6(11):824–832, 2007.

[9] Yasuhiko Shirota. Photo-and electroactive amorphous molecular materials—molecular design, syntheses, reactions, properties, and applications. *Journal of Materials Chemistry*, 15(1):75–93, 2005.

[10] Stephen R Forrest and Mark E Thompson. Introduction: organic electronics and optoelectronics. *Chemical Reviews*, 107(4):923–925, 2007.

[11] Peter Jenniskens and David F Blake. Structural transitions in amorphous water ice and astrophysical implications. *Science*, 265(5173):753–756, 1994.

[12] CA Angell. Relaxation in liquids, polymers and plastic crystals—strong,fragile patterns and problems. *Journal of Non-Crystalline Solids*, 131:13–31, 1991.

[13] M. D. Ediger, C. A. Angell, and Sidney R. Nagel. Supercooled liquids and glasses. *The Journal of Physical Chemistry*, 100(31):13200–13212, 1996.

[14] Ditte Gundermann, Ulf R Pedersen, Tina Hecksher, Nicholas P Bailey, Bo Jakobsen, Tage Christensen, Niels B Olsen, Thomas B Schrøder, Daniel Fragiadakis, Riccardo Casalini, et al. Predicting the density-scaling exponent of a glass-forming liquid from prigogine–defay ratio measurements. *Nature Physics*, 7(10):816–821, 2011.

[15] Andrea Cavagna. Supercooled liquids for pedestrians. *Physics Reports*, 476(4):51–124, 2009.

[16] Hiroshi Shintani and Hajime Tanaka. Frustration on the way to crystallization in glass. *Nature Physics*, 2(3):200–206, 2006.

[17] Ernst-Joachim Donth. *Introduction*, pages 1–10. Springer Berlin Heidelberg, Berlin, Heidelberg, 2001.

[18] Michael P Allen and Dominic J Tildesley. *Computer simulation of liquids*. Oxford university press, 2017.

[19] Daan Frenkel and Berend Smit. *Understanding molecular simulation: from algorithms to applications*, volume 1. Elsevier, 2001.

[20] ISAACS program by Central Michigan University, June 2016.

[21] John Edward Lennard-Jones. On the determination of molecular fields. ii. from the equation of state of gas. *Proc. Roy. Soc. A*, 106:463–477, 1924.

[22] Jean-Pierre Hansen and Ian R McDonald. *Theory of simple liquids*. Elsevier, 1990.

[23] Søren Toxvaerd and Jeppe C. Dyre. Communication: Shifted forces in molecular dynamics. *The Journal of Chemical Physics*, 134(8):081102, 2011.

[24] Søren Toxvaerd, Ole J Heilmann, and Jeppe C Dyre. Energy conservation in molecular dynamics simulations of classical systems. *The Journal of chemical physics*, 136(22):224106, 2012.

[25] Loup Verlet. Computer" experiments" on classical fluids. i. thermodynamical properties of lennard-jones molecules. *Physical review*, 159(1):98, 1967.

[26] Dominique Levesque and Loup Verlet. Molecular dynamics and time reversibility. *Journal of Statistical Physics*, 72(3):519–537, 1993.

[27] Shuichi Nose. A unified formulation of the constant temperature molecular dynamics methods. *The Journal of chemical physics*, 81(1):511–519, 1984.

[28] Shuichi Nose. A molecular dynamics method for simulations in the canonical ensemble. *Molecular physics*, 52(2):255–268, 1984.

[29] William G Hoover. Canonical dynamics: Equilibrium phase-space distributions. *Physical review A*, 31(3):1695, 1985.

[30] William Graham Hoover and Carol Griswold Hoover. *Time reversibility, computer simulation, algorithms, chaos*, volume 13. World Scientific, 2012.

[31] Nicholas P. Bailey, Trond S. Ingebrigtsen, Jesper Schmidt Hansen, Arno A. Veldhorst, Lasse Bøhling, Claire A. Lemarchand, Andreas E. Olsen, Andreas K. Bacher, Lorenzo Costigliola, Ulf R. Pedersen, Heine Larsen, Jeppe C. Dyre, and Thomas B. Schrøder. Rumd: A general purpose molecular dynamics package optimized to utilize gpu hardware down to a few thousand particles. *SciPost Phys.*, 3:038, 2017.

[32] Marcos Raydan. On the barzilai and borwein choice of steplength for the gradient method. *IMA Journal of Numerical Analysis*, 13(3):321–326, 1993.

[33] David B Kirk and W Hwu Wen-Mei. *Programming massively parallel processors: a hands-on approach*. Morgan kaufmann, 2016.

[34] Roger Fletcher. *Practical methods of optimization*. John Wiley & Sons, 2013.

[35] Mordecai Avriel. *Nonlinear programming: analysis and methods*. Courier Corporation, 2003.

[36] Joseph-Frederic Bonnans, Jean Charles Gilbert, Claude Lemarechal, and Claudia A Sagastizabal. *Numerical optimization: theoretical and practical aspects*. Springer Science & Business Media, 2006.

[37] Dmitry Kovalev, Konstantin Mishchenko, and Peter Richtarik. Stochastic newton and cubic newton methods with simple local linear-quadratic rates. *arXiv preprint arXiv:1912.01597*, 2019.

[38] William H Press, H William, Saul A Teukolsky, A Saul, William T Vetterling, and Brian P Flannery. *Numerical recipes 3rd edition: The art of scientific computing*. Cambridge university press, 2007.

[39] David G Luenberger, Yinyu Ye, et al. *Linear and nonlinear programming*, volume 2. Springer, 1984.

[40] Carl T Kelley. *Iterative methods for optimization.* SIAM, 1999.

[41] Nicholas P. Bailey, Ulf R. Pedersen, Nicoletta Gnan, Thomas B. Schrøder, and Jeppe C. Dyre. Pressure-energy correlations in liquids. i. results from computer simulations. *The Journal of Chemical Physics*, 129(18):184507, 2008.

[42] Nicholas P. Bailey, Ulf R. Pedersen, Nicoletta Gnan, Thomas B. Schrøder, and Jeppe C. Dyre. Pressure-energy correlations in liquids. ii. analysis and consequences. *The Journal of Chemical Physics*, 129(18):184508, 2008.

[43] Nicoletta Gnan, Thomas B. Schrøder, Ulf R. Pedersen, Nicholas P. Bailey, and Jeppe C. Dyre. Pressure-energy correlations in liquids. iv. "isomorphs" in liquid phase diagrams. *The Journal of Chemical Physics*, 131(23):234504, 2009.

[44] Trond S. Ingebrigtsen, Thomas B. Schroder, and Jeppe C. Dyre. What is a simple liquid? *Phys. Rev. X*, 2:011011, Mar 2012.

[45] Ulf R. Pedersen, Nicholas P. Bailey, Thomas B. Schrøder, and Jeppe C. Dyre. Strong pressure-energy correlations in van der waals liquids. *Phys. Rev. Lett.*, 100:015701, Jan 2008.

[46] Thomas B. Schroder, Nicholas P. Bailey, Ulf R. Pedersen, Nicoletta Gnan, and Jeppe C. Dyre. Pressure-energy correlations in liquids. iii. statistical mechanics and thermodynamics of liquids with hidden scale invariance. *The Journal of Chemical Physics*, 131(23):234503, 2009.

[47] Thomas B. Schrøder and Jeppe C. Dyre. Simplicity of condensed matter at its core: Generic definition of a roskilde-simple system. *The Journal of Chemical Physics*, 141(20):204502, 2014.

[48] Jeppe C. Dyre. Hidden scale invariance in condensed matter. *The Journal of Physical Chemistry B*, 118(34):10007–10024, 2014. PMID: 25011702.

[49] Jeppe C. Dyre. Isomorph theory beyond thermal equilibrium. *The Journal of Chemical Physics*, 153(13):134502, 2020.

[50] Arno A. Veldhorst, Jeppe C. Dyre, and Thomas B. Schrøder. Scaling of the dynamics of flexible lennard-jones chains. *The Journal of Chemical Physics*, 141(5):054904, 2014.

[51] Nicholas P. Bailey, Lasse Bøhling, Arno A. Veldhorst, Thomas B. Schrøder, and Jeppe C. Dyre. Statistical mechanics of roskilde liquids: Configurational adiabats, specific heat contours, and density dependence of the scaling exponent. *The Journal of Chemical Physics*, 139(18):184506, 2013.

[52] Elijah Flenner, Hannah Staley, and Grzegorz Szamel. Universal features of dynamic heterogeneity in supercooled liquids. *Phys. Rev. Lett.*, 112:097801, Mar 2014.

[53] Saurav Prasad and Charusita Chakravarty. Onset of simple liquid behaviour in modified water models. *The Journal of Chemical Physics*, 140(16):164501, 2014.

[54] Trond S. Ingebrigtsen, Thomas B. Schrøder, and Jeppe C. Dyre. Isomorphs in model molecular liquids. *The Journal of Physical Chemistry B*, 116(3):1018–1034, 2012. PMID: 22251282.

[55] Dan E. Albrechtsen, Andreas E. Olsen, Ulf R. Pedersen, Thomas B. Schrøder, and Jeppe C. Dyre. Isomorph invariance of the structure and dynamics of classical crystals. *Phys. Rev. B*, 90:094106, Sep 2014.

[56] Andreas Kvist Bacher, Thomas B. Schrøder, and Jeppe C. Dyre. The exp pair-potential system. ii. fluid phase isomorphs. *The Journal of Chemical Physics*, 149(11):114502, 2018.

[57] Lorenzo Costigliola, Thomas B. Schrøder, and Jeppe C. Dyre. Freezing and melting line invariants of the lennard-jones system. *Phys. Chem. Chem. Phys.*, 18:14678–14690, 2016.

[58] Wence Xiao, Jon Tofteskov, Troels V. Christensen, Jeppe C. Dyre, and Kristine Niss. Isomorph theory prediction for the dielectric loss variation along an isochrone. *Journal of Non-Crystalline Solids*, 407:190 – 195, 2015. 7th IDMRCS: Relaxation in Complex Systems.

[59] H.W. Hansen, A. Sanz, K. Adrjanowicz, B. Frick, and K. Niss. Evidence of a one-dimensional thermodynamic phase diagram for simple glassformers. *Nature Communications*, 9(518), 2018.

[60] Laura Friedeheim, Jeppe C. Dyre, and Nicholas P. Bailey. Hidden scale invariance at high pressures in gold and five other face-centered-cubic metal crystals. *Phys. Rev. E*, 99:022142, Feb 2019.

[61] D. Fragiadakis and C. M. Roland. On the density scaling of liquid dynamics. *The Journal of Chemical Physics*, 134(4):044504, 2011.

[62] K. Koperwas, A. Grzybowski, and M. Paluch. The effect of molecular architecture on the physical properties of supercooled liquids studied

by md simulations: Density scaling and its relation to the equation of state. *The Journal of Chemical Physics*, 150(1):014501, 2019.

[63] D. Fragiadakis and C.M. Roland. Intermolecular distance and density scaling of dynamics in molecular liquids. *The Journal of Chemical Physics*, 150(20):204501, 2019.

[64] Thomas B. Schrøder, Ulf R. Pedersen, Nicholas P. Bailey, Søren Toxvaerd, and Jeppe C. Dyre. Hidden scale invariance in molecular van der waals liquids: A simulation study. *Phys. Rev. E*, 80:041502, Oct 2009.

[65] Jeppe C Dyre. Simple liquids' quasiuniversality and the hard-sphere paradigm. *Journal of Physics: Condensed Matter*, 28(32):323001, jun 2016.

[66] Jeppe C. Dyre. Perspective: Excess-entropy scaling. *The Journal of Chemical Physics*, 149(21):210901, 2018.

[67] GK Batchelor. Fluid mechanics. by ld landau and em lifshitz. 2nd english edition. pergamon press, 1987. 539 pp.£ 45 or 29.50 (paperback). *Journal of Fluid Mechanics*, 205:593–594, 1989.

[68] Uri M. Ascher and Linda R. Petzold. *Computer Methods for Ordinary Differential Equations and Differential-Algebraic Equations.* Society for Industrial and Applied Mathematics, USA, 1st edition, 1998.

[69] Lasse Bøhling, Trond S Ingebrigtsen, Andrzej Grzybowski, Marian Paluch, Jeppe C Dyre, and Thomas B Schrøder. Scaling of viscous dynamics in simple liquids: theory, simulation and experiment. *New Journal of Physics*, 14(11):113035, 2012.

[70] Mikhail Dzugutov. addendum: A universal scaling law for atomic diffusion in condensed matter. *Nature*, 411(6838):720–720, 2001.

[71] Yaakov Rosenfeld. A quasi-universal scaling law for atomic transport in simple fluids. *Journal of Physics: Condensed Matter*, 11(28):5415, 1999.

[72] Gary S. Grest and Kurt Kremer. Molecular dynamics simulation for polymers in the presence of a heat bath. *Phys. Rev. A*, 33:3628–3631, May 1986.

[73] Kurt Kremer, Gary S Grest, and I Carmesin. Crossover from rouse to reptation dynamics: A molecular-dynamics simulation. *Physical review letters*, 61(5):566, 1988.

[74] Kurt Kremer and Gary S Grest. Dynamics of entangled linear polymer melts: A molecular-dynamics simulation. *The Journal of Chemical Physics*, 92(8):5057–5086, 1990.

[75] M. Aichele, Y. Gebremichael, F. W. Starr, J. Baschnagel, and S. C. Glotzer. Polymer-specific effects of bulk relaxation and stringlike correlated motion in the dynamics of a supercooled polymer melt. *The Journal of Chemical Physics*, 119(10):5290–5304, 2003.

[76] Kurt Binder, Jørg Baschnagel, and Wolfgang Paul. Glass transition of polymer melts: test of theoretical concepts by computer simulation. *Progress in Polymer Science*, 28(1):115–172, 2003.

[77] F Puosi and Dino Leporini. Scaling between relaxation, transport, and caged dynamics in polymers: from cage restructuring to diffusion. *The Journal of Physical Chemistry B*, 115(48):14046–14051, 2011.

[78] F Puosi and Dino Leporini. Communication: Fast and local predictors of the violation of the stokes-einstein law in polymers and supercooled liquids, 2012.

[79] Jean-Louis Barrat, Jørg Baschnagel, and Alexey Lyulin. Molecular dynamics simulations of glassy polymers. *Soft Matter*, 6(15):3430–3446, 2010.

[80] Sharon C Glotzer and Wolfgang Paul. Molecular and mesoscale simulation methods for polymer materials. *Annual Review of Materials Research*, 32(1):401–436, 2002.

[81] Guillaume Galliero, Christian Boned, and Josefa Fernandez. Scaling of the viscosity of the lennard-jones chain fluid model, argon, and some normal alkanes. *The Journal of chemical physics*, 134(6):064505, 2011.

[82] Guillaume Galliero and Christian Boned. Thermal conductivity of the lennard-jones chain fluid model. *Physical Review E*, 80(6):061202, 2009.

[83] Teena Goel, Chandra Nath Patra, Tulsi Mukherjee, and Charusita Chakravarty. Excess entropy scaling of transport properties of lennard-jones chains. *The Journal of chemical physics*, 129(16):164904, 2008.

[84] Evangelos Voyiatzis, Florian Müller-Plathe, and Michael C Böhm. Do transport properties of entangled linear polymers scale with excess entropy? *Macromolecules*, 46(21):8710–8723, 2013.

[85] Roger Edberg, Denis J Evans, and GP Morriss. Constrained molecular dynamics: Simulations of liquid alkanes with a new algorithm. *The Journal of chemical physics*, 84(12):6933–6939, 1986.

[86] Søren Toxvaerd, Ole J. Heilmann, Trond Ingebrigtsen, Thomas B. Schrøder, and Jeppe C. Dyre. Time-reversible molecular dynamics algorithms with bond constraints. *The Journal of Chemical Physics*, 131(6):064102, 2009.

Declaration of co-authorship

Co-authors should fulfill the requirements of the Vancouver rules[i]

1. Title of article Predicting Scaling properties of fluids from individual configurations: Pseudoisom rph

2. Declaration of the individual elements

The extent of the candidate's contribution to the article is assessed on the following scale.

- A. has contributed to the work (0-33\%)
- B. has made a substantial contribution (34-66\%)
- C. did the majority of the work (67-100\%)

	Author 1	Author 2	Author 3	Author 4	Author 5
1. Formulation in the concept phase of the basic scientific problem on the basis of theoretical questions which require clarification, including a summary of the general questions which it is assumed will be answered via analyses or actual experiments/investigations.	A,B or C A	A,B or C A	A,B or C C	A,B or C	A,B or C
2. Planning of experiments/analyses and formulation of investigative methodology in such a way that the questions asked under (1) can be expected to be answered, including choice of method and independent methodological development.	A,B or C B	A,B or C A	A,B or C B	A,B or C	A,B or C
3. Involvement in the analysis or the actual experiments/investigation.	A,B or C C	A,B or C A	A,B or C C	A,B or C	A,B or C
4. Presentation, interpretation and discussion of the results obtained in the form of an article or manuscript.	A,B or C B	A,B or C A	A,B or C B	A,B or C	A,B or C

3. Signatures

Date	Name	Author #	Signature
28/5-21	Zahran Sheydaakaw	1	Zahra Sheydaakaw
Jeppe Dyk	Jeppe Dyk	2	Jeppe Dyk
	Thomas Schröder	3	Th...

Declaration of co-authorship

Co-authors should fulfill the requirements of the Vancouver rules[i]

1. Title of article *Predicting scaling properties of fluids from individual configurations: Small Molecules*

2. Declaration of the individual elements

The extent of the candidate's contribution to the article is assessed on the following scale.

- A. has contributed to the work (0-33\%)
- B. has made a substantial contribution (34-66\%)
- C. did the majority of the work (67-100\%)

Z.Sh. Jcb TBS

	Author 1	Author 2	Author 3	Author 4	Author 5
1. Formulation in the concept phase of the basic scientific problem on the basis of theoretical questions which require clarification, including a summary of the general questions which it is assumed will be answered via analyses or actual experiments/investigations.	A,B or C A	A,B or C A	A,B or C C	A,B or C	A,B or C
2. Planning of experiments/analyses and formulation of investigative methodology in such a way that the questions asked under (1) can be expected to be answered, including choice of method and independent methodological development.	A,B or C B	A,B or C A	A,B or C B	A,B or C	A,B or C
3. Involvement in the analysis or the actual experiments/investigation.	A,B or C C	A,B or C A	A,B or C C	A,B or C	A,B or C
4. Presentation, interpretation and discussion of the results obtained in the form of an article or manuscript.	A,B or C B	A,B or C A	A,B or C B	A,B or C	A,B or C

3. Signatures

Date	Name	Author #	Signature
28/5 -21	Zahraa Sheydaafar	1	Zahraa Sheydaafar
"	JEPPE DYRE	2	Jeppe Dyre
"	THOMAS SCHRØDER	3	TS